AGARD

ADVISORY GROUP FOR AEROSPACE RESEARCH & DEVELOPMENT

7 RUE ANCELLE 92200 NEUILLY SUR SEINE FRANCE

AGARD LECTURE SERIES 183

Steady and Transient Performance Prediction of Gas Turbine Engines

(Prédiction des Performances des Moteurs à Turbine à Gaz en Régimes Etabli et Transitoire)

This material in this publication was assembled to support a Lecture Series under the sponsorship of the Propulsion and Energetics Panel of AGARD and the Consultant and Exchange Programme of AGARD presented on 27th– 28th May 1992 in Cambridge, MA, United States, 9th–10th June 1992 in Neubiberg, Germany and 11th–12th June in Châtillon/Bagneux (near Paris), France.

North Atlantic Treaty Organization
Organisation du Traité de l'Atlantique Nord

The Mission of AGARD

According to its Charter, the mission of AGARD is to bring together the leading personalities of the NATO nations in the fields of science and technology relating to aerospace for the following purposes:

— Recommending effective ways for the member nations to use their research and development capabilities for the common benefit of the NATO community:

— Providing scientific and technical advice and assistance to the Military Committee in the field of aerospace research and development (with particular regard to its military application);

— Continuously stimulating advances in the aerospace sciences relevant to strengthening the common defence posture;

— Improving the co-operation among member nations in aerospace research and development;

  Exchange of scientific and technical information;

— Providing assistance to member nations for the purpose of increasing their scientific and technical potential;

— Rendering scientific and technical assistance, as requested, to other NATO bodies and to member nations in connection with research and development problems in the aerospace field.

The highest authority within AGARD is the National Delegates Board consisting of officially appointed senior representatives from each member nation. The mission of AGARD is carried out through the Panels which are composed of experts appointed by the National Delegates, the Consultant and Exchange Programme and the Aerospace Applications Studies Programme. The results of AGARD work are reported to the member nations and the NATO Authorities through the AGARD series of publications of which this is one.

Participation in AGARD activities is by invitation only and is normally limited to citizens of the NATO nations.

Preface

The quality of the design of gas turbine type propulsion systems strongly depends on the aero-thermodynamic system performance and on the accuracy of modelling of the performance of the components. These prediction models are used during the design phase, for flight performance calculations of the airframe-propulsion system and also for engine test analysis during the development phase. In addition, modern engine monitoring systems also need reliable engine performance prediction methods. This is valid for steady and transient operation of the engines.

The Lecture Series will therefore cover topics of aero-thermodynamic performance prediction methods for gas turbine engines with respect to steady and transient operation. This includes advanced cycle calculation methods, also taking into account variable cycle engine types. A very important objective will be the consideration of installation effects, i.e. Reynolds number and inlet distortions, as well as advanced control concepts for increasing engine surge margins.

This Lecture Series, sponsored by the Propulsion and Energetics Panel of AGARD, has been implemented by the Consultant and Exchange Programme.

Préface

La qualité de la conception des systèmes de propulsion du type turbine à gaz dépend fortement des performances aérothermo namiques du système et de la fidélité de la modélisation des performances de ses composants.

Ces modèles prédictifs sont employés lors de la phase de conception, pour le calcul des performances en vol du système cellule-propulseur et pour l'analyse des tests de moteurs lors de la phase de développement. En outre, les systèmes modernes de gestion et de surveillance du moteur demandent, eux aussi, des méthodes fiables de prévision des performances des moteurs, tant en régime transitoire qu'en régime établi.

Ainsi, ce Cycle de conférences portera sur les méthodes employées pour la prévision des performances aérothermodynamiques des turbines à gaz en ce qui concerne le fonctionnement en régime transitoire et en régime établi. Ceci comprend les méthodes modernes de calcul de cycle, en tenant compte des moteurs à cycle variable. L'un des principaux objectifs de la conférence sera la prise en compte des effets d'installation, c'est à dire les distorsions produites au niveau des nombres de Reynolds et des entrées d'air.

Ce Cycle de conférences est présenté par le Panel AGARD de Propulsion et d'Energétique et organisé dans le cadre du programme des Consultants et des Echanges.

List of Authors/Speakers

Lecture Series Director: Prof. Dr-Ing. L. Fottner
Institut für Strahlantriebe
Universität der Bundeswehr München
Werner Heisenberg Weg 39
8014 Neubiberg
Germany

AUTHORS/SPEAKERS

Mr R. Carrillo, Mr J.-P. Duponchel and Mr J. Loisy
SNECMA — Direction Technique
Centre de Villaroche
77550 Moissy-Cramayel
France

Mr A. H. Epstein, Prof. Dr E. M. Greitzer, Mr G. R. Guenette
Mr D. L. Gysling, Mr J. Haynes, Mr G. J. Hendricks
Mr J. Paduano, Mr J. S. Simon and Mr L. Valavani
Gas Turbine Laboratory
Massachusetts Institute of Technology
Cambridge, Massachusetts 02139
United States

Dr Ing. J. Kurzke
Motoren und Turbinen Union München
Postfach 50 06 40
8000 Munich 50
Germany

Mr J. P. Longley
Whittle Laboratory,
Cambridge University
Cambridge
United Kingdom

Dr B. D. MacIsaac
GasTops Ltd
1011 Polytek Street
Gloucester
Ontario K1JS 9J3
Canada

Prof. W. F. O'Brien
Professor of Mechanical Engineering
Virginia Polytechnic Institute
Virginia State University
Blacksburg, VA 24061
United States

Dr M. G. Philpot
Superintendent, Performance and Control
RAE Pyestock
Farnborough, Hants, GU14 0LS
United Kingdom

Prof. Dr H. I. H. Saravanamuttoo
Department of Mech. & Aerospace Engineering
Carleton University
Ottawa
Ontario K1S 5B6
Canada

Contents

OVERVIEW ON BASIS AND USE OF PERFORMANCE PREDICTION METHODS

H. Saravanamuttoo
Department of Mechanical and Aerospace Engineering
Carleton University
Ottawa K1S 5B6, Ontario
Canada

SUMMARY
The lecture outlines the basic methods of component matching which are central to the prediction of gas turbine performance. Steady state prediction of off-design performance must be done at the beginning of an engine development program, to ensure that the engine can satisfy all the mission requirements. The matching techniques can be extended to predict transient performance, which is essential for controls development and to ensure good engine handling. The large amount of computation required demands the use of computer modelling and the role of modelling in the development program and the basic requirements for performance modelling are described.

SYMBOLS

m	air flow rate	I	polar moment of inertia
C_p	specific heat at constant pressure	ω	angular acceleration
T	temperature	N	rotational speed
P	pressure	t	time
G	torque	W_f	fuel flow
η_m	mechanical efficiency	τ	rotor time constant

1.   INTRODUCTION

This lecture series will deal with advanced methods for performance prediction, covering both steady state and transient operation of different types of aero-engines. It is instructive to consider the role of performance calculations in the overall design process of a gas turbine. An overall view of the design process, showing the inter-relationship between thermodynamic, aerodynamic, mechanical and control system design is given in Fig. 1 (1). It should be clearly understood that the mechanical design cannot begin until preliminary thermo-dynamics and aerodynamic designs have been carried out; the thermodynamic design determines the most suitable cycle conditions. fixing the required air flow, cycle pressure ratio and turbine inlet temperature. Knowing these basic parameters, the aerodynamic design can begin, defining the number of stages, annulus dimensions and rotational speed. Once these are available the mechanical design can start. Fig. 1 shows some of the feedback loops involved, and clearly indicates that the various specialist groups can not work in isolation and each must realize how their contributions affect other design groups.

The previous material has concentrated on the design point of the proposed engine. It is equally important, however, to consider the off-design performance at a very early stage. Off-design performance must consider the behaviour of the engine over a wide range of conditions which may vary either as a result of variable power settings, ambient conditions or flight conditions. The manufacturers must be able to make accurate predictions of performance at key flight conditions or for critical airport locations, for example, at the design stage, to provide information required by the aircraft customer. The off-design performance predictions are of major importance to the controls designer, providing such information as maximum fuel flow requirements, acceleration and deceleration fuel schedules, control limits and selection of parameters for display to the pilot. Information can also be provided to the stress group on the variation in loading with operating conditions, e.g. the maximum torque produced by a turboshaft in extreme cold conditions. Methods of keeping the engine within prescribed limits may then be determined and built in to the design of the control system. Fig. 2 shows a suitable method for controlling a simple jet engine to limit the thrust at low ambient temperatures, often required for aircraft directional control in the event of engine failure in a multi-engined aircraft, or to limit the turbine inlet temperature on hot days. These limiting functions may be achieved by placing limits on other parameters such as compressor delivery pressure, fuel flow or engine pressure ratio

2. THE ROLE OF ENGINE MODELLING

The evaluation of engine performance obviously requires a large computing effort and mathematical models are now an integral part of the design phase. It is obvious that engine manufacturers must be deeply involved in mathematical modelling, but it should also be realized that users may also have a significant interest in the use of mathematical models for investigation of in-service problems; these might include handling problems in particular flight regimes or the application of diagnostics in Engine Health Monitoring (EHM).

Computer modelling will be used throughout an engine development program, but there are many certification tests which must be demonstrated on actual engines, e.g. bird strike, blade-off testing and water ingestion, and the development period of engines has not changed significantly following the widespread use of computing.

2.1 Performance Evaluation

One of the first requirements for an engine program is to predict the performance of the engine over the full range of conditions from take-off to a variety of flight regimes such as low altitude penetration, high altitude cruise and combat manoeuvring with maximum afterburning. This requires sophisticated modelling which can be done with a high level of confidence before the engine has run; both design point and off-design performance must be accurately predicted. This must be done before any component testing has been carried out and the component characteristics must be estimated and then updated as the program unfolds. In a later lecture, the topic of component peformance changes between test rigs and actual engine operation will be discussed.

As the need for ever improving aircraft performance drives the engine designer to continually improve engine performance, engines are steadily becoming more complex. Variable stator compressors, for many years found only on GE engines, are now used on virtually all high performance engines to cope with steadily rising pressure ratios. Blow-off valves are frequently used on starting or when operating at low power. Variable final nozzles are becoming more sophisticated, with the first fully variable convergent-divergent nozzle introduced on the Olympus 593 in Concorde; the use of variable nozzle area to optimize Concorde engine performance is well described in (2); variable geometry turbines have not yet been introduced in aeroengines, but have been used for some years in industrial engines for performance improvement at part load. Future military, and probably civil, engines will introduce variable cycle technology. As an example, a future supersonic transport engine will need to operate at high by-pass ratio and low jet velocity at take-off, to minimize noise, while operating with a very low by-pass ratio and high jet velocity for efficient supersonic cruise.

The evaluation of all of these new technologies requires an ever increasing use of mathematical models at the design stage; many initially promising schemes may turn out to be impractical, but considerable man effort and computations may be req ed to provide the information to support or abandon a new concept.

2.2 Controls Design

With increasingly complex engines the control system requirements become much more complicated. Early engines had no variable geometry to control and simple hydro-mechanical controls capable of adjusting fuel flow with altitude and providing simple acceleration schedules were used. The use of variable geometry compressors, intakes and nozzles allows the engine operating conditions to be optimized for widely differing flight conditions. The variable geometry can also be used to optimize transient response, both during accelerations and decelerations, to provide rapid thrust changes without over-temperature or flame out.

Comprehensive mathematical models of the complete power plant (intake-gas generator-exhaust) plus the control system can be used to devise control strategies and limiting parameters (3); these can be investigated in great detail, without endangering an engine. The acceleration and deceleration fuel schedules can be optimized, along with the required variable geometry settings. The predictions from the mathematical model must eventually be validated on actual engines, first on the test bed and later in flight. The judicious use of models should reduce the amount of testing required and minimize the high cost of engine failures.

2.3 Engine Test Direction and Analysis

Engine modelling may be used in advance of engine testing to investigate possible hazardous operating conditions and also to familiarize test crew with the likely behaviour of the engine on test. This will become increasingly important as complex variable cycle engines appear, because the test operators will have no previous experience to rely on; indeed, following past practice for simple engines could be quite the wrong action. Both steady state and dynamic models could be used for operator training.

Engines under development are heavily instrumented, leading to prodigious amounts of experimental data. This must be rapidly analyzed and then assessed by the test crew before moving to another operating condition. The use of models to analyze experimental data is invaluable to both ground test beds and flight operations.

2.4   Engine Health Monitoring

Once the engine has entered service, many of the problems transfer to the operator. It is nearly two decades since the introduction of Airborne Integrated Data Systems (AIDS) in the airline world; these systems primarily dealt with trend monitoring and were not notably successful. Engine Health Monitoring (EHM) systems are considerably more ambitious, with the prime goal of diagnozing performance deterioration and identifying the fault. With the widespread introduction of fully modular engines, it is critically important to diagnoze to the module level.

Mathematical modelling can be used to predict performance deterioration, by implanting faults at the component level in a performance model and developing fault matrices showing the effect of different faults. This eventually leads to the concept of expert systems, the main problem being that the rules for performance degradation are not fully understood and will probably be quite engine specific. Mathematical models of performance deterioration can give a good insight into likely indications of trouble (4), but it is still necessary to obtain experimental evidence of the quantitative effects of damage on engine components to replace the asumptions about changes in efficiency or flow capacity that must currently be used.

Ideally, the manufacturer and the user would work together on this problem but the user may find a lack of suport from the manufacturer or even that the manufacturer does not understand the problem. This leads to the situation where the user, or a third party, becomes deeply involved in mathematical modelling.

3.   OFF-DESIGN PERFORMANCE

Methods for calculating the design point performance of gas turbines are well understood, and can be done with great accuracy by making the appropriate assumptions regarding component efficiencies, pressure losses, air bleeds and the variation of fluid properties with temperature and composition. Off-design performance is often not well understood, largely because of the manner in which the results are presented. Performance figures from a typical engine manufacturer's brochure are shown in Figures 3 and 4; these results could be obtained on a test bed, from flight test or by mathematical modelling and all three methods would be used in practice. It is not clear, however, how these results could be predicted by mathematical modelling without understanding the underlying principles.

3.1   Basic Method for Performance Analysis

In its simplest form, the gas turbine consists of a compressor, combustor, turbine and exhaust; this configuration could be used for either a turboprop or turbojet. When the gas turbine is operated at any condition other than the design point its performance will depend on the matching of the compressor and turbine; both compressors and turbines have well defined variations of flow with pressure ratio and speed, and when the compressor power is supplied by the turbine there is a very restricted range of operating possibilities. The configuration of the gas turbine has a major bearing on its off-design performance. A turboprop may be designed with a single shaft or free turbine configuration; two engines may be designed with almost identical cycle conditions, but totally different operational characteristics. This is exemplified by the Garrett 331 and PW Canada PT-6 turboprops.

The majority of high performance modern engines use multi-spool compressors, the most common configuration being the twin-spool with the low pressure (LP) fan/compressor driven by the LP turbine and the high pressure (HP) compressor driven by the HP turbine; typical examples are shown in Fig. 5. A notable exception is the three-spool RB-211 family of high by-pass commercial turbofans. The three-spool arrangement has also been used on the Turbo Union RB-199 military turbofan.

Irrespective of the configurations used, the off-design behaviour is determined by the matching of the compressor(s) and turbine(s). The matching process is categorized by two main conditions, these being

1.   Compatibility of Flow
2.   Compatibility of Work

In the case of transient operation the turbine work is not equal to the compressor work, resulting in acceleration or deceleration of the rotor system.

The basis of the compressor-turbine matching process was first laid down by Mallinson and Lewis (5); it is perhaps worth noting that the process was originally done by slide rule, before even the most rudimentary computers were available.

1-4

3.2 Basic Application of Method

The prediction of off-design performance requires the availability of compressor and turbine characteristics, which are presentations of the flow/pressure ratio/speed variation of the components. These are usually given in terms of 'non-dimensional' qualities such as $m\sqrt{T}/P$, pressure ratio and $N/\sqrt{T}$ as shown in Fig. 6. The 'non-dimensional' flow, $m\sqrt{T}/P$, is related to the axial Mach number of flow, while $N/\sqrt{T}$, is related to the Mach number corresponding to the tangential blade speed (see (1)).

It should be realized at the outset that it is difficult to obtain these characteristics, and this will be discussed further in a later lecture. Methods exist for predicting characteristics, either based on knowledge of similar components or from estimates of the head-flow characteristics of individual stages. Component characteristic data are often highly proprietary to the manufacturer, and this can present problems to the user who wishes to create an engine model.

The basis of the method will be illustrated using the examples of a single shaft turboprop and a simple jet engine, using an abbreviated treatment of material from (1). For simplicity and ease of understanding engine, stations are numbered consecutively starting with 1 at the compressor inlet. The SAE have recommended a unified method applicable to all gas turbine types in SAE Aerospace Recommended Practice ARP 755A "Gas Turbine Engine Performance Station Identification and Nomenclature." This system uses 2 for inlet to the first compressor, 3 for the exit from the final compressor, 4 for inlet to the first turbine and 5 for exit from the last turbine; this allows the use of numbers such as 4.5 for entry to the LP turbine of a twin spool engine.

3.2.1 Single Shaft Turboprop

Consider a single-shaft turboprop with station numbering as in Fig. 7; to illustrate the basic simplicity of the method, secondary effects such as inlet and exhaust pressure losses and bleed will be neglected. It will also be assumed that the turbine characteristic is independent of speed, giving a single line characteristic as shown.

Select any arbitrary point on the compressor characteristic, A, defining $m_1\sqrt{T_1}/P_1$, P_2/P_1 and η_c. From Compatibility of Flow

$$m_1 = m_3 \text{ (neglecting bleed and fuel addition)}$$

Re-writing in terms of non-dimensional groups

$$\frac{m_1\sqrt{T_1}}{P_1} = \frac{m_3\sqrt{T_3}}{P_3} \cdot \frac{P_3}{P_2} \cdot \frac{P_2}{P_1} \cdot \sqrt{\frac{T_1}{T_3}} \cdot \frac{m_1}{m_3}$$

where P_3/P_2 is the combustion pressure loss. Simplifying, with $m_1 = m_3 = m$

$$\therefore \quad \frac{m\sqrt{T_1}}{P_1} = \frac{m\sqrt{T_3}}{P_3} \cdot \frac{P_3}{P_2} \cdot \frac{P_2}{P_1} \cdot \sqrt{\frac{T_1}{T_3}}$$

This gives an expression for T_3/T_1, i.e.

$$\sqrt{\frac{T_3}{T_1}} = \frac{\dfrac{m\sqrt{T_2}}{P_3} \cdot \dfrac{P_3}{P_2} \cdot \dfrac{P_2}{P_1}}{\dfrac{m\sqrt{T_1}}{P_1}}$$

With inlet and exhaust pressure losses ignored, $P_3/P_4 = P_2/P_1$; thus $m\sqrt{T_3}/P_3$ can be obtained directly from the turbine characteristics and we have all the information required to determine T_3 at our selected point A.

Turning to Compatibility of Work,

(Turbine work) η_m = Compressor work + propeller output

$\therefore$ $\qquad$ m C_{p34} ΔT_{34} η_m = m C_{p12} ΔT_{12} + power $\qquad\qquad$ II

Now, $\Delta T_{34}/T_3$ can be found from P_3/P_4 and η_t and $\Delta T_{12}/T_1$ from P_2/P_1 and η_c hence both ΔT_{34} and ΔT_{12} can be calculated as we know T_3 (from Eqn. (I)) and T_1, the ambient temperature. Thus the power developed can be calculated from Eqn (II); all other data required for cycle calculations are available, and it would now be possible to calculate fuel flow, sfc etc. as required.

The key question to be resolved, however, is whether point A is valid or not. This, in turn, depends on the power-speed characteristic of the driven load. If a fixed pitch propeller were used, power varies with $(N)^3$, and for any specified speed the power is known; there is no reason why our arbitrary choice of point A should give the correct power and it would be necessary to find the unique point on the constant speed line which gave the correct power by trial and error.

For a variable pitch propeller (or electric generator) we can vary power at constant speed and by choosing a series of points on the compressor characteristic we could readily establish the variation of power, turbine inlet temperature, fuel flow, sfc as pressure ratio is varied. This could determine the point where zero power was obtained and also the power at maximum allowable temperature or at the surge limit, whichever came first.

Calculations for the single shaft engine are intrinsically simple because the pressure ratio across the turbine is directly related to the compressor pressure ratio. This simple relationship is lost when we consider either a free turbine or a propelling nozzle.

3.2.2 Jet Engine

The simple jet engine considered is shown in Fig. 8; the flow characteristics of a propelling nozzle and a turbine are virtually identical, so the following analysis can be applied to either a jet engine or a turboprop/turboshaft with a free turbine.

Let us start again by choosing any point A on the compressor characteristic. Considering Compatibility of Flow, we get

$$\frac{m\sqrt{T_1}}{P_1} = \frac{m\sqrt{T_3}}{P_3} \cdot \frac{P_3}{P_2} \cdot \frac{P_2}{P_1} \sqrt{\frac{T_3}{T_1}}$$

giving

$$\sqrt{\frac{T_3}{T_1}} = \frac{\dfrac{m\sqrt{T_3}}{P_3} \cdot \dfrac{P_3}{P_2} \cdot \dfrac{P_2}{P_1}}{\dfrac{m\sqrt{T_1}}{P_1}} \qquad\qquad I$$

which is the same result as for the previous case.

Compatibility of Work gives

$$(m\ C_{p34}\ \Delta T_{34})\ \eta_m = m\ C_{p12}\ \Delta T_{12}$$

i.e. the gas generator turbine provides just enough work to drive the compressor

Re-writing in terms of non-dimensional temperature ratios,

$$\frac{\Delta T_{34}}{T_3} = \frac{\Delta T_{12}}{T_1} \cdot \frac{T_1}{T_3} \cdot \frac{c_{p12}}{c_{p34}\ \eta_m}$$

or
$$\frac{T_3}{T_1} = \frac{\left(\dfrac{\Delta T_{12}}{T_1}\right)}{\left(\dfrac{\Delta T_{34}}{T_3}\right)} \left(\frac{c_{p12}}{c_{p34}\,\eta_m}\right)$$
II

The values of T_3/T_1, from Eqns. I and II must be equal. In this case, however, we do not know P_3/P_4. If we assume a value of P_3/P_4, we can get $m\sqrt{T_3}/P_3$, η_t and $\Delta T_{34}/T_3$ from the turbine characteristic; this will, in general, give different values of T_3 from Eqns. I and II and it is necessary to iterate until a suitable value of P_3/P_4 is found.

Having found the value of P_3/P_4 that gives the same value of T_3 from both Compatibility of Flow and Compatibility of Work, we have satisfied the matching requirements of the gas generator.

We can also calculate conditions at exit from the turbine, i.e.

$$\frac{m\sqrt{T_4}}{P_4} = \frac{m\sqrt{T_3}}{P_3} \cdot \frac{P_3}{P_4} \cdot \sqrt{\frac{T_4}{T_3}}$$

where
$$\sqrt{\frac{T_4}{T_3}} = \sqrt{1 - \left(\frac{\Delta T_{34}}{T_3}\right)}$$

This also gives us P_4, because

$$P_3 = P_1 \cdot \frac{P_2}{P_1} \cdot \frac{P_3}{P_2}$$

and
$$P_4 = P_3 \cdot \frac{P_4}{P_3}$$

Knowing P_4/P_a, the nozzle characteristic gives us a value of $m\sqrt{T_4}/P_4$; this, unfortunately, will not in general be the same as the value calculated at exit from the turbine. In other words, we still have to satisfy Compatibility of Flow between the turbine and the exhaust.

This would require the selection of a series of points along the selected speed line until the unique point satisfying both the gas generator and nozzle requirements was found. If this procedure were repeated for each speed line on the compressor characteristic the result would be a single operating line, determined by the swallowing capacity of the nozzle or power turbine. It is important to note that for a free turbine turboprop the operating line is fixed by the power turbine characteristic rather than the power output as in the case of the single shaft turboprop. Thus, power changes must be obtained by changes in gas generator speed for the free turbine engine; the single shaft can change power at constant speed, by means of propeller pitch control. The transient behaviour of the two types of turboprop is totally different, as is their mode of operation.

3.2.3 *Effect of Choked Nozzle*

It is useful to consider the behaviour of a turbine and nozzle, or two turbines, in series. If we start with a conventional turbine characteristic, knowing $m\sqrt{T_3}/P_3$ and η_t as functions of P_3/P_4, we can calculate the turbine exit flow function $m\sqrt{T_4}/P_4$, i.e.

$$\frac{m\sqrt{T_4}}{P_4} = \frac{m\sqrt{T_3}}{P_3} \cdot \frac{P_3}{P_4} \cdot \sqrt{1 - \left(\frac{\Delta T_{34}}{T_3}\right)}$$

Thus, for _each_ value of P_3/P_4 we can calculate $m\sqrt{T_4}\,/P_4$ and draw the two characteristics as shown in Fig. 9. It is immediately obvious that the pressure ratio P_3/P_4 is limited by choking of the downstream components. With the final nozzle choked, the gas generator turbine operates at a fixed non-dimensional point with the values of $m\sqrt{T_3}\,/P_3$, P_3/P_4 and $\Delta T_{34}/T_3$ constant. It is for this reason that over a very wide range of operating conditions the HP turbine continues to operate efficiently. The choked nozzle gives a unique operating line on the compressor characteristic which is independent of flight speed; for modern jet engines the nozzle will be choked for all normal flight conditions, only becoming unchoked during descent or ground operations when the engine is throttled back.

3.2.4   *Off-design Performance Presentation*

Assuming a unique operating line on the compressor characteristic, it can readily be seen that at each point along the line all performance parameters are known, having been determined from the matching calculations. It is more useful to select one of these as the independent variable and display all other parameters as a function of the selected parameter. The most obvious independent parameter is the gas generator speed, and this results in the presentation previously shown in Fig. 3; this can also be used to present the performance at various altitudes as a function of Mach number and compressor speed. From Fig. 3 it can readily be seen that the setting of take-off, climb and cruise ratings on the basis of gas generator speed implies both reduction in centrifugal stress and turbine inlet temperature. Calculations yield the values of all significant temperatures, e.g. Turbine Inlet Temperature, Inter Turbine Temperature or Exhaust Gas Temperature; the value of EGT corresponding to the maximum allowable TIT can then be determined and used as a control limit.

Any of the thermodynamic parameters could be selected as the independent variable, including Engine Pressure Ratio (EPR); this was widely used for thrust setting purposes on jet engines. It can be shown that the thrust is directly related to the EPR, and even for a deteriorated engine knowledge of the jet pipe pressure will give a good indication of thrust. EPR is not an intuitive indicator of thrust; it can be seen, however, that the variation of parameters with EPR is directly obtained from the off-design matching calculations.

3.2.5   *Multi-Spool Engines*

With multiple spools it becomes necessary to solve for work compatibility on all rotors and for flow compatibility between components. For a twin-spool turbojet, for example,

LP compressor work = LP turbine work
HP compressor work = HP turbine work

and

$$\left(m\frac{\sqrt{T}}{P}\right) \text{ at exit from LPC} \qquad = \left(m\frac{\sqrt{T}}{P}\right) \text{ at entry to HPC}$$

$$\left(m\frac{\sqrt{T}}{P}\right) \text{ at exit from HPT} \qquad = \left(m\frac{\sqrt{T}}{P}\right) \text{ at entry to LPT}$$

$$\left(m\frac{\sqrt{T}}{P}\right) \text{ at exit from LPT} \qquad = \left(m\frac{\sqrt{T}}{P}\right) \text{ at entry to nozzle}$$

The level of complexity of the calculation increases rapidly as more components are added, but the basic simple methods described earlier still apply.

In the cases of a twin-spool turbojet, the LP turbine stators are normally choked over most of the operating range. The HP spool can be thought of as a simple jet engine with a choked final nozzle, giving rise to a unique operating line on the HPC characteristic as long as the LP turbine is choked. Incorporation of a variable final nozzle affects the operation of the LP system, while the HP system is shielded from disturbances downstream of the choked LP turbine. Methods of analyzing twin-spool performance, both for turbojets and turbofans, are given in (1).

4. TRANSIENT PERFORMANCE

The steady state performance of the engine can be calculated using the methods described in the previous section, one of the key outputs being the steady state fuel flow. To accelerate the engine, excess fuel must be added, giving a higher turbine inlet temperature; this, in turn, gives a higher turbine temperature drop resulting in more power available than required by the compressor. The engine speed then increases until the torques are again in balance. Decreasing the fuel has the opposite effect.

The simplest way to understand the transient behaviour of engines is to assume that compatibility of flow is still satisfied, but compatibility of work is not.

4.1 Acceleration Torque

If the engine is operating in equilibrium and is then subjected to a sudden increase in fuel flow, the turbine temperature will increase much more rapidly than any increase in rotor speed because of the inertia of the rotor system. For a simple jet engine, the effect is an excursion along the constant speed line on the compressor characteristic towards surge; a sufficiently large step change will cause the engine to surge.

Considering the case of accelerating the gas generator, the acceleration torque, ΔG, is given by

$$\Delta G = G_t - G_c$$

where G_t and G_c are the turbine and compressor torques. Assuming $\Delta T_{34}/T_3$ to be determined by the turbine operating point, increasing T_3 will cause an increase in ΔT_{34} and the torque is given by

$$\Delta G = m\ C_{p34}\ \Delta T_{34}\ \eta_m - m\ C_{p12}\Delta T_{12}$$

The rotor acceleration is then obtained from Newton's Second Law of Motion as

$$\Delta G = J\ \dot{\omega}$$

where J is the polar moment of inertia and $\dot{\omega}$ is the angular acceleration. The accelerating torque can then be integrated with respect to time to get the change in rotor speed.

It should be noted that the i.e. torque is the difference between two quantities of similar magnitude and a small change in either may result in a much larger change in the torque available for acceleration. Accurate transient calculations therefore require very good estimates of both compressor and turbine torques; this is especially difficult at low speeds, e.g. during starting or windmilling.

4.2 Fuel Schedules

The fuel required for acceleration or deceleration is normally scheduled, the requirements being to provide safe operation, rapid response and long life. Rapid response requires a large amount of over-fuelling, causing high temperatures and thermal shock which is undesirable from the viewpoint of long life. Safe operation implies maintaining a large surge margin and avoiding flame-out on deceleration; again, the need for a large surge margin is directly in conflict with the requirement for rapid response.

Selection of a suitable fuel schedule is very dependent on the engine application, and is greatly helped by the use of mathematical modelling of the engine transient performance.

Typical fuel schedules are shown in Fig. 10. The use of a computer model to optimize acceleration performance of a simple turbojet is described in (6) and for a variable geometry turbofan in (7).

5. THE EVOLUTION OF MODELLING TECHNIQUES

It is the availability of extremely powerful computing facilities which have made possible the very advanced thermodynamic models in widespread use to-day. It is instructive, however, to examine the evolution of modelling techniques realizing that the basic investigations into the engine response problem began in the late 40's, when computers were in their infancy; at that period in time, control engineering was very much in the field of electrical engineering and there was a very considerable gulf between the disciplines of control and engine performance.

5.1 Linear Models

Although this pioneering work may now be regarded as somewhat elementary, it is important to realize that the early attempts to quantify engine dynamics were very successful in identifying and understanding the parameters which affect the response rate. Probably the earliest published work was that of NACA, where Gold and Rosenzweig (8) showed, in 1952, that the rotor of a turbojet responded to sudden changes in fuel flow as a first-order system which could be conveniently expressed in terms of a rotor time constant; their expression for time constant, however, appeared in terms of partial derivatives which were not readily available and also were difficult to interpret quantitatively. A major advance was made by the Lucas Company (9), whose analysis assumed that a sudden increase in fuel flow would cause an instantaneous increase in turbine torque but zero increase in compressor torque. As a result of this simplified analysis, the rotor time constant could be expressed in terms of thermodynamic parameters which were readily obtained from normal performance calculations. The expression obtained was

$$ \tau = \frac{K I N}{\left(\dfrac{\Delta T_{34}}{T_3} \right) \left(\dfrac{dW_f}{dN} \right)} $$

The variation of τ as a function of N could thus be determined as soon as the off-design performance had been evaluated. Referring to Fig. 3, it can be seen that fuel flow changes relatively slowly at low speeds and then changes much more rapidly as speed increases. Fig. 11 shows typical variations of $\Delta T_{34}/T_3$ and dW_f/dN for a simple turbojet, and it can be seen that both terms decrease with reducing speed causing a significant increase in time constant; it can readily be seen that the dominant effect in determining τ is dW_f/dN. Thus, the simple theory yields the important practical result that <u>response is much more sluggish at low speeds</u>. Despite its simplifying assumptions, the Lucas method gives quite respectable results when compared with engine tests, as shown in Fig. 12, and improvements on this method are still in use for preliminary investigations.

Another important deduction following from the simple expression for the time constant is that, at high altitudes, where dW_f/dN will be much lower because of the reduction in fuel flow, the time constant will be increased. It is possible (but hardly convincing!) to express the moment of inertia in non-dimensional form, but a much more reasonable explanation is to consider that the engine inertia remains fixed while the energy release decreases with altitude.

It is important to realize that it is <u>quite fundamental</u> that response from low values of compressor speed will be sluggish, and much sophisticated modelling for a wide variety of engines of differing complexity has shown that it is essential to keep the HP rotor speed as high as possible for good response rates.

The major disadvantage of the time constant approach, however, was that it was limited to small changes in speed (say ± 5%) and it did not give much information beyond the rotor speed response; it was primarily of use to control system designers, and was of little use to the engine or airframe designer.

5.2 Analog Computer Models

It was clear that for mathematical modelling to be useful to the engine designer, models capable of operation over the complete running range were essential. The computations required for continuous calculation of engine dynamics were greatly in excess of the capacity of early digital computers, and attention was initially focused on analog computers because of their capability of operating in real time. Notable work was carried out by Larrowe and Spencer (10), sponsored by the US Air Force, in the hope that, with a model operating in real time, the control hardware could be developed using a simulator rather than an actual engine. The anticipated advantages were not immediately realized, mainly because of the difficulty of integrating hydromechanical control systems and their required sensors and actuators with analog computers. A further major problem was the use of conducting surface bi-variant function generators for compressor characteristics, as these introduced both inaccuracies and dynamic effects on their own. Larrowe and Spencer, however, are due credit for the first real time simulation based on component characteristics using the approach of the engineering thermodynamicist. The problem of bi-variant function generators was overcome by using three single function generators to generate a function of two variables, and Saravanamuttoo (11) used this to develop full range analog methods which were used to predict dynamic behaviour of the Orenda OT-4 at the design stage. The analog proved fully capable of carrying out real time dynamic performance investigations on the Olympus 593, (12). It is interesting to note that 25 years ago the analog could simulate the Olympus 593 in real time, while a typical 5 second acceleration took approximately 20 minutes on a University main frame digital computer of that era. While analog models proved extremely useful in predicting engine behaviour, their greatest use has been in providing an understanding of different control strategies.

Once full range models, based on known component characteristics, became established, major efforts were focused on effects such as heat transfer to and from engine parts, changes in clearances during transients, transient combustion efficiencies and changes in component characteristics during transients. Bauerfeind (13) discussed many of these effects in an earlier AGARD paper. It is clear that these can only be considered because of the enormous developments in computing capability, and also that they can lead to a vast increase in modelling complexity.

Hybrid computers were used for a few years, augmenting the high speed integration capability of the analog with the stored program capability of the digital computer. In recent years, however, developments in high speed digital computers has made both the analog and hybrid machines obsolete, and all future activity in modelling will be based on digital computing; the advent of parallel processing in particular permits much higher computing speeds.

5.3   Modelling Requirements

It is appropriate at this point to consider the requirements for a successful mathematical model, bearing in mind that the model should be kept as simple as possible consistent with the needs of the particular user. The prime requirement of any model is that it should faithfully and accurately represent the behaviour of the engine over its complete running range and flight envelope. Further important requirements include:

1.   Flexibility: The simulation must be capable of handling all the obvious requirements, such as scheduled accelerations and the operation of variable geometry devices; it must also be capable of dealing with situations which were not anticipated initially. During the development of an engine compressors and turbines may be modified to improve their performance, and the simulation must be able to keep abreast of the latest developments.

2.   Credibility: The simulation must be readily understandable to performance, development and management engineers who are not simulation specialists; for this reason, the simulation should produce results in a form similar to a real engine and should make use of commonly available data.

3.   Availability: Once the simulation has been verified it must be capable of being rapidly brought into use whenever required without the necessity of lengthy setup times.

4.   Reliability: A high degree of reliability and repeatability is clearly essential, and the simulation must be capable of easy checking to ensure that it is functioning correctly; this is especially important for complex engine simulations.

REFERENCES

1.   Cohen, H., Rogers, G.F.C. and Saravanamuttoo, H.I.H., 'Gas Turbine Theory', 3rd Edition, Longman 1987.

2.   Young, P.H., 'Propulsion Controls on the Concorde', Journal of the Royal Aeronautical Society, Vol. 70, 1966, pp. 863-881.

3.   Cottington, R.V., 'Overall Powerplant Control', AGARD Conference Proceedings 151, 'Power Plant Control for Aero Gas Turbine Engines', 1974.

4.   Saravanamuttoo, H.I.H. and MacIsaac, B.D., 'Thermodynamic Modelling for Pipeline Gas Turbine Diagnostics', Transactions ASME, Journal of Engineering for Power, vol. 105, 1983, pp. 875-884.

5.   Mallinson, D.H. and Lewis, W.G.E., 'The Part Load Performance of Various Gas Turbine Engine Schemes', Proceedings of I. Mech. E., Vol. 159, 1948, pp. 198-219.

6.   Saravanamuttoo, H.I.H. and MacIsaac, B.D., 'The Use of a Hybrid Computer in the Optimization of Gas Turbine Control Parameters', Transactions ASME, Journal of Engineering for Power, Vol. 95, 1973, pp. 257-264.

7.   MacIsaac, B.D. and Saravanamuttoo, H.I.H. 'Aerothermodynamic Factors Governing the Response Rate of Gas Turbines', AGARD Conference Proceedings 151, 'Power Plant Control for Aero Gas Turbine Engines', 1974.

8.   Gold, H. and Rosenzweig, S., "A Method for Estimating Speed Response of Gas Turbine Engines", NACA RM E51 K21, 1952.

9.   Lawrence, J.O.N. and Powell, R.D., "The Application of Servo-Mechanism Analysis to Fuel Control Problems", Proc. I. Mech. E., Vol. 172, pp. 439-469, 1958.

10. Larrowe, V.L., Spencer, M.M. and Tribus, M., "A Dynamic Performance Computer for Gas Turbine Engines", Transactions of the ASME, Oct. 1957, pp. 1707-1714.

11. Saravanamuttoo, H.I.H., "Analog Computer Study of the Transient Performance of the Orenda 600 HP Regenerative Gas Turbine", ASME paper 63-AHGT-38, 1963.

12. Saravanamuttoo, H.I.H. and Fawke, A.J., "Simulation of Gas Turbine Dynamic Performance", ASME paper 70-GT-23, 1970.

13. Bauerfeind, K., "A New Method for the Determination of Transient Jet Engine Performance Based on the Non-Stationary Characteristics of the Components" AGARD Conference Proceedings No. 34, Paper 32, 1968.
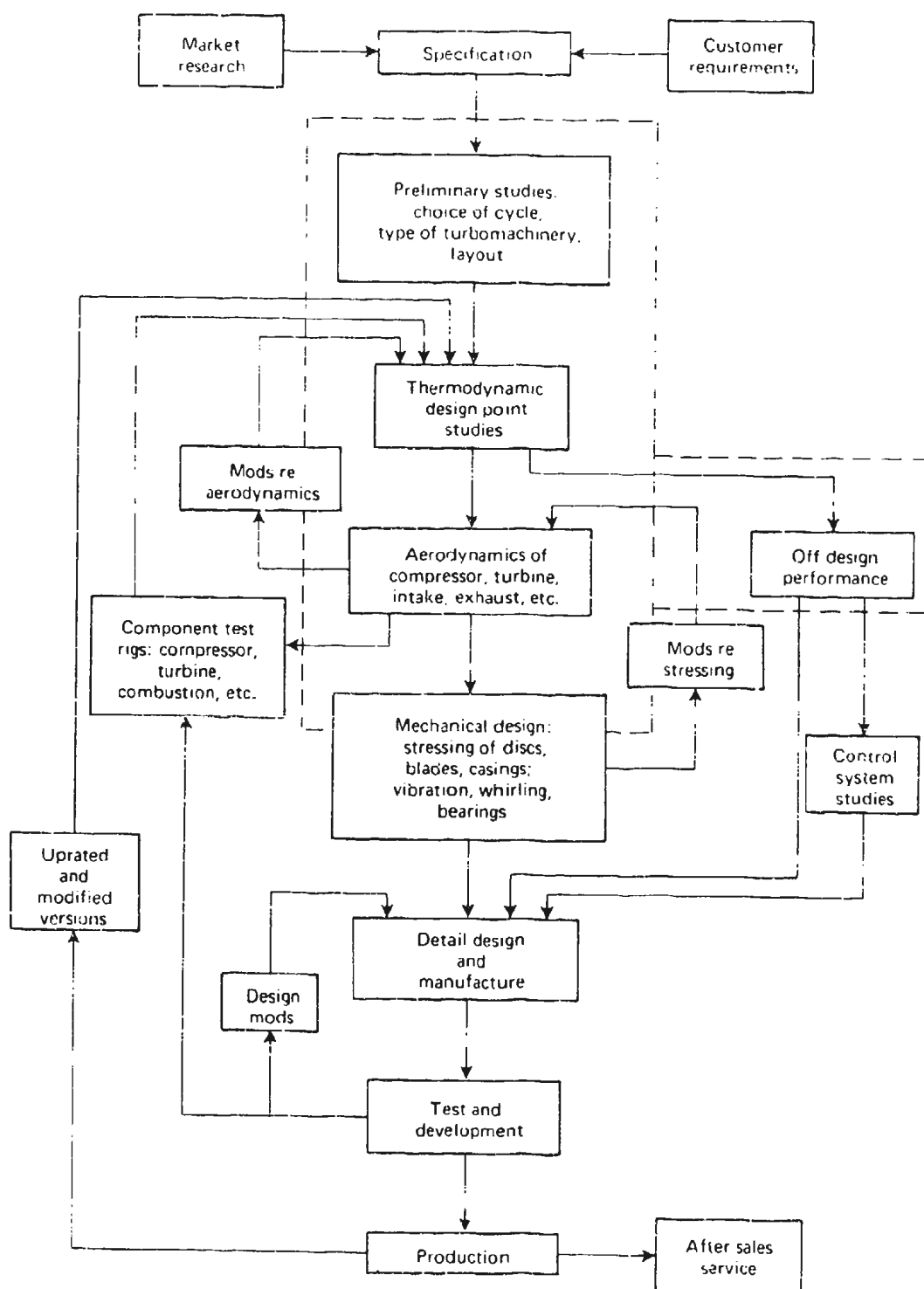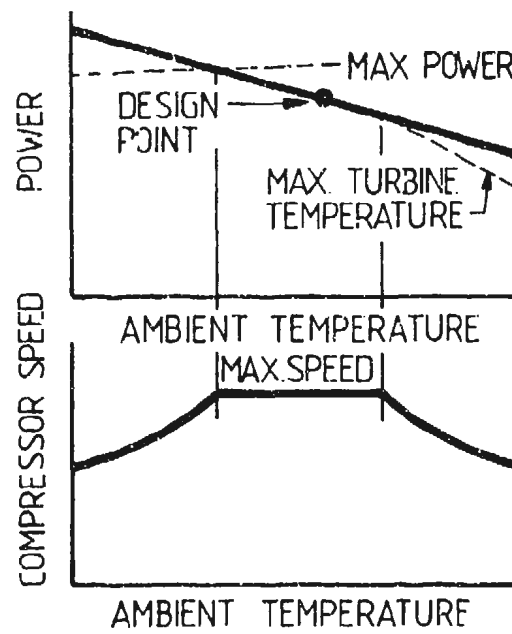
Fig. 1   Typical gas turbine design procedure
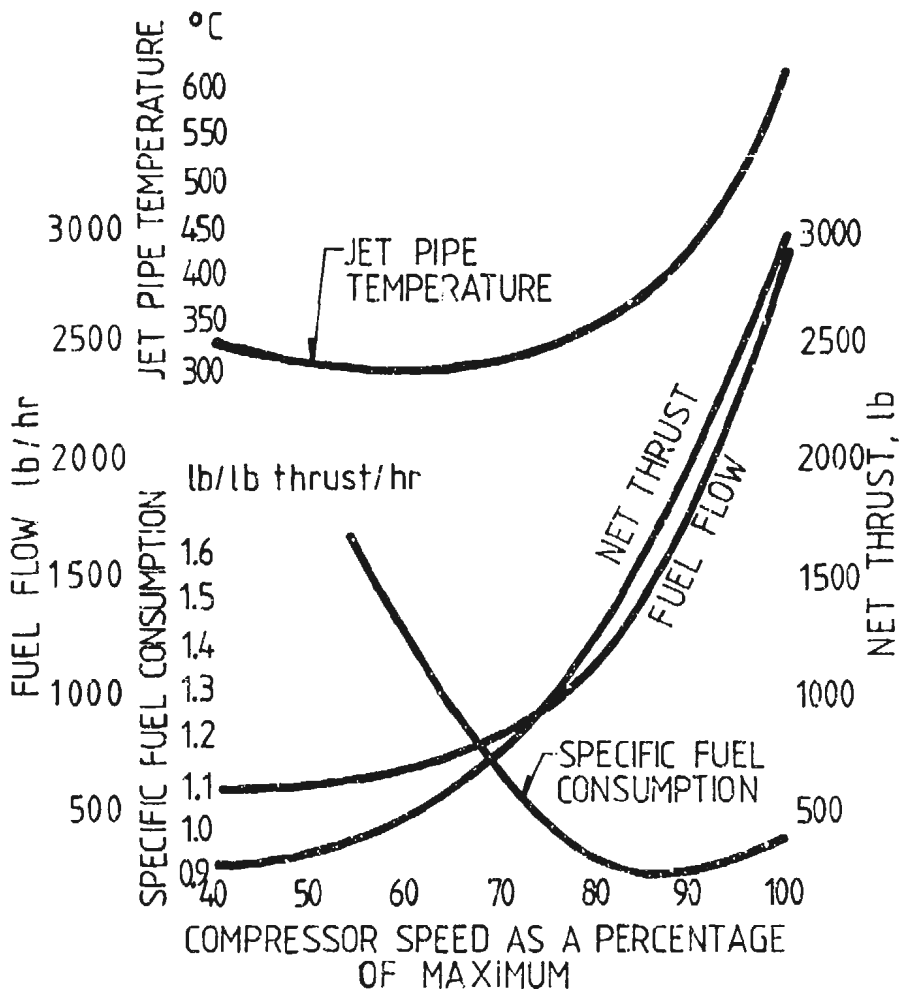
FIG.2 POWER AND TEMPERATURE LIMITING.
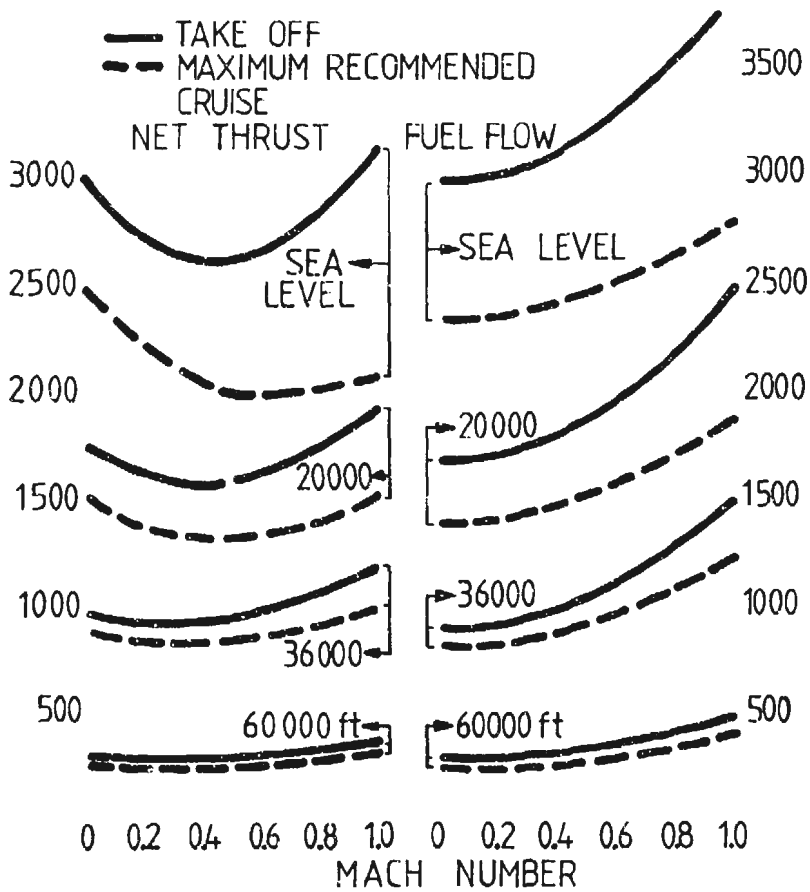

FIG.3 SEA LEVEL STATIC PERFORMANCE

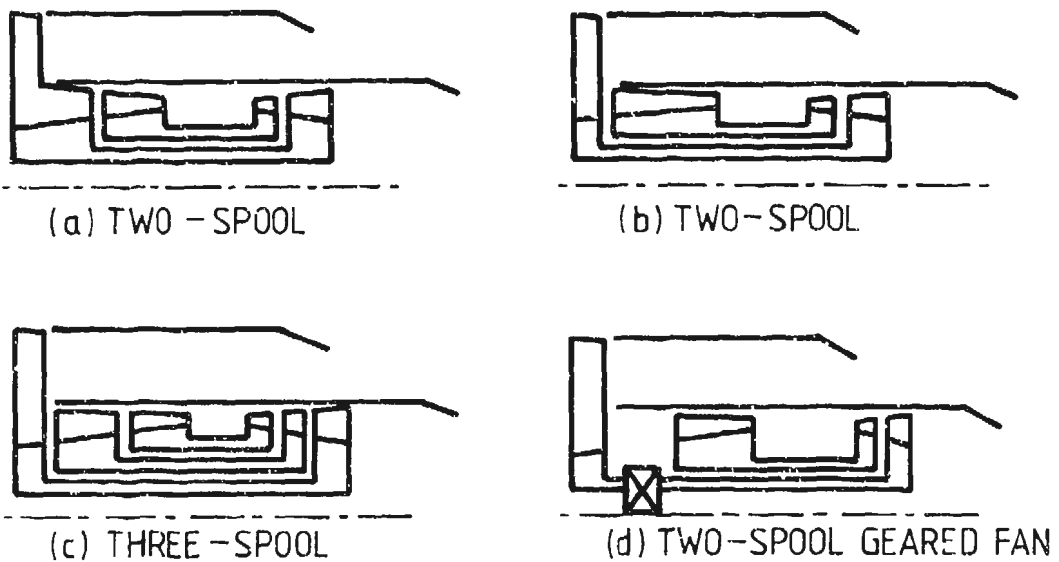**FIG. 4 TAKE-OFF AND MAXIMUM RECOMMENDED CRUISE RATINGS**

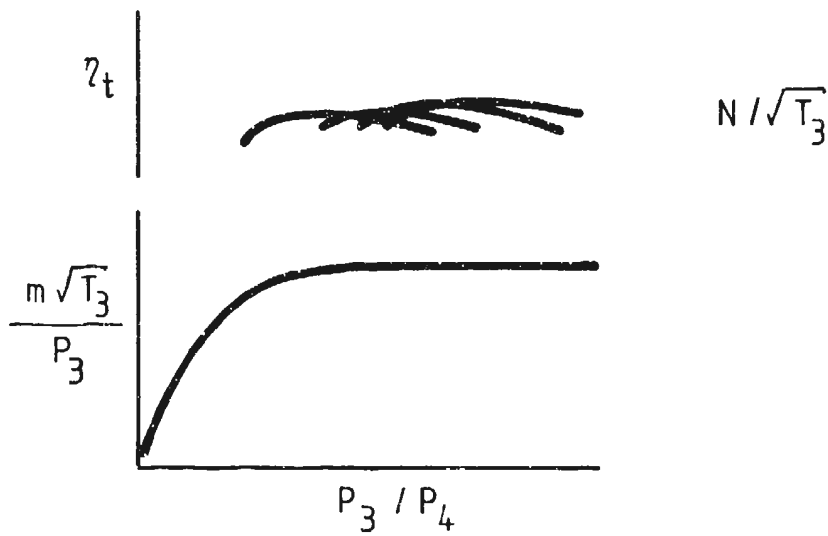**FIG. 5 CONFIGURATIONS FOR HIGH BY-PASS RATIO TURBOFANS**
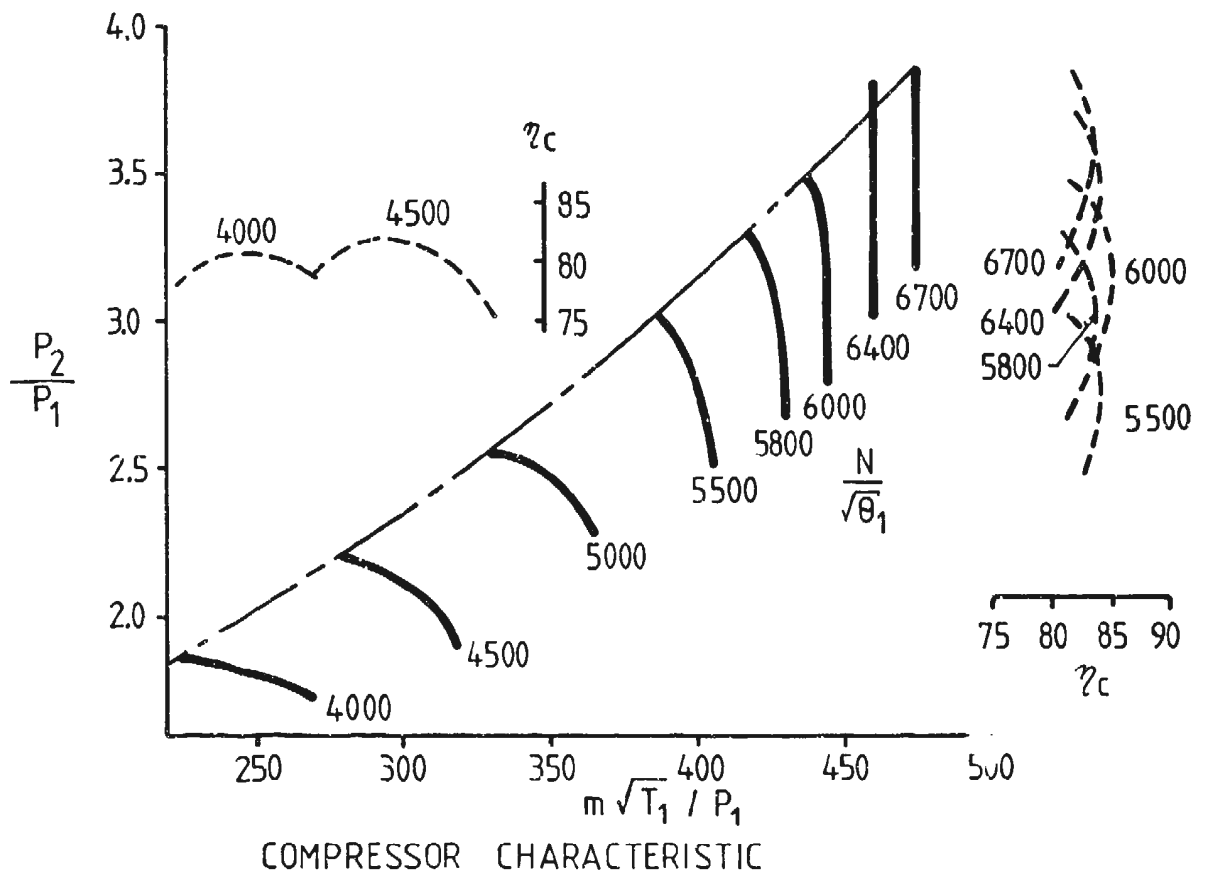
FIG. 6   TURBINE   CHARACTERISTIC

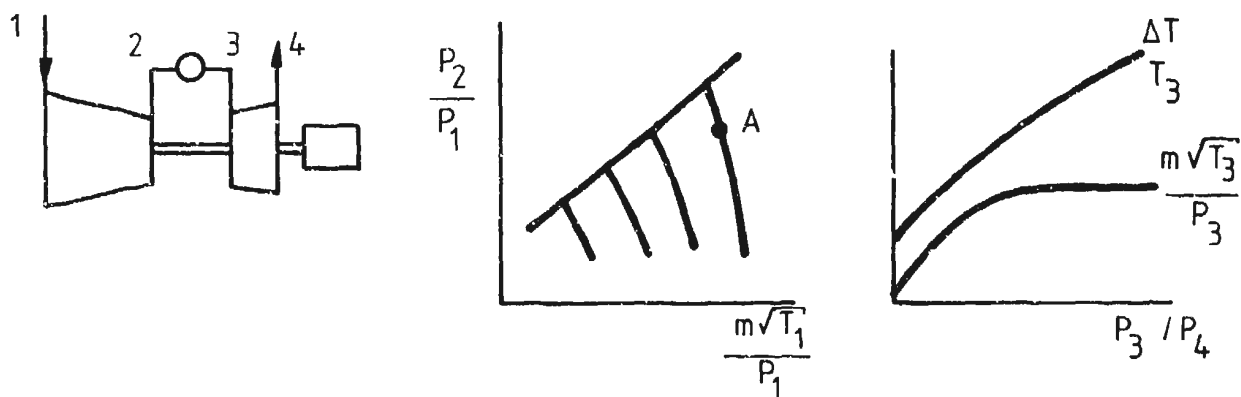FIG. 7   SINGLE   SHAFT
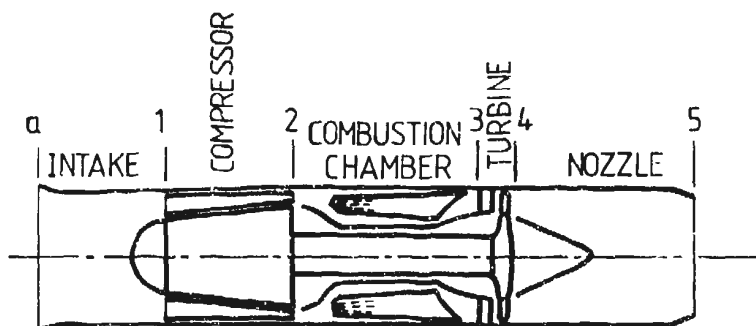

FIG. 8   SIMPLE   TURBOJET   ENGINE
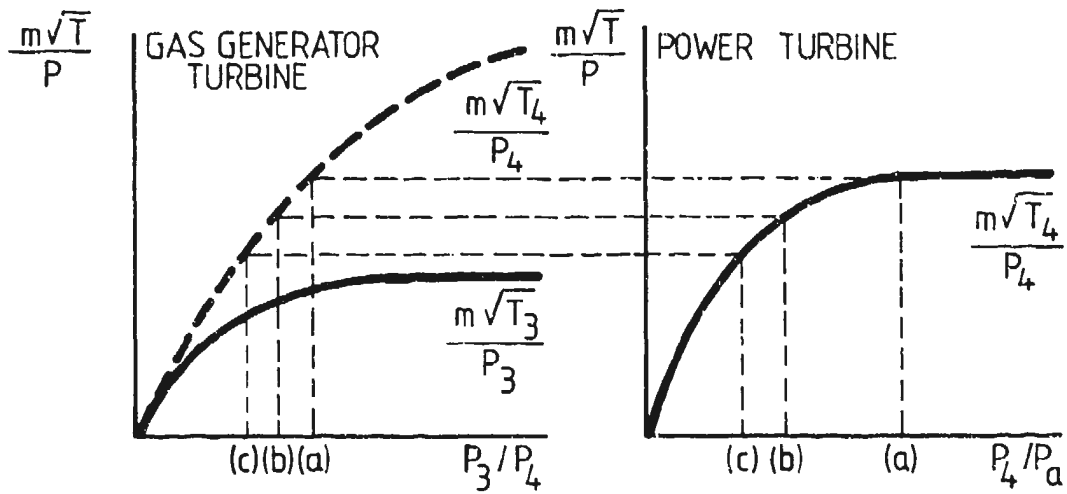
FIG. 9   OPERATION OF TURBINES IN SERIES
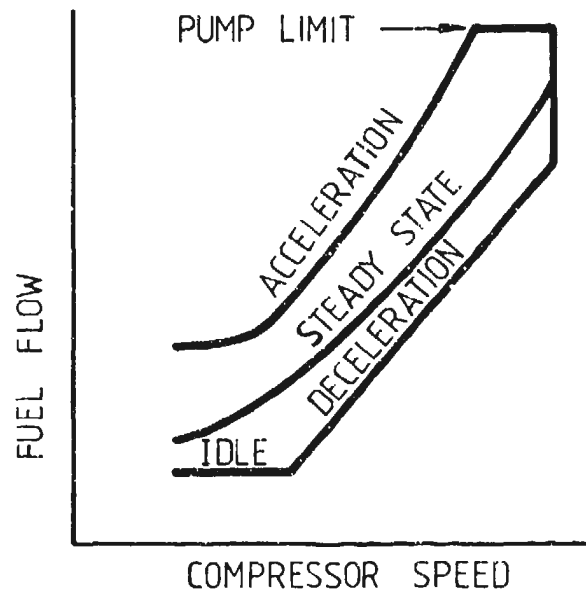

FIG. 10   TYPICAL FUEL SCHEDULE
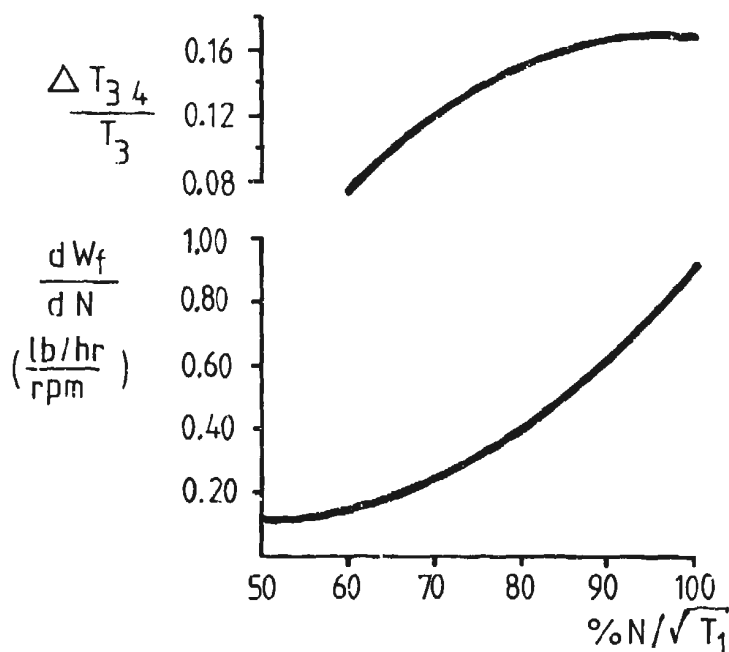
$$\frac{\triangle T_{3\,4}}{T_3}$$

$$\frac{dW_f}{dN}\left(\frac{lb/hr}{rpm}\right)$$

$$\%N/\sqrt{T_1}$$

FIG. 11 PARAMETERS DETERMINING TIME CONSTANT

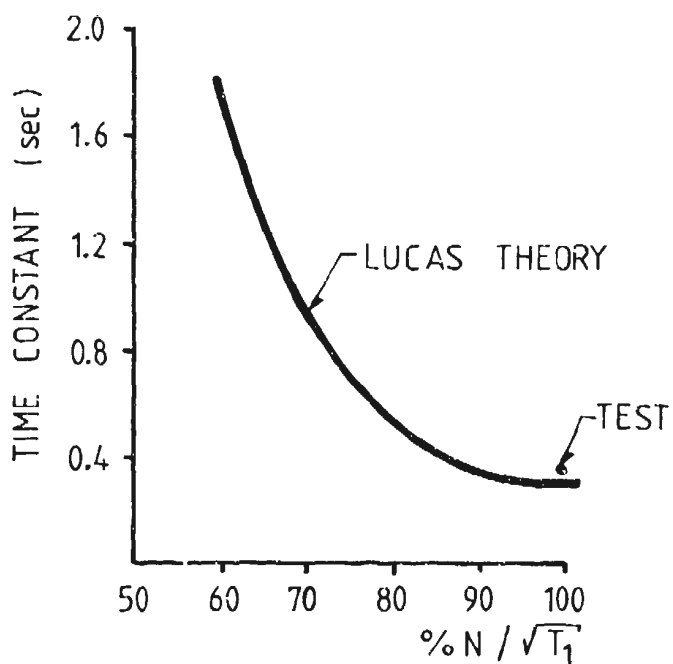TIME CONSTANT (sec)

LUCAS THEORY

TEST

$$\%N/\sqrt{T_1}$$

FIG. 12 VARIATION OF TIME CONSTANT WITH SPEED

PRACTICAL CONSIDERATIONS IN DESIGNING THE ENGINE CYCLE

M G Philpot

Air Vehicle Performance Department
Royal Aerospace Establishment
Defence Research Agency,
Pyestock, Farnborough, UK

SUMMARY

When it is required to define the cycle parameters and calculate the performance of a real engine, there are numerous practical constraints that need to be taken into account. These fall into two main categories: the limitations of available component technologies, and the operational considerations that are dependent on aircraft application. The lecture discusses the main technology limiters and indicates how they are incorporated into the cycle definition process. Operational factors include the extent of the intended flight envelope and range of critical flight conditions for which performance must be assured, and the balance to be struck between minimising fuel consumption, maximising installed power and constraining costs of ownership. Taking these technology and operational influences into account, the basic cycle characteristics and approach to cycle choice are examined for three main classes of aircraft: subsonic transports, military combat aircraft and helicopters.

LIST OF MAIN SYMBOLS

C_p = Specific heat
H = Enthalpy
h = Enthalpy/unit mass flow
LCV = Fuel lower calorific value
M_a = Aircraft flight Mach no
P_n = Total pressure at station n
Q_n = Air mass flow at station n
Q_f = Fuel mass flow
R = Compressor pressure ratio
R_{oa} = Overall (cycle) pressure ratio
T_n = Total temperature at station n
U = Blade tangential speed
V_a = Aircraft flight speed
V_j = Jet velocity relative to aircraft
X_G = Gross thrust
X_N = Net thrust
η_{isen} = Component isentropic efficiency
η_{oa} = Overall cycle efficiency
η_p = Propulsive efficiency
η_T = Transfer efficiency
η_θ = Thermal efficiency
ρ = Density
μ = Bypass ratio

1   INTRODUCTION

In the first lecture (Ref 1), Prof Saravanamuttoo has outlined the basic principles of aircraft gas turbine cycle analysis and performance. In applying these principles to specific cases, the gas turbine designer must take a multitude of practical factors into account in order to select the most appropriate cycle parameters.

Most obviously, the available component technologies impose aerodynamic, thermal and mechanical limits which set upper bounds on cycle pressure ratios and temperatures. Gas turbine R and D is being pursued vigorously in government laboratories, manufacturing companies, universities and other research institutes and these barriers are being progressively pushed back, with little sign that a plateau of technology is being reached. Nevertheless, while the acceptable limits may move with time, they remain firm ones which the designer must observe, his only freedom being the judgement of precisely where to set them for the envisaged application at the time of design freeze. The application itself is equally important. The type of aircraft - military combat, civil or military transport, helicopter, etc - and the planned service life and mission operating requirements, will all have major influence on the choice of cycle parameters.

In this lecture we will examine some of the key technology limiters, how they affect cycle choice and how they can be taken into account in cycle analysis. This will provide a basis on which to consider the cycle requirements and characteristics of the three main types of application mentioned above.

2   TECHNOLOGY CONSIDERATIONS

2.1   Compressor loadings and running lines

For any engine, choice of compressor design is one of the crucial issues facing the designer at the start of the engine definition process. It involves a complex compromise between efficiency targets, numbers of stages, surge margin requirements across the intended flight envelope and various mechanical considerations, such as stress limits, vibration, etc.

Fig 1 shows the typical trend in pressure ratio/stage for in-engine efficiencies at the engine aerodynamic design point. In general, increasing the work done per stage reduces compressor efficiencies, although thanks to the considerable improvements in the understanding of detailed compressor aerodynamics and in CFD design methods, this effect is less marked than it used to be. On the other hand, reducing the number of stages tends to bring advantages in reduced engine length, weight and cost.
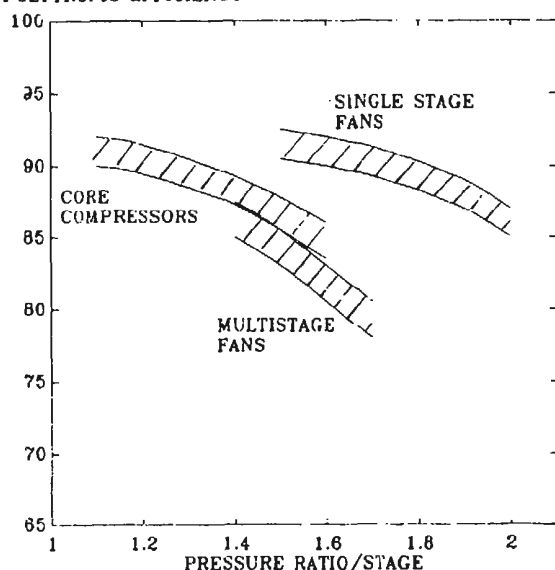
POLYTROPIC EFFICIENCY

FIG.1 COMPRESSOR EFFICIENCIES - EFFECTS OF LOADING

PRESSURE RATIO

FIG.2 TYPICAL MILITARY HP COMPRESSOR CHARACTERISTIC

For combat aircraft, the latter considerations generally dominate and high stage loading designs are almost always chosen, at least for the core. For civil applications, while cost and weight are still important, the need to minimise fuel burn places more stress on high component efficiencies and leads to more modest core compressor stage loadings.

The situation is reversed for the fan on the low pressure spool. Stage pressure ratios of up to 1.8 are commonplace in high bypass civil engines, but largely because of the problems of stage matching, the multistage fans needed for low bypass combat engines are struggling to reach such high levels at acceptable efficiency and stability. Even so, fan stage pressure ratios can be considerably higher than for core compressors. This is because high blade speed transonic designs are habitually used for fans, reducing the aerodynamic loading in terms of $\Delta h/U^2$. For HP compressors, the combination of rear stage stresses and temperatures and narrow flow annuli demand much lower blade speed designs and hence lower stage pressure rises.

From a practical point of view, it is essential that the fan and core compressor are each provided with sufficient working surge margin to ensure stable operation over the entire flight envelope and under all likely transient conditions. Achieving this at high stage loadings is always a challenge. Fig 2 shows an operating map for a military engine high pressure compressor, with a typical engine running line superimposed. This runs roughly parallel to the surge line, the difference between the two being the surge margin, which may be defined as:

$$\text{Surge Margin} = \frac{\text{Rsurge} - \text{Rop}}{\text{Rop}} \quad \text{at fixed } Q_2\sqrt{T_2}/P_2$$

$Q_2\sqrt{T_2}/P_2$ = compressor entry mass flow function

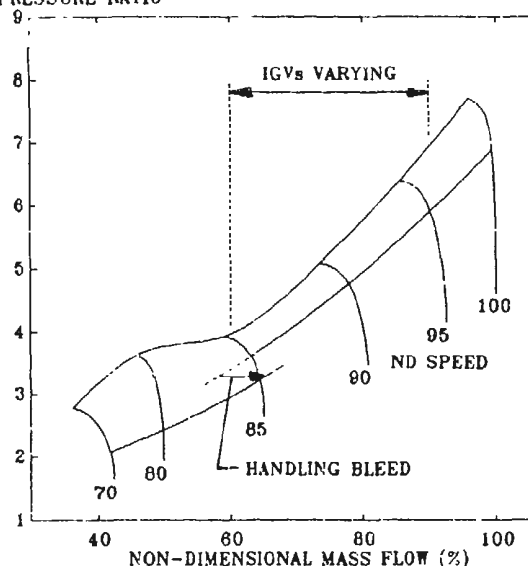(the station numbers follow the convention defined in Fig 5 of Ref 1)

The required surge margin is built up empirically from a consideration of the various sources of instability. The main factors, which contribute roughly equally are:

- Allowance for build tolerances, in-service deterioration etc.

- Allowance for intake flow distortions due to cross-wind and/or severe pitch/yaw aircraft manoeuvres.

- Allowance for running line shift during engine transients (eg slam accelerations).

Assessment of these effects for specific cases may yield surge margins as low as 15% or as high as 25% at the design point, but a figure of around 20% is fairly normal and this has been used in Fig 2. Unfortunately, modern high duty compressors, particularly LP system transonic designs, tend to achieve peak efficiency close to the surge line (perhaps at a surge margin of 10% or less). The shift to a realistic surge margin may cost 3% or more in compressor efficiency. The cycle designer must be aware of this in evaluating claimed compressor technology achievements.

Account must also be taken of Reynolds number (Re), which has a significant effect on compressor efficiencies. This operates in a complex way and generally has to be modelled empirically. Various experimentally-based relationships may be used, but typically:

$$(1 - \eta_{isen}) \quad \alpha \quad Re^{-0.1}$$

From sea level to altitude cruise, Re can change by a factor of around 2.5, giving a compressor efficiency loss of some 1½%. As

well as affecting engine fuel burn or thrust performance, this reduction causes the engine to rematch to a slightly higher compressor running line and must be included in the surge margin assessment.

2.2 Turbine aerodynamics

The turbines introduce few cycle modelling problems. For example, Reynolds number effects are small and can safely be ignored. The main concern is to achieve proper representation of the bleed flows in cooled turbines. In modern, high temperature engines the cooling bleeds are extracted from the compression system at two or more points and returned to the cycle at several points through the turbine system. Up to 25% of the core entry flow may be utilised in this way, see Fig 3. The flows provide cooling for two or more nozzle guide vane (NGV) rows, at least one and more probably two rows of rotor airfoils, and the front and back faces of the associated rotor discs.

In cycle analysis it is usually assumed that cooling bleed flows entering the mainstream before a given turbine rotor (ie the NGV and front disc face cooling) contribute to the work done in that turbine stage. The cooling flow for the rotor blades is deemed to re-enter the cycle downstream of the turbine and thus does no work in the stage. The effective mass flow through the turbine for work calculation purposes includes all the pre-rotor in-bleed, with a simple energy balance calculation assuming perfect mixing to determine the appropriate stream temperature. The coolant is assumed to have the total temperature of the compressor out-bleed point (a readily calculable quantity), so that all the heat transfer takes place at the in-bleed point. This is clearly an over-simplification, but the error involved is negligible. Taking the first NGV row in the HP turbine as an example, the cooling flow comes from HP compressor exit (station 3):

$$Q_{4.1}Cp_{4.1}T_{4.1} = Q_4 C_{p_4}T_4 + Q_{cool}Cp_3T_3$$

Station 4 is at entry to the NGV row (see Ref 1) and station 4.1 is at entry to the turbine rotor.

The bleed in-flows have complex effects on the turbine aerodynamics due to flow disturbance, boundary layer thickening, etc. These can be estimated by turbine specialists using a mix of CFD and empirical methods. Typically in-engine aerodynamic turbine efficiencies are some 2% lower than might be measured on a cold turbine rig, with no simulation of the cooling flows.

The temperature $T_{4.1}$ is of fundamental importance for cycle analysis because it represents the beginning of the work-producing expansion process. It is variously termed: Turbine Entry Temperature, Stator Outlet Temperature, or simply, Cycle Temperature (to avoid confusion T_4 is best termed Combustor Exit Temperature, CET).
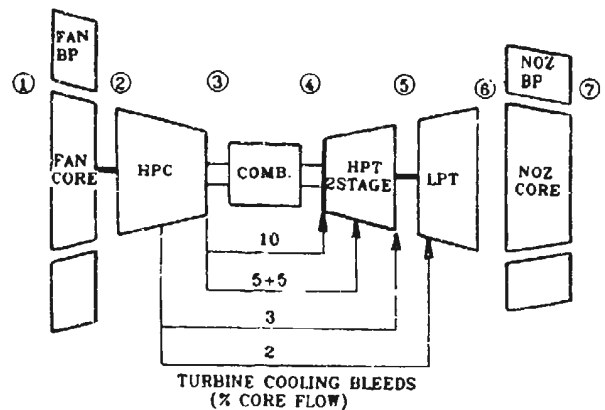

FIG.3 ENGINE CYCLE DIAGRAM (CIVIL TURBOFAN)

The extent and efficiency of the turbine blade cooling, together with the temperature capabilities and mechanical strengths of the blade and disc materials are equally important because they determine the upper limits on achievable cycle temperature. These crucial thermal aspects will be considered in Section 2.4.

2.3 Combustor considerations

Before that it is necessary to examine the influence of the combustion system. Fig 4 shows a typical modern combustor with the main airflow patterns. The air exits from the HP compressor through a dump diffuser and enters the burning zone via a complex arrangement of large and small holes, slots, etc. These are designed to promote the recirculation and turbulent mixing on which the whole burning process depends, while at the same time ensuring adequate cooling of the metal walls. With flame temperatures in the primary zone reaching 2300K or more, well above the melting point of any usable alloy, this is no mean feat. Nevertheless, it has so far been achieved with sufficient success for combustor wall temperatures not to out-pace the turbines as cycle temperature limiters.

The dump diffuser and wall resistance contribute to an aerodynamic pressure loss of typically 4% to 5% at design conditions. In cycle terms this appears as a parasitic loss, but it is nevertheless vital because it ensures sufficient pressure differential to drive the turbine cooling flows. Anything less than 4% would imperil the flow of the cooling air and risk turbine over-heating. At off-design conditions the loss must be recalculated, which can be done by dynamic similarity using:

$$\frac{\rho \Delta P}{Q^2} = \text{constant}$$

Despite the extreme conditions, combustion efficiency is almost always close to 100% (falling off significantly only at flight idle or below, and often not even then). Nevertheless the temperature profiles at the combustor exit plane are far from uniform. A circumferential traverse shows large peaks in line with the burners and considerable troughs mid-way between them.
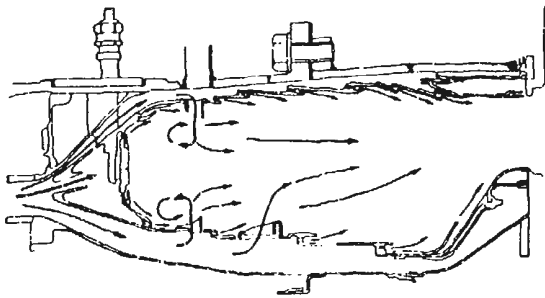
FIG.4 TYPICAL GAS TURBINE COMBUSTOR

FIG.5 GAS TURBINE MATERIALS (FROM REF 4)

A radial traverse at any circumferential point shows low temperatures close to the inner and outer walls, rising to a peak at around mid-annulus. These temperature distributions must be taken into account in determining the turbine metal temperatures. Their numerical description is a normal part of the definition of combustor characteristics. Two factors are used:

Circumferential Temperature Pattern Factor or Overall Temperature Distribution Factor:

$$OTDF = \frac{T_{max} - T_4}{\Delta T_{comb}}$$

Radial Temperature Profile or Radial Temperature Distribution Factor:

$$RTDF = \frac{\overline{T}_{max} - T_4}{\Delta T_{comb}}$$

T_{max} = maximum temperature anywhere in the combustor exit plane

$\overline{T}_{max}$ = radial peak temperature, circumferentially averaged

T_4 = mean temperature at combustor exit plane

The levels of these factors depend on the details of the combustor design, but typically:

OTDF = 20% to 35%
RTDF = 7% to 15%

With combustor mean temperature rises reaching 800K to 1000K, it is evident that the local gas temperatures impinging on the turbine airfoils can be very much greater than simple cycle analysis would indicate.

The value of OTDF is most relevant for the first row of NGVs, since it may be expected that at least some airfoils will experience the hottest streaks. RTDF is the relevant factor for the rotor blades, because the rotation creates automatic circumferential averaging. It is assumed that the radial profile passes through the NGV row without change. There is little detailed knowledge of what happens to the temperature profiles thereafter, but experimental evidence indicates that they can persist through several turbine stages, although becoming
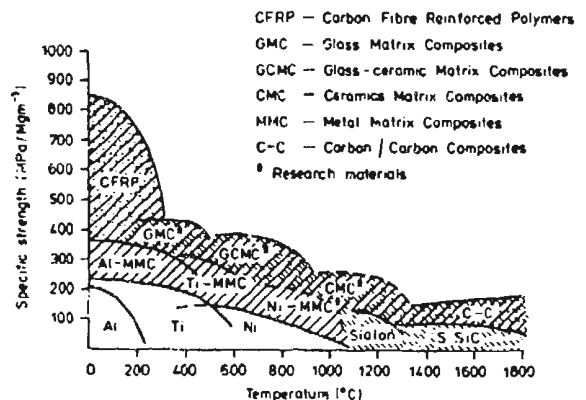
progressively attenuated. A reasonable working assumption is that the factors may be halved for each successive turbine stage.

2.4 **Materials and cooling**

The upper limits on the main core cycle parameters - overall pressure ratio Roa and Turbine Entry Temperature $T_{4.1}$ - depend most fundamentally on the materials and their associated engineering. Temperatures and stresses throughout the engine must be constrained to what the available materials can withstand at acceptable component lives. The lifing of high stress components like discs and rotor blades is a major topic in itself (see eg Refs 2,3). Suffice to say that "acceptable" life varies from component to component as well as depending on the application. The shortest lives are usually allowed for turbine blades, with 1000 to 2000 hours being typical for military engines and 10000 to 20000 hours being required for much higher utilisation civil engines.

Fig 5, taken from Ref 4 shows the range of current and future gas turbine materials in terms of specific strength (ie strength/density) versus temperature. Currently, the conventional metal alloys are used for virtually all structural components. The next steps are expected to feature increasing use of the "cold" carbon fibre reinforced polymers and the medium/high temperature metal matrix composites. It can be seen from Fig 5 that the latter materials may confer a small temperature gain, but the main advance will be in specific strength, which promises considerable reductions in engine weight. For a step-change in temperature capability it will be necessary to go to the ceramic matrix composites, such as silicon carbide-silicon carbide or carbon-carbon. But while these are beginning to be used for non-load-bearing applications like nozzle petals, they remain future long term hopes for major structural components rather than presently available technology. Here, we will confine ourselves to the conventional alloys.

Examining these in more detail, Fig 6 taken from Ref 2, shows how temperature capability has advanced over the years for
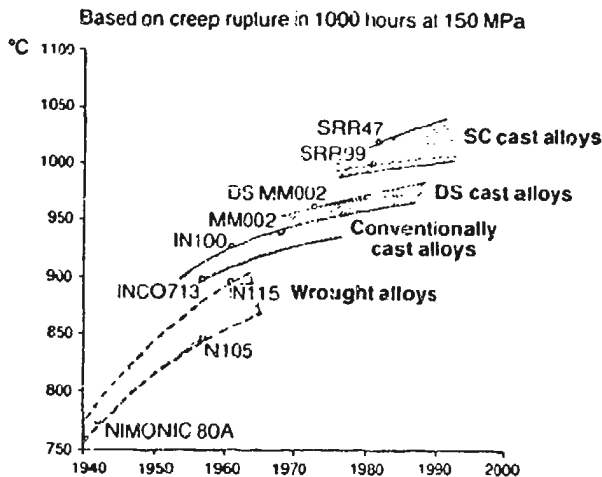
Based on creep rupture in 1000 hours at 150 MPa

FIG.6 TURBINE BLADE ALLOY CAPABILITIES (FROM REF 3)

FIG.7 RB211535E4 NOZZLE GUIDE VANE (FROM REF 6)

the main classes of turbine airfoil materials. Progress in both alloy chemistry and processing technology has gradually shifted the lines upward, for example through the move from poly-crystal, "conventional" castings for turbine blades to first and second generation single crystals. The highest temperature materials may however be considerably more costly, or have significantly higher density so that centrifugal stresses are higher. Use of these alloys therefore tends to be confined to applications where their temperature capability is essential. Specific material choice is always carefully optimised for the particular application.

For any given material, creep life is highly dependent on temperature, with every extra 15°C reducing life at a given stress by some 50%. This means that the relatively low stress NGVs can operate up to 100°C hotter than the rotor blades for the same material and life. This is helpful in view of the higher gas temperature peaks the NGVs must withstand. The typical rotor stress shown in Fig 6 is appropriate for the mid-span region. Because of centrifugal loading, the stress in the blade is high at the root and low at the tip (zero if the blades do not have tip shrouds). However, as discussed in the last section, the radial peak gas temperature occurs at around mid-span and because of the very steep exchange rate with temperature, it is usually best to assess the blade capability at the gas temperature peak.

For the current "best" materials, allowable rotor metal temperatures at mid-span will be around 1250K to 1300K (980°C to 1030°C) for a 1000 hour turbine. A 10000 hour turbine would need to operate 50°C to 70°C lower. In most cases when blade cooling aspects are taken into consideration (see next section), it turns out that rotor metal temperature has the controlling influence on attainable cycle temperature.

Turning to the discs, these operate at very much higher stresses and allowable temperatures in the high stress zones are
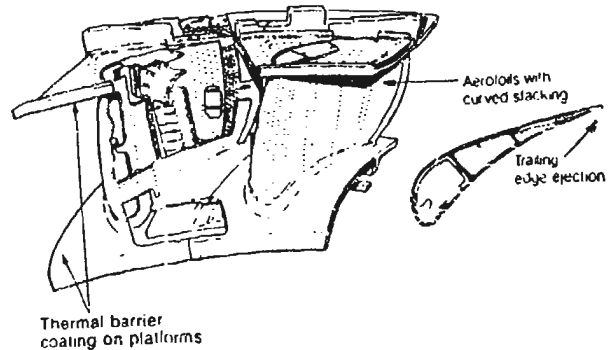
typically around 850K to 900K. The problem is to some extent eased by the fact that the high stresses occur near the bore of the disc, well away from the main gas path. Nevertheless the final HP compressor disc and the first turbine disc are bathed in air, effectively at compressor delivery temperature T_3 (in fact slightly above because of effects like windage heating). As with the airfoils, materials development is gradually increasing temperature capability, but disc temperature effectively sets an upper limit on allowable engine overall pressure ratio.

2.5 **Turbine blade cooling**

Modern turbine blades are extremely complex castings, as Fig 7 illustrates. Cooling technology is therefore another highly developed science, involving multiple internal air passages, an array of bleed holes to create external film cooling of the blade surfaces, and the careful prediction of internal and external heat transfer coefficients (see for example Refs 5, 6). The amount of cooling achieved is expressed in terms of cooling effectiveness ε:

$$\varepsilon = \frac{Tgas - Tmetal}{Tgas - Tcool}$$

Tmetal may be either the mean temperature across a given airfoil section, or the local temperature at a particular point, and the value of ε will vary accordingly. Local metal temperature can vary considerably across the section, with the leading and trailing edges, which are more difficult to cool, being hotter than the mid-chord region (see Fig 8). For present purposes it is convenient to use the mean value (εmean).

The value of εmean is dependent on the complexity of the cooling design and also on the cooling flow rate through the blade. Turbine cooling engineers use a cooling flow coefficient which incorporates a heat transfer term (Ref 5), but for cycle analysis purposes it is necessary to convert this to simple cooling mass flow. Fig 9 shows the variation of εmean with percentage cooling flow (Qcool/Qgas at the blade row concerned) for typical modern technology designs.

Being static, the NGVs can be provided with rather more complex internal cooling configurations, including the use of non-
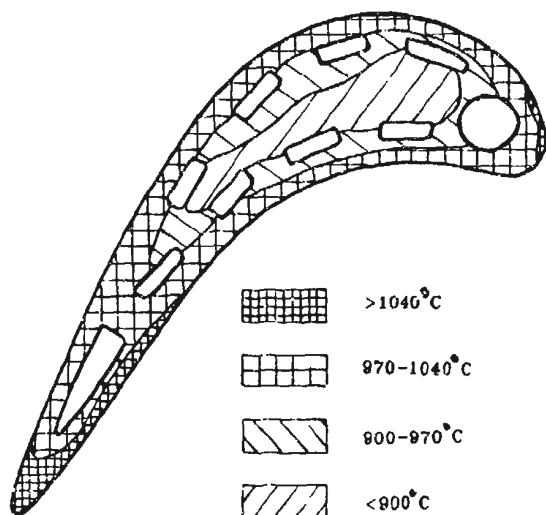
FIG.8 TEMPERATURE VARIATIONS IN TURBINE ROTOR AIRFOIL

FIG.9 TYPICAL BLADE COOLING EFFECTIVENESS TREND

cast inserts, and they usually have larger airfoil sections so that higher cooling flow rates can be accepted. Both effects contribute towards the higher cooling effectiveness values for the NGVs shown in Fig 9, with εmean as high as 0.75 to 0.80 being possible. For rotor blades, values of 0.55 to 0.60 are more typical, with cooling flow rates seldom exceeding 4.5% to 5.0%. Since the NGVs suffer the more severe temperature environment, the additional cooling capability is needed.

For the rotor blades, one other important and beneficial effect must be taken into account. Due to the rotation, the rotor effectively "runs away" from the NGV exit flow, thereby reducing the stagnation temperature relative to the blade. From a consideration of the velocity triangles it can be shown that:

$$T_R = T_T - \frac{U^2}{2C_P}\left[\frac{\Delta h}{U^2} + 1 - 2Rn\right]$$

where T_R = Gas stagnation temperature relative to rotor

T_T = stagnation temperature in stationary coordinates ($T_{4.1}$ for the HP turbine)

U = tangential blade speed

Δh = turbine work

Rn = Reaction

Most turbines for jet engine applications are designed close to 50% Reaction (ie $Rn \sim 0.5$), so the calculation is easily done. Moreover, if we take RTDF to be about 0.1 (see Section 2.3), and assume a typical moderate to high turbine stage loading, the following is a reasonable empirical

approximation for the first stage rotor temperature:

$$T_{Rmax} \sim 0.93 T_{4.1}$$

In combination with the cooling effectiveness, the above procedure enables TET to be related to rotor metal temperature. Despite the advantage of rotation, it is most often the first stage rotor temperature that sets the upper limit on TET in any given case.

2.6 Afterburners

Afterburners are used in the majority of high performance combat aircraft as a means of greatly increasing thrust for short periods of time, albeit at the cost of a huge increase in fuel consumption. Fig 10 shows a typical modern afterburner. Outwardly simple, it is in practice a sophisticated piece of engineering design with a long and careful development pedigree. The burner is placed close to the bypass/core stream mixer plane, so that the outer radii are working with un-vitiated bypass air, while the centre section is using the core exit gas, in which the fuel/air ratio may already be around 0.025.

In principle, fuel/air ratio can be increased until both streams are close to the stoichiometric limit of 0.0687. In

FIG.10 AFTERBURNER AND VARIABLE NOZZLE

practice, it becomes increasingly difficult for the fuel droplets in the core stream to find oxygen molecules to react with and combustion efficiency begins to fall. Also, rising afterburner temperature requires more bypass air to pass round the burning zone in order to cool the jet pipe line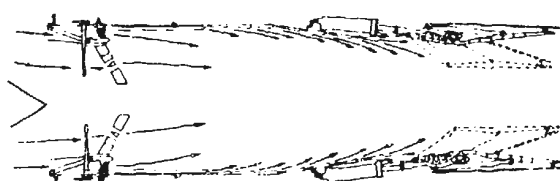r and nozzle, thus reducing the quantity available for combustion. Thirdly, high heat release in the afterburner leads to the burning stability problems known as "buzz" and "screech", when severe pressure oscillations in the jet pipe can cause rapid structural failure.

The precise limits on afterburner fuelling due to the above considerations are very dependent on the precise geometry and aerothermodynamic parameters. It must suffice to note that for the range of bypass ratios and core cycles most commonly used in combat engines, maximum overall fuel/air ratio is likely to be around 0.06 (85% to 90% stoichiometric). There is also a minimum fuelling limit, determined by burner blow-off characteristics. This is again highly dependent on the design parameters, but generally it means that moving from maximum "dry" (ie non-afterburning) throttle setting to minimum afterburner causes a distinct step change in thrust. Although combustion efficiency falls off towards this minimum, over most of the range a good afterburner design will give close to 100% efficiency.

2.7 The final nozzle

The simplest form of final nozzle is the fixed area convergent nozzle, typically used for subsonic transport engines. Here, nozzle pressure ratios vary from around 2.0 at take-off to 4.0 at cruise altitude maximum thrust. Although the exhaust flow is under-expanded at the latter condition, so that excess total pressure exists in the jet downstream of the nozzle lip, the losses involved are small and thrust coefficient C_x is very close to 1.0. For a high specific thrust engine at supersonic flight conditions, this would no longer be the case and a convergent-divergent nozzle is required. The difference in thrust coefficient is indicated in Fig 11. Strictly, the divergent part of the nozzle can only be designed for one flight condition, but in practice a high value of C_x can be maintained over a fairly wide range.

Afterburning engines demand variable area nozzles in order to match the exhaust mass flow function $Q\sqrt{T}/P$ over a wide range of nozzle temperatures. Modern, variable condi nozzles are complex but usually allow the divergence angle to be varied to some extent independently of throat area. This greatly increases the range over which the nozzle is well-matched. The variability may also be needed for good engine matching at throttled-back conditions in dry engine mode.

Like the jet pipe, the nozzle in an afterburning engine requires cooling, although this can now be reduced by using materials like carbon-carbon for the nozzle petals. Nevertheless, the cooling needs of
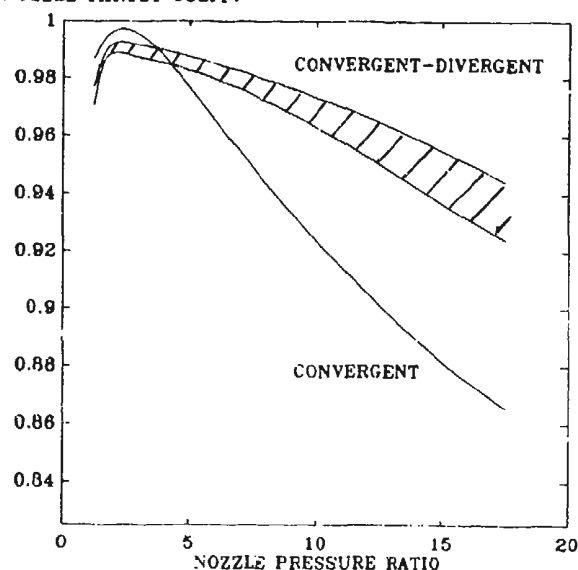
NOZZLE THRUST COEFF.

FIG.11 CONVERGENT AND CONVERGENT-DIVERGENT NOZZLES

jet pipe and nozzle mean that bypass ratio cannot generally be reduced below 0.1 to 0.15. Such engines are often described as "leaky turbojets".

3 TRANSPORT ENGINE CYCLES

In this next part of the lecture, the characteristics of practical engine cycles will be examined, taking into account the technology issues outlined in Part 2. The high bypass engines used for subsonic airliners and military transports will be considered first, because these powerplants are relatively simple and enable the basic trends to be readily highlighted. For additional simplicity, attention will be confined to un-mixed cycles, where the bypass and core streams discharge through separate nozzles. This allows fan pressure ratio R_{fan} to be a separate variable, not directly dependent on the core cycle (provided the latter provides enough power to drive the fan). In fact, a number of current engines have mixed cycles, with full length cowls, common nozzles and at least partial flow mixing in the jet pipe. Internal mixing offers a small improvement in fuel consumption, although nacelle weight tends to be slightly greater. The physical requirement for equal static pressures in both streams at the mixer plane links the fan to the core cycle, so that R_{fan} is no longer an independent variable. This is an important constraint at low bypass ratio, but for the bypass ratios typical of civil engines, it has only minor influence on cycle optimisation and can conveniently be ignored here.

3.1 Selection of the core cycle

Most current civil engines have bypass ratios of around 5 and we will start with this case. For virtually all transport engines, there are two pre-eminent requirements - minimum fuel consumption, and long overhaul life. Engines are designed for a careful balance between these two properties and as a result the
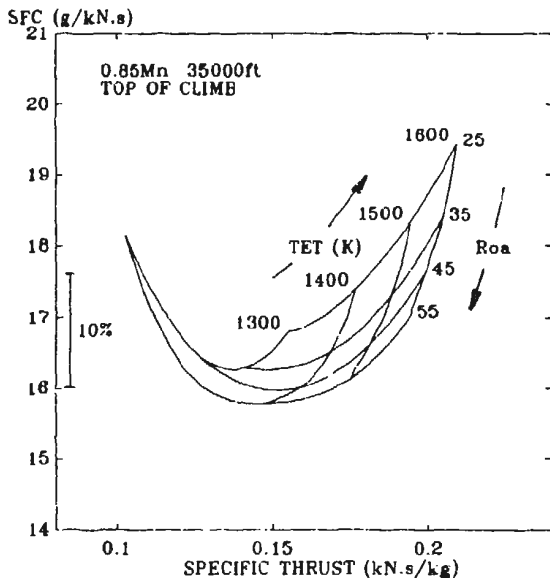
SFC (g/kN.s)

0.85Mn 35000ft
TOP OF CLIMB

TET (K)   Roa

1600 25
1500   35
1400   45
1300   55

10%

SPECIFIC THRUST (kN.s/kg)

FIG.12 AERODYNAMIC DESIGN POINTS – CIVIL ENGINES

SFC (g/kN.s)

SEA LEVEL STATIC
ISA+15deg.C

DESIGN TET   DESIGN Roa

1600 25
1500   35
1400   45
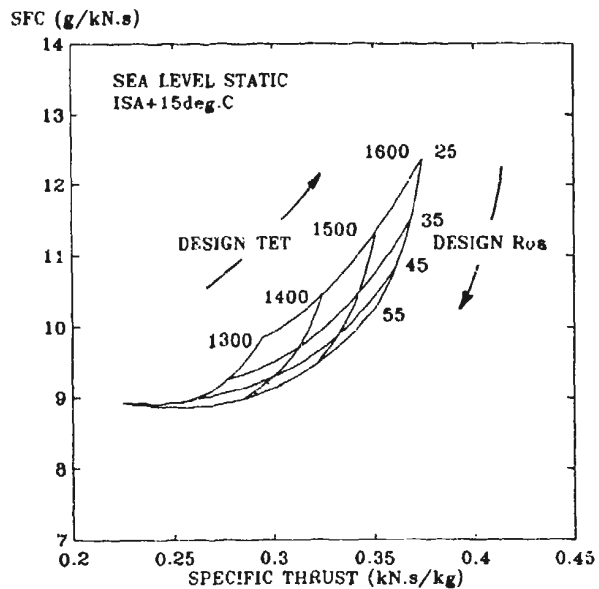1300   55

SPECIFIC THRUST (kN.s/kg)

FIG.13 HDTO OFF-DESIGN POINTS – CIVIL ENGINES

core cycle parameters are largely optimised round three operating conditions:

a.   The maximum thrust condition at nominal cruise flight speed and altitude. This point, often termed "Top of Climb", determines the maximum overall pressure ratio (Roa), dimensionless spool speeds ($N/\sqrt{T_1}$) and engine inlet mass flow function ($Q\sqrt{T_1}/P_1$), required by the engine anywhere in the flight envelope. For this reason it is usually used to define the engine Aerodynamic Design Point (ADP).

b.   The average thrust rating for normal cruise at steady speed and altitude, obtained by throttling back from the ADP to say 70% thrust. This is where the engine will operate most of the time and where the specific fuel consumption (sfc) requirement will normally be defined.

c.   The maximum thrust at sea level static conditions for take-off on a hot day (typically ISA + 15°C). This point (HDTO) defines the maximum cycle temperature and metal temperatures required; it therefore relates strongly to component life.

Figs 12 and 13 show how the engine performance and core cycle parameters vary at the ADP and at HDTO respectively, for a range of design point cycles. Specific fuel consumption (fuel flow/unit net thrust, Qf/Xn) is plotted against specific thrust (thrust/unit airflow, Xn/Q_1). The engines are "uninstalled", so that no allowance is made for nacelle drag, customer air bleed and power off-take, etc. Component efficiencies typical of current achievement have been assumed. All the engines have an ADP fan pressure ratio of 1.8. Strictly, as will be seen later, FPR should be re-optimised for each cycle, but at 5 bypass ratio, the effect is small. More importantly the nominal optimum tends to be at a higher FPR and higher tip speed than would normally be acceptable on mechanical, noise or fan efficiency grounds; the above figure has been selected

in the light of these constraints.

The HDTO points have been obtained by off-design calculations, using the following relationship:

$$\frac{X_g(SLS)}{X_N(TOC)} = 4.0 \,(for\ 0.85M_d/35Kft,\ 10.67KN)$$

The precise thrusts required at the two points depend on the aircraft lift/drag characteristics and the thrust-rating rules used for take-off and climb, but the above figure is broadly typical of current practice. It should be noted that the ratio would be different for a different flight speed or altitude.

The two plots show broadly similar trends, although the sfc levels are much higher and the specific thrusts much lower for the flight condition in Fig 12. This apparently worse performance is caused by the forward speed effect, which creates the ram effect known as inlet momentum drag. This must be subtracted from X_G to give X_N.

$$X_N = X_G - \frac{Q_1\ Va}{g} \quad (Va = flight\ speed)$$

Other than this it is seen that increasing Roa always improves sfc and reduces specific thrust (so that engine diameter increases for a given thrust). Increasing cycle temperature for the most part has the opposite effect. It can be shown that these two trends occur over a wide range of cycles and many different bypass ratios and represent basic properties of the jet engine cycle.

Specific fuel consumption is effectively

the reciprocal of overall engine efficiency η_{oa}:

$$\eta_{oa} = \frac{X_N Va}{Qf.LCV} = \frac{1}{sfc} \times \frac{Va}{LCV}$$

The overall efficiency comprises three main elements:

$$\eta_{oa} = \eta_p \, \eta_\theta \, \eta_T$$

where η_p = Propulsion efficiency
η_θ = Gas generator thermal efficiency
η_T = Transfer efficiency

The first two of these are generally explained in text books on the jet engine (see, eg Refs 7, 8, 9). The Transfer Efficiency is an additional term to account for the losses in transferring energy via the LP spool and fan outer section to the bypass stream (in a turbojet, η_T = 1). It becomes more significant as bypass ratio increases and is typically 85% to 90% for bypass ratio 5.

η_p = $\dfrac{\text{Energy used in driving a/c forward}}{\text{Energy available in engine jets}}$

$$\bar{\eta}_p = \frac{X_N V_a}{X_N Va + \sum KE}$$

$$\sum KE = \sum \frac{Qj}{2g} \, (Vj - Va)^2$$

Whe $\sum KE$ is the residual jet energy "lost" behind the aircraft (summed for the core and bypass streams).

With b ass ratio fixed, any increase in TET will feed through the turbine system and result in higher core jet pipe temp ure and Vj. Or, the fan must be redesigned to a higher pressure ratio to absorb the additional energy and bypass Vj will go up. In either case propulsion efficiency will drop. It is always the case that maximising propulsive efficiency requires cycle temperature to be reduced as much as possible.

The pressure ratio effect in Figs 12 and 13 is governed by the thermal efficiency, which can be defined as:

η_θ = $\dfrac{\text{Energy delivered by core}}{\text{Energy supplied by fuel}}$

$$\approx \frac{Q_{core}(C_{p5}T_5 - C_{p0}T_0)}{Qf.LCV}$$

where Station 5 = LP turbine entry
Station 0 = Ambient air static conditions

The gas generator can be regarded as that part of the engine that provides the energy
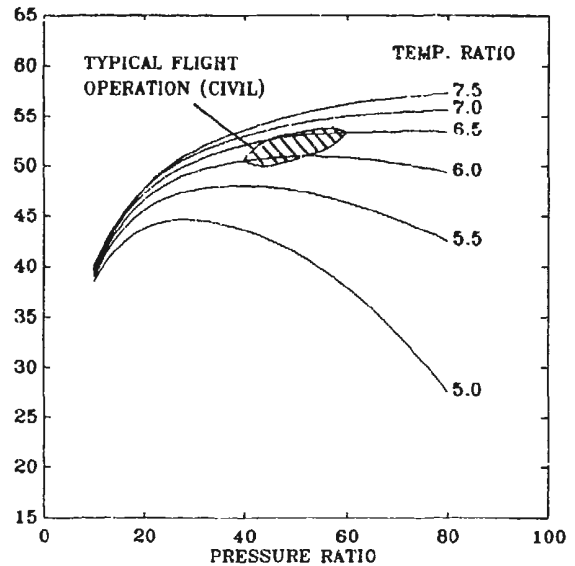
THERMAL EFF.

FIG.14 ENGINE THERMAL EFFICIENCY VARIATIONS

to drive the fan outer (bypass) section as well as the energy for the core jet. Strictly it should include the small proportion of the LP turbine required to drive the fan inner section, but this is neglected in the above approximation.

The thermal efficiency is analogous to the ideal Brayton air cycle efficiency, but takes into account the irreversible losses in the system. Unlike the ideal efficiency it turns out to be a function of total pressure ratio P_3/P_0 (ie including the ram effect) and total temperature ratio $T_{4.1}/T_0$. Fig 14 shows the behaviour of η_θ, assuming typical component efficiencies and cooling bleeds.

At the cycle conditions appropriate to a modern high bypass engine at altitude, thermal efficiency is seen to increase with both cycle pressure ratio and temperature, although a law of diminishing returns operates for both parameters. The beneficial effect of cycle temperature here is in contrast to its adverse effect on propulsive efficiency. For most of the cases shown in Fig 12 the propulsive effect is the stronger so that the net effect on fuel consumption of reducing cycle temperature is advantageous. However, beyond a certain point, the gain in η_p is outweighed by the increasingly deleterious effect on η_θ. The two trends are balanced at the bottoms of the curves in Fig 12.

It should be noted that at sea level static conditions, Fig 13, propulsive efficiency has no meaning (in effect it becomes equal to unity, so that $\eta_{oa} = \eta_\theta.\eta_T$. It should also be noted that η_θ and η_T can always be increased by increasing component efficiencies and reducing cooling bleeds and other parasitic losses. At a typical cruise condition, example trade-offs are:

Increase all turbomachinery Δsfc = -2.8%
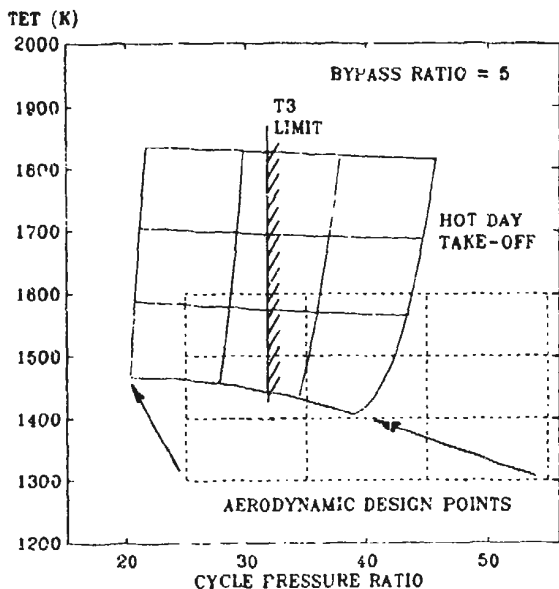component efficiencies
by 1 percentage point

TET (K)

FIG.15 CORE CYCLE PARAMETERS AT AERO DESIGN POINT
AND OFF-DESIGNED TO HOT DAY TAKE-OFF

MEAN ROTOR Tm (K)

FIG.16 HP TURBINE ROTOR METAL TEMPERATURES AT HDTO

Reduce HP turbine stage 1 $\Delta sfc = -0.4\%$
cooling bleed by
1 percentage point

Reduce HP turbine stage 2 $\Delta sfc = -0.6\%$
cooling bleed by 1
1 percentage point

Reduce bypass duct pressure $\Delta sfc = -1.2\%$
loss by 1 percentage point

These trade-offs are quite strong and there is therefore considerable incentive to improve internal performance by these means.

3.2 Materials temperature limits

Fig 15 shows what happens to the matrix of design point Roa and TET values, when the engines are off-designed to the HDTO sea level static point. Roa is always significantly reduced, while TET becomes considerably higher, as would be expected given the much greater inlet air temperature on the ground. The engine is throttled back relative to the ADP, essentially because there is no inlet momentum drag to overcome at SLS conditions. As the aircraft climbs and flight speed increases, the inlet drag steadily increases while inlet temperature drops. Top of Climb thus normally gives the engine aerodynamic maximum.

As discussed in Section 2.4, one of the major materials limiters is the temperature of the final compressor stage disc. This runs at close to compressor delivery temperature T_3 and thus is dependent mainly on Roa, although the efficiency of the compression system is also a factor. A typical T_3 limit is shown on Fig 15, although the precise position in any given case will be dependent on the particular material, stress and life selected for the disc design. Any cycles to the right of the limit line are disqualified because T_3 is too high. As the diagram suggests,
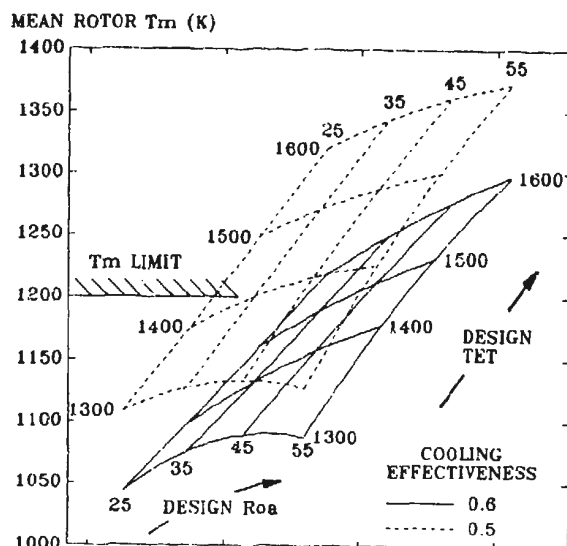
design point Roa in practical engines of bypass ratio 5 is at present generally less than 40.

Fig 16 shows the calculated turbine rotor metal temperatures at the HDTO point for two different levels of cooling technology, $\varepsilon_{mean} = 0.5$ and 0.6 respectively. The difference between the two is worth around 50°C of metal temperature. The diagram is in the form of a carpet plot for added clarity. Again a hatched zone is shown to indicate working limits for typical blade materials. Cycles above the limit line are disqualified.

We thus find that practical solutions are "boxed into" quite a small area of the original design point matrix in Fig 12, with Roa less than about 40 and TET less than about 1500K (1700K at HDTO). In fact this temperature exceeds that required for minimum sfc. Fig 12 suggests that a 1400K cycle (1600K at HDTO) or less would normally be preferred. The margin will allow a less costly and lighter blade alloy to be used and/or a smaller cooling bleed, which will be advantageous for sfc, as already noted. Often, an engine will enter service at a lower TET still, thereby allowing room for thrust growth by "throttle push", as demand for higher thrust versions develops.

3.3 The sfc loop

Fig 17 shows sfc plotted against percentage thrust at cruise speed and altitude, for one particular engine in the matrix of Fig 12 (Roa = 35; TET = 1400K). Two curves are shown, one assuming constant component efficiencies, the other assuming typical variations in fan and core compressor efficiencies along the engine running line. Both show a characteristic "catenary" shape, with minimum sfc occurring at around 70% thrust. This is convenient because the engine will normally be throttled back at least to around 80% thrust at the start of
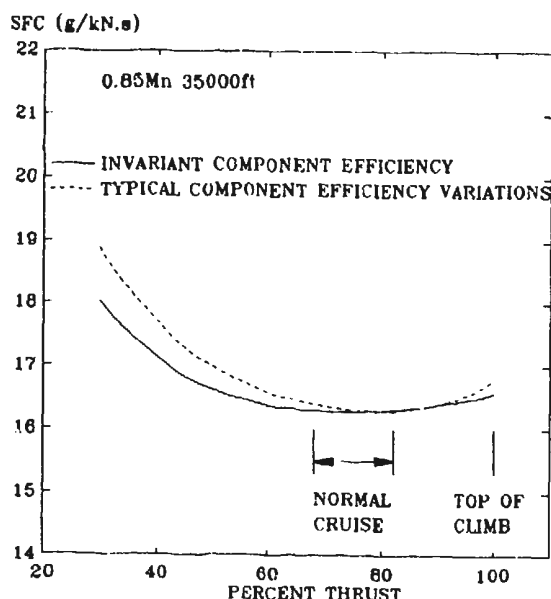
FIG.17 THRUST/SFC LOOPS FOR BPR=5 ENGINE

FIG.18 AERO DESIGN POINTS - EFFECT OF BYPASS RATIO

steady, level cruise and will be gradually throttled further back as fuel is burned off and the aircraft becomes lighter. The shape of the curve stems from the opposing behaviour of propulsive efficiency and thermal efficiency as described in Section 3.1. As the engine is throttled back and TET drops, propulsive efficiency increases, while thermal efficiency falls. Initially the former wins, but below about 70% thrust, the thermal efficiency effect becomes increasingly dominant.

When the compressor efficiency variations are taken into account, the shape of the loop is accentuated. It is usually the case for both fan and core compressors that maximum component efficiency occurs over a fairly wide range, but somewhat below the maximum thrust point - say in the 60% to 90% thrust band. Above and below this zone, the compressor efficiencies fall off and may indeed do so quite sharply at the top end. This can be acceptable because maximum thrust is only required for a small proportion of each flight. In fact the compressor designer may deliberately incorporate such a characteristic in order to "buy" more efficiency in the key cruise thrust band.

3.4 The effect of bypass ratio - ultra high bypass engines

Bypass ratios of conventional civil turbofans have stayed at around 5 for the last twenty years. During that time there has been a continuous improvement in sfc, to the extent that 1990s generation engines are around 15% more fuel efficient than their 1970s predecessors. This improvement has been achieved largely through increases in Roa and the internal component efficiencies. In other words, the gains have been mainly in thermal efficiency (and to some extent in transfer efficiency). As has been shown, current materials put a top limit on Roa, while component efficiencies are reaching such high levels that further
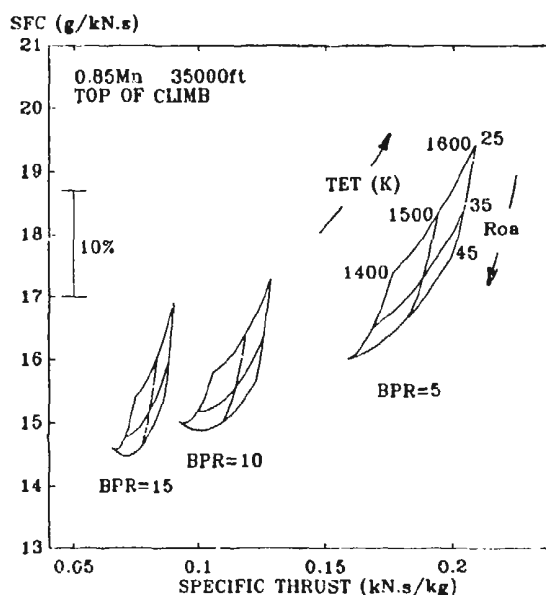
improvements are becoming more difficult to achieve. The ultra high bypass (UHB) engine and the advanced open rotor (which is a logical extension of the UHB) provide an alternative strategy, approaching the problem from the propulsive efficiency end.

Fig 18 shows the effects of increasing bypass ratio from 5 to 10 and then to 15 for the 'best' group of core cycles emerging from the previous discussion. The plot assumes constant polytropic efficiencies for the components and is for uninstalled performance, so that the effects of nacelle drag, etc, are not yet taken into account. However the fan pressure ratios are re-optimised for the higher bypass ratios, as shown in Fig 19. At $\mu = 5$, performance is not very sensitive to R_{fan} as noted earlier. But as μ is
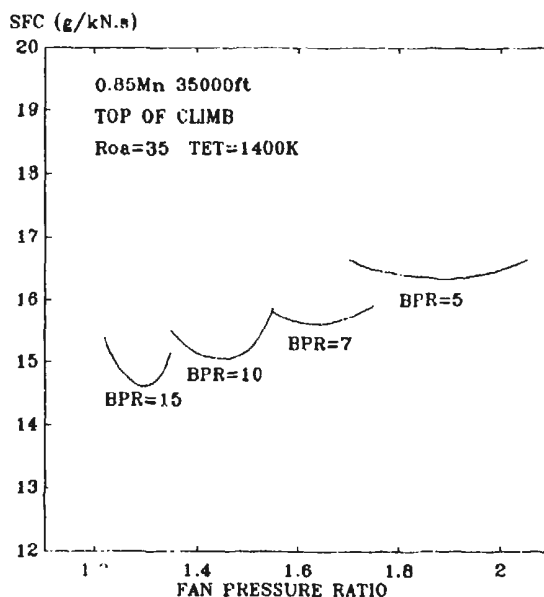
FIG.19 AERO DESIGN POINTS - FPR OPTIMISATION
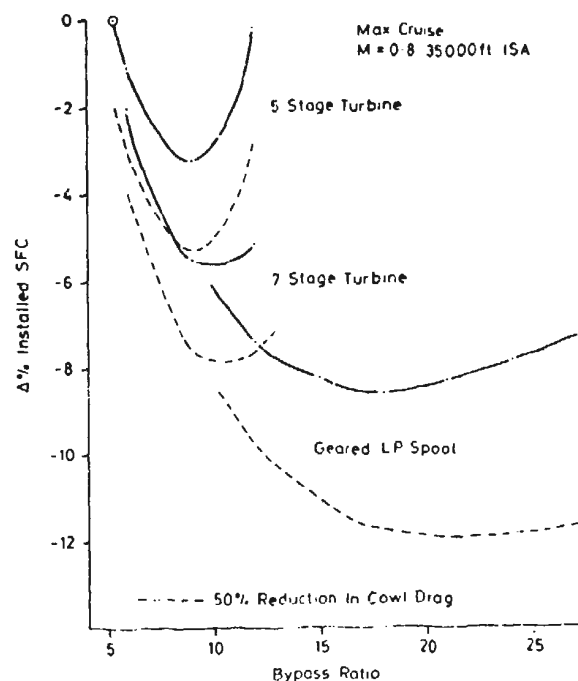
FIG.20 EFFECT OF BYPASS RATIO ON INSTALLED SFC
(FROM REF 10)

increased, the sensitivity becomes increasingly marked, while the optimum value itself is greatly reduced. It is clearly essential to get R_{fan} right.

Fig 18 indicates the considerable potential for improvement in fuel consumption offered by the increased bypass ratio route, with some 12% gain in uninstalled performance in going from $\mu = 5$ to $\mu = 15$, for the same core cycle. This is achieved because of the reduction in specific thrust and the resultant reduction in lost kinetic energy in the jets. In essence the required thrust is achieved by transferring more energy into a high mass flow, low jet velocity bypass stream, thereby improving propulsive efficiency, albeit at a small cost in transfer efficiency.

In practice there are a number of considerations that lead to qualification of these trends (Ref 10). Firstly, installation factors become increasingly important. The reduced specific thrust means that engine diameter is increased by nearly 50% at $\mu = 15$. All things being equal, nacelle drag will be increased by perhaps 60% at a cost in installed sfc of around 3%. The increased diameter also adds to the difficulty of aircraft installation and, to achieve sufficient ground clearance, the nacelle must be closely-coupled to the wing and be as "slim-line" as possible. The former may cause adverse nacelle/wing interference, although careful design and integration can minimise this problem. The latter requires a sharp lip to the intake, which will make the engine more sensitive to cross-winds at low aircraft speeds (eg during ground handling). The weight of the powerplant will also be significantly greater.

The increased fan diameter has other major implications. Mechanical considerations generally limit fan tip speeds to around 460 m/s. Thus as diameter goes up, LP spool speed must be reduced, with a growing mismatch between the operating requirements of the fan and the LP turbine. The latter requires spool speed to be kept high in order to retain acceptable stage loadings ($\Delta h/u^2$). Initially this problem can be met by increasing turbine stage numbers in order to reduce Δh in line with u^2. However there are practical limits to this process and 6 or 7 stages are about the most that might be accepted (current $\mu = 5$ engines have 3 or 4 LP turbine stages). One way to side-step this is to use the contra-rotating turbine principle, which was successfully demonstrated by General Electric in their UDF open rotor engine. This effectively doubles the blade tangential speed for a given shaft rotational speed. A similar turbine concept, matched to a novel contra-rotating fan, was proposed by Rolls-Royce for their RB529 UHB cowled engine design. The alternative is to couple the fan to the turbine via a step-up gearbox. It is difficult to be precise about where either this or the contra-rotation alternative needs to be introduced, but it would appear to be somewhere around $\mu = 9$ or 10.

The net effect on engine performance is shown in Fig 20, which is taken from Ref 10. This shows that when the effects of installation and turbine loading are taken into account, the 12% gain in sfc becomes reduced to around 8% (even with a gearbox), with the best result occurring between $\mu = 15$ and $\mu = 20$. A 50% reduction in cowl drag would be needed to approach the gain indicated by the uninstalled data.

There are two other effects which should be mentioned. Low specific thrust and high mass flow mean that inlet momentum drag in flight is very much higher at $\mu = 15$ than at $\mu = 5$. As a result the engine is considerably over-powered at SLS conditions and must be throttled back further to meet the take-off requirement. The effect on Roa and TET is shown in Fig 21. In performance terms this is an advantage. It means that design point Roa can be set at a considerably higher level (say 45 to 50) without infringing the compressor disc materials limit. Thus the gain in propulsive efficiency can be augmented by a small increase in thermal efficiency. The TET levels at take-off are also much reduced compared to a $\mu = 5$ engine and are now scarcely greater than those at top of climb. This should benefit turbine life and may also allow some reduction in the turbine cooling bleed flows.

The second effect concerns the operating characteristics of the fan. At high bypass ratio, there is a greater shift in fan working line from the altitude/cruise speed condition to SLS conditions. This is illustrated in Fig 22 for $\mu = 5$ and $\mu = 10$. At the higher bypass ratio the SLS working line is much closer to the surge line. It is likely that at bypass ratios above 10, some additional variability will be required to ensure stable operation (Ref 10). This is most likely to take the form
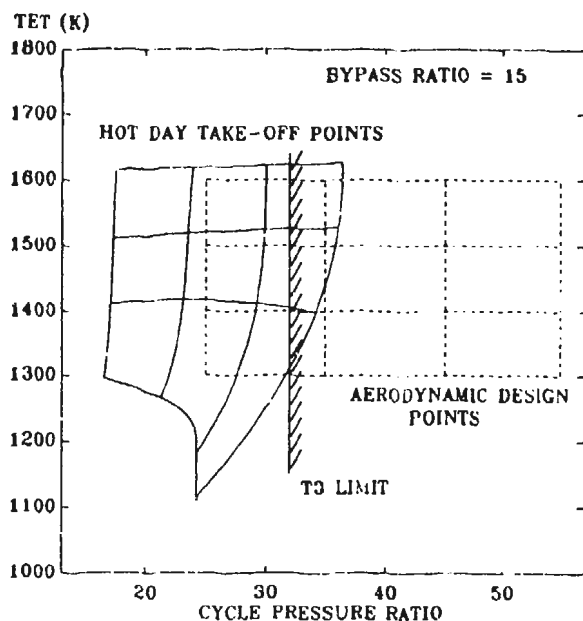
TET (K)

FIG.21 CORE CYCLE PARAMETERS AT AERO DESIGN POINT
AND OFF-DESIGNED TO HOT DAY TAKE-OFF
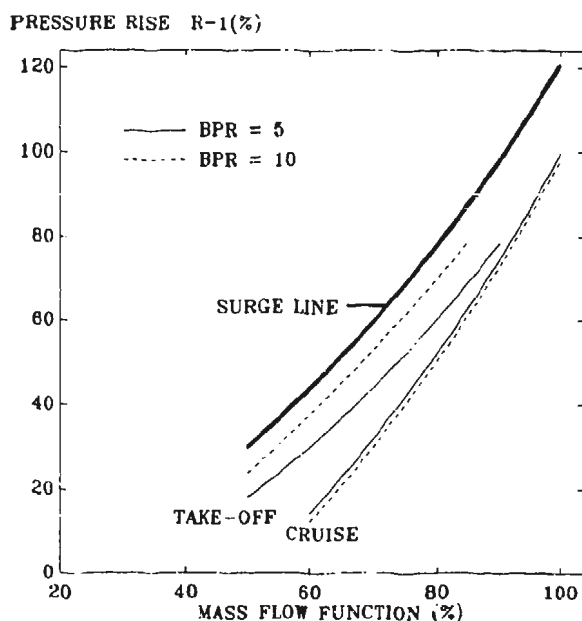
PRESSURE RISE R-1(%)

FIG.22 EFFECT OF BYPASS RATIO ON FAN RUNNING LINE

of a blow-off bleed in the bypass duct, to unload the fan, but could entail a variable bypass nozzle, or variable stagger rotor blades. Whatever the solution, additional complexity is involved and it must be taken into account in deciding where to fix the bypass ratio.

3.5 Environmental constraints

No discussion of civil engine cycles is complete without some mention of the two key environmental issues - noise and emissions. Engine noise has been a critical concern since the widespread introduction of jet airliners at the beginning of the 1960s. For the turbojets and very low bypass ratio engines of that period, with their high specific thrusts and high jet velocities, the far field

noise was largely dominated by jet noise. With the magnitude of the latter varying roughly as $Q_jV_j^8$, increasing engine power was causing the problem to get worse very rapidly. The need to circumvent this trend was as much responsible for the adoption of the high bypass turbofan as the performance benefits. Despite the huge improvement in noise that resulted, the problems are still with us and are now much more complex (Refs 11, 12); in high bypass engines, the far field noise comes in fairly equal measure from the fan and compression system, the LP turbine and the jets.

For a subsonic aircraft, the noise issue does not at present affect cycle choice fundamentally. The supersonic transport is a different matter - cycle choice for a future SST is likely to be very largely dominated by the noise problem, but consideration of this must lie outside the scope of the present lecture. In the subsonic case, while noise criteria are important, their influence tends to be confined to "fine-tuning" the cycle, eg to control jet velocities. It has been found that the use of a mixed exhaust brings some noise benefits and provides additional justification for selecting a mixed cycle. In general, increasing the bypass ratio will tend to reduce jet velocities so that a higher μ engine should have some advantage from the jet noise point of view, even though a mixed exhaust will be less effective and be more difficult to install.

Turbomachinery noise is largely dependent on the internal configurations of the compressor and turbine systems (blade numbers, spacings, etc), although tip speeds are also important. The relationship between the noise and the engine cycle is therefore indirect and fairly weak. Increasing bypass ratio will however raise the noise contribution from the fan. A major means of noise control is the use of acoustic linings in the duct both upstream and downstream of the fan. These are likely to become less effective with increasing bypass ratio, particularly as the need to minimise cowl length and diameter for external drag reasons will restrict the space available for the linings. The low fan pressure ratios required will alleviate the noise to some extent because fan tip speed can be reduced. Nevertheless, although difficult to quantify, it is possible that the noise problem could introduce an additional upper constraint on choice of bypass ratio.

Turning to the emissions question, the important factor from the cycle point of view is the production of oxides of nitrogen (NOX). These occur mainly at full power and are sensitive to combustor entry temperature T_3 and therefore to overall cycle pressure ratio. Fig 23, shows the general trend, with measured points from many different current engines. These are compared with the present international limit for NOX emissions and a lower regulatory limit to be imposed by the year 2000 (Ref 13); in fact this limit could be set lower still. The data are very variable, but an upward trend of NOX with Roa is apparent, as is the fact that many of the current engines will have difficulty
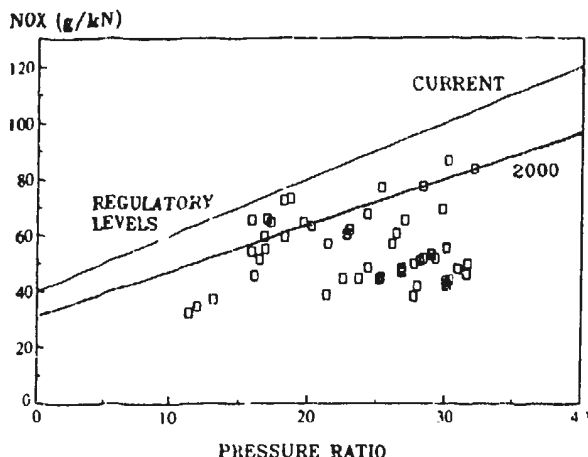
NOX (g/kN)

FIG.23 VARIATION OF NOX WITH CYCLE PRESSURE RATIO

ALTITUDE(KM)

FIG. 24 MILITARY AIRCRAFT FLIGHT ENVELOPE

in meeting the more stringent limit without modification. Various techniques are being developed by combustion technologists to overcome the problem, with particular attention being given to staged burning. However some sensitivity to cycle pressure ratio is likely to remain and this could lead to an additional upper constraint here. Certainly, the cycle designer will not be able to complete his task without an appraisal of both NOX emissions and noise.

4   CHARACTERISTICS OF COMBAT ENGINES

The basic principles we have just discussed for transport engines — thermal, propulsive and transfer efficiency and the effects of the cycle parameters - apply with equal force to combat engines. However both operational needs and cycle selection criteria are quite different. In the first place, except for one or two very specialised roles, combat aircraft are required to operate effectively and efficiently over a wide range of flight speeds, altitudes and thrust demands (see Fig 24). While the transport engine has only about three critical flight conditions to satisfy (albeit several secondary ones), the military engine may have to meet 20 or more cardinal points.

Secondly, the predominant aim is almost always to achieve high aircraft thrust/weight ratio, in the interests of speed, agility and/or weapons carrying capability. This means engine thrust/weight ratio needs to be high, but more importantly it places stress on engine specific thrust. High specific thrust means small engine cross-section and hence reduced aircraft fuselage cross-section. Any growth in engine size has a considerable knock-on effect on airframe size and weight.

This does not mean that fuel consumption is unimportant; far from it - the military operator is always seeking more range and endurance. Cycle choice remains a careful balance between thrust capability and endurance; engines optimised for different roles can have quite different cycle parameters (Refs 14, 15). Nevertheless the
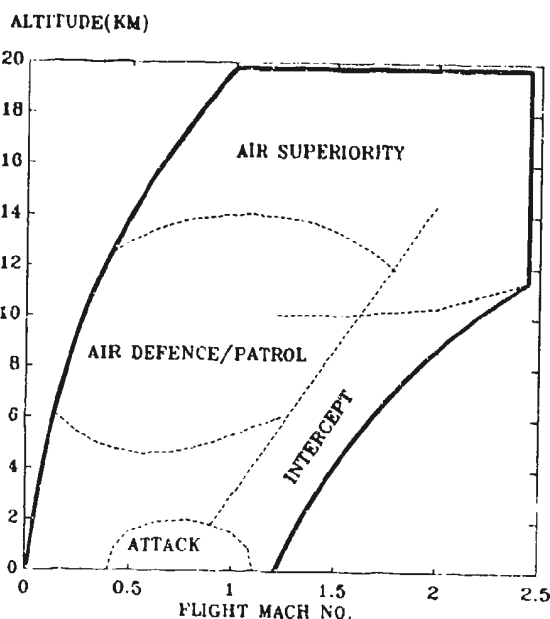
first priority is usually to satisfy the aircraft requirements for thrust and size, leaving the engine designer to achieve the best mission fuel burn he can, within these constraints.

4.1   Specific thrust

Figs 25 to 27 show how specific thrust varies over a range of design point cycle temperatures and bypass ratios, for three different flight conditions. The engines are assumed to be typical mixed exhaust afterburning turbofans, plus a datum turbojet with $\mu = 0$. The latter is included as a frame of reference. As was noted earlier, the requirements for jet pipe and nozzle cooling mean that in practice bypass ratio cannot be reduced below about 0.15. All the engines are assumed to have the same core efficiency, ie the same component polytropic efficiencies, same percentage turbine cooling bleeds and the same cycle pressure ratio Roa. These parameters have been set at levels typical of current designs; Roa has been taken as 25 (the effect of varying Roa will be considered later). These assumptions effectively turn the TET scale into a measure of engine hot parts technology standard. The afterburner lines are nominal limit lines based on a fully-mixed final fuel/air ratio of 0.06 (see discussion in Section 2.6).

Strictly, specific thrust is a function of fan pressure ratio (or more precisely nozzle pressure ratio), but the static pressure equilibrium condition at the mixer creates a unique relationship between R_{fan}, bypass ratio and TET, as shown in Fig 28. As TET increases, R_{fan} is increased at a given μ because additional power is available from the core to drive a higher duty fan.

Returning to Figs 25 to 27, these show three typical conditions of interest - the SLS hot day take-off point which is most

SPECIFIC THRUST (kN.s/kg)

FIG. 25 MILITARY ENGINE SPECIFIC THRUST TRENDS

SPECIFIC THRUST (kN.s/kg)

FIG. 26 MILITARY ENGINE SPECIFIC THRUST TRENDS

SPECIFIC THRUST (kN.s/kg)

FIG. 27 MILITARY ENGINE SPECIFIC THRUST TRENDS

commonly cited in published performance statements for military engines, a high subsonic flight speed/low level performance point, and a high altitude supersonic point. All three plots show the same general trends.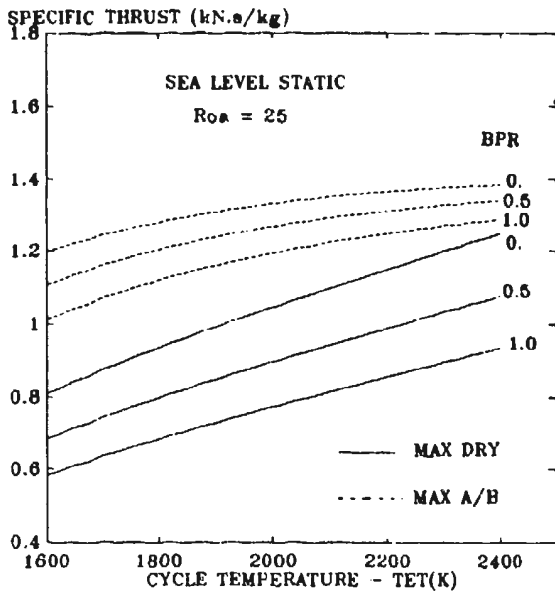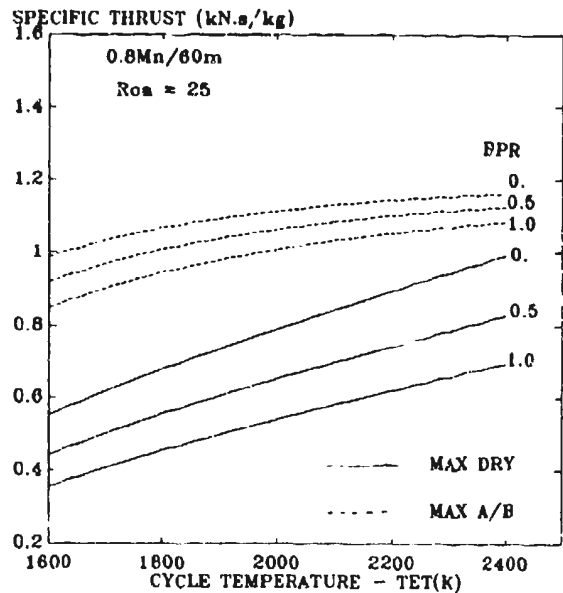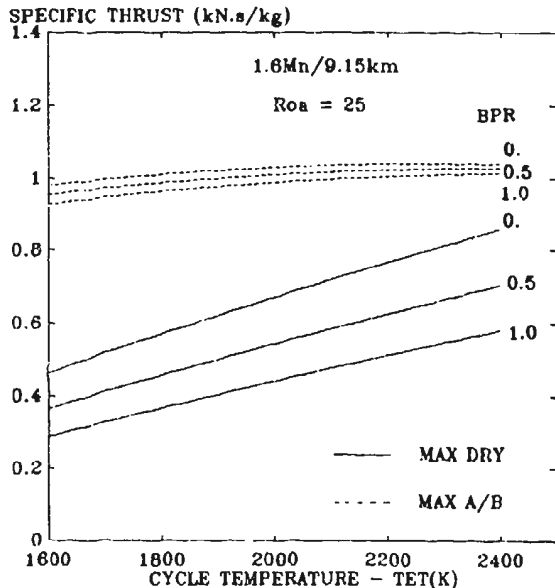 Non-afterburning, or 'dry', specific thrust can be increased by selecting a low bypass ratio and setting cycle temperature as high as the technology will allow. But applying maximum afterbuner always provides a substantial thrust boost, although the extent of this depends on TET. Comparison of the three figures shows that the magnitudes of all three effects are strongly dependent on flight speed, with sensitivity increasing as flight speed increases. For TET and bypass ratio the sensitivity is approximately doubled in going from SLS to Mach 1.6; afterburner boost goes up from +50% to +150%. These increases arise from

the fact that the cycle changes operate on gross thrust. As flight speed and hence inlet momentum drag go up, the effect on net thrust becomes magnified.

Irrespective of flight speed, afterburner boost always becomes less marked at the higher TET levels, particularly for low bypass ratio. This is because an increasing proportion of the oxygen in the engine airflow is used up in the main combustor, leaving less available for the afterburning process. Extrapolation of the two $\mu = 0$ curves would cause them to meet at around 2700K TET. This point would represent the so-called "stoichiometric engine", when all the oxygen would be consumed in the main burner, leaving nothing for the afterburner. No materials yet exist with enough strength and temperature capability to allow anything approaching such a cycle. In any case it is doubtful whether its fuel consumption characteristics would make it a desirable goal from the all-round performance point of view.

By using a similar estimation process to that described earlier for transport engines (Section 3.2) it is possible to establish practical TET limits corresponding to the selected materials and cooling technology standards. These will be independent of bypass ratio and could therefore be drawn as vertical boundaries on Figures 25 to 27. The major influence that TET has on thrust capability means that the cycle temperature details of any new combat engine design are always treated as sensitive information, both militarily and commercially. But broadly it can be said that TETs have advanced from the 1600K to 1700K of designs introduced at the beginning of the 1980s, to a potential 1900K to 2000K for engines coming into service during the present decade. Further progress beyond this is undoubtedly possible.
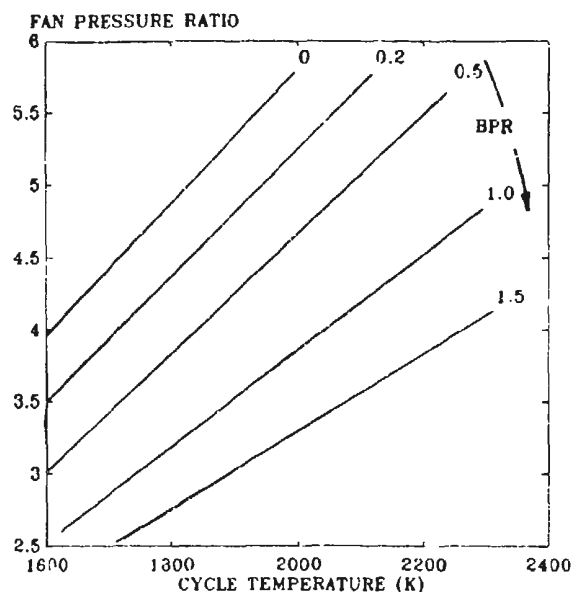
FAN PRESSURE RATIO

FIG. 28 FAN PRESSURE RATIO/BYPASS RATIO RELATIONSHIP
MILITARY TURBOFAN

FIG. 29 MILITARY ENGINE SFC TRENDS

It is to be noted that these temperatures are considerably higher than those indicated for civil engine applications, although the same basic technologies are used for both. There are a number of reasons why this is possible. In the civil case as discussed earlier, design optimisation is biased towards relatively modest cycle temperatures and any technology margins tend to be used to minimise cooling bleed requirements and/or extend turbine lives. In the military engine, the design emphasis is generally on achieving maximum TET. Also, while cost of ownership pressures are leading to much greater emphasis on military engine life, it remains a fact that annual utilisation may seldom exceed 300 hours; in the civil field, 3000 hours/year and more are commonplace. The military designer can therefore trade a considerable amount of component life for increased cycle temperature and still meet the customer's enhanced life requirements. He will also use different turbine alloy specifications, optimised for high temperature at the expense of higher cost, density or other properties.

4.2 Specific fuel consumption

As already remarked, despite the importance of specific thrust, fuel consumption cannot be neglected. It comes as no surprise that the trends are in generally the opposite sense. Fig 29 shows the sfc variations for SLS conditions and thus complements Fig 25. Similar plots could be shown for flight conditions and would show the same increased disparity between dry and afterburner operation. The figure demonstrates very clearly the inherent drawback of afterburner operation, which gets worse as bypass ratio increases. Using fuel to heat the low pressure bypass air is a highly inefficient process, whose only attractions are that it is basically simple and it provides the engine with a
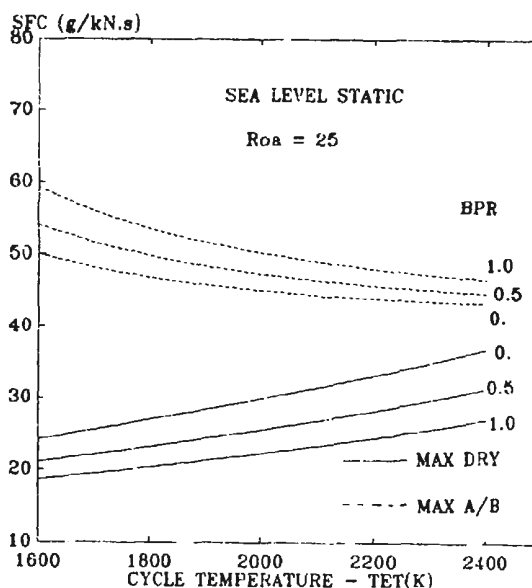
greatly increased thrust capability without increasing diameter. Because of the very high fuel consumption, afterburning can seldom be used for more than a few minutes during any mission. Its main function is to provide short bursts of power for take-off, high rate climbs, acceleration (particularly through the transonic drag rise region) and high alpha combat manoeuvring.

Fig 29 naturally highlights the very big increases in sfc when the afterburner is switched on. However closer study of the curves shows that dry performance also varies quite considerably with bypass ratio; eg, changing from $\mu = 0$ to $\mu = 1.0$ reduces sfc by some 25%, a difference that can have a strong impact on mission endurance. The issue is more readily apparent when the different bypass ratios are compared in terms of the sfc loops. Fig 30 shows sfc plotted against percentage thrust (ie throttle setting) for a group of engines all having the same core cycle pressure ratio and TET. The diagram also shows typical throttle bands corresponding to different types of mission segment.

Long range penetration or combat air patrol missions usually involve extended subsonic cruise or loiter, with high endurance being an important requirement. To optimise for this, a relatively high bypass ratio is likely to be preferred, it being accepted that the small bursts of high power will have to depend largely on afterburning. The Panavia Tornado GR1 with its $\mu = 1$ engines is a good example of this approach.

On the other hand an air superiority or interceptor fighter will require sustained operation at high speeds and make much more use of the medium to high power throttle settings. Crucially, much of this may span the point at which the afterburner has to be switched on. As noted in Section 2.6, there is a minimum fuelling rate for stable
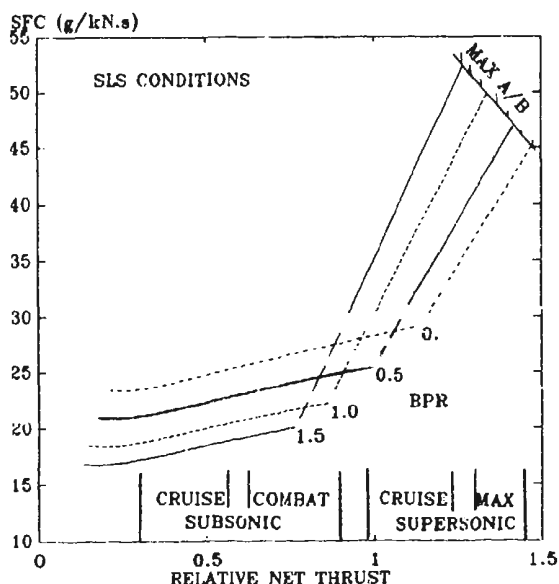
FIG. 30 MILITARY ENGINE PERFORMANCE
– EFFECT OF BYPASS RATIO

FIG. 31 MILITARY TURBOFAN – TYPICAL RATING DIAGRAM

afterburner operation, with the result that there is a considerable step change in fuelling rate, as shown in the Figure by the dashed lines. There is clearly big advantage in keeping as much of this mid-power operation as possible in the non-afterburning regime, even at the expense of poorer fuel consumption at low power. In part this is secured by selecting a relatively low bypass ratio, as typified for example by the F15 and F18 fighters (0.3 to 0.6 bypass ratio). But the further contribution to be obtained by increasing TET is clear and the resultant reduced dependence on afterburning is one of the more important prizes from the pursuit of high cycle temperature.

4.3 Rating structures and the influence of cycle pressure ratio

Because of the wide range of altitudes and flight speeds required for typical combat aircraft operation, the engine has to be rated to meet a number of different mechanical and aerodynamic limits. These will affect the detailed engine performance capability in different parts of the flight envelope. Fig 31 shows a typical rating diagram with TET plotted against engine inlet face temperature T_1. Also shown on the diagram are some selected flight points to illustrate the significance of the rating specification.

Allowable TET provides an overriding limit and the previous discussion has focused on that aspect. It appears on the rating diagram as a horizontal line, or sometimes as two such lines as shown in Fig 31. The lower line represents the normal limit for continuous operation, while the higher one provides for some additional thrust performance on a short-term basis – allowable on the basis that its use is sufficiently brief not to have too drastic an impact on hot end life. The higher rating may for example be programmed into the engine controller as a "combat" rating,
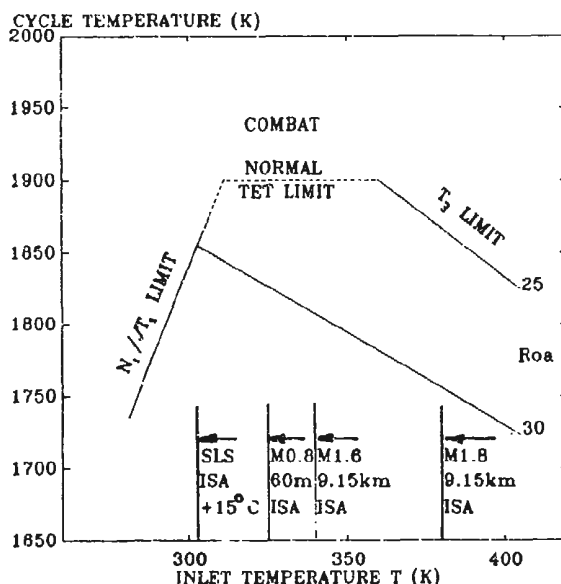
to be operative only when the afterburner is in use. Or, it might be invoked when operational circumstances demand exceptionally high thrust – ie the concept of the "peace/war switch".

Moving to the left side of the diagram, ie towards low T_1, causes the compressor dimensionless spool speeds and especially the low pressure spool speed to increase until the latter takes over from TET as the ruling limitation. This $N_1/\sqrt{T_1}$ limit appears as a line sloping steeply down to the left; for a given flight speed it is in effect a constant Roa and constant maximum thrust line. To the right of the kink point, Roa must be progressively reduced to avoid exceeding the limiting TET. At high inlet temperatures, the problem becomes one of high temperature at compressor delivery – the T_3 limit. This appears as a sloping line on the right hand side of the diagram. Some designers may incorporate further elaborations, but most rating structures are based essentially on these three main criteria.

How a particular engine is rated within these general principles will depend on the required usage pattern. The most important flight conditions for a general purpose combat aircraft usually include low altitude operation at speeds around or just below M1.0 and medium altitude operation at M1.4 to M1.8 (say). These span the T_1 range from around 325K to 355K and it is desirable to ensure that the engine is flat-rated over at least this range. To avoid over-sizing the engine it will probably be necessary to place the SLS point in the N_1 limited region, so that design TET cannot actually be reached in real take-offs. However this enforced de-rating is unlikely to be a problem for a modern combat design, since both engine and aircraft will be sized by certain critical flight conditions. These leave more than enough installed thrust to meet normal take-off requirements.

SFC (g/kN.s)

FIG. 32 EFFECT ON THRUST PERFORMANCE
OF HIGH PRESSURE RATIO CYCLE

SPECIFIC THRUST (kN.s/kg)

FIG. 33 MILITARY ENGINE SPECIFIC THRUST TRENDS
WITH AIRCRAFT SPEED DEMANDS

The rating structure does however have an important influence on overall pressure ratio. As for civil engines, increasing Roa has a beneficial effect on dry engine sfc, with around 7% improvement being obtained by raising Roa from 20 to 30, for example (Ref 16). However, this shifts the T_3 limit line considerably to the left, reducing the attainable TET at several of the important high T_1 conditions. The effect on performance is illustrated in Fig 32, which compares a 30 pressure ratio engine with the 25 Roa engine considered hitherto. For this particular example it is seen that both maximum dry and maximum afterburner thrusts are considerably reduced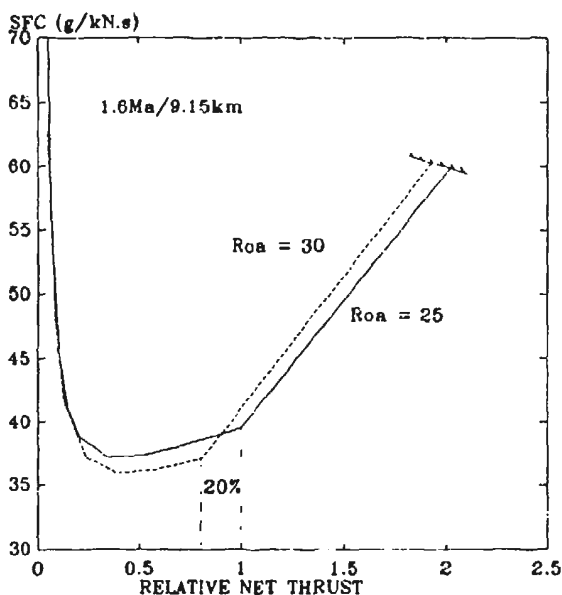 at the higher pressure ratio (by 20% and 10% respectively). This would normally be unacceptable and the general rule is to select the highest possible Roa, but only to the point where the T_3 limit begins to restrict performance in important parts of the flight envelope. It explains why combat-engine pressure ratios are generally limited to the 25 to 30 range, when their civil counterparts are reaching 35 to 40.

4.4 Supercruise

Given sufficient dry specific thrust, it is possible to provide the aircraft with the capability for sustained steady state operation at speeds well into the supersonic regime - so-called 'supercruise'. Engine technology has now reached the point where this type of operation can be achieved in a practical, versatile fighter and it has become a favoured approach for future high capability interceptors. The US Advanced Tactical Fighter will embody the principle. It may be remarked in passing that the idea is far from new. The Anglo-French Concorde airliner, which has been in service for over 15 years, is a classic supercruiser; so too is the Lockheed SR71 Blackbird, albeit in a very specialised role. However, neither of these aircraft has a
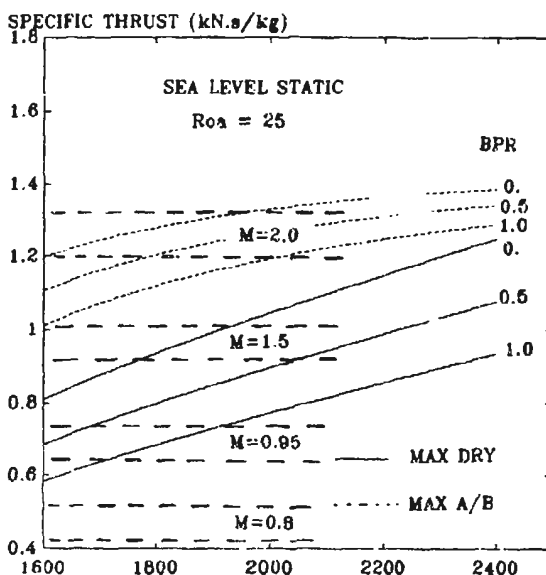
wide operational envelope and the supercruise capability was achieved by providing big externally-mounted engines rather than particularly high specific thrust. To maximise the latter within the technology constraints of the time, turbojet (μ = 0) cycles were chosen and overall pressure ratios were set very low by today's normal standards in order to avoid the T_3 limit problem. These two factors combined to give severe fuel consumption penalties at lower flight speeds.

What is needed for a fighter, with engines conventionally housed in the aft fuselage, is illustrated in Fig 33. This repeats the specific thrust/TET plot of Fig 25 with the approximate bands of SLS specific thrust typically required to sustain steady flight at different speeds in a fighter. It shows how the technology advances of the past 10 to 20 years have made supercruise a practical proposition. It must however be reiterated that this capability is still only obtained at the expense of worse fuel consumption at low throttle settings, even with a relatively high Roa. If mission doctrine calls for sustained combat patrol at say 0.6 flight Mach no, a lower specific thrust design and a lesser or perhaps no supercruise capability may remain a better solution (see for example Ref 17).

The supercruiser may give enough power for steady flight at 1.3 to 1.5 Mach no (at medium to high altitudes), but it still needs afterburning to accelerate to this speed in the first place, as well as to provide a margin for higher speed supersonic dash and for high turning-rate combat manoeuvring. These requirements will demand perhaps 30% to 40% thrust boost from the afterburner at the SLS rating, so the provision of afterburning is far from superfluous.

Could afterburning be avoided altogether without recourse to over-sized engines? In principle the answer is clearly yes. Such

SFC(g/kN.S)
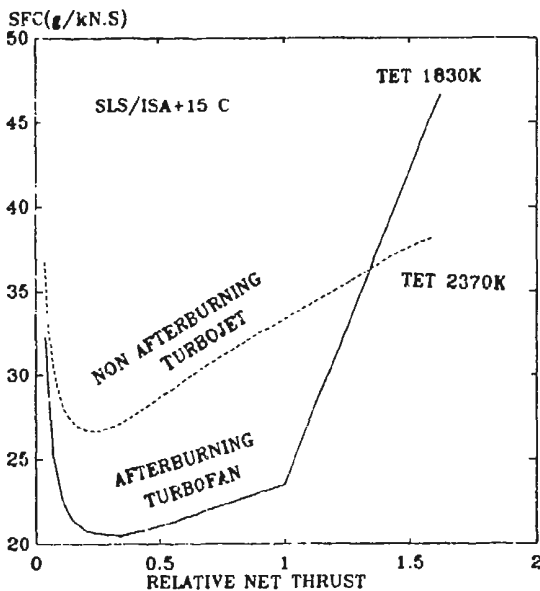
FIG. 34 AFTERBURNING TURBOFAN COMPARED
W.TH NON-AFTERBURNING TURBOJET

an engine would have to be as near to a turbojet as possible and have very high TET, although not necessarily going as far as the stoichiometric engine mentioned earlier. Fig 34 shows a non-afterburning turbojet compared with a more conventional afterburning turbofan of 0.5 bypass ratio; both engines are sized to give the same maximum specific thrust. The turbojet turns out to require approximately 300K higher TET, so that the difference in technology is very substantial. On this ground alone, the dry engine is probably not achievable for another 20 years. Perhaps more importantly, it only shows to advantage at the highest thrust levels. Below about 75% thrust, fuel consumption is some 30% worse than the conventional engine. On this basis the high performance dry turbojet is unlikely to offer any advantage except in the occasional highly specialised role.
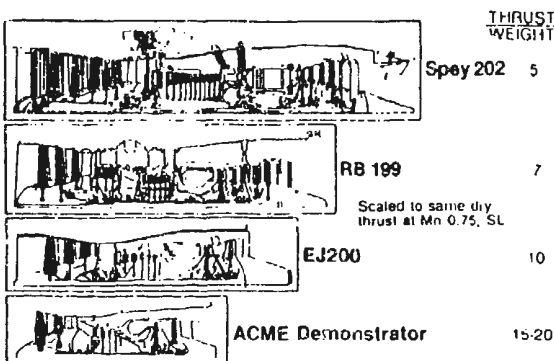
There remains an important place for the non-afterburning engine, but for applications not requiring high specific thrust. Such engines are particularly appropriate for the long range subsonic penetrator, where high agility or significant self-defence are not prime requirements. This is typified by aircraft like the Grumman A6 or BAe Buccaneer and more recently by the Lockheed F117 (which relies primarily on its low signatures for self-protection).

4.5 Engine thrust/weight ratios

Engine thrust/weight ratio is one of the commonly quoted measures of technical progress for combat engines. The engines in current operational fighters, which are mostly based on designs dating from the mid-1970s, generally have T/W ratios of around 7 (based on the nominal maximum SLS thrust on full afterburner). The 1990 class of engines being developed for the new generation of fighters coming into service in the next five years have T/W ratios of around 10. Foreseen technology developments will bring a T/W of 15 within reach in a few years time and advanced research and technology programmes are setting 20 as a longer term goal.

Achieving high T/W has a significant direct benefit in terms of aircraft size, but it also symbolises gains in other ways. One of these - the progressive increase in attainable cycle temperatures and hence in specific thrust - has underpinned most of the preceding discussion. It means for example that more thrust can be generated from a given size of engine. At the same time, improvements in internal aerodynamics have enabled the job to be done with less turbomachinery and this has hitherto also contributed in some measure to improved T/W. However, with stage numbers now becoming quite low, there is less to come by this means in the future. As implied in

	THRUST WEIGHT
Spey 202	5
RB 199	7
EJ200	10
ACME Demonstrator	15-20

Scaled to same dry thrust at Mn 0.75, SL

FIG.35 ENGINE THRUST/WEIGHT RATIO TRENDS
(FROM REF 18)

A/C WEIGHT (%)

FIG.36 EFFECT OF ENGINE THRUST/WEIGHT ON AIRCRAFT

Section 2.4 further direct weight reductions will be very largely through increasing use of ra ically new materials like the metal composites and the non-metallics. Smaller engines and fewer components meanwhile imply lower costs, at least notionally, and improvements in T/W therefore provide some figure of merit in this regard as well. Fig 35, taken from Ref 18, provides a graphic illustration of these trends.

Returning to the direct benefits of high T/W, the estimation of engine weight itself is much less straightforward than calculating cycle performance and will not be addressed here. However various studies on the impact of engine T/W on aircraft weight have been published (Refs 16, 19, 20). The trade-offs do not appear to be greatly sensitive to aircraft role, with similar figures being obtained for an interceptor and for a CAP-optimised aircraft (Ref 16). A generalised plot, encapsulating the published trends and assuming constant airframe technology, is shown in Fig 36. Raising the engine T/W from 10 to 20 will save around 15% 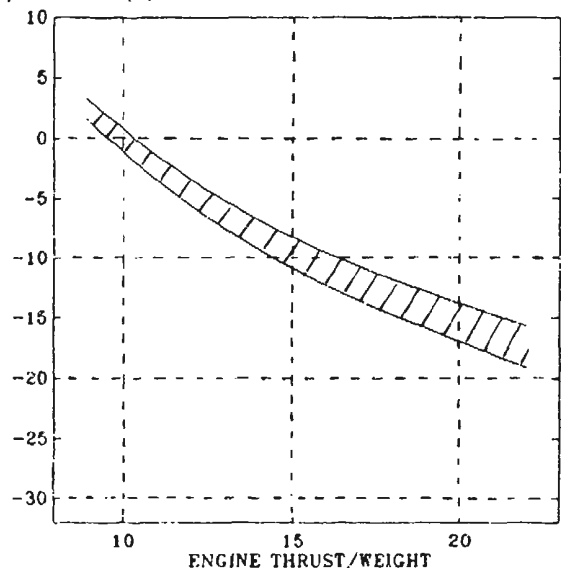of aircraft weight for the same mission. This represents an appreciable saving and helps to explain why T/W attracts so much attention.

5   SHAFT POWER ENGINES

In this section we will consider the cycles for aircraft shaft power engines, concentrating mainly on helicopter powerplants. Some reference will be made to turboprops, but in most respects there is little fundamental difference between the two applications.

For the helicopter engine, unlike the transport and fighter applications, it is more difficult to focus on any one performance attribute as a design driver. Considerations of helicopter size, flight performance and payload create some pressures towards high power/weight and high power/volume ratios. However, the engines (excluding transmission system) normally represent only around 6% to 8% of gross take-off weight and even big changes in engine weight can have only a small impact on total vehicle weight. The pursuit of improved fuel consumption has rather more importance and low sfc may be a cardinal point requirement in roles where long endurance is a major factor - eg maritime reconnaissance and anti-submarine warfare. But in most applications, endurance and low sfc are not critical issues and while performance must be satisfactory and competitive in these respects, the design will not necessarily be optimised around minimum sfc.

In the majority of cases, particularly at the present time, the most sought-after qualities tend to be low acquisition cost, low maintenance burden and high reliability (helicopters have a generally poor record in the latter two respects). The military customer is facing shrinking defence budgets and tends in any case to commit the lion's share of his resources to front-line combat aircraft and other "prima donna" projects. He expects to pay much less for his helicopter fleet. The civil customer is often a small operator who has limited resources anyway. Cycle choice may therefore be dominated by these cost issues, rather than by what is technologically possible for maximum performance.

5.1   The basic cycle trends

The basic thermodynamics of the helicopter engine are rather simpler than the civil and mili ary jets we have already considered. The helicopter is a slow speed machine, operating mainly below 140kts, so that inlet momentum drag is low and can largely be ignored. The usable power is extracted almost fully in the power turbine, so that the gas leaves the turbine with only sufficient pressure to overcome the exhaust system losses. Moreover the exhaust is often ejected through a sideways pointing nozzle rather than being directed rearwards, so that usable jet thrust energy is equally negligible. As a result the only significant component of cycle efficiency is the thermal efficiency $\eta_\bullet$.

The above comments need some qualification in the case of the turboprop. Aircraft speeds are higher, typically reaching 350kts (0.6 Mach no) or more, so that ram pressure ratio becomes sufficiently high to give a significant up-lift to thermal efficiency at cruise conditions. There will also be significant inlet momentum drag, although this will be counter-balanced by the pressure ratio across the exhaust nozzle in flight; the latter will normally point rearwards. It is not unusual for the final nozzle to be sized to give a small but significant net thrust to augment the shaft power to the propeller. At sea level static conditions, this may leave the nozzle with a pressure ratio of 1.1 to 1.2. To account for it turboprop engine performance may be quoted both in normal shaft power terms and in effective shaft power (ESP), where:

$$\text{Static ESP} = \text{Shaft Power} + \frac{M_j V_j^2}{2g}$$

and M_j and V_j are exhaust mass flow and jet velocity respectively. ESP may be up to 10% higher than nominal shaft power. However, in what follows, attention will be confined to the latter.

The basic trends in sfc and specific power over a range of cycle pressure ratios and temperatures are shown in Fig 37, for SLS conditions. Note that the performance parameters are now defined in terms of shaft power (KW) rather than thrust force (KN). It is seen that for the range covered here, increasing TET at constant Roa always improves sfc, in contrast to the case for the jet engine, where the opposite trend was shown (Figs 12, 13). This demonstrates how elimination of the propulsive efficiency element affects overall cycle behaviour.

Fig 37 suggests that there is every advantage to be gained by pushing the cycle as far to the bottom right of the diagram as possible, ie to go for both high Roa and high TET. Clearly this will be subject to
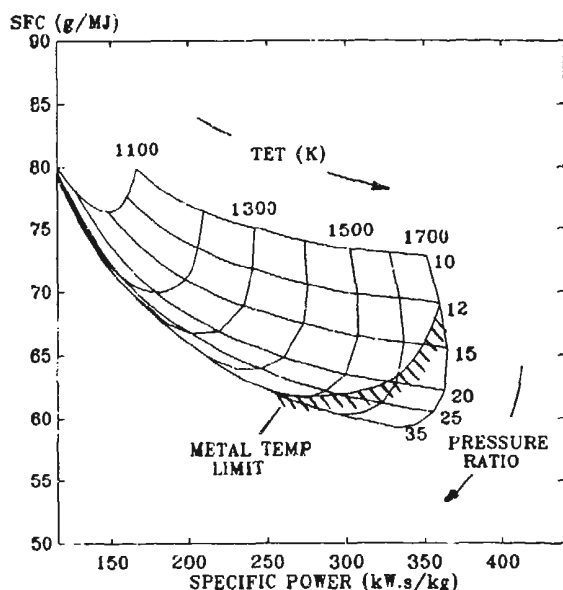
SFC (g/MJ)

FIG.37 BASIC SHAFT POWER ENGINE PERFORMANCE

FIG.38 COMPRESSOR SIZE EFFECT (FROM REF 22)

FIG.39 TURBINE SIZE EFFECT (FROM REF 22)

turbine materials temperature limitations in exactly the same way as before. A typical materials limit line has been superimposed on the plot and as would be expected shows that attainable TET reduces as Roa is increased. In practice, other factors provide additional constraints, most notably the effect of size.

5.2 The size effect

Helicopter engines are generally small, with air flows typically being an order of magnitude lower than the core flow in the average fighter engine. Moreover, the compression systems usually include a final centrifugal stage, or may consist entirely of centrifugal stages. As a result, blade and vane sizes and annulus heights are very small, so that boundary layer and other losses become magnified. The component efficiencies of helicopter engines are therefore much more strongly size-sensitive than for other engines and this must be taken into account in selecting the engine cycle (Refs 21, 22, 23). The magnitudes of the effect for compressors and turbines are shown in Figs 38, 39 which are taken from Ref 22. The ranges of interest for engines in the typical 750 to 1500 KW power bracket are indicated. Two curves are given, one for "current technology", broadly representing what is achievable now, and one for "advanced technology" representing what should become possible within a few years by full application of advanced cfd methods, etc, for component aerodynamic design. The latter are expected to make component efficiency by increases of around 2% possible.

It is apparent from the specific power trends that increasing TET can reduce engine size quite considerably. This will generally be beneficial in terms of cost, as well as weight, but the components will have to slide significantly down the size/efficiency curves. If Roa is also increased, annulus height at compressor exit and in the gas generator turbine will
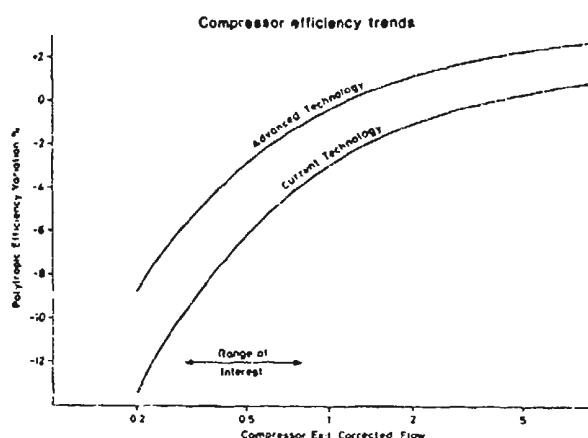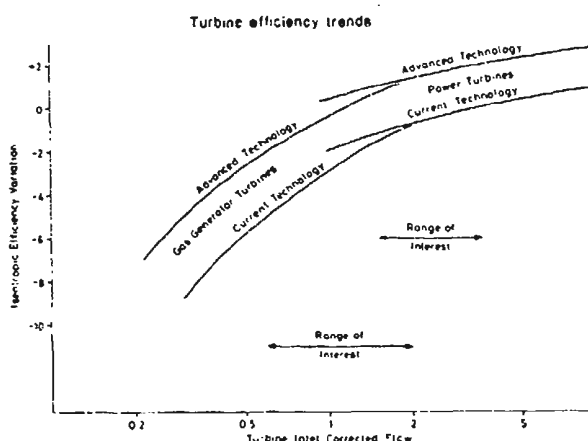
be further reduced, with a similarly detrimental effect on component efficiencies. For a shaft power engine a 1% reduction in every turbomachinery component will increase sfc by 4% to 5% and reduce specific power by a similar amount. These losses considerably undermine the potential benefits of the more advanced cycles.

Small size also adds to the difficulties of turbine cooling. With such small blades, both the cooling flow rates and the sophistication of the blade cooling design have to be less than those achievable in larger engines. Cost considerations also tend to discourage the use of cooled blading for more than two NGV rows and perhaps only one rotor row. The problem can to some extent be alleviated by using a single stage, heavily loaded gas generator turbine, rather than a two stage design. The single stage design will have larger blades which are easier to cool, while the high loading requires a higher tangential speed and a larger temperature drop through the turbine. The net result is a turbine with up to 100K more TET capability than the equivalent two stage design. However, this is at the expense of some 5% higher sfc because high stage loading penalises the turbine efficiency (Ref 22).
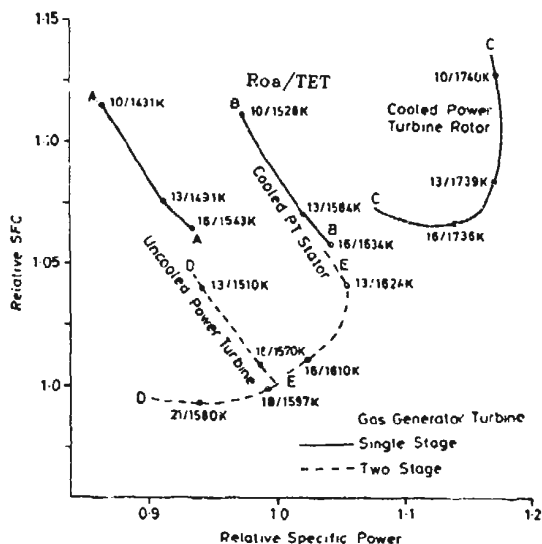
FIG.40 SMALL TURBOSHAFT ENGINE PERFORMANCE
(FROM REF 22)

FIG.41 SMALL TURBOSHAFT - EFFECTS OF ADVANCED
TECHNOLOGY

The combination of the above considerations leads to the result illustrated in Fig 40, which is taken from Ref 22 and is based on current component efficiency levels. The gas generator turbine is assumed to have cooling on all blade rows and the first power turbine stage is either uncooled or cooled, as indicated on the diagram. The curves represent the boundaries of "best" performance for realistic engine designs in the 1000 KW class, with all practical solutions lying above or to the left of the lines. If the aim is to minimise sfc, a two stage gas generator turbine would be preferred, but the performance "bottoms out" at around Roa = 20. Higher Roa would bring no benefit and would normally be worse on both sfc and specific power, because the adverse size effects outweigh the cycle benefits.

In the example shown, allowable TET tends to be governed by metal temperature at the first uncooled blade row, so that extending the cooling to the first power turbine NGV and then to the first rotor, allows specific power to increase, but generally at the expense of sfc. If small size is the aim, Fig 40 shows that a single stage gas generator combined with a cooled power turbine would be the best option. This could operate at high TET (up to 1740K) but at relatively modest pressure ratio (less than 15). Low pressure ratio has a cost advantage in reducing the number of compressor stages, but if low cost is the primary requirement power turbine cooling would be avoided altogether, moving the choice back to the left of curve A in Fig 40. Thus practical cycle choice and engine configuration may vary significantly depending on design priorities.

Improving component efficiencies or other component technologies can improve performance considerably. Fig 41 shows the effect of two anticipated trends. Firstly metal temperature capability is increased by 50°C - a step that is well within the bounds of evolving conventional alloy technology. This allows an increase of 80K in TET and a 10% increase in specific power, with no effect on sfc. In practice, this sort of measure would most probably be used to extend the power capability of an existing design, rather than produce a new and smaller design. The second step is to move to the advanced technology component efficiencies of Figs 38 and 39. With an increase of around 2% in each component, this gives a further 10% increase in specific power and a 10% improvement in sfc. However it is noteworthy that maximum Roa still scarcely exceeds 20.
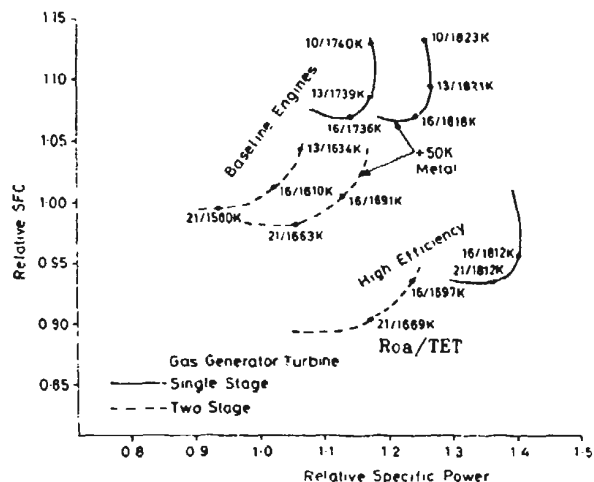
5.3 The sfc loop and engine ratings

A consequence of the basic thermodynamics of shaft power engines is that the sfc loop does not have the catenary shape of the jet engine. As the engine is throttled back, sfc rises continuously, the minimum normally being at the maximum power point, see Fig 42. Like the civil turbofan, the helicopter engine spends little time at maximum power and may be well throttled back for most of its duty cycle. Thus, as we saw for the former, there is advantage to the designer in allowing compressor efficiency to fall off at top power, in exchange for improved part power performance. This will have the effect of flattening out the curve slightly over the top part of the range, but typically sfc at 50% power is 15% to 20% greater than at 100% power.

Fig 42 also shows the power bands required for different phases of helicopter flight. Normal maximum power is required for fully-laden take-off and maximum vertical climb rate, but as soon as the helicopter starts moving forward the main rotor generates much more lift and the power requirement falls off, reaching a minimum in the 70 to 100kt range. Beyond that, increasing drag from both rotor and airframe begins to dominate and maximum forward speed is reached when power demand is back up to the maximum continuous rating.

SFC (%)
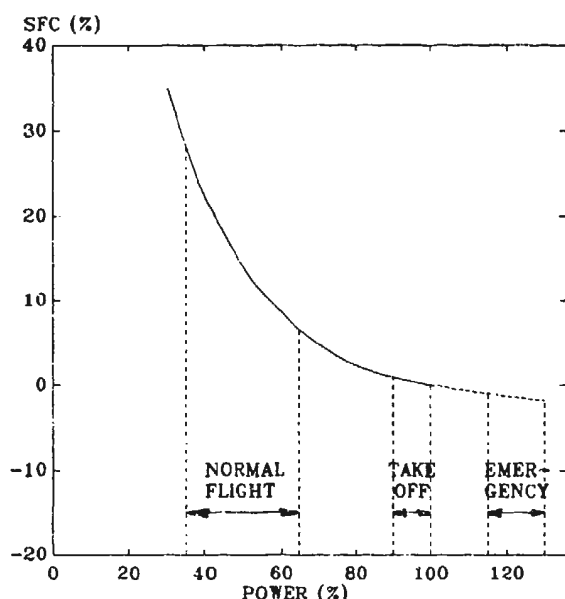
FIG.42 TURBOSHAFT ENGINE – TYPICAL SFC LOOP

Maximum continuous rating is the maximum power setting that can be used without time limit or discrimination. In theory, the pilot could choose to use it all the time, although in practice the designer specifies it at a level consistent with the predicted mission usage for the helicopter. This may tell him that the rating will be required for say 5% of total flight hours. If the engine overhaul life is 5000 hours, the rating is set at a level where the engine would last 250 hours if run continuously there. The difference between these two lives is 80°C to 100°C in metal temperature or around 150K in terms of TET. It is clearly essential to predict the power utilisation pattern correctly. Over-prediction of the maximum power requirement will lead to a low temperature, conservative design, which is over-sized and costly. Under-prediction will lead to a short life, unreliable design. It should however be added that new designs are invariably intended to have a degree of conservatism at initial entry into service, in order to leave room for power growth in later years without complete redesign.

Above the maximum rating, there is always one and sometimes two emergency ratings, mainly to cater for the one engine inoperative case in a twin engine helicopter (Ref 24). Safety considerations require that above a prescribed minimum height, a helicopter in hover must be able to suffer a single engine failure and still accelerate forwards without striking the ground. Rating philosophy for this case varies from manufacturer to manufacturer, but typically a 120% rating may be provided with a maximum allowed time of say 5 minutes for each application; there may also be a higher emergency rating still of perhaps 130% or more, with a maximum permissible time of perhaps 1 or 2 minutes. The specification may even require a borescope inspection after every application of the latter rating and may even call for engine removal and strip for refurbishment.

5.4 Engine installation factors

The discussion has so far dealt with the uninstalled engine. As would be expected, installed performance will be slightly worse than for the bare engine, because allowance must be made for intake and exhaust losses. There is a growing requirement for military helicopters to be fitted with inlet particle separators or dust screens to prevent the ingestion of sand or dust, which would otherwise have a very rapid and disastrous effect on the engine blading. Similarly, because helicopters are highly vulnerable to ground-launched infra-red homing missiles, it may be necessary to fit some form of infra-red suppressor. This is an extra unit fitted to the exhaust to prevent line of sight to hot metal and to cool the exhaust plume by internal mixing with ambient air, probably drawn in on the ejector principle. Both devices add pressure losses to the engine system and these must be allowed for in the performance calculation. Broadly, every 1% of pressure loss at either intake or exhaust increases fuel consumption by 0.5% and decreases power by a similar amount.

6 CONCLUDING REMARKS

In this lecture we have discussed many of the practical considerations that influence cycle choice for the three main types of aircraft application. Even so it has only been possible to scratch the surface of the subject. There is a multiplicity of additional factors, both technical and commercial, that the engine designer must take into account and which will affect his choice of cycle parameters. These include mechanical constraints such as shaft torque loadings and overspeed limits, vibration avoidance and damage containment. The commercial issues include perceived market size and the possibility of alternative applications, availability and cost of raw materials, processing methods and fabrication techniques, etc. When all such aspects are taken into consideration, the engine cycle may deviate significantly from the optimum as indicated by the simple, logical rules outlined here.

It has also not been possible to address a number of important specialist applications, eg short take-off/vertical landing fighters (STOVL), variable cycles, supersonic transports and high performance open rotors. However there are many good papers in the open literature on all these topics that are available for further study. While they introduce a number of extra influences on cycle choice, these applications are still subject to the basic materials, aerodynamic and thermodynamic constraints that have provided the bed-rock of this lecture. These constraints are fundamental to the whole process of gas turbine cycle design and are universally relevant to every type of engine.

REFERENCES

1 Saravanamuttoo, H I H, "An Introduction to Engine Performance Prediction and Modelling Techniques", AGARD Lecture Series LS 183, Paper 1, May 1992.

2 Hicks, M A, "New Metallic Materials for Gas Turbines", AGARD PEP72, Bath, UK, October 1988.

3 Harrison, G F and Shepherd, D P, "Lifing Philosophy for Aero-engine Fracture Critical Parts", Inst Mech Engineers/Roy Aero Soc, Aero-engine Reliability, Integrity and Safety Conference, Bristol, UK, October 1991.

4 Kirk, G E, "Composite Materials for Future Aero-engines", ASME 89-GT-313.

5 Oates, Gordon C (Ed), "Aerothermodynamics of Aircraft Engine Components", AIAA Eduction Series, 1985.

6 Scrivener, C T J, "Heat Transfer in Aero-engine Gas Turbines", J. Gas Turbo Soc. of Japan, 1990.

7 McMahon, P J, "Aircraft Propulsion", Pitman Press, 1971.

8 Shepherd, Dennis G, "Aerospace Propulsion", American Elsevier Publishing Co Inc, 1972.

9 Cohen, H, Rogers, G F C and Saravanamuttoo, H I H, "Gas Turbine Theory", Longman Scientific and Technical, Third Edition 1987.

10 Ivey, M S, "The Impact of Bypass Ratio on the Performance of Future Civil Aero Engines", Inst Mech Engineers, Aerotech 89 Conference, Seminar 15, Birmingham, UK, November 1989.

11 Smith , M J T, "Aircraft Noise", Cambridge University Press, 1989.

12 Jamieson, J B, "21st Century Aero-engine Design: The Environmental Factor", Proc Inst Mech Engineers, Vol 204, p.119, 1991.

13 Lister, D H, "Aircraft Emissions and Environment", Inst Mech Engineers, Seminar on 21st Century Aero-engine Design, Oxford, UK, May 1992.

14 Kamman, J H and Perryman, D C, "Propulsion System Requirements for Advanced Fighter Aircraft", AIAA-82-1143, June 1982.

15 Plourde, G A, Sims, R E and Cea, R A, "Fighter Engine Cycle Selection", AIAA-83-1300, June 1983.

16 Litchfield, M R and Philpot, M G, "An Examination of the Impact of Potential Advances in Component Technology for Future Military Engines", AGARD PEP 69, Paper 3, Paris, May 1987.

17 Denning, R M and Mitchell, N A, "Trends in Military Aircraft Propulsion", Inst Mech Engineers, Aerotech 87 Conference, Birmingham, UK, October 1987.

18 Ruffles, P C, "Current and Future Aero Engine Development", Inst Mech Engineers, Aerotech 89 Conference, Seminar 15, Birmingham, UK, November 1989.

19 Denning, R M and Mitchell, N A, "Critical Propulsion System Parameters for Future STOVL Combat Aircraft", American Helicopter Society, 42nd Annual Forum Proceedings, Vol II, p1047, June 1986.

20 Dollyhigh, S M and Foss, W E, "The Impact of Technology on Fighter Engine Requirements", SAE 851841, October 1985.

21 Bewley, A D, "Cycle Analysis for Helicopter Gas Turbine Engines", ASME 89-GT-328, ASME Gas Turbine and Aeroengine Congress, Toronto, June 1989.

22 Philpot, M G and Bewley, A D, "Performance Prospects for Future Helicopter Engines", Inst Mech Engineers, Aerotech 89 Conference, Seminar 20, Birmingham, UK, November 1989.

23 Niedzwiecki, R W and Meitner, P "Small Gas Turbine Engine Technology ", NASA/Army Rotorcrart Technology Conference, Moffett Field, Cal, 1987.

24 Cosner, A A and Rutledge, G S, "Successful Performance Development Program for the T800-LHT-800 Turboshaft Engine", SAE 891048, 1989.
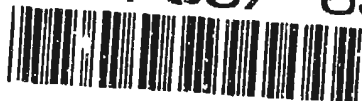
Steady and transient performance calculation method for prediction, analysis and identification

by
Jean Pierre DUPONCHEL
Jean LOISY
René CARRILLO

SNECMA Engineering Division
VILLAROCHE Center
77550 MOISSY-CRAMAYEL/FRANCE

AD-P007 892

92-20691

SUMMARY

The detailed design and development of turbofans involves the prediction and identification, by means of test analysis, of the performance of the engine and its components. The thermodynamic simulation and analysis codes integrate existing knowledge and interpretations of the detailed operating procedure of the components of the engine being developed. The relevance of the predicted performance depends on the quality of the representation of the various physical phenomena affecting the characteristics of the components and, consequently, on the incorporation of experimental correlation in the modelling.

In this context, the representation of compressor and turbine characteristics is particularly important. Firstly, we will analyze the ability of corrected parameters to represent MACH similitude at the component inlet under various conditions.

The various measurements achieved on the engine during development are used to enhance the modelling. The methods of identifying the thermodynamic calculation code with the various measurements, considered here with their uncertainties, are then presented and described. The analysis of the tests performed on the powerplant, designed to identify the real characteristics of the engine components, can be undertaken, considering one or more engine test points and incorporating knowledge acquired through experimentation or on the component test bench.
There are many possible fields of use for these identification methods ranging from the rematching of components to the optimization of the control system.

Symbols and notations

The symbols, notations and station identifications correspond to the SAE ARP 755A recommendations.

A	area
[C]	influence matrix
cg	correction factor for compressor/turbine characteristics map
CL	radial clearance
E	adiabatic efficiency
EP	polytropic efficiency
FAR	fuel: air ratio
H	stagnation enthalpy per unit mass
HS	static enthalpy per unit mass
IC	confidence interval
IDC	unstationary inlet distortion index, circumferential
m	measurement number
n	unknowns number (structural coefficents)
n	HPC inlet temperature exponant (acceleration schedule)
p	test point number
P	total pressure
PLA	power level angle
PR	total pressure ratio
PRS	compressor surge margin (%)

$$PRS = 100 \frac{PR_{Surge} - PR_{Operating\ point}}{PR_{Surge}} \text{ at constant corrected mass flow}$$

PRS2	fan surge margin
PRS25	HP compressor surge margin
PRS2P	fan surge margin fixed by engine performance considerations
PRS2R	fan surge margin required for aerodynamic stability
PS	static pressure
PW	power
P3Q25	HPC pressure ratio
R	gas constant per unit mass
RH	relative humidity (%)

$$RNI = \frac{\frac{P}{1.01325}}{\left(\frac{T}{288.15}\right)^{1.24}}$$

RNI	REYNOLDS number index	
S	entropy per unit mass	
t	time	
T	total temperature	
TK	critical temperature	
TS	static temperature	
V	gas velocity	
W	mass flow rate	
WAR	water (vapor):air ratio	
WB30	aircraft bleed mass flow	
WF32	gas generator fuel flow	
XMO	aircraft flight MACH number	
XN	rotational speed	
Z	turbine loading parameter	
α	aircraft angle of attack	
αA	anticipated aircraft angle of attack	
β	angle of sideslip	
γ	ratio of specific heats	
Δ or D	change in parameter	
ΔX	unknown vector (structural coefficients)	
ΔY	Y model - Y measurement	

$$\theta = \frac{T}{288.15}$$

σ	measured engine parameter uncertainty (coverage factor k=3)
Σ	summation
τ	thermal time constant
φ	entropy function

Subscripts after the basic symbols

C	correction operator for compressor/turbine characteristics taking into account molecular weight and specific heats ratio

$$\text{i.e.: } XN2C = \frac{XN2}{\sqrt{\gamma RT2/\text{standard values}}}$$

d	discharge
e	estimated value
i	inlet
K	critical state (MACH number unity)
L	turbine power limit
Q	quotient
R	conventional correction factor for compressor/turbine characteristics taking into account temperatures and pressures

$$\text{i.e.: } XN2R = \frac{XN2}{\sqrt{T2/288.15}}$$

s   steady state
S   static state (No. subscript for total state)

1. INTRODUCTION

Elaboration of an engine, designed to meet a new level of military or civil specifications, provides the opportunity to introduce modern technologies developed within advanced research and technology demonstration programmes. Carefully coordinated and targeted, this new product combines the capacities of the advanced components and of all the systems making up the powerplant, dealt with here from the point of view of the functions contributing to propulsion performance.

Mastering design and development implies global modelling and simulation studies for the various engine functions. During the engine design and development phases, global thermodynamic modelling of the powerplant is used intensively. The engine operation simulation precedes and supports its development. In the initial phase, computer calculation code simulation is used to analyze several engine configurations and architectures, combining the use of current and advanced technologies, in order to assess, for example, the impact of each technological characteristic on engine performance factors. At this stage of design, the thermodynamic calculation code is used primarily for prediction.

Given that these studies lead to the selection of performance options and guarantees, it is essential that the thermodynamic modelling used in the design phase should be based on a previously acquired accurate understanding of the operation of the engine components and systems and also on experimental data relating to advanced compressors and turbines acquired on the component test bench. Extensive data from theoretical calculations, measurements taken on components and test analyses performed on previously developed engines is compiled for the thermodynamic calculation of the performance.

In the second phase of engine development the engine's real performances become accessible through tests conducted in the various installations, such as the ground level test cell, the simulated altitude test cell and the flight test bed. Testing program and specification of measuring instrumentation are then directed towards the determination of the real characteristics of the engine components. After this, an adjustment phase, during which the calculation code is identified with the real cycle, starts. The interpretation of the measured characteristics, using a special identification version of the thermodynamic calculation code, enables performance to be predicted more accurately and, after analysis of the repercussions of the current configuration, engine component improvements and rematchings to be defined.

The purpose of this lecture is to describe:

. techniques for modelling component characteristics maps,

. methods of identifying the thermodynamic calculation code so that it represents, as far as possible, the real cycle of the engine under development.
These methods are applied to engine test analysis as well as to the development of the control logic.

2. THERMODYNAMIC PROCESS DURING ENGINE DEVELOPMENT PREDICTION/SIMULATION, ANALYSIS/IDENTIFICATION STUDIES

2.1 Thermodynamic modelling - General

In his analysis, the thermodynamicist will consider the whole powerplant as a single system. Due to the extent of this system, the thermodynamicist is unable, at present, to fully use the detailed models (e.g. on the scale of the blade) developed by the aerodynamicist. In general, the engine is considered to be composed of a set of modules, the various flows are separated, the air streams are split into a series of stations and average parameters are assigned to the flows (monodimensional calculations). This simplification, inherent to this system, as a whole, means that the analyst will resort to correlations and global characteristics for the engine components, in particular, compressor or turbine characteristics maps. This method of expressing the operation of the component constitutes the interface between the fields of aerodynamics and thermodynamics. Analysis involving the division of the air stream into a series of modules requires the use of a simplified description, approximation and correlation to define the characteristics of each module. The advantage of global modelling of the powerplant is that it is possible to rapidly assess the contribution of the characteristics of each detailed module to the global performance and consequently to carry out numerous studies for optimization, rematching and trade-off. However, this type of modelling has a number of restrictions, model identification using measurements enables the duct pressure loss to be expressed as a function of various parameters such as MACH number/inlet corrected mass flow rate or dynamic pressure/kinetic energy, but will not indicate the respective contributions of the various types of pressure loss: friction, diffusion, shock, secondary flow.

2.2 Specifications with respect to thermodynamic modelling

On the basis of the detailed description of the component characteristics, the thermodynamic cycle calculation code will satisfy the mass flow rate, momentum and energy conservation equations throughout the powerplant. Calculations will take into account the component degrees of freedom and the control system laws. The result of these calculations is a detailed representation of the engine cycle, in the characteristics maps specific to each component (operating point).

The characteristics of the modules will evolve during the various phases of engine development: they start as predicted characteristics, are measured on the component test bench and are then confirmed by engine tests in the ground test cell, the altitude test cell and on the flight test bed. This implies that the thermodynamic calculation code is of a semi-analytic nature providing a flexible and dynamic tool the contents of which reflect the best state of knowledge concerning component characteristics at the current stage of engine development.

Engine thermodynamic modelling is primarily used to accurately predict the performance of the engine and its cycle throughout the contractual flight envelope of the aircraft, and particularly for the phases of flight corresponding to performance guarantees. Throughout all the engine development phases, the real status of engine performance, in relation to the guarantied levels, has to be known. For these specific flight cases, the performance predicted by the calculation code will be based successively on:

- a prediction based on the measured compressor/turbine characteristics,

- a prediction readjusted on the basis of the first engine ground tests.

At a later stage, the calculation code will allow certain tests in the altitude test cell or in flight to be extended or transposed according to contractual requirements.

For this purpose, it is necessary to perform tasks to validate the engine thermodynamic modelling. The various tests carried out on the engine being developed

may be used to readjust the calculation code. During the various phases, it is important to know the accuracy of the model to represent the behaviour of the various components over wide-ranging flight envelope conditions. This validation phase has to be performed as early as possible in the development programme for the following reasons:

- thermodynamic modelling is used to diagnose the shortcomings in the engine cycle; it is used to orient component improvement and rematching phases.

- it is very important to rapidly define the ability of the engine to meet guaranteed performance with an adequate degree of confidence. It is therefore necessary to assess the level of modelling representation at all times.

The quality of modelling will be expressed by the consistency of engine testing in the different installations; the accuracy of the predicted engine performance will depend on the confidence interval of the experimental correlations, included in the model that will be derived from identification studies.

To facilitate the process of identifying and validating modelling, it is appropriate to confer a specific structure to the calculation code:

- a large number of modules must be anticipated and for each the addition of formulations corresponding to the presence of the various physical phenomena.

- the degrees of freedom, as empirical correlations, should be introduced to allow these formulations to be readjusted on the basis of the available measurements.

3. MODELLING OF COMPRESSOR AND TURBINE AEROTHERMODYNAMIC CHARACTERISTICS

The principles of thermodynamic modelling described in the following paragraphs refer to the JANUS calculation code designed by SNECMA for the development of the M88-2 military engine. The M88-2 is an advanced technology dual rotor turbofan engine, incorporating a three-stage fan and a six-stage high pressure compressor, each driven by a single-stage turbine.

Its degrees of freedom are:

- variable fan inlet guide vane position,

- variable compressor stator vane position,

- core engine fuel flow,

- afterburner fuel flows,

- nozzle position.

3.1 Basic thermodynamic modules

A certain number of subroutines on the thermodynamic characteristics of the fluid that will undergo a series of evolutions as it passes through the engine must be available beforehand. At the engine inlet, the fluid consists of a mixture of dry air and water vapor, characterized by a certain WAR specific humidity. The combustion of hydrocarbon CH_β, with a certain fuel/air ratio FAR, in the air, in the presence of water vapor, generates a new mixture characterized by the WAR and FAR ratios. The per unit mass enthalpy is described by a function H (T, FAR, WAR). The fluid function

$$(1) \quad \phi = \int_o^T \frac{dH}{T} = \phi \ (T, FAR, WAR)$$

is required, this function being linked to the entropy variations by the relation

$$(2) \quad S_2 - S_1 = (\phi_2 - \phi_1) - R.\log_e \frac{P_2}{P_1}$$

The ϕ function applied to the isentropic evolutions (3) (calculation of static state or critical state), to a compressor (4) or a turbine (5).

$$(3) \quad \phi - \phi_s = R.\log_e \frac{P}{P_s}$$

$$(4) \quad \phi_d - \phi_i = \frac{R}{EP} \log_e \frac{P_d}{P_i}$$

$$(5) \quad \phi_d - \phi_i = R.EP.\log_e \frac{P_d}{P_i}$$

is used for the simple calculation of the state parameters without resorting to the thermal capacity γ ratio (thus avoiding the mean γ choice).

The functions H_{mix} and ϕ_{mix} relative to the unit of mass of the mixture comprising:

- 1 kg of pure air

- WAR of water vapor

- FAR of burnt gases

are deduced from the values H and ϕ of the constituent parts of the mixture by the relations (6) and (7).

$$(6) \quad H_{mix} = \frac{H_{pure\ air}\ (T) + WAR.H_{water\ vapor}\ (T) + FAR.H_{burnt\ gases}\ (T)}{1 + WAR + FAR}$$

$$(7) \quad \phi_{mix} = \frac{\phi_{pure\ air}\ (T) + WAR.\phi_{water\ vapor}\ (T) + FAR.\phi_{burnt\ gases}\ (T)}{1 + WAR + FAR}$$

The mass enthalpies and the ϕ functions, of the three constituent parts of the mixture, vary with temperature and are represented by high order polynomials.

The notation for the thermodynamic parameters and the main engine stations, are those recommended in the document SAE ARP 755 A.

The incorporation of water vapor, which has a significantly different molecular weight to that of pure dry air, implies the creation of several specific subroutines.

As an indication, the principal modules relative to water vapor are:

- calculation of the saturating pressure of water vapor as a function of the static temperature. Deduction of the correspondence between the relative humidity RH and the specific humidity WAR,

- condensation test,

- calculation of the latent heat of vaporization, the quantity of water condensation and the temperature rise ΔT_{RISE} of the gaseous mixture following condensation.

The presence of water vapor in free (atmospheric) air will affect the various thermodynamic functions H, φ and γ and will also increase the mixture mass constant. Thus, for a mixture of dry air and water vapor

$$(8) \quad R_{mix} = \frac{287.05287 + WAR.461.522}{1 + WAR}$$

The various parameters of m- odimensional flow that correspond to the critical stat (MACH = 1) and the static state for the given total flow arameters, can be calculated directly or by iter ion when the different thermodynamic modules ar appropriately combined. Figure 1 summarizes the concatenation of calculations to assess the main thermodynamic parameters corresponding to the static state and the critical state.
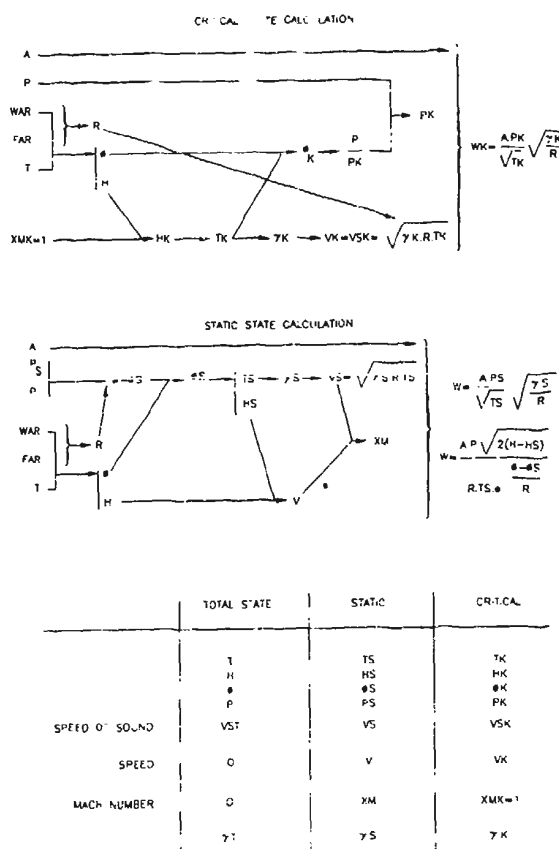
3.2 Modelling of compressor and turbine characteristics

COMPRESSOR

The characteristics of the compressor are usually modelled for a reference state, i.e.

- for clean inlet flow (low space-time pressure and temperature distortion),

- for a given variable stator vane schedule,

- for rated (and identified) clearances,

- in steady thermal operation,

- for rated engine ventilation air bleed values,

- for an accurately defined inlet REYNOLDS number.

This method takes for granted that appropriate specific corrections, such as those developed in conference No. 8, can be incorporated in these compressor reference characteristics to describe compressor behaviour under real conditions.

Searching for a method for representing the characteristics of a compressor, implies questioning the variance of the physical phenomenon and then choosing reduced variables apt to represent similar functions in terms of velocity triangles. The standard method considers several independent variable categories:

- variables qualifying the fluid passing through the compressor,

- variables characterizing a reference state for this fluid,

- the geometry and kinematics of the compressor,

- variables characterizing the energy exchanges between the compressor and the fluid.

If the effects of viscosity are disregarded (independently accounted for by the REYNOLDS analogy), the conventional dimensional analysis leads to the selection of similitude parameters such as the pressure ratio and efficiency as a function of two parameters,

$$\frac{W\sqrt{T}}{P} \quad \text{and} \quad \frac{XN}{\sqrt{T}} \quad ,$$

representative of MACH numbers:

. the flow axial MACH at the compressor inlet

. the formed MACH with the rotational speed of the blades.

By the following points SNECMA's choice differs slightly from this conventional representation of the compressor similitude parameters. In the expressions of the reduced parameters, we have retained the quantities γ and R, characterizing the fluid, to more accurately signify the constancy of the velocity triangles with regard to MACH similitude for fluids with different characteristics at the compressor inlet (temperature, humidity, etc.). However, we have chosen not to retain the two MACH numbers (the axial MACH at the inlet, and the formed MACH with the rotational speed). The use of these MACH numbers implies an iteration on the fluid static state and we have preferred to keep the property enabling a direct access of the similitude parameters of the characteristics map on the basis of the total flow parameters.

These considerations oblige us to represent the compressor characteristics map by the following corrected parameters (example given for a high pressure compressor):

- corrected speed, $XN25C = \dfrac{XN25}{\sqrt{\gamma R T25}}$

- the throttling or position parameter on the corrected speeds isograms,

$$W3QK = \frac{W3}{W3K}$$

(ratio of real mass flow rate to critical flow rate corresponding to the annular discharge station A3, for discharge conditions)

- non-dimensional parameter representing the MACH number at the inlet,

$$W25QK = \frac{W25}{W25K}$$

(ratio of real mass flow rate to critical flow rate corresponding to the annular station A25, for inlet conditions)

- the corrected total enthalpy rise.

$$\frac{H3 - H25}{\gamma RT25}$$

2 TABLES AND AREAS A25–A3
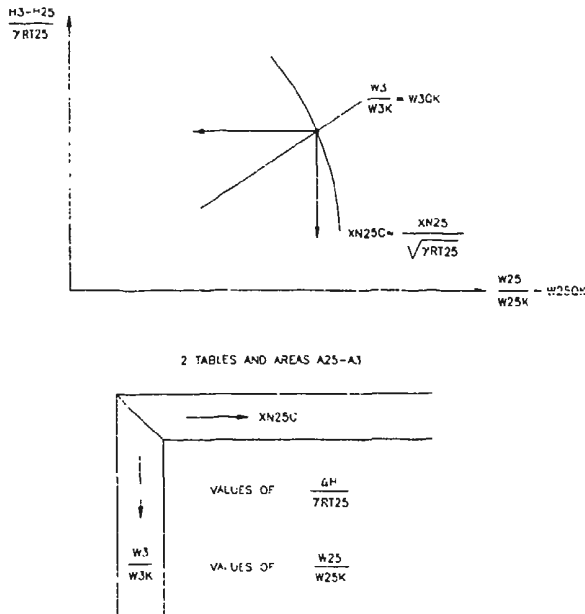
FIGURE 2 – REPRESENTATION OF COMPRESSOR CHARACTERISTICS FOR REFERENCE STATE

Figure 2 summarizes this representation of the compressor characteristics for the reference state. The integration of this compressor map representation into the engine thermodynamic calculation code is reduced to the establishment of two matrices

$$\left. \begin{array}{c} \dfrac{H3 - H25}{\gamma RT25} \\[2em] W25QK \end{array} \right\} = f(XN25C, W3QK)$$

associated with sections A25 and A3 and with the coefficient linking the real discharge flow rate W3 with the real inlet flow rate W25.

The introduction of the reference compressor map surge line executes independently. It is expressed by

$$P3Q25 = F(W25C)$$

with $W25C = W25 \sqrt{\dfrac{T25}{288.15}} \sqrt{\dfrac{1.01}{P25}} \sqrt{\dfrac{R}{287.05}} \sqrt{\dfrac{1.400}{\gamma}}$

associating the specific values for the stator setting schedule, the radial clearances, the viscosity and distortion, to make the appropriate corrections to the position of the surge line.
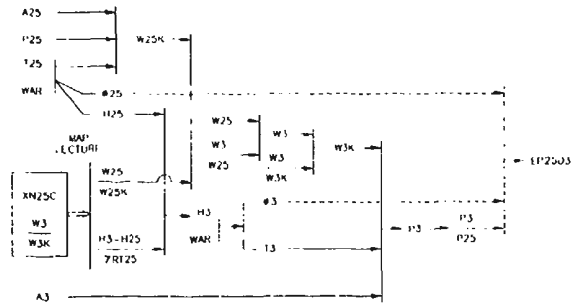
FIGURE 3 – POLYTROPIC EFFICIENCY CALCULATION, USING THE CORRECTED PARAMETERS OF AN HP COMPRESSOR MAP

The block diagram in figure 3 shows the sequence of calculations of the compressor discharge conditions, the compression ratio and the polytropic efficiency, for an operating point within the compressor characteristics map and for fixed inlet conditions.
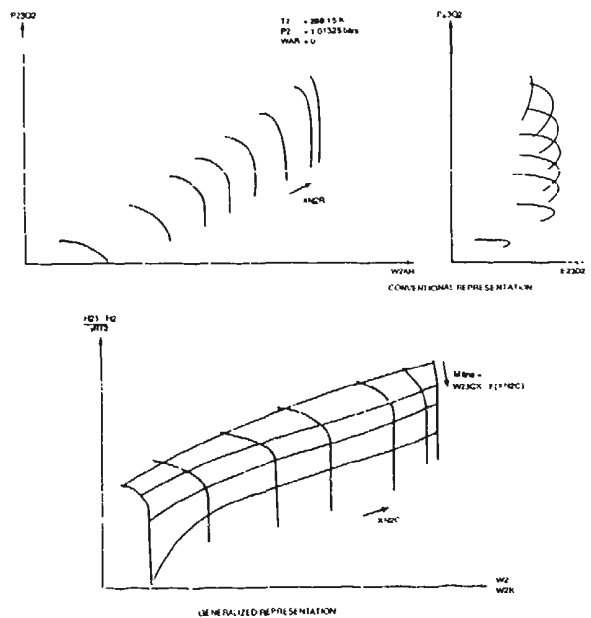
FIGURE 4 – REPRESENTATION OF CHARACTERISTICS OF A LP COMPRESSOR

An example of the representation of the LP compressor map (primary flow) is given in figure 4:

- a new representation with more complete invariants on the lower part,

- the representation of the characteristics of the same compressor with conventional invariants on the upper part, for standard conditions

$P_2 = 1.01325$ bars

$T_2 = 288.15$ K

and for a reference fluid (WAR = 0, dry air), that is, $R = 287.05287$ J/kgK.

The representation of a compressor characteristics map, the basis of these new similarity parameters, is also used on the basis of the measurements taken on the

compressor partial test bench. To the standard measurement of the flow rate, pressure and temperature at the compressor inlet and discharge, must be added the measurement of ambient humidity and the use of the same thermodynamic functions, as those composing the engine calculation code, to calculate the four similitude parameters (Figure 3).

TURBINE

A similar method has been developed to represent the turbine reference characteristics (here, notation for HP turbine).
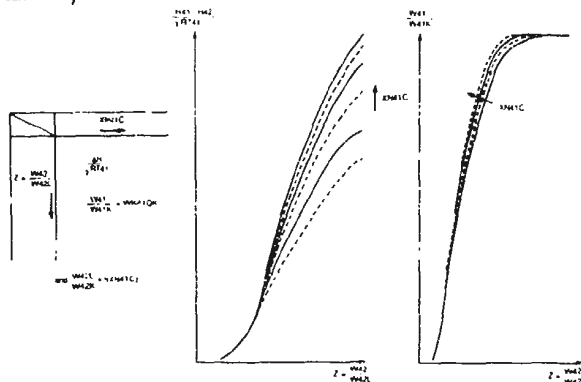
FIGURE 5 REPRESENTATION OF CHARACTERISTICS OF AN HP TURBINE

The four similitude parameters used are as follows:

- corrected speed, $XN41C = \dfrac{XN25}{\sqrt{\gamma RT41}}$

- position parameter on the corrected speed isograms,

$$Z = \frac{W42}{W42L}$$

W42L corresponds to the turbine power limit conditions (with regard to the power limit a proximity indicator is available)

- similitude parameter representing the MACH number at the inlet,

$$W41QK = \frac{W41}{W41K}$$

(the real mass flow rate to critical flow rate ratio corresponding to station A41, for inlet conditions).

- the drop in the corrected total enthalpy, $\dfrac{H41 - H42}{\gamma RT41}$

Figure 5 illustrates this representation. The introduction of this turbine characteristics map into the engine thermodynamic calculation code is reduced to the establishment of two tables

$$\left. \begin{array}{c} \dfrac{H41 - H42}{\gamma RT41} \\[2mm] W41QK \end{array} \right\} = f\,(XN41C,Z)$$

associated with stations A41 and A42 and a relation W42L/W42K = f(XN41C) defining the turbine power limit.

3.3 Quality of the representation of the MACH number using corrected parameters

In this paragraph, we examine the ability of the similitude parameters to represent the MACH number for different inlet conditions and for varied fluids. The problem of the generalization of the compressor or turbine characteristics map arises when the ratio γ of the heat capacities and the R fluid mass constant (that is to say the molecular weight) diverge markedly from the reference values corresponding to the cases of calculation or measurement on the component partial test bench. For a compressor, the problem consists in the extension of a map measured on the partial test bench supplied under atmospheric conditions at the estimated characteristics map of this same HP compressor mounted on an engine, therefore downstream from the LP compressor and under aircraft flight conditions.

For a turbine, this implies the transposition of the characteristics measured on the partial test bench by warm supply for the particular engine.

With regard to the representativeness of the axial MACH number at the entry to the annular zone by a corrected flow, we have successively examined the three following invariants:

(1) $\quad \dfrac{W\sqrt{T}}{P}$

(2) $\quad \dfrac{W\sqrt{T}}{P}\sqrt{\dfrac{R}{\gamma T}}$

(3) $\quad \dfrac{W}{WK}$

for two axial MACH number values: 0.6 (representative value for a compressor) and 1 (case of a turbine) and for the combined cases of pure air with richness in burnt gases of 0.03 and specific humidity WAR = 0.03 (corresponding to t_a = 35°C at a relative humidity RH = 80%). The results of the calculations are described in figures 6 to 8. The invariants (1) and (2) are represented as specific flow rate units and as ratios, taking the standard specific flow rate as the reference (T_{std} = 288.15K, pure air WAR = 0, FAR = 0); The invariant (3) in W/WK was not represented for a MACH number equal to 1 because it is evident that its unitary value, by definition, is then independent of the component supply conditions.

In tables 1 and 2, we have treated the relative deviations caused by the use of a same type of invariant, both for the partial test of the component and for the engine flight test, and this for a HP compressor and for a HP turbine.

The results of these calculations reveal the shortcomings

of the simplified similitude parameter (1) $\dfrac{W\sqrt{T}}{P}$ and

illustrate its inaptitude to transpose the large variations of the ratio γ of the heat capacities ratio and above all the R gas per unit of mass constant, when considering important deviations in the component inlet temperature or a heterogeneous gas mixture of water vapor and burnt gas. Its role must therefore be limited to low-amplitude transpositions.

Table 1 HP compressor axial MACH number XM :0.6

	T_{ss} (K)	FAR	WAR	Flow rate invariant		
				(1) $\frac{W\sqrt{T}}{P}$	(2) $\frac{W\sqrt{T}}{P}\sqrt{\frac{R}{\gamma T}}$	(3) $\frac{W}{W_K}$
				(Kg/cm²)	(Kg/cm²)	
Partial bench test, ambient conditions	288.15	0	0	203.041	203.041	0.84164
Engine flight test	550	0	0.03	200.07	203.55	0.8405
Relative discrepancy (in %)				- 1.46%	+0.25 %	- 0.13%

Table 2 HP turbine   MACH number : XM = 1

	T_{41} (K)	FAR	WAR	Flow rate invariant		
				(1) $\frac{W\sqrt{T}}{P}$	(2) $\frac{W\sqrt{T}}{P}\sqrt{\frac{R}{\gamma T}}$	(3) $\frac{W}{W_K}$
				(Kg/cm²)	(Kg/cm²)	
Partial bench test, (when cold)	288.15	0	0	241.244	241.244	1
Engine flight test	1800	0.03	0	234.09	244.74	1
Relative discrepancy (in %)				- 2.97%	+1.45 %	0

introduction of in the invariant (2) $\frac{W\sqrt{T}}{P}\sqrt{\frac{R}{\gamma T}}$ For this, the residual deviation comes from the use of total parameters in this expression because the same quantity written in static parameters expresses the MACH number perfectly.

The invariant (3) in $\frac{W}{W_K}$ that we have chosen to represent the compressor and turbine maps further attenuates the representativeness deviations at XM = 0.6. These deviations cancel out when the invariant (3) is defined for XM = 1, by its very definition.
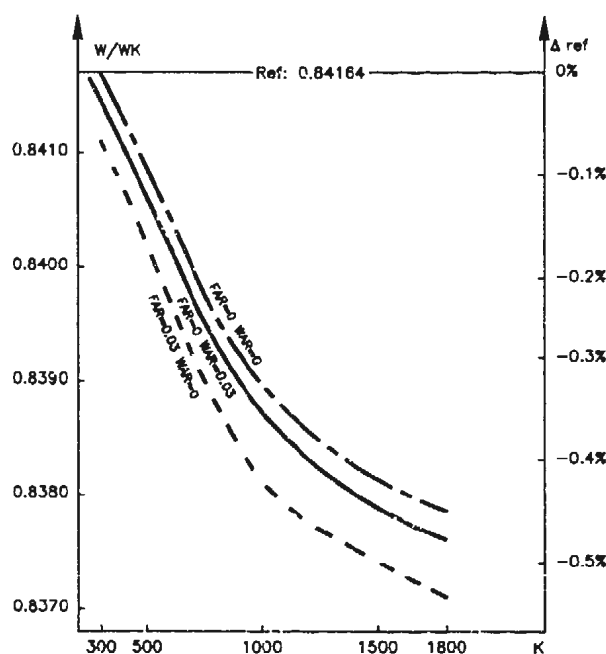
FIGURE 8 — EFFECTS OF
— FLOW TOTAL TEMPERATURE T
— WATER (VAPOR) : AIR RATIO WAR
— FUEL: AIR RATIO FAR
ON THE RATIO : FLOW RATE/CRITICAL FLOW RATE
FLOW MACH NUMBER = 0.6

FIGURE 6 - VARIATIONS OF THE CORRECTED MASS FLOW (1) (2) WITH
— FLOW TOTAL TEMPERATURE T
— WATER (VAPOR) : AIR RATIO WAR
— FUEL: AIR RATIO FAR
FLOW MACH NUMBER = 0.6
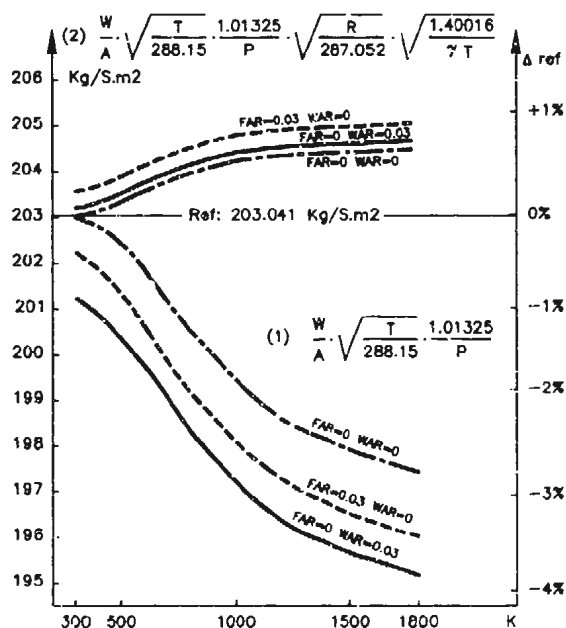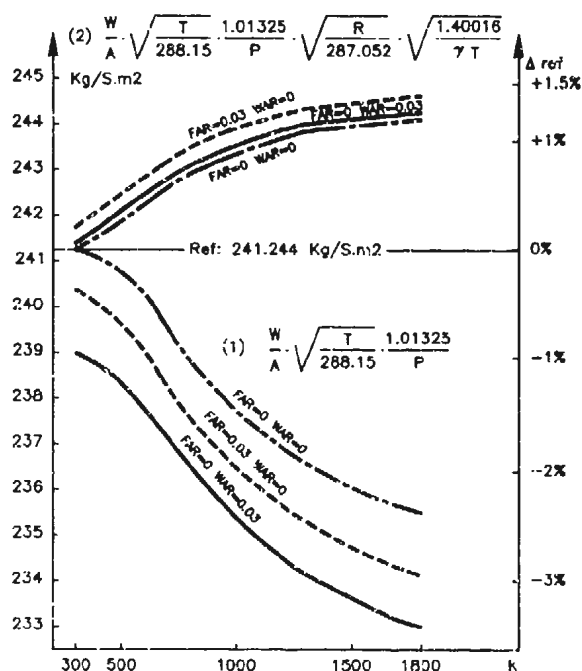

FIGURE 7 - VARIATIONS OF THE CORRECTED MASS FLOW (1) (2) WITH
— FLOW TOTAL TEMPERATURE T
— WATER (VAPOR) : AIR RATIO WAR
— FUEL: AIR RATIO FAR

The greater part of the correction, coming from the variation of fluid molecular weight, is generated by the

4. METHODS FOR IDENTIFYING A THERMODYNAMIC MODEL BY MEASUREMENTS

4.1 Test analysis process

Once the prediction and simulation code of the engine's thermodynamic behaviour has been obtained on the basis of component characteristics, either predicted or measured on the component test bench, this modelling must be validated and decisions must be taken as to the orientation the engine performance tests will take. During the initial stages of modelling or at the beginning of the development programme, many uncertainties remain concerning both the data that comprise the calculation code and the real characteristics of the engine components. The thermodynamicist's main concern is to reduce the uncertainties in the initial modelling, quantify the real characteristics of each component and then validate the calculation code. This is achieved by performing tests on engines fitted with detailed instrumentation. The thermodynamic analysis cannot be confined to observations of the overall performances or to measured cycle parameters. It is therefore necessary to assess the real characteristics of the components. Any deviation from the expected characteristics of a component causes the other engine components to be mismatched resulting in operating point migrations, including components with nominal characteristics. Consequently, directly comparison of the efficiencies deduced from the measurements with the expected values, can lead to an erroneous interpretation of the quality of the components. The analysis must be conducted for each component to show up the origin of the deviations observed on the cycle.
This task is performed using the identification methods described further on. The real characteristics of the components are then discussed with the aerodynamicists. The role of the thermodynamic specialist is to describe the confidence interval corresponding to the real characteristics of the component, the consequences on the overall engine performance and the potential possibilities of rematching the components.

For a single definition of the engine, the process for

validating the thermodynamic calculation code progressively requires all the different categories of engine tests: the ground level test cell, the simulated altitude test cell, and the flying test bed. All these data are linked together by the thermodynamic simulation tool. The experiments on the simulated altitude test cell can be used to adjust the viscosity corrections of the modelling used for ground level tests. They also highlight the effects linked to the untwisting of the blades and the extended characteristics of the exhaust system. An initial quantification of flow-distortion effects, at engine intake, can also be measured on the engine at this stage using an unstationary distortion generation system. This initial individual quantification, performed for each effect for experiments on the simulated altitude test cell, is essential for the calibration and validation of the thermodynamic calculation code; only this rigourous progression in identifying each influence on the component characteristics can lead to a satisfactory interpretation of the other numerous effects inherent in the in-flight tests: installation, transient, thermal, throttle-dependent effects, etc.

4.2 Component characteristics correction factors

In order to quantify the deviations between the modelling and the experimental results, it is common practice to define correction factors used to adjust the model characteristics to the measurements obtained. In general terms, the thermodynamic process taking place in the compressor or turbine can be described by using four parameters such as (table 3):

. axial MACH number at the inlet, i.e. the ratio W_i/W_{iK}
. efficiency EP
. corrected speed XNC
. axial MACH number at discharge, i.e. the ratio W_d/W_{dK}

The operating point in the characteristics map is fixed by two of these four parameters. The four related correction factors are defined in table 3. The permeability and efficiency deficits are usually expressed as cg_1 and cg_2. The correction factors concerning the other components apply to the aerodynamic pressure loss coefficient and the combustion efficiency.

	correction factors cg	for constant map values of		
compressor	$\left(\dfrac{W_i}{W_{ik}}\right)_{map} \times cg_1 = \left(\dfrac{W_i}{W_{ik}}\right)_{real}$	EP	XNC	$\dfrac{Wd}{Wdk}$
	$EP_{map} \times cg_2 = EP_{real}$	$\dfrac{Wi}{Wik}$	XNC	$\dfrac{Pd}{Pi}$
	$XNC_{map} \times cg_3 = XNC_{real}$	$\dfrac{Wi}{Wik}$	EP	$\dfrac{Pd}{Pi}$
	$\left(\dfrac{W_d}{W_{dk}}\right)_{map} \times cg_4 = \left(\dfrac{W_d}{W_{dk}}\right)_{real}$	$\dfrac{Wi}{Wik}$	EP	XNC
turbine	$\left(\dfrac{W_i}{W_{ik}}\right)_{map} \times cg_1 = \left(\dfrac{W_i}{W_{ik}}\right)_{real}$	EP	XNC	$\dfrac{Wd}{Wdl}$
	$EP_{map} \times cg_2 = EP_{real}$	$\dfrac{Wi}{Wik}$	XNC	$\dfrac{\Delta H}{\gamma RT_i}$
	$XNC_{map} \times cg_3 = XNC_{real}$	$\dfrac{Wi}{Wik}$	EP	$\dfrac{\Delta H}{\gamma RTi}$
	$\left(\dfrac{W_d}{W_{dl}}\right)_{map} \times cg_4 = \left(\dfrac{W_d}{W_{dl}}\right)_{real}$	$\dfrac{Wi}{Wik}$	EP	XNC

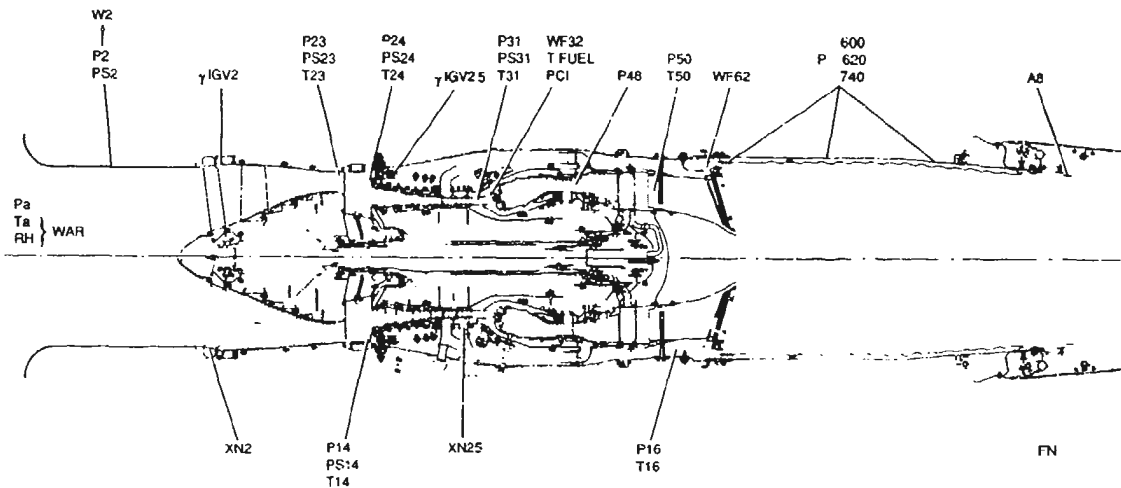Table 3 Definition of correction factors

FIGURE 9 - LOCATION OF FLOW PATH MEASUREMENTS ON M88-2 ENGINE

	UNKNOWNS		EQUATIONS TO BE MET		
7 OPERATING VARIABLES	LPC - MAP LOCATION PARAMETER	W23QK	W2A = W2A MAP		
	HPC - MAP LOCATION PARAMETER	W3QK	W25 = W25 MAP	AIRFLOW RATE	
	HPT - MAP LOCATION PARAMETER	W42QL	W41 = W41 MAP	CONTINUITY	
	LPT - MAP LOCATION PARAMETER	W5QL	W49 = W49 MAP		COMPATIBILITY EQUATIONS
	CYCLE AIRFLOW RATES	W2A	PW42 = PWHP		
		BPR	PW5 = PWLP	POWER BALANCE	
		T40	PS57 = PS17	CONFLUENCE STATIC PRESSURES	
STRUCTURAL COEFFICIENTS	LPC PRIMARY	CG1	FN CYCLE = FN SENSED		
		CG2	W2A = W2A		
	LPC SECONDARY	CG1	WF32 = WF32		
		CG2	A8 = A8		
	HPC	CG1	P CYCLE = P SENSED	23	
		CG2		23A	
	HPT	CG1		24	
		CG2		31	
	LPT	CG1		48	
		CG2		50	
	PRESSURE LOSS	23/24		13	
		50/55		14	
		13/14		16	MEASURES
		14/15		PS57	
	EFFECTIVE LPT OUTLET SECTION	CK57		PS17	
			T CYCLE = T SENSED	23	
				23A	
				24	
				31	
				50	
				13	
				14	
				16	

FIGURE 10 - SINGLE TEST POINT IDENTIFICATION METHOD - EQUATION SYSTEM

The aim of analyzing tests through identification is to distort the modelled component characteristics (efficiencies, flow rates, pressure losses, etc.) in such a way that, for a given operating point, the values calculated by the model of the operating parameters (pressures, temperatures, etc.) are equal, or as close as possible, to the engine during the test. Figure 9 illustrates the typical instrumentation of a development engine on a ground level test cell. The various engine stations are equipped with pressure and temperature probe rakes, linked to static pressures on the walls. The other conventional thermodynamic measurements are the rotational speeds, the fuel flow rate and temperature, the nozzle positions, the variable fan inlet guide vane positions, the variable HP compressor stator vane positions, the thrust and the ambient conditions. Processing and averaging of these measurements generates the parameters that will be used to analyze the engine cycle.

4.3 Single-test point identification methods

For each test point, characterized by a set of measurements obtained on the engine, the values of the various correction coefficients to be applied to the modelling characteristics are determined in such a way that the simulated parameters of the cycle correspond to the measured values.
This correspondence is established by resolving equation systems by iterative numeric methods with regard to the non-linearity of the modelled phenomena.
Figure 10 illustrates the equation system to be resolved in the most usual case. There are two sub-systems to be solved. The first equation sub-system comprises the cycle compatibility equations, i.e. generation of the various continuities of the flow rate, shaft power equilibrium and static pressure at the confluence; where the unknowns are the operating variables, i.e. the operation point position parameters in the characteristics maps and the air flow rates.

This sub-system, that is characteristic of the presented engine model structure, will be found in all the identification methods described below. It is this sub-system that ensures the physical validity of the calculated cycle (notion of loop). This first sub-system, by its very nature, must be exactly resolved. It is generally considered to have been satisfied when the relative error on each equation is less than a predefined epsilon.

The second equation sub-system is composed of the identity between the m measurements and the parameters simulated by the model, where the unknowns are the model's structural coefficients, i.e. the various correction factors of the compressor, turbine and pressure loss characteristics. It is clear that an accurate solution cannot be achieved when the number of measurements exceeds the number of structural coefficients.

One method consists of using only a limited set of measurements corresponding to the number of structural coefficients and therefore ignoring some of the measurements. The non-linear equation system can then be solved accurately within the limits of convergence accuracy, by a NEWTON-RAPHSON type method. This type of identification method is known as a "square" method, since it contains an equal number of equations and unknowns.

Another approach consists of using all the measurements. Since the equation system cannot be solved accurately, uncertainty related to each measurement should be taken into account. In this case, the solution that minimizes the quadratic deviation is sought,

$$\Sigma_m \left(\frac{Model\ value\ -\ Measurement}{\sigma} \right)^2$$

the compatibility equations being satisfied accurately. This type of identification method is known as a "rectangular" method. Additional equations can also be introduced in order to take into account the experience acquired by adding estimated parameter values associated with their confidence interval. Both these equation sub-systems:

. compatibility equations, to be satisfied accurately,
. equations identifying the model with the measurements, to be matched as best as possible,
are solved using a NEWTON method coupled with a regression method.

When the measurements relative to a given engine component are not accurate or when the component modelling is not representative, the identification results concerning other components may be affected. In this case, an other method, enabling to identify the structural coefficients of each component with the measures specific to this component in particular, is advisable. The system is then constituted of several rectangular sub-systems and of only one common square sub-system (compatibility equations).

The use of the rectangular identification method highlighted the need for an extremely accurate calculation of the derivatives. Applying these methods to a set of test points covering the entire operation envelope of the engine component characteristics leads to a set of values for the various correction factors. At this stage, pertinent correlations must be obtained between these correction factors and the intrinsic component parameters using regression methods, in order to obtain an overall description of the behaviour observed in this component over the operating range covered by the tests.

4.4 Multi-test point identification method

This is the result of extending the single-test point rectangular identification method to a set of test points p. In this case, the local structural coefficients of the single-

test point methods are replaced by global coefficients (values common to all the points). These coefficients, characterizing functions f given below, therefore constitute new unknowns.

The solution sought should be along the following lines:

HPC cg_1 25 = f(XN25C)
cg_2 25 = f(XN25C)

LPC cg_1 2A = f(XN2C, W23QK)
cg_2 2A = f(XN2C, W23QK)

HPT ...

that accurately solves all the compatibility equations for each test point and:

. matches the measurements as well as possible -->
  minimisation of the quadratic deviation

$$\Sigma_p \ \Sigma_m \left(\frac{Model\ value\ -\ Measurement}{\sigma} \right)^2$$

. takes into account any previous experiments by introducing the estimated parameter e, associated with its confidence interval IC

$$\Sigma_p \ \Sigma_e \left(\frac{Model\ value\ -\ Estimated\ value}{IC} \right)^2$$

A direct search is therefore made for the coefficients of these correlations (e.g. polynomial correlations) that express the changes in the model's correction coefficients. This requires the expression of the different functions f to be defined beforehand.

Methods, splitting the rectangular sub-system into several other ones, may also be applied.

Notion of "rectangular utilization with a new orientation":

Our understanding of the engine's behaviour is made all the more easier because of the available additional non-redundant information. When the number of sensors cannot be increased, the multi-test point identification method results in an original solution: in this case, the quantity of additional information comes from the **simultaneous incorporation of the various points**. The utilization of this method can be understood through algebraic representation, rather than time-consuming developments.

Let us assume that we wish to identify a vector of an unknown $\overrightarrow{\Delta X}$ (coefficients) and that we have a vector $\overrightarrow{\Delta Y}$ whose components are the differences between the model's values and the measured values for a test point. By linearizing and taking the operating point as our viewpoint, formally, we have:

$$\overrightarrow{\Delta Y} = [C] \ . \ \overrightarrow{\Delta X}$$

dimensions   (m x 1) (m x n) (n x 1)
(line x column)

where [C] is the influence matrix given by the engine model at the point being studied. This system can only be solved if $n \leq m$
(if m = n: square system to be solved using the NEWTON method
 if n < m: a "pure" rectangular system to be solved by a regression method).

If it is considered that the coefficients sought do not evolve during the different test points taken into account, the previous relation can then be written as follows for p points:

$$\overrightarrow{\Delta Y}_1 = [C]_1 \ . \qquad\qquad \overrightarrow{\Delta X}$$

$$\overrightarrow{\Delta Y}_p = [C]_p \ . \qquad\qquad \overrightarrow{\Delta X}$$

i.e. by combining

$$\overrightarrow{\Delta Y_1} = \begin{bmatrix} C \end{bmatrix}_1$$

$$\overrightarrow{\Delta Y_p} = \begin{bmatrix} C \end{bmatrix}_p \quad \overrightarrow{\Delta X}$$

dimensions   (mp x 1)   (mp x n)   (n x 1)

This gives us mp known values (model minus measurements), whereas the number of unknowns remains the same. This can still be solved due to the non-linearity of the phenomena, insomuch as the selected points are relatively uncoupled and sufficiently numerous.

Note: For the sake of clarity, the compatibility sub-system was not taken into account in the preceding explanation. However, it can be accurately transposed by including in vectors ΔY_i the deviations on the compatibility equations and splitting previous vector $\overrightarrow{\Delta X}$ into:

$\overrightarrow{\Delta X_i}$: local unknown compatibility quantities
ΔX_g: global coefficients to be identified

This type of approach enables more coefficients to be identified than the number of existing measures for a given component (determination of turbine correction coefficients).

5. APPLICATIONS OF THE IDENTIFICATION METHODS - TEST ANALYSIS

5.1 Operational approach:

Test analysis, by mathematical modelling, is justified by the necessity to know with ever increasing depth the characteristics of the engine's components.
Therefore, the real part of each engine component in the engine's overall performance must be ascertained, with consolidation of the initial modelling of our phenomena analysis.

This improvement of the engine model representativeness, then enables the undertaking of several types of studies (prediction, influences, component matching...) with more relevance, to improve the characteristics of the engine's components, as well as their adaptation, in such a way that the engine can satisfy performance targets (understand to act). This results in a reduced number of tests being required to apprehend the engine's behaviour.
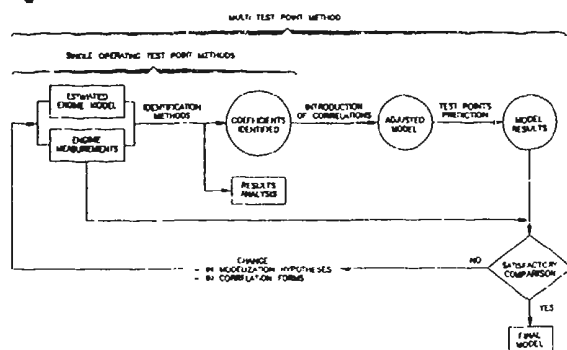

FIGURE 11 - TEST PROCESSING DIAGRAM

This test analysis approach subdivides into several phases that deserve some specific remarks:

. Identification phase: (determination of correction factors)

This is the confrontation phase between the tests and the existing type of modelling, the modelling then being "adapted" to measurements according to criteria of previously developed residual deviation minimisation. Result analysis makes it possible to apprehend the

characteristics of the components that are actually installed in a new environment. The model is then seen as a mean of understanding physical phenomena that enable possible detection, for example, of component peculiarities, defects (weakness).

. Resetting phase (updating our model)

The purpose is to transpose the tendencies of the correction factor evolutions, that systematically appeared on an engine/mounting set with the same technological definition, by correlations depending on characteristic parameters of the components in question.
These correlations are then reintroduced into the engine model. They must comply with the double imperative of reliability and simplicity and be adaptable to very different cases of operation. This approach makes it possible to go from a pin-point level of knowledge to a continuous perception of the engine's behaviour.
It is then possible to simulate, by extrapolation, areas of operation that are difficult, or even impossible, to implement on the test bench.

. Prediction phase

The purpose here is to assess the resetting quality of our engine model by simulating test operation cases.
In particular this will enable hypothesis validation made at modelling level and the types of correlation chosen.
The results deemed unsatisfactory, because they differ too much from the measurements obtained on the test bench, will oblige resumption of the previous identification and resetting phases.
In this respect, the use of statistic analysis tools will be very beneficial for the analysis of our distribution of the model/measurements results deviations for each parameter.

It will then be possible to test:

- the random character of that distribution (research for bias...)

- the hypothesis, in its statistical sense, of a nil average.

At the end of this iterative process the engine model, "reset" in this way, is ready to undergo several research studies.

We have tried to schematize the precedent approach by the synoptic illustrated by figure 11

5.2 Use of the various identification methods in the engine development process :

The three identification methods:

. Square - single-test point }
. rectangular - single-test point } + regression
. rectangular - multi-test point,

the principles of which were given in chapter 4, have their optimum application in the different steps of the engine development process.
The choice of one of these methods will then be guided by:

- the level of knowledge reached at the time of identification,

- the measures at disposal,

- the type of research that we intend to implement.

The disposition and choice of measurements being guided by the analysis that we wish to undertake concerning the engine (for instance, diagnosis of a particular component). We will now define the different characteristics and possibilities of each of the methods mentioned.

5.2.1 Single-test point rectangular identification method

This method particularly applies when we have excess information with respect to the number of correction factors to be identified.
This information can consist of measurements, on the engine, or estimated characteristics of components. In the latter case, we shall talk about constraints imposed on the operation of the engine. Each item of information being matched with a certain amount of confidence corresponding, for measurements, to the uncertainty about the measurement, and in the case of constraints, to the uncertainty on the knowledge of the estimated characteristic value.
Depending on the state of progress in the development of the engine, the composition of this set of information, to be matched, changes.

The main cases of application are then:

- the first development tests in which instrumentation is usually abundant and the characteristics of the components on the engine are little or badly known.

- engine tests with the integration of one or more new components: there is little excess instrumentation but the behaviour of the old components on the engine is very well known.

- engine tests in a new environment (for instance the beginning of flight tests): the instrumentation is less developed but the behaviour of the components is well known on the entire operating envelope that has already been explored during tests on ground and simulated altitude benches.

In the two latter cases, it will be possible to impose constraints on the known characteristics of the components, taking into account the influence of the new component or new environment for the degree of confidence granted for that constraint.

5.2.2 Single-test point square identification method:

The square method has the particularity of using only one part of the measurements available on the engine. As a matter of fact, the method imposes an exact correspondence with the information taken into account (within the precision of convergence accuracy). Because of the uncertainty of the implemented measurements, it is not possible to match all the measurements, this eventuality usually leads to a double determination of the engine calculated parameters such as the primary air flow-rate for instance. A badly reset model then imposes the use of several calculation channels in order to make sure the results are consistent with one another.
However, this method has the advantage of being very sensitive to measured disturbances. Therefore its application is optimum for the analysis of small performance deviations, for instance for engine acceptance tests or endurance tests. It is however necessary to have at one's disposal a reliable model and to choose a reference calculation channel.

5.2.3 Multi-test point identification method

The generalization of the rectangular single-test point identification principles leads to the method called multi-test point.
Obviously, this method has a large field of application:

- The first one is test synthesis.
The use of the multi-test point method necessitates hypotheses as to the form of the correlations to be introduced into the engine model. However, test analysis makes it possible to obtain "stable" (conventional) forms of correlation that can therefore be used from one synthesis to the next. The physical meaning and the accuracy required to match the

measurements then give the user the possibility of refining his choice. The introduction of such correlations can in principle be performed with relevance only at an advanced stage of knowledge of the engine's behaviour.

The multi-test point method then makes it possible to avoid the degradation of results due to the successive identifications specific to the single-test point methods. As a matter of fact, the single-test point methods separate the point analysis and correlation parameter identification phases, thus causing error "stacking". This taking into account of the identification of the correlations for the purpose of method convergence, presents an important aid to facilitate computerization. The analysis of the whole sample of chosen points, and the simultaneous identification of related correlations, is carried out in a single computer job. As a result, use of this method under such conditions greatly improves productivity.

- The multi-test point method also offers an undeniable interest for research on the engine-model's behaviour. Let's suppose that on the basis of a sample of reference test points, we want to analyse the influences (repercussions) of a change in hypothesis, for instance, a modification of the form of a correlation: the coefficients of all the correlations then adapt automatically to reset our model in these new conditions in the best possible way.

It is thus possible to easily assess the interdependence between the various components and maintain at the same time our general approach (taking into account all the operation cases corresponding to the points of the sample).

- The primary idea, to improve our knowledge of the engine's behaviour, consists in increasing the quantity of information available: this can be achieved by installing new sensors.

However, two important obstacles hinder this approach.

. Supplementary instrumentation is not possible for all the engine stations (technological constraints in the hot parts).

. Adding more sensors is a lengthy operation when the casings have not been designed for that purpose.

The multi-test point identification method makes it possible under certain conditions to avoid these limitations. The quantity of required information then comes from simultaneously taking into account the various test points.
The rectangularization of the equation system, having for each individual point, less available information for cross-checking than unknowns, is then obtained by considering a set of test points for which the same unknowns have to be searched for. This particular use is called "rectangular, with a new orientation", in the development of the principles of the method.

5.3 Implementation of the identification methods

In order to implement each of the methods mentioned above, it is necessary to carefully check all the data taken into account, this includes the measurements matched by the method as well as the hypotheses implemented in the model and the choice of the correction factors.

5.3.1 Instrumentation

The quality of the estimates of the engine and component performance during identification depends greatly on the quality of the measurement system. This quality of the measurement system can be estimated through three

criteria: location, number of measurements and uncertainty about the measurements. Indeed, a perfect knowledge of the performance of each engine component would imply having at one's disposal a great number of measurements in each of the engine stations, both upstream and downstream with respect to the components to be characterized. However, this idealistic vision of the measurement system does not resist the reality of the limitations met with when implementing the measurement system on the engine.

Generally speaking, the installation of probes depends on the technical feasibility:
- bosses on the engine to install probes while preserving the mechanical integrity of the engine,
- sensors adapted to the measurement environment, particularly regarding temperature or vibrations.

The number of sensors per measurement station is, barring location problems, a compromise to be made between the minimum number of sensors installed, in order to obtain a good representation of the fluid working in the powerplant, and the maximum number of sensors that will not disrupt powerplant operation.

The uncertainty with regard to the engine parameter gives an indication as to the quality of the measurement chain performed. This uncertainty depends on the type of measurement, namely:
- for an individual measurement, it is the uncertainty related to the measurement chain of the engine parameter (sensor, measuring device),
- for an indirect measurement, it is the calculated uncertainty from the engine uncertainty parameters that have been directly measured, by the error propagation method,
- for an average measurement in an engine station, it is the uncertainty related, on the one hand, to the uncertainty about each individual measurement in the station, and on the other hand, to the mean calculation method in the measurement station.

Each one of these three criteria plays a part in the test analysis process, at different levels. The compromise concerning the number of sensors to be installed in each measurement station will have an influence on the quality and consequently on the uncertainty about the mean measured in the measurement station. The possibilities of installing probes will have an influence on the hypotheses to be implemented for the model, depending on whether the information is available or not, and consequently, on the choice of the resetting coefficients concerning this model. The uncertainty, as we have seen before, is the image of the degree of confidence granted to each parameter that the resolution system tries to match. In this way, the uncertainty determines the quality of the identification achieved whatever the method used.

5.3.2 Choice of hypotheses for resetting the model

The identification of the engine parameters with the measurements makes it necessary, in the same way as a degree of confidence in the measurement is established, to choose and grant confidence to a number of hypotheses concerning the model.

These hypotheses are of two kinds:

- First, the hypothesis of model monodimensionality that imposes a description, necessarily simplified, of the physical phenomena and consequently of the components intervening in the powerplant.
- Then, all the hypotheses made on the knowledge of the actual operation of the powerplant through component tests or engine tests already analysed.

These hypotheses bring us to describe the operation of each component through specific parameters, such as the corrected speed or flow-rate for a rotating component. These specific parameters are generally linked to one

another by relationships established during component tests (component characteristics map).

These descriptions of physical relationships in the model can be questioned during test identification. For that purpose, correction coefficients that can be adapted according to the information available are attributed to all the relationships that are to be questioned.

It seems evident that, depending on the measurements available, it will not be possible to simultaneously identify all the degrees of freedom offered by the engine model. While, either by the relations of equilibrium linking the components inside the engine, or by the measurements sufficiently complete on the components located upstream and downstream, it is possible to attain certain characteristics of a component for which there is no direct measurement, for the other characteristics of that same component, estimates originating from component tests or from specialists calculations will have to suffice.

The choice of the resetting coefficients will then depend essentially on the instrumentation of the engine, on the confidence granted to the estimates obtained by calculation, or by component tests, and on the structure of the engine.

5.3.3 Construction of equation systems

The rematching of the model resetting coefficients to the test engine is obtained by resolving an equation system chosen by the user. This system will consist of:

- unknowns:
  - operating variables (parameters for positioning in component maps, engine control parameters).
  - structural coefficients (correction coefficients).

- equations:
  - compatibility equations (continuity of flow-rates, power equilibrium).
  - identification equations (measured or estimated parameters matched by the values of the model).

Whatever the identification method chosen, the system shall include the compatibility equations ensuring that the modellings of the various components within the model are compatible with each other. Depending on the identification method chosen, the equation system will be more or less developed. Apart from the compatibility equations which are always present, it is the number of identification equations implemented that will differentiate the analysis methods.

We have seen in the previous chapters that the square method, by its very principle and because of the uncertainty inherent to each measurement, imposes that only the measured values leading to a univocal mode for the calculation of the engine's internal parameters shall be matched. As a result, not all the engine measurements available will be processed, depending on the calculation channel used (critical distributor, secondary duct, etc.)

Conversely, if the analysis method chosen is the rectangular method, it is possible to use all the measurements made on the engine simultaneously. The identification equation system will include, in addition to each measurement matching equation, a weight corresponding to the uncertainty estimated about the measured value. Compared to the square equation system, the rectangular system will be much more developed in terms of measurements to be matched and also in terms of information contained in the identification equation, since the latter contains the weight granted to that measurement in the resolution of the system.

5.3.4 Correlations

The identification of p test points using our engine model provides, together with other results, the same number of values for each correction factor. In paragraph 5.1, we emphasized the need to include a summarized form of this quantity of information in the initial modelling; compiling correlations, that express the tendencies of the correction factor changes, fulfils this requirement.

These correlations, characteristic of the engine that provide the test points, are subsequently re-introduced into the model, this model can then be considered as a computerized twin version of the particular engine.

This approach requires explanation:
- the regression methods used smooth the results: the correlations obtained in this way correspond to an approximation of the observed behaviour of the engine,
- converting point data (the discrete set of values of the correction factors) into analytical forms (e.g. polynomial correlations) completes the area of our understanding. The practical remarks given below will enable the validity of this operation to be tested.
- by extrapolating the laws obtained, the areas of operation, that are difficult or even impossible to implement on the test bench, can be simulated.

The simplicity of the process and the ease with which it can be used can only too often conceal certain subtle realities.
We would like to indicate a certain number of recommendations to ensure that correlations can be compiled in the best possible conditions. Rather than giving a complex explanation, it would seem more appropriate to list a few practical remarks:

- Make sure that the following basic statistical conditions are met:

a) are the points satisfactorily distributed over a relatively wide range?
b) does the examination of residuals (deviations between experimental points and correlated points) or reduced residuals (residuals/estimated standard deviation) show any anomalies? It is useful to make a graphic representation of these residuals or of a function of the characteristics that could influence them. If the correlation model is correct, the reduced residuals should lie between approximately -2 and +2, assuming that their mean is zero. They should not be structured in any particular way, but if they are, it means that a structure exists that has not been taken into account, in which case attempts should be made to determine what it is.

- Appropriate correlation parameters should be chosen, i.e. they must be adaptable to other operating cases. Representative parameters can be chosen based on experience and according to physical meaning. They are usually the parameters inherent to the component.

- The correlations should meet both reliability and simplicity requirements. The uncertainty bandwidth of the various correlations should be relatively coherent throughout the model.

- During convergence, the numeric methods can use highly extrapolated areas that have no physical reality.

This border phenomenon should be taken into account when correlations are compiled.

5.4 Comparison of test analysis methods

In order to achieve a comparison of different test analysis methods that highlight the specific qualities of each method, we have to start from the same set of data. This set of data is composed of measurement points, a model

and hypotheses about the overall behaviour of the powerplant.

The measurement points used constitute a homogeneous series distributed over the entire operation envelope, from idle rating to full dry power, for various nozzle sections. The model shared by all the methods is a development model comprising exactly the same physical hypotheses (turbine permeability, leaks, cooling, etc.). The hypotheses on the form of the correlations (on the overall operation of the engine) have been drawn up using the single-test point rectangular identification. Depending on the method used, the number of these hypotheses, concerning both the engine model and its overall behaviour that are called into question varies. How well the model represents the engine depends on the doubt or confidence attached to the data obtained through component tests or tests on previous engines. In both square and rectangular single-test point methods, the hypotheses on the behaviour of the engine components at each point and the incorporation of the measurement uncertainty in the analysis of the test point, determine the quality of the representation. As in the previous paragraph, matching the measurements accurately in the square method means attributing excessive confidence to certain measurements (knowing the uncertainty of these measurements) and therefore, introducing dispersions on the analysis of component and engine performance. This quality can be assessed by the spread of test points around the mean value representing the overall mean behaviour of the engine when correlations are being sought. Figure 12 illustrates this uncertainty in the determination of the mean value for the single-test point square and rectangular methods.
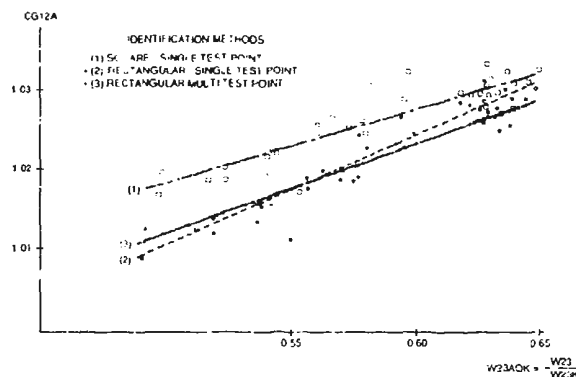
FIGURE 12 FAN FLOW CORRECTION FACTOR
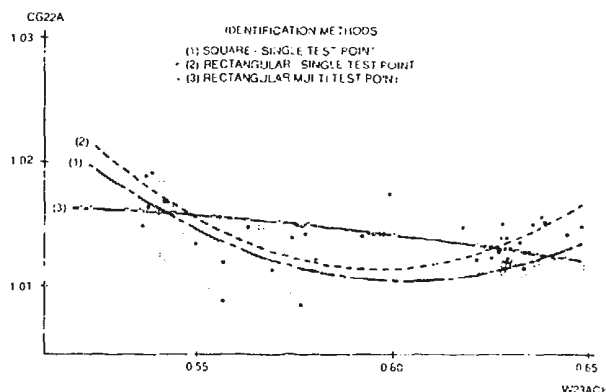
FIGURE 13 FAN EFFICIENCY CORRECTION FACTOR

In comparing single-test point and multi-test point rectangular methods, another type of hypothesis (concerning the overall operation of the engine) is called into question. The quality of the identification must therefore be assessed on the level of coherence between the various correlations. No significant deviations in the description of the component behaviour over the entire envelope are found in figure 12, but in figure 13,

significant deviations do appear when coherence between all the regressions has to be ensured.
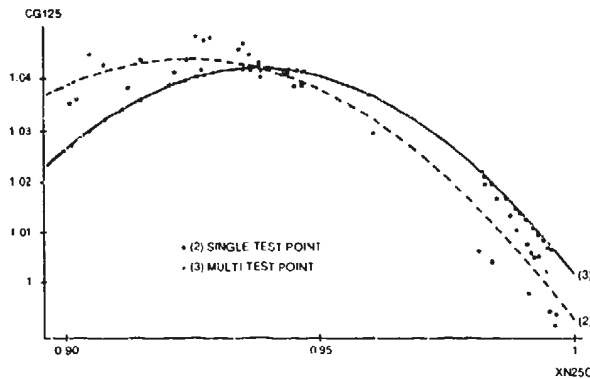
FIGURE 14 - HPC FLOW CORRECTION FACTOR (RECTANGULAR METHODS)
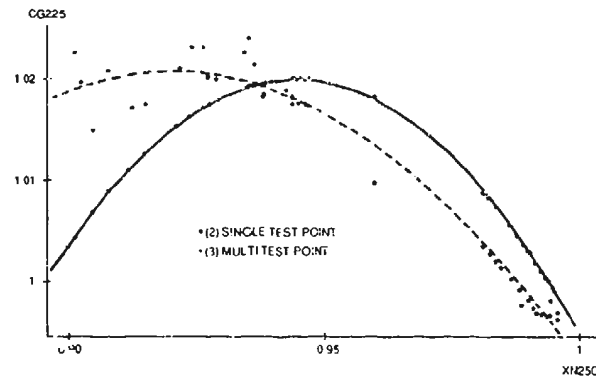
FIGURE 15 - HPC EFFICIENCY CORRECTION FACTOR (RECTANGULAR METHODS)

Similarly, figures 14 and 15 show extremely different engine behaviours, particularly at low rotational speed, depending on whether the coherence between the correlations is included in the analysis or not. Similarly, the comparisons between the single-test point methods, and the single-test point and multi-test point rectangular methods can be made by taking into account the global nature of the identification and repeated prediction process of the engine characteristics.

FIGURE 16 - MEAN OF RELATIVE DIFFERENCE. CONSIDERED IN ABSOLUTE VALUE (%) - P23A -

FIGURE 17 - MEAN OF RELATIVE DIFFERENCE. CONSIDERED IN ABSOLUTE VALUE (%) - T31 -

Figures 16 and 17 clearly indicate characteristic differences between the methods.
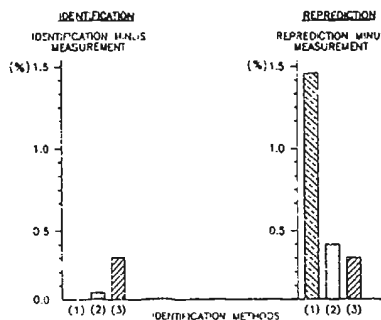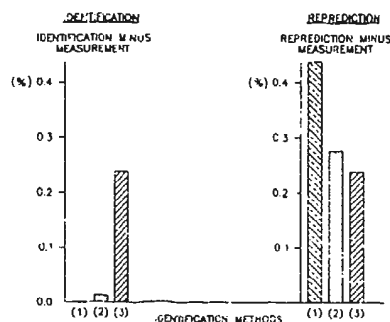Although using the single-test point square method for identification purposes, results in an almost perfect match with the measured value, the hypotheses that are not called into question in this identification and the additional hypotheses made when the correlation is constructed, will introduce imperfections into the engine description leading to a wide confidence band during repeated prediction.
In contrast, in its identification, the single-test point rectangular method takes into account a measurement confidence band that will limit both the measurement accuracy matching and the number of reducer hypotheses used to obtain accurate matching of the measured values. However, the spread of identified points around the correlated mean value, seen in the previous figures, gives an idea of the approximation performed during the repeated prediction of the test point. Incorporating correlation hypotheses during analysis, (concerning the overall engine behaviour) into the multi-test point rectangular method, means that test point identification and repeated prediction are included in the same operation that solves the equation system.

IDENTIFICATION METHODS	MEAN OF RELATIVE DIFFERENCES	STANDARD DEVIATION
(1) SQUARE - SINGLE TEST POINT	0 559	2 091
(2) RECTANGULAR SINGLE TEST POINT	- 0 004	0 529
(3) RECTANGULAR MULTI TEST POINT	- 0 032	0 429
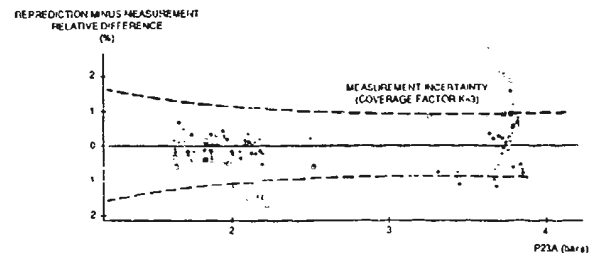
FIGURE 18 - MEASUREMENT REPREDICTION COMPARISON FAN EXIT PRESSURE P23A

IDENTIFICATION METHODS	MEAN OF RELATIVE DIFFERENCES	STANDARD DEVIATION
(1) SQUARE SINGLE TEST POINT	- 0 104	0 529
(2) RECTANGULAR SINGLE TEST POINT	0 059	0 327
(3) RECTANGULAR MULTI TEST POINT	0 011	0 289
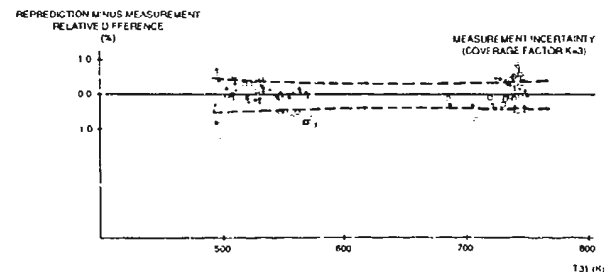
FIGURE 19 - MEASUREMENT REPREDICTION COMPARISON HPC EXIT TEMPERATURE T31

Therefore, we can only assess the quality of the results obtained, using this method, by comparing the repeated predictions with the other methods. Figures 18 and 19 show that:
- major deviations exist between the square method and the rectangular methods, particularly by the bias existing on the mean that is linked to the physical hypotheses incorporated in the square method,
- the deviations between the single-test point rectangular method and the multi-test point method in the dispersion of values around the mean.
Let us emphasize that this set of data is particularly well-suited to the rectangular method. As we have explained in the previous chapters, these methods are best applied at different stages of engine development. It is therefore likely that the deviation between the single-test point methods would have been less significant with a more suitable model.
However, the results obtained illustrate the specific features of each method developed in terms of the quality of both identification and repeated prediction.

6. ANALYSIS BY IDENTIFICATION OF TRANSIENT STATE TESTS

An identification method applied to transient state conditions will allow us to:

- improve our knowledge of the engine during development.

- cut the costs of acceptance tests.

6.1 Use:

6.1.1 Component characteristics maps

Some areas of these maps that are inaccessible on the engine, under steady state conditions, could be identified in the engine context by this method. This is the case, in particular, for the HP core and the LP turbine.

- HP compressor:
The areas located underneath and to a greater extent above the steady state working line: the conditions under which surge occurs will be better known.

- Combustion chamber:
The operation at very high fuel to air ratio (FAR) (acceleration) and high air loading (deceleration).

- HP turbine
High corrected speeds (deceleration) and low corrected speeds (acceleration).

- LP turbine
High corrected speeds and low loads (deceleration), low corrected speeds and high loads (acceleration).

6.1.2 Thermal and pneumatic phenomena

Analysis by identification of transient state tests will allow us to improve our knowledge of thermal phenomena (clearances, heat flux, variations of ventilation flow rates) as well as their impact on the aerodynamic characteristics of the components (flow rates, efficiency and operating limits).
They will also allow us to identify pneumatic capacity phenomena.

6.1.3 Characteristics of control

It will be possible to identify the actual characteristics of control in the engine context, and in particular the delays and the response of the main sensors and actuators.

6.1.4 Flight tests

It is very difficult to obtain very steady operation of the engine.
The use of identification at transient state conditions is therefore advisable, even to treat tests usually considered as steady.

6.1.5 Acceptance tests

The use of this method will allow us to check the characteristics of engines without having to wait for their complete thermal stabilization (short duration testing). This means saving time and fuel.

6.2 Principles of the method

The multi-test point identification method is used at present to identify real-time simulation model on detailed thermodynamic model.
This identification on unbalanced independent test points is only possible because the thermodynamic model provides derivatives with respect to time which are reliable enough.
Whatever way measurements are made, the tests do not provide, with respect to time, sufficiently reliable derivative values, pin-point identification criteria must be replaced by integral criteria.

Therefore, we will look for the minimum of:

$$\int_{t1}^{t2} \Sigma \left(\frac{Y_{model} - Y_{measure}}{\sigma} \right)^2 dt$$

The search for this objective being coupled at every instant with the resolution of:
- compatibility equations
- implicit differential equations

7. THERMODYNAMIC SPECIFICATIONS OF THE ENGINE CONTROL SYSTEM

7.1 General principles

Using the identification methods described above for the test analysis (component tests on component test bench, engine tests in ground/altitude test cells and on flight test bed), the influence of the various factors on the operation of the components can be determined with increasing accuracy and quantified. The compressor reference aerothermodynamic characteristics can be associated with:

- variations in the setting schedule for the HP stators and the LP inlet guide vane,

- the effects of the air bleed. the viscosity, the unstationary distortion of flow at the compressor inlet and the transient variation of the thermal radial clearance, on the mass flow rate and efficiency characteristics, and the position of the compressor surge line. All these informations are either predicted, using theoretical calculations, or emanate from previous experience, or are defined, on the basis of tests performed on the engine being developed, and constitute the logic of the engine thermodynamic calculation code.

The incorporation of digital computers with substantial computing power into the engine control systems provides new light on the thermodynamic principles of powerplant control.
Using these new airborne calculation systems, it is possible to express the various set-points for the fuel flow, the nozzle area and the position of the compressor stators as a function of an increased number of parameters. The ation of the set-points now incorporate a number of factors describing the environment and operation of the engine, allowing the controlled processes to be managed more effectively. Interconnection with the aircraft systems can be envisaged, with the innovation of an engine control system extensively integrated with the aircraft.

Furthermore, we must seek to benefit from the greater flexibility permitted during the development of the software making up the calculation logic of these electronic systems. In order to exploit the flexibility of the software, a highly modular logic must be selected, with a specific function assigned to each module. This ensures that the software is readable and transparent, facilitating developments. It is advisable to closely model the functions and physical representation of the various modules, involved in the calculation of the set-points, on elements of the modelling of the engine thermodynamic programme. This ensures that it is relatively simple to apply the progress, made in the identification studies to the control logic, by incorporating the results of the modelling into the various modules. This concept is applied within SNECMA for the design and development of the software for the calculation of the control set-points for the advanced technology M88-2 military engine.

The designer aims to optimize the operating range permitted by the components (compressors, combustion chamber, afterburner), while respecting their limitations. The highest possible level of steady and transient state performance is sought. To this end, it is vital to limit the margin consumption with respect to these limitations: surge margins for the LP and HP compressors, combustion flammability limits (rich blow-out, lean flame-out).

The following paragraphs describe the principles of:

- management of the fan surge margin by means of nozzle control

- control of the operating point in the HP compressor map during acceleration using the main fuel control.

Particular attention is paid to the incorporation of modelling derived from identification studies in logic.

7.2 Management of the fan surge margin by means of nozzle control

At partial rating and full throttle, the control features selected for the M88-2 engine are as follows:

- the power lever position generates an LP r.p.m. set-point by action on the generator fuel flow.

- the position of the operating point in the fan characteristics map determines the position of the nozzle.

Various parametric studies have justified the choice of these options. For a given flight condition, the LP r.p.m. is representative of the total engine air flow, which is one of the thrust factors. Furthermore, for a given fan corrected speed, the air flow dispersion is very moderate on new engines during acceptance testing and, during operation, the evolution of the air flow remains practically unchanged. The control of a fan operating point, through LP r.p.m. and MACH number set-points in the fan discharge station, has two main advantages:

- when the engine is controlled in this way, the thrust is hardly affected by the variations in flow rate and in the efficiency of the core engine or by modified air bleed or power extractions. The thrust is principally affected by variations in the characteristics of the fan. In this way, the operational engine performance is optimized, with the thrust maintained by natural correction of engine ageing. This feature will be retained, provided that the turbine temperature remains below the red line.

- for a $(P_{23} - PS_{23})/P_{23}$ type set-point, the fan pressure ratio only depends on minor variations in flow rate and and efficiency and is therefore independent of the evolutions of the other components located downstream from the fan. It is possible to program the position of the low pressure compressor operating point, as a function of various engine environmental and operating factors, in order to effectively manage the fan surge margin.

For these concepts, we use the widest possible range of the fan-characteristics map. In order to optimize performance, we define the full throttle value for the LP r.p.m. using a function generator dependent on the flight parameters. Similarly, using fan surge margin set-points we can limit the dimensioning margin consumption considerably and therefore optimize use of all the possibilities of the LP compressor.

By checking the operating point of the fan, we can control its surge margin by incorporating a logic that calculates the fan surge margin PRS2.

- The characteristics reference map of the fan is converted into a network

$$(P_{23} - PS_{23})/P_{23} = f(XN2R, PRS2)$$

This reference corresponds to the engine condition – mean state (dispersion), new, for engine static conditions, with low inlet distortion. For these conditions, the position of the fan surge line will serve as a reference for the various calculations of the surge margin PRS2. Extension to high altitude and low MACH flight conditions necessitates the introduction of viscosity effects. These effects reduce the air flow-rate W2AR as well as the efficiency of the fan and consequently cause a slight migration of the operating point (the latter being defined by parameters XN2, $(P_{23}-PS_{23})/P_{23}$). An LPC surge margin correction expressed as a function of the REYNOLDS index is then incorporated. An other correction of the representativeness of the measurements made in station 23 (fan outlet) allows us to take into account the various deviations that appear in a deterministic way and can therefore be modelled, between the pin-point measurements that are carried out and average parameters from a thermodynamic point of view. Thus, a bi-univocal correspondence is achieved between parameters PRS2 and $(P_{23} - PS_{23})/P_{23}$ (figure 20).
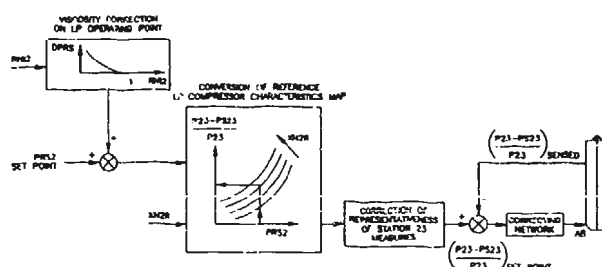
FIGURE 20 - M88-2 EXHAUST NOZZLE CONTROL THROUGH FAN SURGE MARGIN SET POINT

- The principle of introducing modelling, that originates in the detailed thermodynamic calculation code, into the control logic was applied for programming the fan aerodynamic stability stack-up. Figure 21 lists the main destabilizing effects taken into account in the fan aerodynamic stability stack-up in order to envisage extreme operations of the fan. The main factors have been modelled, under a simplified form, by using a number of indicators and describers that characterize the times of appearance and amplitudes of each destabilizing effect.

. The lowering of the surge line in high altitude and low MACH flight conditions is taken into account by an expression that depends on the REYNOLDS index. The effects due to the uncertainties concerning measurements on the position of the operating point, which increase as the measured pressures decrease, were assimilated to this modelling.

. The effects of the engine dispersion and ageing of the characteristics of components such as compressors, turbines, on the fan operating point and surge line, cannot be modelized and are constantly taken into account, in the same way as a stability stack-up. It is the same for the residual error on the representativeness of the measurements in station 23.

. The contribution of distortion is introduced by a modelling of describer IDC2 of the unstationary distortion level, followed by an image of the fan's behaviour with regard to this distortion level. The prediction of describer IDC2 rests on wind tunnel tests, and subsequently, on tests done directly on the aircraft. It is based on the knowledge of flight conditions, corrected air flow-rate, real and anticipated angles of attack and of aircraft side-slip. The sensitivity of the fan

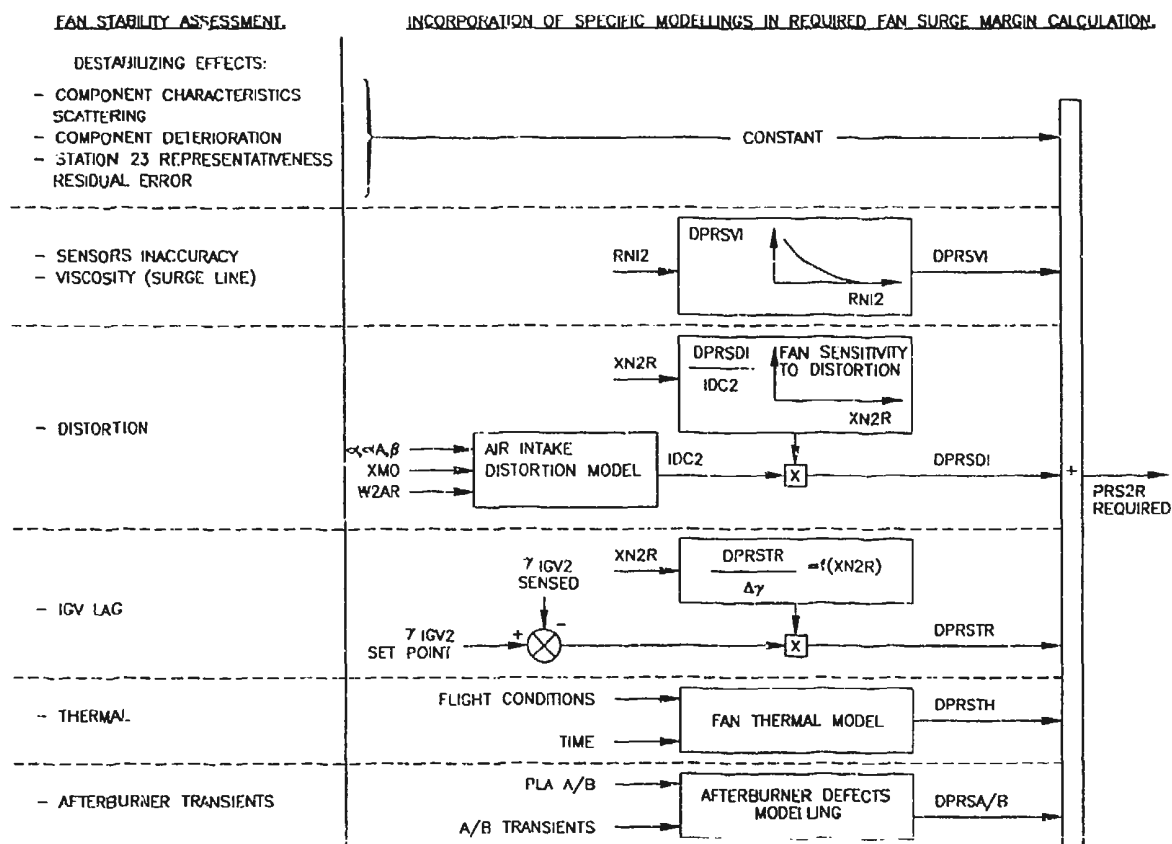FIGURE 21 — M88-2 MODELLING OF LP COMPRESSOR AERODYNAMIC STABILITY BALANCE IN EXHAUST NOZZLE CONTROL.

to distortion, essentially as a function of corrected speed, is extracted from measurements on the partial test bench, with an air supply that presents the unstationary distortion characteristics found on the aircraft.

The shortcomings in the positioning of the inlet guide vane are also modelled, and so are the fan surge margin consumptions on afterburner transients. Also the contribution of the thermal response of the LP compressor parts, to the characteristics of the LP compressor itself, is described more briefly (substantial effect during the various phases of a subsonic flight following a long supersonic flight).

The value PRS2R thus obtained, by summing up each surge margin consumption, reflects the required fan surge margin in the function of the various scenarios originating in the environment of the fan.
- A basic setting of the engine in the form of a surge margin PRS2P set-point, depending on the flight conditions and speed XN2R, is introduced in order to fix the reference level of the engine performance. The required fan surge margin PRS2R being calculated permanently, the control of the nozzle position is performed by a resultant set-point:

PRS2 = Max (PRS2P, PRS2R)

Such a structure for the elaboration of nozzle set-points makes it possible to distribute in a flexible way the engine performance level for usual flight conditions and to ensure at the same time the protection of the engine (with regard to the fan surge) under extreme conditions. By considering the amplitude and the instants that the most destabilizing effects occur (and not just distortion) in the calculations of the required PRS2R surge margin, it is possible to perform a good matching setting of the fan advisedly.

7.3 Gas generator acceleration control

The same principle of introducing modelling originating from the detailed thermodynamic calculation code into the control software has been applied to the generator acceleration logic, in order to optimize acceleration times and comply at the same time with the high pressure compressor surge limitation. As for the fan, the basic idea consists in incorporating in the fuel set-point calculations a modelling of the migrations of the transient state operating point in the HP compressor characteristics map, and of the supposed variations of the surge line during destabilizing scenarios.
The expression retained for the generator acceleration schedule is as follows:

$$\frac{WF32}{P_{S32}\,(\theta_{23})^{n(T41)}} = f\,(XN25R)$$

This expression was elaborated in such a way that it should provide a bi-univocal correspondence, at a given XN25R corrected speed, between a level of the acceleration schedule and an operating point in the compressor characteristics map, whatever the value of the temperature T23 at the compressor inlet. For this purpose, it was necessary to introduce a variable n exponent that is a function of the estimated temperature T41, at the inlet of the HP turbine rotor, to take into account the dissociation effects that are specific to operations at high turbine temperatures.

The basic level of the acceleration schedule is then corrected according to the amplitudes of several effects which are destabilizing as far as the HP compressor is concerned. Each amplitude is quantified in terms of the variation of the DPRS25 surge margin (with respect to a

reference surge line) that applies both to the lowering of the surge line and to the migrations of the transient state operating point in the HP compressor characteristics map.

The main corrections of the acceleration control schedule, envisaged for engine M88-2 are: (figure 22)
- viscosity effect on the HP compressor.
- influence of the amount of airbleed (necessary for the aircraft).
- the distortion of flow at the HP compressor inlet.
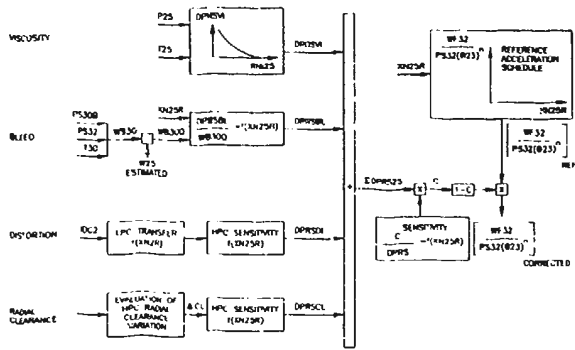- the amplitude of the thermal effects causing variations in the radial clearance.

FIGURE 22 - M88-2 ADAPTIVE ACCELERATION SCHEDULE

- Viscosity effect on the HP compressor:
The lowering of the surge line and the slight migration of the transient state operating point (with constant acceleration schedule), that is due to the decrease of the corrected flow-rate and of the efficiency of the HP compressor during operation at a low REYNOLDS index, are taken into account under the form of a specific DPRSVI correction expressed as a function of the REYNOLDS index at the HP compressor inlet. Other considerations, such as the observance of required surge margins (originating from HP compressor aerodynamic stability stack-ups), the distribution of acceleration times in the flight envelope and HP surge risks (in case the engine operates in a degraded mode or fails, it is preferable for surges to occur first at high rather than low altitude) are also included in this correction.

- Aircraft air bleed extraction:
A real constant transient surge margin rarely occurs with a constant acceleration schedule, whatever the amount of air bleed necessary for the aircraft. In order to attain that objective, the amount of bleed air is measured by a venturi system installed on the engine; a fraction WB30Q = WB30/W25 of the amount of air bled is then calculated on the basis of the estimate of the primary air flow-rate (continuity in the HP turbine nozzle deemed critical); the correction is obtained using the sensitivity of the real surge margin to the percentage of the bleed air flow-rate. A residual surge margin during the acceleration is thus achieved and it is independent of the amount of bleed air. This character presents a definite interest in high altitude and low MACH number flight conditions, as the fraction of WB30Q flow-rate taken is then substantial and the HP compressor surge margin is never too great under these dimensioning conditions. Such a correction improves the generator acceleration times in an airbleed situation.

- distortion of flow in front of the HP compressor:
The transfer, through the fan, of the unstationary pressure distortion at the inlet of the engine, characterized by IDC2 index, has repercussions at the inlet of the HP compressor in terms of pressure and temperature distortions that essentially cause the lowering of the HP compressor surge line. The modelling of this mechanism is introduced by separating transfer phenomena through the fan (depending on the LP XN2R corrected speed) from the HP compressor sensitivity to residual pressure and temperature

distortions (depending on the HP XN25R corrected speed). Such a correction favours accelerations with low distortion and at the same the time fulfils the absence of HP compressor surge with high distortion levels.

- correction of radial clearance due to thermal effects:
Following a first acceleration, the temperature of the flowpath increases sharply in a very short time and the radial clearance increases with time as compared to the thermal steady state, due to the differences in the time constants of metal temperature responses (hence in radial displacement) of the HP compressor casing (faster) and discs (slower).
A throttle operation, consisting of a deceleration that is immediately followed by a new acceleration at the instant of radial clearance increase ("bodies transient") is then dimensioning with regard to the HP compressor surge because the surge line of the latter is lowered following its operation with increased radial clearance. The method for taking this effect into account uses a simplified formulation of the average temperatures of parts (case, disk), hence of displacement, related to a sensitivity to the radial clearance of the HP compressor surge line.

The calculation of the metal temperature (casing, disk) in thermal transient, reposes on a formulation of this type:

$$T_{t+\Delta t} = T_t + (T_{s_{t+\Delta t}} - T_t)(1 - e^{-\frac{\Delta t}{\tau}})$$

where the metal temperature at time $t + \Delta t$ is determined by recurrence using temperature at time t and the estimate of the metal temperature corresponding to the fictitious thermal steady state. This temperature, and the time constant τ, are expressed by flow parameter functions such as T25, T30, P25, W25 and XN25. A similar formulation is applied for the calculation of hot part thermal stresses for the control of the residual potential of the parts. This formulation of metal temperatures in thermal transient state is applied to an upstream stage and a downstream stage of the HP compressor, for the casing and disk. Considering the variations in radial clearance with respect to a reference constituted by steady conditions from the thermal point of view, instantaneous transient state clearance variations can be expressed as follows:

$$\Delta CL = \Sigma\ \alpha(T_{s_{t+\Delta t}} - T_{t+\Delta t})$$

     casing
     blade/vane
     disk

The introduction of this type of correction on the acceleration schedule does not modify the dimensioning acceleration performed at maximum thermal clearance. Nevertheless, it makes it possible to improve the acceleration time in simple acceleration mode in the ordinary and less strict control lever scenarios.

The combination of the 4 corrections described above, expressed in DPRS25, is then translated into a correction to be made on the reference acceleration schedule, resorting to a sensitivity depending on the XN25R corrected speed.

This description of the control of the fan surge margin and of the acceleration schedule modulation is an illustration, in a control software, of the types of modelling inferred from a detailed thermodynamic calculation code, the identification of which was first based on tests.

8. CONCLUSION

The design and development process of a propulsion system is strongly influenced by the quality of modelling and interpretation of the existing aerothermodynamic phenomena permitted by the thermodynamic calculation code.
The first part of this document, concerning the modelling of compressor/turbine characteristics maps, describes a new representation providing an improved expression of MACH similitude, irrespective of the conditions upstream.

To achieve in-depth knowledge of the real characteristics of the components, an extremely detailed analysis of the test results is required. The methods described in this document for identifying the thermodynamic calculation code with the measurements vary depending on the quantity of information considered: number of measurements, number of test points, etc. These methods are applied to the analysis of the tests performed on the M88-2 engine. These types of analysis methods are relatively powerful and enable the maximum amount of information to be extracted from engine tests. One could envisage a potential application of these methods in engine-condition monitoring.

An example of one of the applications benefiting from our knowledge of physical phenomena existing in the engine, which has been acquired through the use of these identification methods is described in the latter part of this document, i.e. the integration of specific modelling in the engine control software of the M88-2 engine.

Acknowledgements

The identification and analysis methods presented in this document were developed at SNECMA as part of an Advanced Research and Studies programme conducted under the authority of Mr. A HABRARD and were put into operation in thermodynamic studies through the impetus given by Mr. M BERTHIER, head of the Thermodynamics and Performance Department.
The authors would like to thank Mr. T. LANDEL and Mr. R. LETURCQ for their contributions concerning numeric calculations and for their assistance in preparing this document. The authors would also like to express their gratitude to SNECMA's General Management and to the Service Technique des Programmes Aéronautiques for giving their permission for this document to be published.

REFERENCES

1. Oates, G.C., "Aerothermodynamics of gas turbine and rocket propulsion", AIAA Education Series (revised and enlarged edition), 1988.

2. Oates, G.C.
"Aerothermodynamics of aircraft engine components", AIAA Education Series, 1985.

3. Oates, G.C.
"Aircraft propulsion systems technology and design", AIAA Education Series, 1989.

4. Covert, E.E.
"Thrust and drag: its prediction and verification", AIAA Progress in Astronautics and Aeronautics - Volume 98 - 1985.

5. Cohen, H., Rogers, G.F.C., Saravanamuttoo, H.I.H. "Gas turbine theory" (Third edition), Longman Scientific & Technical, March 1986.

6. Gordon, S. NASA Lewis R.C.
"Thermodynamic and transport combustion properties of hydrocarbons with air", NASA TP 1906/7/8/9, 1982.

7. Zimmerman, O.T. and Lavine, I.
"Psychrometric tables and charts" (second edition), Industrial Research Services Inc., Dover 1964.

8. Samuels, J.C., and Gale, B.M.
"Effect of humidity on performance of turbojet engines", NACA TN 2119, June 1950.

9. Grabe, W, National Research Council - Canada. "Humidity effects on gas turbine performance", Technical Report TR-ENG-003, 1988.

10. Duponchel, J.P. and Leturcq, R.
"Humidity effects on gas turbine performance - SNECMA methodology", AGARD Committee 72-5, Madrid, May 1990.

11. Koenig, R.W., and Fishbach, L.H., NASA Lewis R.C., "Geneng - A program for calculating design and off - design performance for turbojet and turbofan engines", NASA TN D-6552, February 1972. "Geneng II - A program for calculating design and off design performance of two - and three - spool turbofan with as many as three nozzles", NASA TN D-6553, February 1972.

12. Sellers, J.F., and Daniele, C.J., NASA Lewis R.C., "Dyngen - A program for calculating steady - state and transient performance of turbojet and turbofan engines", NASA TN D-7901, April 1975.

13. Sadler, GG, and Melcher K.J., NASA Lewis R.C., "DEAN: A program for dynamic engine analysis", NASA TM 87033, July 1985.

14. Habrard, A.G., SNECMA
"Characterization of components performance and optimization of matching in jet-engine development", AGARD L.S. 83, June 1976.

15. Rick, H. and Muggli, W., Technische Universität München.
"Generalized digital simulation technique with variable engine parameter input for steady state and transient behaviour of aerogas turbines", AGARD CP324, Engine handling, Paper 26, October 1982.

16. Hörl, F., Technische Universität München,
"Systemtheoretische methode zur dynamischen zustandsüberwachung von gasturbinen", L.F.A. TU München, 1987.

17. Feidt, M.
"Thermodynamique et optimisation énergétique des systèmes et procédés". Techniques et documentation Lavoisier, 1987.

18. Villermaux, J.
"Le génie des procédés". La Recherche, Septembre 1991.

19. Tomassone, R., Lesquoy, E., and Millier C.
"La régression - Nouveaux regards sur une ancienne méthode statistique". INRA Masson 1983.

20. Couot, J., ENSAE 1973.
"Eléments de la théorie de l'approximation - Résolution des équations linéaires".

21. Abernethy, R.B., and Thompson, J.W.
"Handbook - Uncertainty in Gas Turbine Measurements". AEDC - TR - 73-5, February 1973 (revised January 1980).

22. "Definitions and calculations of errors - Uncertainty of measurement". Bureau de Normalisation de l'Aéronautique et de l'Espace B.N.A.E. Recommandation R.M. Aéro 800 01B, Avril 1986.

23. Abernethy, R.B. and ai,
"Uncertainty Methodology for In-flight thrust
determination". SAE pape   31438, October 1983.
"Application of In-flight thrust determination
uncertainty". SAE paper 831439, October 1983.

24. Abernethy, R.B., and Ringhiser, B. - Pratt and
Whitney Engineering Div.
"The history and statistical development of the new
ASME - SAE - AIAA - ISO Measurement Uncertainty
Methodology". AIAA-85-1403, July 1985.

25. Poti, N.B. and Rabe, D.C. AFWAL Wright-Paterson
AFB.
"Verification of compressor data accuracy by
uncertainty analysis and testing methods".
Journal of turbomachinery, April 1988, Vol. 110,
pp 255-269.

26. Cohen, E.R.
"Guide to the expression of uncertainty in
measurement". ISO/TAG4/WG3, July 1990.

27. "Recommended practices for measurement of gas
path pressures and temperatures for performance
assessment of aircraft turbine engines and
components". AGARD-AR N° 245, June 1990.

28. "Suitable averaging techniques in non-uniform internal
flows". AGARD-AR 182, June 1983.

29. "The uniform engine test programme".
AGARD-AR 248, February 1990.

30. "Measurement uncertainty within the uniform engine
test programme". AGARDograph N° 307, May 1989.

31. "Comparative engine performance measurements".
AGARD L.S. N° 169, May 1990.

32. Stamatis, A., and Papailiou, K.D., - Athens National
Technical Univ.
"Discrete operating conditions gas path analysis"
AGARD CP 448, June 1988, paper 33.

33. Stamatis, A., Mathioudakis, K., Berios, G., and
Papailiou, K.D.- NTUA.
"Jet engine fault detection with differential gas path
analysis at discrete operating points". ISABE 89-7133.
9th International Symposium on Air Breathing
Engines, Athens, September 1989.

34. Stamatis, A.,Mathioudakis, K., and Papailiou, K.D.-
NTUA.
"Adaptive simulation of gas turbine performance".
ASME paper 89-GT-205.

35. Stamatis, A.,Mathioudakis, K.,Smith, M. and
Papailiou, K.D.- NTUA.
"Gas turbine component fault identification by means
of adaptive performance modeling". ASME paper
90-GT-376.

36. SAE Committee S-16
"Gas turbine Engine inlet flow distortion guidelines".
ARP 1420, March 1978.

37. SAE Committee S-16.
"Inlet total pressure considerations for gas turbine
engines". AIR 1419, June 1981.

38. Williams, D. D., Rolls-Royce.
"Review of current knowldge on engine response to
distorded inflow conditions". AGARD CP 400,
September 1986.

39. Yugov, O. K. Institute of Aviation Motors - Moscow,
USSR.
"Some aspects of development of power plant
optimum control to increase aircraft fuel efficiency".
AIAA 83-7040.

40. French, M. W. General Electric Co.
"Development of a compact real-time turbofan engine
dynamic simulation". SAE 821401, 1982.

41. Brown, H., and Fisk, W. General Electric Co.
"Integrated flight and propulsion operating modes for
advanced fighter engines". ASME 83-GT-194.

42. Vizzini, R. W. Naval Air Propulsion Center - Trenton -
N. J.
"Integrated flight/propulsion control system
considerations for future aircratf applications".
Purdue University short course on engine-airframe
integration 8/1984.

43. Ray, R. J. and Myers, L. P. NASA Ames R. C.
"Test and evaluation of the HIDEC engine uptrim
algorithm". NASA TM 88262, July 1986.

COMPONENT PERFORMANCE REQUIREMENTS

H.I.H. Saravanamuttoo
Department of Mechanical and Aerospace Engineering
Carleton University
Ottawa, Canada K1S 5B6

SUMMARY

Component data are essential for modelling the overall performance of gas turbines. The component characteristics are not easily obtained, and much of the data is proprietary and not available in the open literature. Several methods are available for estimating component characteristics and are briefly described. The requirements of users and manufacturers are quite different, but both can produce fully credible performance models.

SYMBOLS

m	mass flow rate	U	blade speed
T	temperature	C_a	axial velocity
p	pressure	C_w	whirl velocity
ψ	temperature coefficient	α	stator air angles
ϕ	flow coefficient	β	rotor air angles

1.   BASIC FORM OF CHARACTERISTICS

The component characteristics for a turbomachine basically show the relationship between flow, pressure ratio, efficiency and rotational speed over the complete operational range and typical curves were shown in Chapter 2 for compressors and turbines. The nozzle characteristic can be predicted from fundamental gas dynamics, and the ideal characteristics obtained are a good starting point for engine performance modelling. Most modern engines are turbofans and the shape of the fan characteristic is to some extent dependent on the application. In the case of military turbofans, the fan pressure ratio is relatively high and the by-pass ratio low. For a typical fighter engine the fan would have 3 - 4 stages with a pressure ratio of 3.5 - 4.0 and a by-pass ratio of 0.3 - 0.5; the low by-pass ratio is needed to minimize frontal area for high speed. If longer range is required, the by-pass ratio may increase to about 1.0 and the fan may have 2 - 3 stages. The characteristics for these high pressure ratio 'fans' are basically the same as for those for a conventional axial compressor. In the case of a high by-pass ratio turbofan, however, a single stage fan is always used in civil aircraft because of both noise and weight considerations and this results in a rather different shape. The characteristic for a single stage fan from a small turbofan is shown in Fig. 1 from Ref. (1), showing the much flatter shape of the constant speed lines.

It was mentioned earlier that component characteristics are proprietary to the engine manufacturer and are seldom published in the open literature, especially during an engine development program; on the rare occasions when they are published it is normally several years after the successful completion of the development program. One widely used method for preliminary estimation of compressor characteristics is the use of <u>Generalized Compressor Characteristics</u>, an example being shown in Fig. 2 from Ref. (2). In this case pressure ratio, flow, speed and efficiency are related in terms of the Design Point values, with the generalized characteristic obtained from a number of compressors of differing flows and pressure ratios designed using similar aerodynamic design methods; this method, although essentially crude, is an excellent starting point for compressors of moderate pressure ratio. The compressor characteristics of the LM1600, the industrial derivative of the GE F404, were successfully estimated by Zhu and Saravanamuttoo (3) using this simple approach; the model developed gave excellent agreement with field test data from a pipeline operator. The model was based on openly published overall performance data with no information of any sort obtained from the manufacturer.

For preliminary model development, in the absence of any turbine data, turbine characteristics can be estimated using the design point values of m, T and p and the basic shape of the nozzle curve calculated from ideal gas dynamics; this can be done because the flow characteristic of the turbine stators, or nozzles, is the same as that of a propelling nozzle. It is for this reason, of course, that a shaft power engine can be developed from a jet engine by substituting

a power turbine for the final nozzle. Conversely, a nozzle can be substituted for a power turbine; this principle is widely used for the overhaul of aero-derivative gas turbines, where the gas generator is brought back for overhaul and tested as a jet engine, with the power turbine and driven load left in the field. Turbine characteristics based on nozzle curves were successfully used in (2).

A preliminary model using these simple methods is a good starting point, and the model could be updated and refined as test results become available either from component rig testing or overall engine testing. The methods used to refine the model would be different for the manufacturer and a user; the manufacturer would have much more detailed test results, with more parameters measured during test bed development, where the user would normally only have the production engine instrumentation fit.

2. USE OF TEST RIGS TO DETERMINE CHARACTERISTICS
Compressor and turbine characteristics can be experimentally determined using component test rigs. This, however, presents considerable difficulties and is not always done; some of the problems encountered will be outlined.

2.1 Compressor Test Rigs
Ideally a compressor test rig would have a bellmouth intake giving a uniform, undistorted flow at the compressor face, and a throttle or butterfly valve in the outlet duct permitting the compressor to operate over the required range of pressure ratios. The compressor drive should be capable of precise speed control over the operating range, making it possible to carry out testing at any selected speed with the delivery pressure increased in small increments until the surge point is determined.

The first problem encountered is the very large power input required at Sea Level conditions. As an example, the Olympus 593 at take off has a mass flow of about 200 kg/s and a pressure ratio of about 15; the power requirements are about 25 MW for the low pressure compressor and 75 MW for the high pressure compressor. A typical large fan will have a flow of 700 kg/s and a pressure ratio of 1.6, giving a power requirement of about 32 MW. These powers are prohibitive for electric motor drive, and some modern compressor rigs are driven by an industrial gas turbine; but even then it is still not usually possible to test at full power.

The first possible solution is to throttle the intake to the compressor, giving a reduction in inlet pressure and hence mass flow. Unfortunately, a major decrease in inlet pressure means a similar reduction in density and hence Reynolds Number. Dimensionless analysis reveals that the performance of turbomachinery is dependent on both Mach Number and Reynolds Number; in particular, performance decreases at low values of Reynolds Number due to the increasing effect of viscous forces. The overall result is that reducing the power requirement can introduce significant effects on the measured performance, which must be allowed for in predicting the compressor efficiency at the full Reynolds Number.

Another approach, more commonly used with single stage fans, is to make use of scale model fans; by decreasing the diameter, the mass flow can be reduced with a corresponding decrease in power input, with the rotational speed increased to give the correct tip speed. The use of models permits operation at the correct Mach and Reynolds Numbers with considerably reduced power requirements. The cost of constructing an accurate scale model of the fan to be tested is obviously high, but this appears to be the only feasible way of obtaining fan data over the complete running range.

Another problem is that the mechanical configuration and thermal loading of a compressor on a test rig may be significantly different to those on an actual engine; this can result in differences in tip clearances which can have a major effect on compressor performance, affecting both efficiency and surge margin. Some companies test compressors on a gas-generator rig using the actual engine configuration; a variable nozzle is then required to permit operation over the operating range, which is restricted by turbine inlet temperature operating limits and the need to avoid surge.

Further problems occur with multi-spool compressors, where each compressor may be influenced by the other. The high pressure compressor, for example, may have a distorted intake flow resulting from the presence of the inter-compressor support frame; thus the actual performance of the compressor on the engine may be inferior to the results predicted by rig tests. Conversely, the performance of the low pressure compressor could be improved due to the beneficial effects of the high pressure compressor in removing the flow. Stubner (4) of Pratt and Whitney has described the construction of a twin-spool compressor rig; this approach has not been widely used, and requires careful matching of the two rotor speeds corresponding to actual engine operation.

A limited amount of compressor data may be obtained from actual engine testing; this, of course, is due to the fact

that data can only be collected along the operating line, giving a unique operating point for each speed for an engine with fixed geometry.

2.2 Turbine Test Rigs

Turbine test rigs present even more problems than compressors. The most obvious difficulty is the provision of a steady flow of gas at the required pressure and temperature. The next major problem is the need for a suitable dynamometer with the ability to measure power output very accurately, this being needed for accurate evaluation of turbine efficiency. Turbine test rigs may be tested with 'cold' air, using a compressed air supply, but the flow rate available is seldom sufficient for full scale testing; in addition, the intake air must be partially heated to prevent moisture in the air from freezing in the turbine following expansion to a low pressure. It will readily be recognized that running a turbine rig at low temperatures will result in major problems in establishing realistic tip clearances, giving rise to large errors in performance.

Air cooled turbines are universally used for the high pressure stages of large, high performance engines and the discharge of cooling air can have a considerable effect on turbine efficiency. It is therefore necessary to provide appropriate levels of cooling flow at the correct pressure and temperature, greatly increasing the difficulty of realistic testing of turbines.

Turbines may be tested on gas generator rigs, permitting operation under realistic engine conditions including secondary and blade cooling flows. It should be remembered that for the case of a choked downstream component (power turbine or propelling nozzle), the gas generator turbine will operate at a fixed non-dimensional point; this means that only a restricted running range can be obtained on a gas generator rig, but that is exactly what happens in an engine. Power turbines, on the other hand, can operate over a wide range of speeds and loads and would be best tested on a fully instrumented engine driving a dynamometer.

Turbine performance is also a function of Reynolds Number, and may be significantly affected at high altitudes. Typical variation of Reynolds Number with flight condition for the low pressure turbine of a civil turbofan (5) is shown in Fig. 3.

2.3 Rig to Engine Differences

The foregoing has outlined the main reasons why component characteristics obtained from rig tests may differ from the results actually achieved in complete engines, the prime reason being the difficulty of simulating actual engine conditions on rigs. Further differences may also occur when installed in an aircraft as a result of intake flow distortion; the same engine may exhibit different surge margins and operating characteristics in different aircraft. Engine performance may also be affected by location, a good example being the centre engine of a three engined installation, which is usually situated behind a lengthy S-bend intake. Methods of accounting for rig to engine differences will be described in a later lecture.

It can be seen that there are considerable difficulties in obtaining accurate component data even when well instrumented test rigs are available. It should be noted that test rigs are primarily concerned with performance at the important operating conditions such as cruise or take-off. The surge margin must be established over the range from idle to maximum power, but in general not too much attention is paid to the low speed end. Very little useful information is found at sub-idle speeds, but this is essential if a model capable of simulating start up is required.

3. USE OF STAGE CHARACTERISTICS

An alternative approach to generating overall component characteristics is the use of <u>individual stage characteristics</u> which can be <u>stacked</u> to yield the overall performance of the compressor. Stage stacking methods are described by Huppert and Benser (6), Stone (7) and Howell and Calvert (8). The concept of using individual stage data is essential for the analysis and performance prediction of compressors with variable stators; it is also essential for predicting performance deterioration in compressors where some, but not all, stages are subjected to phenomena such as Foreign Object Damage (FOD), fouling or erosion, for use in diagnostic models for EHM studies (9, 10). An elementary introduction to stage characteristics based on (11) follows.

The theoretical form of the stage characteristic can readily be deduced. Referring to the simplified compressor velocity diagram given in Fig. 4, combining the Steady Flow Equation with the Euler Turbine Equation,

$$m\, C_p \Delta T_o = m\, U\, (C_{2w} - C_{1w})$$

$$\therefore\ C_p \Delta T_o = U\, C_a\, (\tan\alpha_2 - \tan\alpha_1)$$

From the velocity triangles,

$$\frac{U}{C_a} = \tan\alpha_1 + \tan\beta_2, \quad \text{also} \quad \frac{U}{C_a} = \tan\alpha_2 + \tan\beta_1$$

It therefore follows that

$$\tan\alpha_2 - \tan\alpha_1 = \tan\beta_1 - \beta_2$$

where β_1 and β_2 are the rotor blade air angles. The equation for temperature rise can then be rewritten as

$$\Delta T_o = \frac{U\, C_a}{c_p}\, (\tan\beta_1 - \tan\beta_2)$$

This can be recast to give

$$\Delta T_o = \frac{U}{c_p}\, [\, U - C_a\, (\tan\alpha_1 + \tan\beta_2)\,]$$

The angle α_1 is the outlet air angle from the preceding stator, β_2 is the rotor outlet air angle, and these can be considered essentially constant, being determined by the blading geometry; β_1, on the other hand, will vary widely as C_a and U change at off-design operation. Dividing the previous equation throughout by U^2 and rearranging we get

$$\frac{c_p \Delta T_o}{U^2} = 1 - \frac{C_a}{U}\cdot (\tan\alpha_1 + \tan\beta_2)$$

The term C_a/U is known as the flow coefficient (ϕ) and $c_p \Delta T_o/U^2$ as the temperature coefficient (ψ). With the stage operating at the design value of ϕ the incidence will be at its design value and a high efficiency will be achieved. With the assumption that α_1 and β_2 are constant

$$\psi = 1 - \phi K$$

where $\qquad K = \tan\alpha_1 + \tan\beta_2$.

As a result of this simple analysis we can predict the shape of the stage characteristic, as shown in Fig. 5; the performance of the stage can be presented in terms of flow coefficient, temperature coefficient and efficiency (or pressure coefficient). Ideally, if α_1 and β_2 were constant, ψ would be given by the dotted line. In practice α_1 and β_2 will not remain constant due to increased deviations as conditions change from the design point. In regions of blade stalling, both at positive and negative incidence, there will be a considerable divergence giving the shape shown. Choking will occur at a high value of flow coefficient, leading to a very large drop in efficiency and placing an upper limit on the flow which can be passed at a given blade speed. Stage characteristics may be predicted from cascade data or obtained from analysis of inter-stage data on a complete compressor or testing of a single stage. In practice, not all the constant speed lines would collapse into a single curve as shown, but for a simplified explanation a single line characteristic will be assumed.

The ψ-ϕ curve shown in Fig. 6 is drawn for the case where the efficiency is a maximum at the design flow coefficient, ϕ_d. Moving away from ϕ_d results in a change in incidence and increasing losses. Reducing ϕ results in increased positive incidence and stall at ϕ_s; increasing ϕ eventually results in choking of the stage and a severe

drop in efficiency. It is essential that all individual stages of a compressor operate in the region of high efficiency without encountering either stall or choke at normal operating conditions; at conditions far removed from design it may not be possible to achieve this without remedial action involving changes in compressor geometry.

The difficulties involved in achieving correct matching of the stages can be understood by considering the operation of several identical stages in series; this procedure is known as <u>stage stacking</u> and is an invaluable tool for the aerodynamicist concerned with overall performance and determining the reasons for sub-standard performance. As an example, consider a compressor with several identical stages as shown in Fig. 6, with all stages operating at the design flow coefficient (ϕ_d) at the design point. If the mass flow through the compressor were reduced, the flow coefficient ϕ_1 entering the first stage would be reduced, resulting in an increase in pressure ratio causing the density at entry to the second stage to be increased. The axial velocity at entry to the second stage is determined by the Equation of Continuity and both effects combine to give a further decrease in flow coefficient for that stage to ϕ_2. This effect is propagated through the compressor and eventually some stage will stall at ϕ_n. Increasing the flow coefficient has the opposite effect and will drive some stage into choke.

3.1 Variable geometry compressors

As compressor pressure ratio increases, the density ratio from front to rear changes dramatically, resulting in a large change in blade length for an axial flow unit. At reduced power settings, or at idle, the pressure ratio will be much lower and this will result in very high axial velocities towards the rear of the compressor, resulting in choking. Possible methods of alleviating this problem include the use of blow off, multi-spool compressors or several rows of variable stators; all of these methods are used in practice.

The use of variable stators can be understood from the concepts of stage characteristics. If the stators are rotated away from the axial direction, increasing α_1 as shown in Fig. 7, the effect is to decrease the axial velocity and mass flow for a given speed. This delays stalling of the first few stages and choking of the last stages at low rotational speeds. It was shown that ideally $\psi = 1 - K\phi$ where $K = \tan \alpha_1 + \tan \beta_2$. Using variable stators it is possible to increase α_1 with β_2 remaining constant. The effect is to decrease the temperature coefficient for a given flow coefficient; the pressure coefficient will also be reduced. The stage characteristic will be shifted to the left as shown.

3.2 Typical stage characteristics

Much of this information would be proprietary, but it is possible to take openly published data and produce a generalized stage characteristic, which can be used for preliminary modelling purposes. An example is given in Fig. 8 from (9), this information being used successfully in producing an overall compressor characteristic for a 16:1 pressure ratio compressor; although no published compressor data were available, the engine model gave excellent results compared with published overall performance. The same data were used in (10) for two engines of widely differing size and pressure ratio, again giving excellent agreement with field performance results.

4. CONCLUSIONS

Component data are difficult to obtain, but are absolutely essential for engine modelling. Various methods can be used to estimate component performance, but these estimated maps must be updated and modified as engine performance results are obtained. Rig testing is expensive and often difficult, and results would be proprietary to the manufacturer. Both manufacturers and users may be involved in the process, with considerable differences in the information available and the end requirements.

REFERENCES

1. Boyd, D.L., "Development of a New Technology Small Fan Jet Engine," Canadian Aeronautics and Space Journal, Vol. 33, No. 2, June 1987.
2. Saravanamuttoo, H.I.H. and MacIsaac, B.D., "Thermodynamic Models for Pipeline Gas Turbine Diagnostics," Trans ASME, 105, Series A, 1983 pp. 875-84.
3. Ping Zhu and Saravanamuttoo, H.I.H., "Simulation of an Advanced Twin-Spool Industrial Gas Turbine," ASME Paper 91-GT-34, June 1991.
4. Stubner, A.W., and Canal, E., "Utilization of a Dual-Spool Compressor Test Facility to Aid Development of Turbofan Engines," SAE Paper 740823, 1974.
5. Hourmouziadis, J. "Aerodynamic Design of Low Pressure Turbines," AGARD Lecture Series No. 167 "Blading Design for Axial Turbomachines," 1989.
6. Huppert, M.C. and Benser, W., "Some Stall and Surge Phenomena in Axial Flow Compressors," Journal Aero Science, Vol. 20, 1953, p. 835.
7. Stone, A. "Effects of Stage Characteristics and Matching on Axial Flow Compressor Performance," Trans ASME, 80, 1958, pp. 1273-93.

8.   Howell, A.R. and Calvert, W.J., "A New Stage Stacking Procedure for Axial Flow Compressor Performance Prediction," Trans ASME, 100, p. 698-703, 1978.

9.   Muir, D.E., Saravanamuttoo, H.I.H. and Marshall, D.J. "Health Monitoring of Variable Geometry Gas Turbines for the Canadian Navy," Trans ASME, Vol. 111, April 1989, pp. 244-250.

10.   Aker, G.F. and Saravanamuttoo, H.I.H., "Predicting Gas Turbine Performance Degradation Due to Compressor Fouling Using Computer Simulation Techniques," Trans ASME, Vol. 111, April 1989, pp. 343-350.

11.   Cohen, H., Rogers, G.F.C. and Saravanamuttoo, H.I.H., "Gas Turbine Theory," 3rd Edition, Longman 1987.
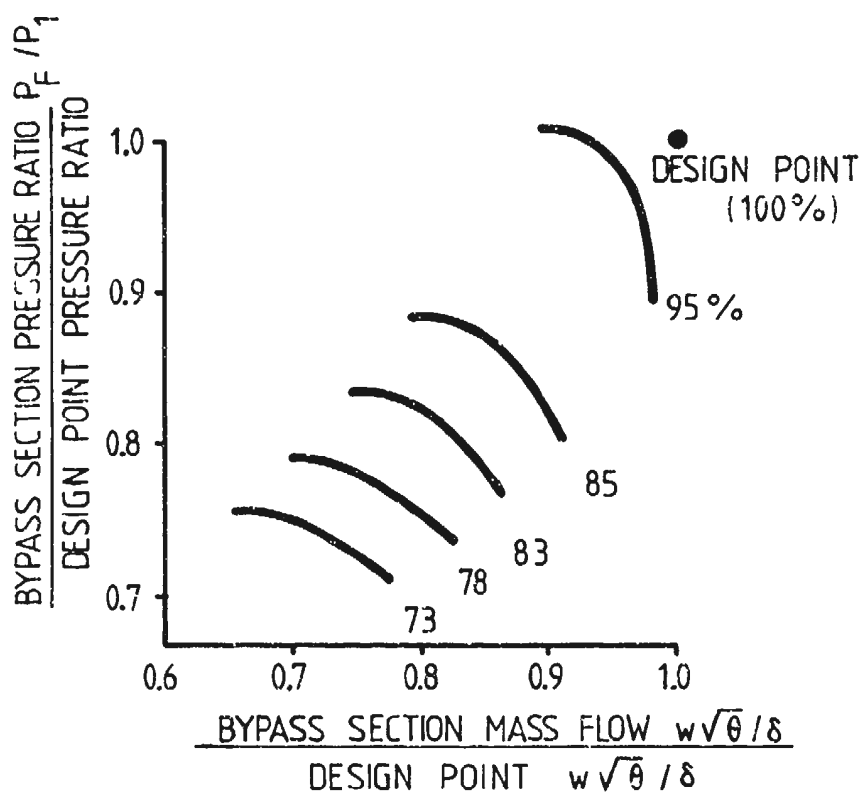
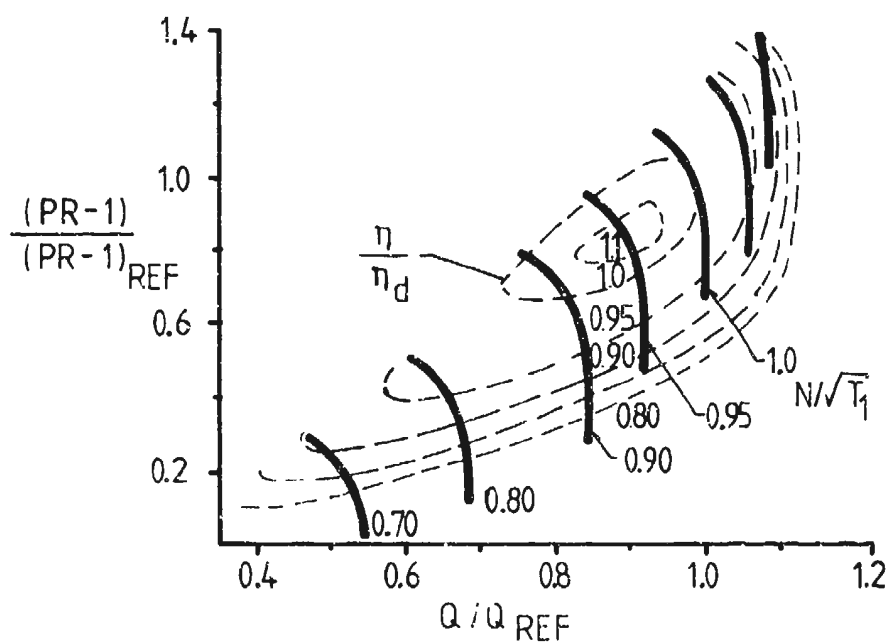FIG.1 SINGLE STAGE FAN CHARACTERISTIC (FROM REF.1)

FIG. 2 GENERALIZED COMPRESSOR CHARACTERISTIC
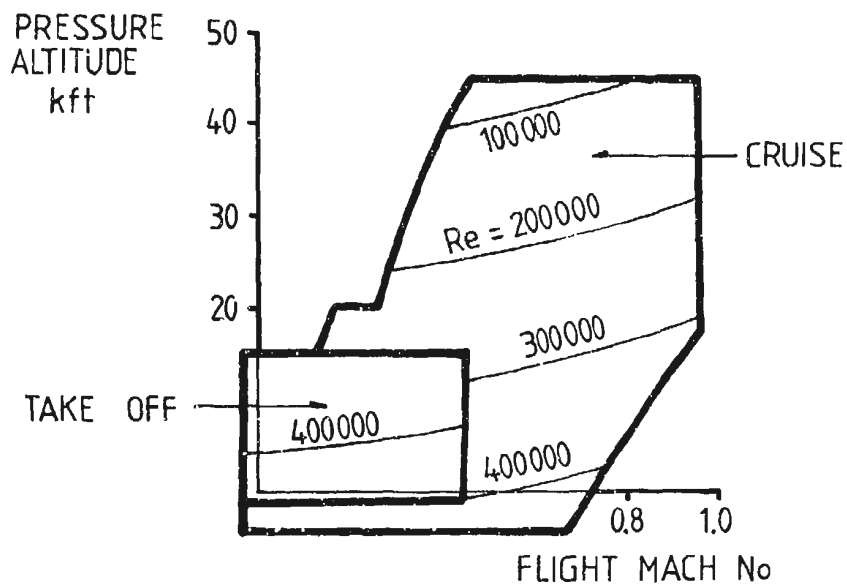
PRESSURE
ALTITUDE
kft

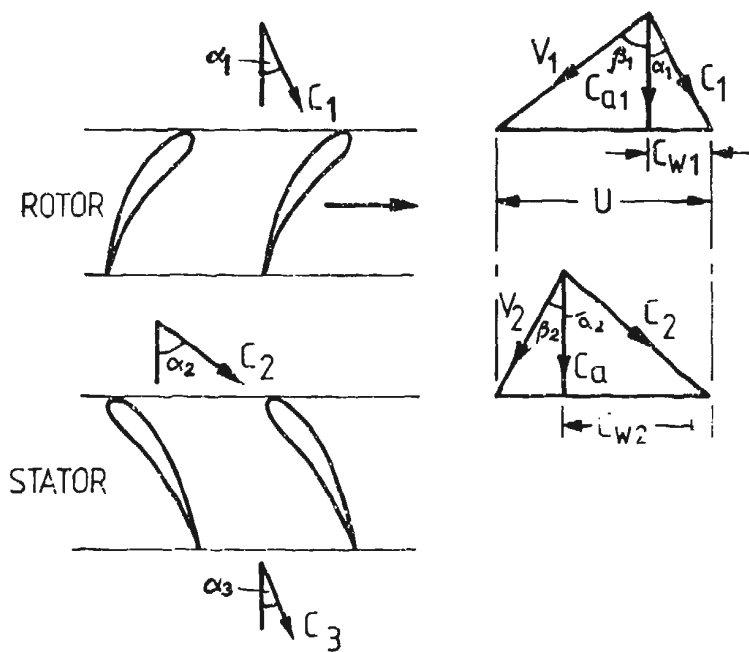FIG. 3 REYNOLDS NUMBER VARIATION, LP TURBINE (FROM REF. 5)

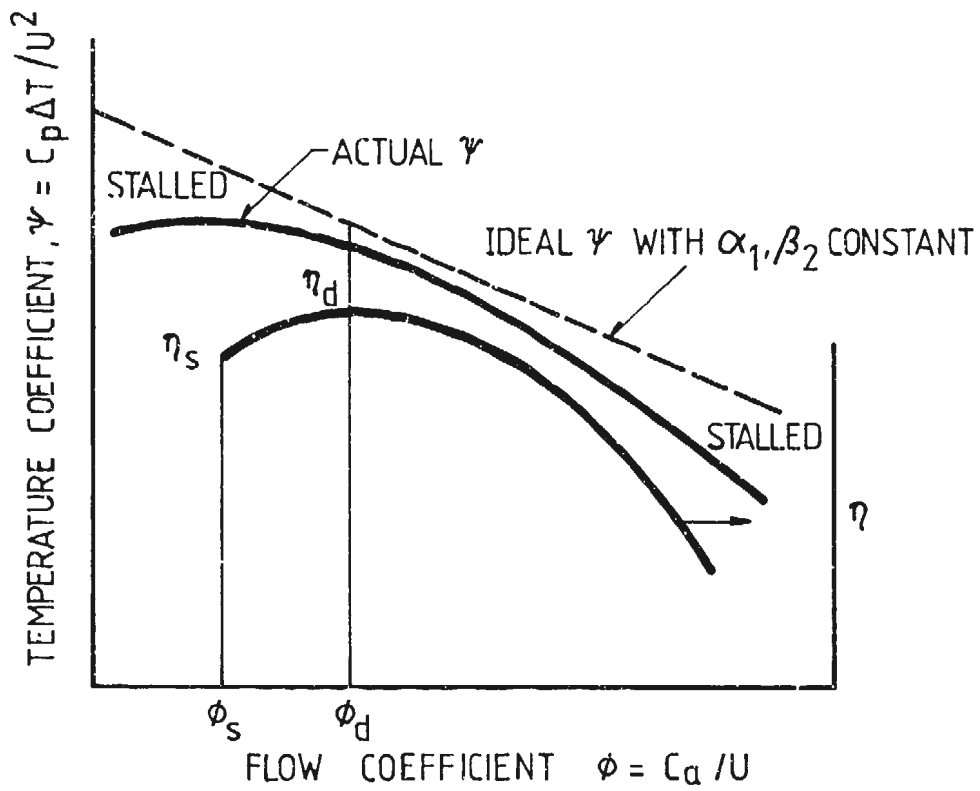FIG. 4 VELOCITY TRIANGLES (AXIAL FLOW COMPRESSOR)
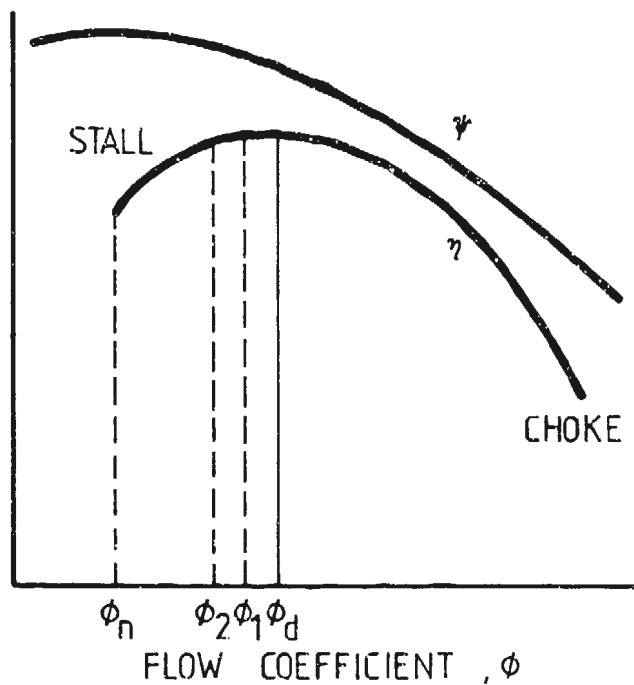
FIG. 5   STAGE CHARACTERISTIC.

FIG. 6 EFFECT OF REDUCTION IN ϕ AT INLET
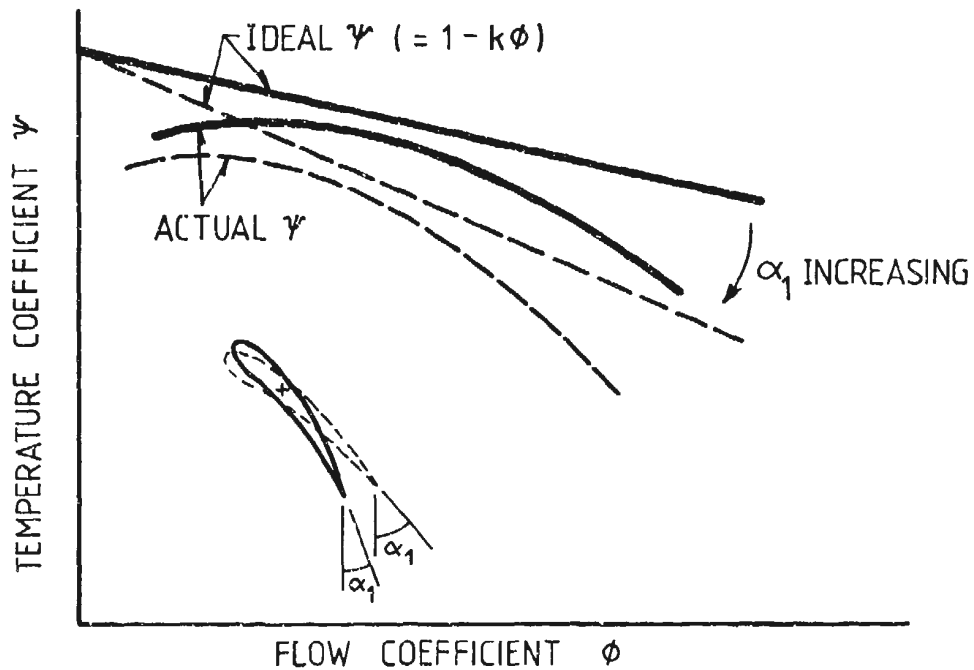
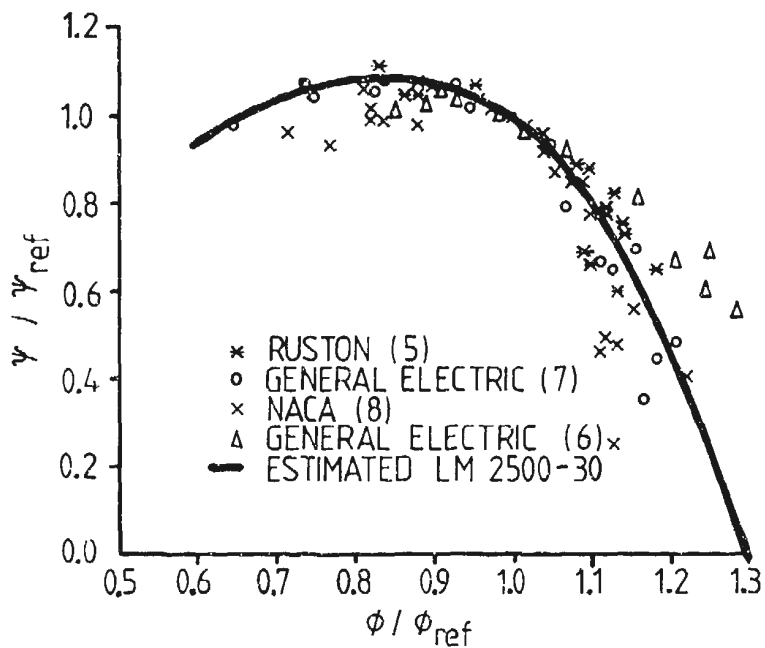FIG. 7   EFFECT OF VARIABLE STATORS

FIG. 8   GENERALIZED STAGE PRESSURE COEFFICIENT
CURVE (FROM REF 8)

DYNAMIC SIMULATION OF COMPRESSOR AND GAS TURBINE PERFORMANCE

Walter F. O'Brien
Mechanical Engineering Department
Virginia Polytechnic Institute and State University
Blacksburg, Virginia 24061-0238 USA

SUMMARY
Dynamic simulation of compressor and gas turbine perform-
ance is useful in a variety of design, analysis, and test appli-
cations. Mathematical models employing estimated or
experimentally-derived component characteristics have been
widely used, especially for near-design-point studies of
acceleration and deceleration transients and control strategies.
With recent progress in simulation methods and
computational power, it has become possible to build models
with detail at the stage level, and with fundamental fluid
mechanics input. Such models are more useful because of the
ability to study the details of inter-component flow property
behavior during machine transients, even including stall and
surge.

Dynamic performance simulation models are discussed with
emphasis on the fundamental principles of the models and the
methods used to represent component and stage flow charac-
teristics. Results of several simulations of the dynamic be-
havior of multistage compressors are shown with comparisons
to experimental data. Possibilities for advanced computa-
tional techniques for near-real-time simulations of compres-
sors and gas turbines are reviewed.

LIST OF SYMBOLS

A	=	area
A_c	=	compressor cross-sectional area
a	=	acoustic velocity
B	=	"B" parameter
CV	=	control volume
Cx, ν	=	axial velocity
C	=	specific heat of conducting metal
c	=	blade chord
c_p	=	specific heat at constant pressure
D_{eq}	=	equivalent diffusion ratio
H	=	blade span
H_2	=	blade wake form factor
i	=	blade incidence angle
IGV	=	inlet guide vane
M	=	Mach number
$\dot{m}$	=	mass flow rate
E	=	energy function
e	=	internal energy
F_a	=	force of compressor blading
F_{ss}	=	steady state force
FX	=	force of compressor blading and casing acting on fluid, including wall pressure area force
H	=	total enthalpy, blade span
IMP	=	impulse function

L_c	=	compressor length
M_T	=	mass flow function based on total condition
N	=	compressor rotor speed
NC	=	compressor corrected rotor speed
P	=	pressure
PR	=	total pressure ratio
Q	=	rate of heat addition to control volume
SW	=	rate of shaft work
T	=	temperature
TR	=	total temperature ratio
t	=	time
U	=	wheel speed
u, C_X	=	axial velocity
V	=	absolute velocity
V_p	=	plenum volume
W	=	mass flow rate, relative velocity
x	=	axial coordinate
α	=	absolute flow angle, or angle of attack
β	=	relative flow angle
β'	=	blade metal angle
δ	=	flow deviation angle
γ	=	blade stagger angle, or ratio of specific heats
η	=	stage isentropic efficiency
σ	=	blade solidity
ρ	=	density
θ	=	blade camber
θ^*	=	wake momentum thickness
τ	=	time constant
ϕ	=	flow coefficient
$\bar{\omega}$	=	total pressure loss coefficient
ψ^P_{S-S}	=	static-to-static pressure coefficient

$$\psi^P_{S-S} = \frac{P_{se} - P_{si}}{\frac{1}{2}\rho u^2}$$

ψ^P_{T-S} = total-to-static pressure coefficient

$$\psi^P_{T-S} = \frac{P_{se} - P_{Ti}}{\frac{1}{2}\rho u^2}, \text{Forward Flow}$$

$$\psi^P_{T-S} = \frac{P_{Te} - P_{si}}{\frac{1}{2}\rho u^2}, \text{Reversed Flow}$$

ψ^T = stage temperature coefficient (stage loading parameter)

$$\psi^T = TR - 1$$

Subscripts

a	=	annulus
B	=	pertaining to bleed
e	=	exit conditions
i	=	inlet conditions
p	=	profile
R	=	rotor
ref	=	reference conditions
S	=	static condition, stator
SS	=	steady-state condition
S-S	=	static-to-static
s	=	secondary
T	=	total conditions
T-S	=	total-to-static
x	=	axial direction
0	=	total property
1	=	rotor or stage inlet
2	=	rotor or stage exit

INTRODUCTION

Dynamic analysis of gas turbine performance is a specialized subject, drawing from the widely-used steady-state aerothermodynamic performance analysis methods. Whereas steady state methods primarily seek to predict fuel and thrust performance values for a given engine cycle, dynamic methods can approach genuine simulations of gas turbine operation. Properly formulated dynamic analyses can predict gas turbine component response to acceleration and deceleration, changes in inlet and exit conditions, and excursions into far-off-design and unstable operating regions.

The roots of present-day dynamic analysis methods are in conventional, steady state cycle analysis procedures. These methods can be directly applied to off-design and transient analysis, if the time scale for adjustment of the local fluid processes is much shorter than the time required for changes of the overall operating state. The description of rapidly changing dynamic events, such as compressor stall and surge and engine response to sudden inlet distortions, requires attention to the dynamic response of both the fluid states and the mechanics components.

The present discussion addresses principles and methods for the development of dynamic analyses, with detail down to the stage level in turbomachinery. A short review of related work and analysis methods is followed by the mathematical development of the stage-by-stage dynamic analysis method for multistage compressors, and some example results. The development of appropriate stage characteristics is discussed. Advanced computational methods and extension of the dynamic analysis method to full gas turbine simulations concludes the discussion.

UNSTEADY PERFORMANCE ANALYSIS

For purposes of classification, we will refer to steady-state, "transient" and "dynamic" performance analysis methods. Steady-state methods draw from thermodynamic cycle analy-

sis, and are widely used for performance prediction and analysis. There are many descriptions of such analyses in the literature, dating from the beginnings of gas turbines. Computer codes based on steady state cycle analysis are in wide use by operators, research organizations and engine manufacturers. As an example, in the United States NASA makes available computer codes for steady-state design point and off-design propulsion analysis from the work of Fishbach, et al [1,2]. The NASA-Navy code NNEP [2] permits the modular assembly of engines with variable cycles, duct burners, and most conceivable arrangement of components. The addition of performance maps for components allows off-design performance predictions.

Transient analyses of turbine engine performance are defined here as those which add to off-design cycle analysis the ability to account for the inertia of the rotating components. Fluid transport delay may be included to improve the prediction of rapid transients. These methods permit the study of engine and component dynamics over the range of normal operation, and up to the compressor stall point. They are widely used in the development of controls and operating schedules. Examples of such analyses include the work of Sadler and Melcher [3], Saravanamuttoo and Fawke [34], and Szuch [4].

Dynamic analyses include the elements of steady-state and transient analysis, and add expressions for the description of dynamic fluid mechanics processes over the full range of possible operating states. Thus, the progress of a multistage compressor through a surge cycle may be studied, and development and recovery from stall may be simulated. Dynamic analyses may use lumped representations of the performance of an entire component, or may include detailed characteristics for stages or even blade rows of the simulated machine. Davis and O'Brien [5] have presented a stage-by-stage model for a multistage compressor, which is reviewed here to develop the mathematical methods and illustrate applications.

DYNAMIC ANALYSIS METHOD

Results of several related experimental investigations can be found in Refs. 6-10. Previous compression system mathematical models have been developed using lumped-volume techniques. A lumped-volume approach makes certain assumptions about compressibility within the system. More specifically, the lumped-volume model neglects Mach number effects, uses an isentropic relationship to relate the time-dependent change in density to a time-dependent change in total pressure, and uses a steady-state form of the energy equation. Initially, models (whether overall simulations or stage-by-stage) were limited in range to the onset of system instability [11-13]. Over the last decade, poststall behavior has been of more interest, which encouraged the development of numerous models capable of exhibiting aspects of surge or rotating stall [14-21]. In general, whether overall or stage-by-stage, poststall models have been previously developed using lumped volume techniques. The model presented here removes assumptions inherent in lumped-volume models (i.e., treats compressibility explicitly) and does so on a stage-by-stage basis.

Illustrated in Fig. 1 is a representative single-spool, multistage compressor and ducting system. Included in this system is a portion of the compressor inlet and the combustor vol-

ume. The compressor and ducting system are modeled by an overall control volume shown in Fig. 1b. The time-dependent inlet-boundary condition is the specification of total pressure and temperature. The exit-boundary condition is either the specification of static pressure or unity Mach number. The overall control volume is divided into a set of elemental control volumes.
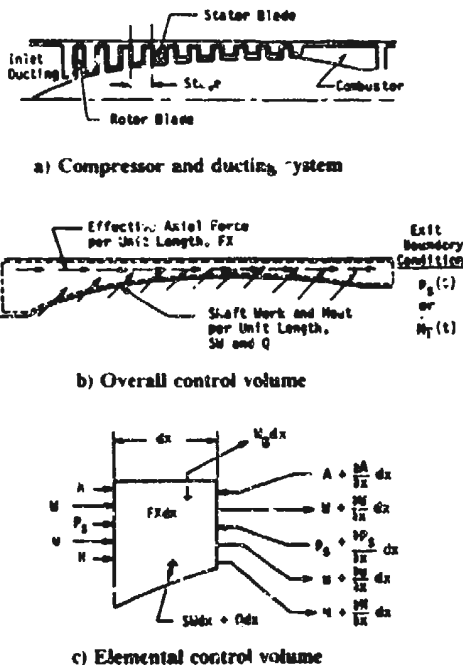

a) Compressor and ducting system

b) Overall control volume

c) Elemental control volume

Figure 1   Physical Compression System and Control Volume Concepts.

The governing equations are derived by application of mass, momentum, and energy conservation principles to the elemental control volume of Fig. 1c. In the compressor section, a stage elemental control volume consists of a rotor followed by a stator, and associated volume representing the complete stage. Acting on this fluid control volume is an axial force distribution, FX, which is attributable to the effect of compressor blading and walls of the system. In addition, the rate of heat transfer to the fluid and shaft work done to the fluid are represented by distributions, Q and SW, respectively. The mass transfer rate across boundaries other than the inlet or exit (such as interstage bleed) is represented by the distribution, W_B.

Applying the continuity principle to the elemental control volume yields

$$\frac{\partial(\rho A)}{\partial t} = -\frac{\partial W}{\partial x} - W_B \qquad (1)$$

where W_B is the interstage bleed flow per distributed length.

Applying conservation of momentum gives

$$\frac{\partial W}{\partial t} = -\frac{\partial(IBP)}{\partial x} + FX \qquad (2)$$

where

$$IMP = Wu + P_s A$$

is a momentum impulse term, and

$$FX = F_B + P_s \frac{\partial A}{\partial x}$$

is an axial-force distribution consisting of blade force and the force produced by the walls of the system. Energy conservation yields

$$\frac{\partial(EA)}{\partial t} = -\frac{\partial H}{\partial x} - H_B + SW + Q \qquad (3)$$

where

$$E = \rho\left(e + u^2/2\right); \quad H = c_p W\left(T_t - T_{ref}\right); \quad T_{ref} = 0$$

and H_B is the enthalpy associated with bleed flow.

To provide stage force and shaft work inputs to the momentum and energy equations, a set of quasi-steady stage characteristics must be available for input to the model. These stage characteristics provide the pressure and temperature performance for each stage as a function of the steady airflow. A typical set of steady-state characteristics for both pre- and post- stall operation is presented in Fig. 2. The stage characteristics are divided into three distinct regions: prestall, rotating stall, and reversed flow. The prestall characteristic is the performance of a blade row in normal operation. The transition to a rotating stall characteristic is approximated as a continuous characteristic along a postulated throttle line. The performance in the rotating stall region is based upon a flow-weighted average of a fully developed rotating stall cell. The pressure and temperature ratios in this region represent the average pressure and temperature rise across the stage for both stalled flow and unstalled flow. The reversed-flow characteristic region represents the pressure loss and temperature rise associated with full-annulus reversed flow. The discontinuity at zero flow has been experimentally shown to exist for a three-stage low-speed compressor[10]. This aspect of the quasi-steady flow characteristic has been incorporated into the modeling technique.

For prestall and poststall reversed-flow, steady characteristics can be used as they exist. However, for dynamic events such as rotating stall or surge, use of steady characteristics is not necessarily correct. In the rotating stall region, rotating stall develops very rapidly and the globally steady characteristic is no longer applicable. To provide a dynamic stage characteristic, a first-order time lag on the stage force has been incorporated into the modeling technique in the rotating stall region only. The first order lag equation used is

$$\tau \frac{dFX}{dt} + FX = FX_{ss} \qquad (4)$$

This lagging technique has been previously applied to several models using overall compression system characteristics [15-17].

The governing equations of the compressor model are solved numerically using the second-order accurate MacCormack explicit finite difference scheme [18], described in Appendix A.
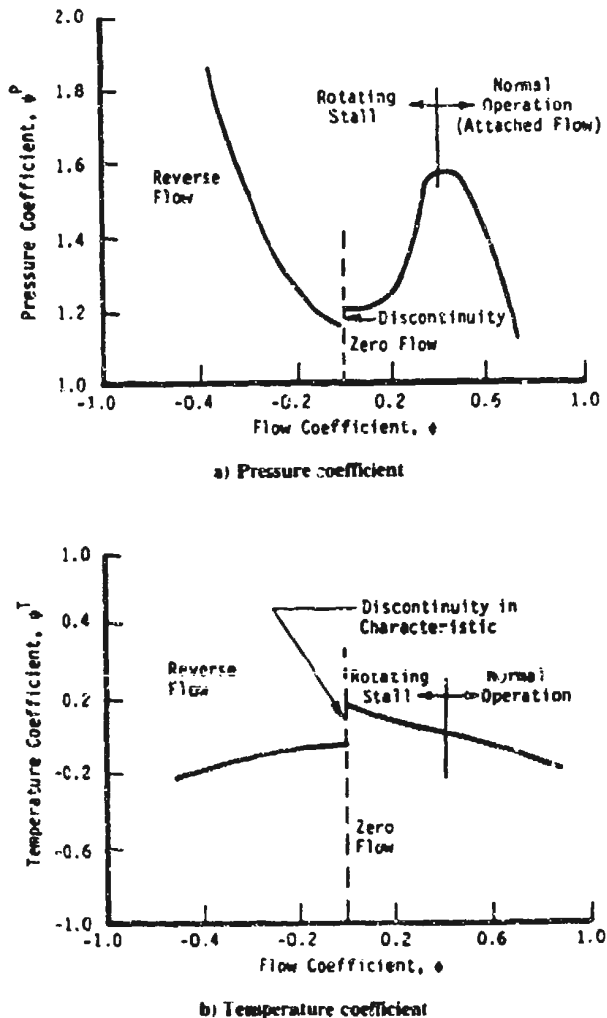

a) Pressure coefficient

b) Temperature coefficient

Figure 2 Typical Stage Characteristics.

The compressor model is not only an initial value problem but a boundary problem as well. Because the treatment of the boundaries can be a cause of stability problems, method-of-characteristics (MOC) boundary formulations were employed. The numerical computational volume is divided into three areas: inlet, exit, and interior. MacCormack's scheme is applied in the interior; the MOC scheme is applied at the inlet; and either an MOC scheme for unchoked flow or an isentropic nozzle model for choked flow is applied at the exit.

A more detailed explanation of the modeling technique can be found in Ref. 19.

THREE STAGE RIG SIMULATION
The available experimental results from tests of the three-stage, low-speed compressor research rig of Gamache were utilized [10]. Transient interstage or overall performance data for surge and rotating stall events were not reported.

However, steady-state data were available from which stage characteristics could be synthesized. Overall system performance during surge and rotating stall was available from tests of a similar system, reported in Ref. 6.

The three-stage, low-speed compressor rig consisted of three nonrepeating stages with a constant cross-sectional annulus area. The hub and tip diameters were 53.63 and 60.96 cm, respectively, which produced a hub-to-tip ratio of 0.88. The major emphasis was the study of the performance of the compressor rig during steady reversed flow. The rig was configured to hold a constant speed while forcing reversed flow through the compressor. By accomplishing this for many flow points, it was possible to obtain overall and stage performance in the reversed flow region. From the previous work of Eastland [20], a complete set of steady state stage pressure characteristics and corresponding overall steady system performance was available.

A complete temperature rise characteristic was not given for each stage, but energy input to the overall system was given in terms of a torque coefficient. For the present purposes, stage temperature rise characteristics were synthesized as total temperature ratios based upon the overall torque characteristic and two isolated flow points in rotating stall. Temperature characteristics were synthesized which would give the same overall torque as observed experimentally. Lacking any other criteria for stage work division, all stage temperature characteristics were synthesized identically.

Measured stage pressure and synthesized temperature rise characteristics for the three-stage, low speed research compressor are presented in Fig. 3. Pressure rise characteristics were based upon reported experimental stage performance measurements which described individual stage pressure behavior during unstalled operation, rotating stall, and reversed flow. Stage temperature rise characteristics have been synthesized as described above.

While the referenced three-stage compression system tests provided excellent stage characteristic data, detailed system behavior during surge and rotating stall was not available from either Refs. 10 or 20. However, the rig was similar to one used in a previous experimental investigation of surge and rotating stall [6]. An extensive experimental investigation to determine system response during poststall events for a variety of compressor/plenum configurations was performed with this rig.

The compression system model was configured to the geometry specified for the compressor/plenum rig of Ref. 6, but using the stage characteristics Fig. 3. For comparison purposes, the "B" parameter [15] was used as a reference variable for both the experimental compressor and the model. The parameter is defined as

$$B = (U/2a)\left(V_p / A_c L_c\right)^{1/2} \qquad (5)$$

The value of the B parameter has been shown to be an indication of whether rotating stall or surge may be expected to occur in a particular compressor [6].
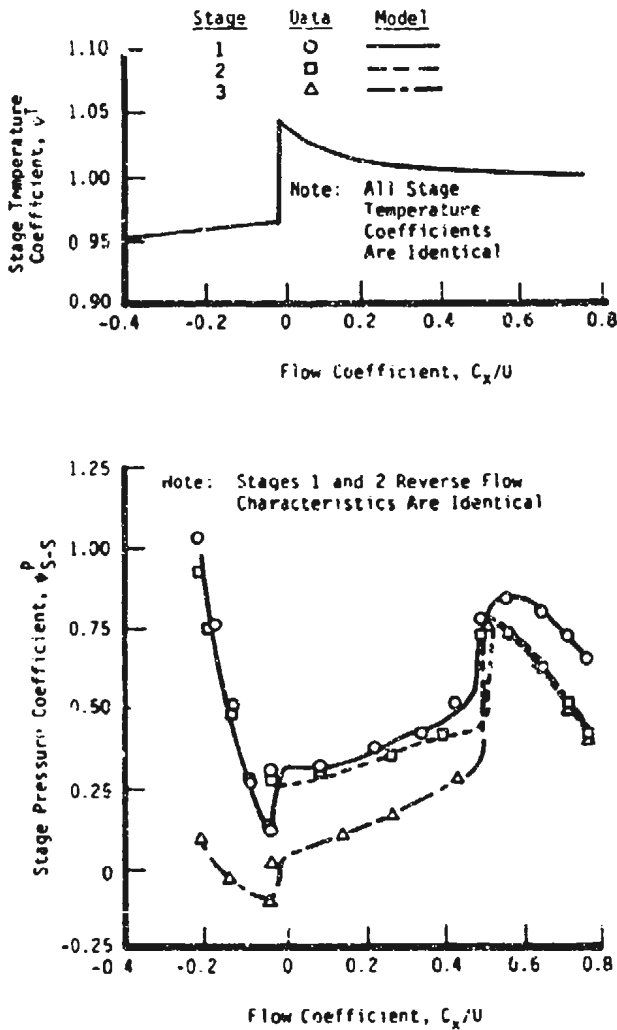
Figure 3 Synthesized Stage Characteristics for a Three-Stage, Low Speed Experimental Compressor Rig and Comparison to Experimental Results.

Three model cases will be compared to experimental results from Ref. 6, corresponding to B parameters of 0.65, 1.00, and 1.58. These B parameters produced rotating stall, classical surge, and deep surge, respectively.

Rotating Stall
The first experimental transient was conducted at a B value of 0.65. The compressor rig throttle was slowly closed to the point of instability and then held constant. The system became unstable at the uniform flow stall point and then traversed to rotating stall (Fig. 4).

The stage-by-stage compressor model was configured in a similar way to a B parameter value of 0.65 at instability initiation. The "throttle" was closed just enough to cause instability and then held constant. The compressor blade force dynamic lagging constant, τ, was set at the model boundary between surge and rotating stall such that the overall system performance traversed immediately to the new operating point indicative of fully developed rotating stall. The modeled poststall behavior is presented in Fig. 5.

Comparison to the general nature of the experimental results (Fig. 4) indicates correctly simulated overall system behavior.

Classical Surge
In a second test, the compressor rig of Ref. 6 was reconfigured to operate at a B value of 1.00. In this condition, the system exhibited classical surge cycles on the order of 1.5 Hz as presented in Fig. 6.

The dynamic model was reconfigured to produce a B value of 1.00. The blade force time constant, τ, was held to the value determined in the previous simulation. Under these conditions, the model also exhibited surge, as presented in Fig. 7. Comparing the time history of the pressure coefficient, one can observe that the change in this parameter is similar in nature and frequency to that observed experimentally (Fig. 6). Comparing the model results as depicted on a compressor map, it can be seen that the surge trajectories are circular in nature and quite similar to those observed experimentally.
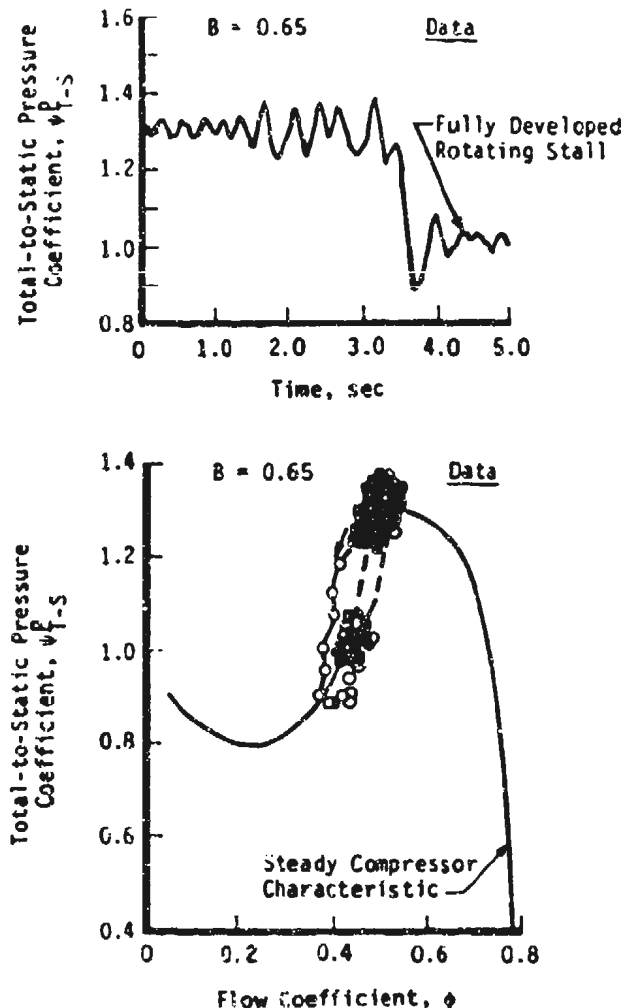
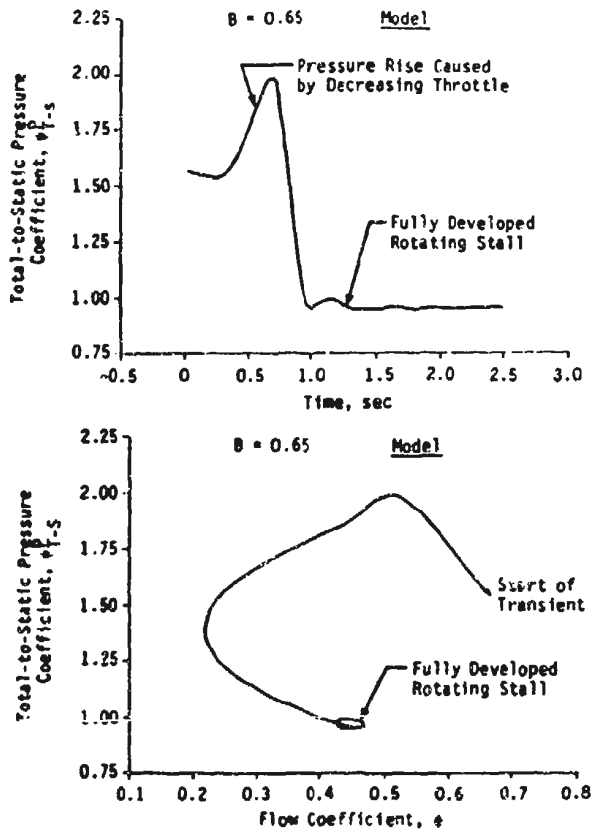**Figure 4 Poststall Behavior of Compressor Rig: Rotating Stall, B = 0.65**

Figure 5 Three-Stage Model Overall Compression System Poststall Behavior: Rotating Stall, B = 0.65.

Deep Surge

The experimental rig of Ref. 6 was operated with a maximum reported B value of 1.58. For this experimental case, a slightly different system behavior was observed. The surge trajectory became larger with near-zero flow during the surge cycle, but still of the classical type. By decreasing the throttle closure point beyond the initial surge position, it was discovered that the nature of the surge cycles could be affected. Indicated in Fig. 8 are surge cycles for the same compressor configuration (B = 1.58), but at a reduced throttle setting. This type of surge cycle has been called a deep surge.

The dynamic model was configured for a B value of 1.58. Again, the blade force time constant, τ, was held at the previous value. The simulated throttle was decreased to a value just small enough to cause compression system instability. Resulting overall system response was indicative of the classical type surge. Further decreasing the throttle function to 60% of the minimum value for system instability caused the model to exhibit deep surge, as was observed experimentally. Modeled overall system response is presented in Fig. 9. Model trajectories are indicative of deep surge poststall behavior with a frequency of 1 Hz.
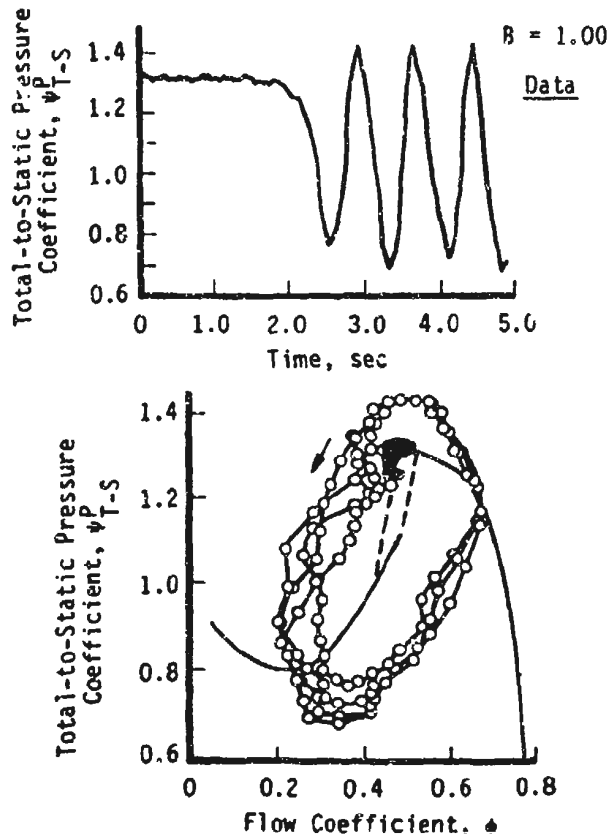

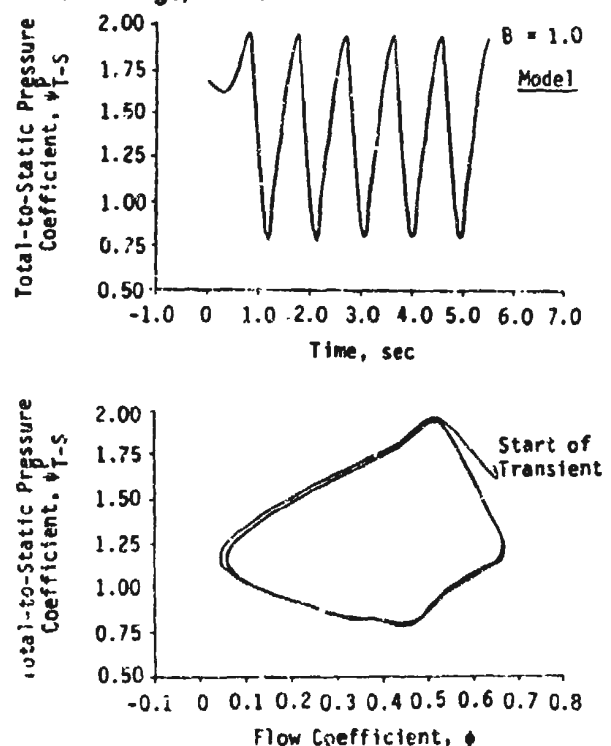Figure 6 Poststall Behavior of Compressor Rig: Classical Surge, B = 1.0

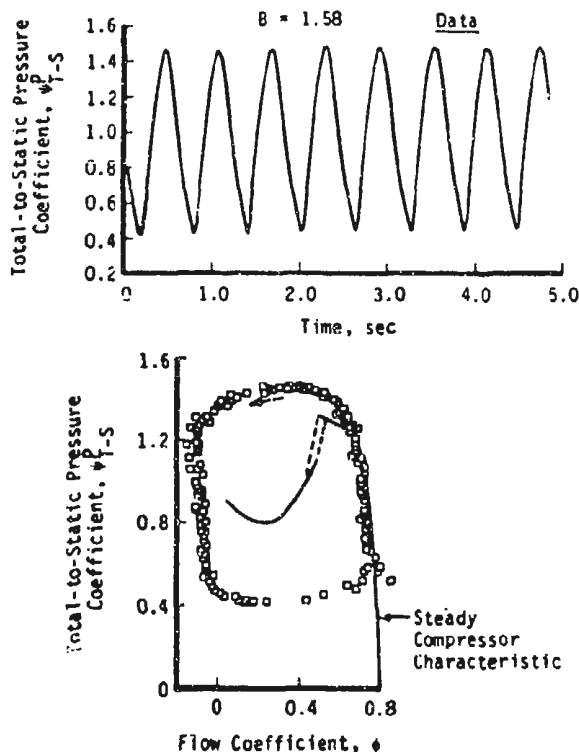Figure 7 Three-Stage Model Overall Compression System Poststall Behavior: Classical surge, B = 1.0.

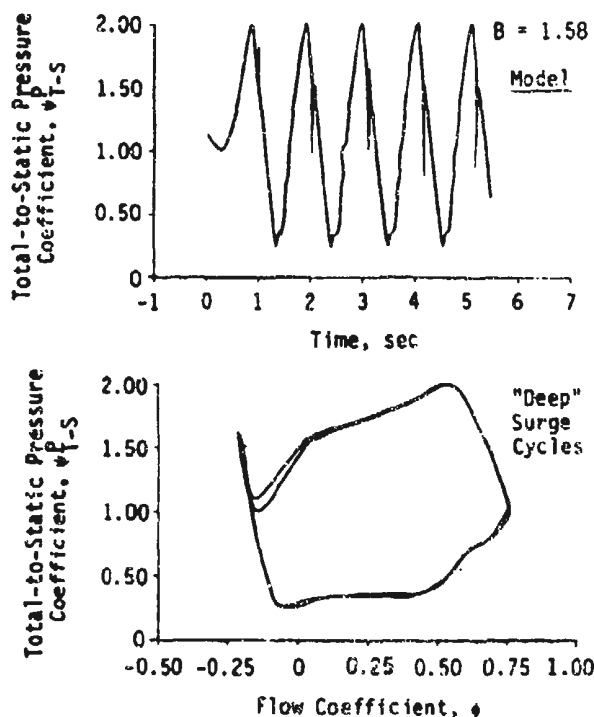Figure 8 Poststall Behavior of Compressor Rig: Deep Surge, B=1.58.

Figure 9 Three-Stage Model Overall Compression System Poststall Behavior: Deep Surge, B = 1.58.

PARAMETRIC STUDIES

To demonstrate the unique capabilities and usefulness of the stage-by-stage, poststall compression system modeling technique, a parametric study was conducted to assess two different effects: 1) the effect of heat transfer due to rapid power lever transients on system poststall behavior employing a nine-stage model and 2) the effect of tip casing treatment on system behavior using the three-stage model.

Effect of Heat Transfer on Poststall Behavior (Nine-Stage Model)

Operation of high-speed, high-pressure ratio compressors results in a large temperature rise through the compressor. A portion of the large amount of energy input is stored in the compressor blades, rotors, and disks. Thus, during engine throttle transients as in a bodie maneuver (maximum power to idle then back to maximum power), heat transfer between the compressor metal and the airflow takes place. The release of energy during the transient from maximum power to idle causes a change in density, which produces a shift in the compressor characteristic and lowers the stability limit. This loss in surge margin can result in a compression system instability during throttle readvance to maximum power.

From a modeling study, MacCallum and Pilidis [21] concluded that the following thermal effects contribute to the loss in stall margin during reacceleration: nonadiabatic flows causing density changes due to heat transfer; changes in boundary-layer development on the blade airfoils; changes in the boundary-layer development near the end walls; changes in tip clearances; and changes in seal clearances. For this study, only the effect of nonadiabatic flows was considered.

An investigation by Crawford and Burwell [22] quantified the magnitude and nature of the heat transfer during turbine engine bodie maneuvers using actual engine test results. A calculation of stage thermal energy was made based upon the following equation:

$$Q_{stage} = mC(T_{max} - T_{idle}) \qquad (6)$$

where

m	=	mass of the blades, platforms and seals
T_{max}	=	stage total temperature at maximum power
T_{idle}	=	stage total temperature at idle power

Stage temperature distributions were obtained from a stage stacking model representing idle and maximum power operation at the flight conditions tested. Stage temperature distributions for maximum and idle power, along with the corresponding stored thermal energy are presented in Fig. 10.

Using a calculation of transient airflow, heat transfer rates (Btu/Sec) were calculated. Typical stage heat-transfer rates calculated from experimental results obtained from current-day high-pressure compressors are presented in Fig. 11. Using these rates as a guideline, stage heat transfer rates were postulated for a nine-stage compression system which had just completed a bodie transient.
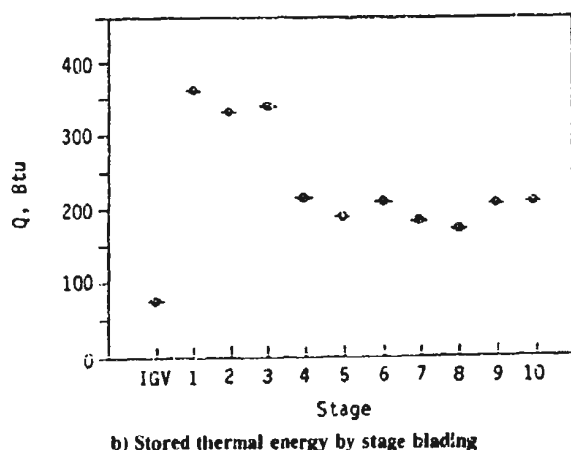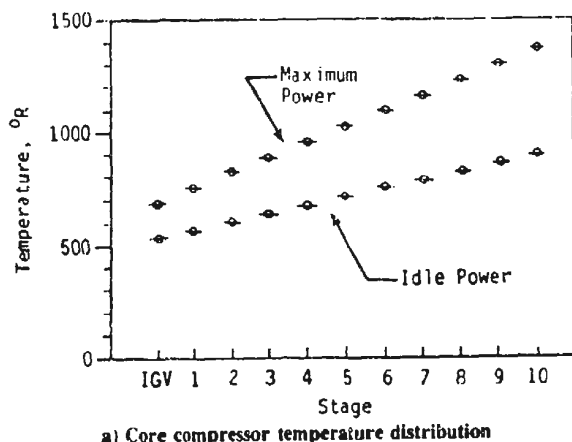
a) Core compressor temperature distribution

b) Stored thermal energy by stage blading

Figure 10 Predicted Stage Temperature Distribution at Maximum and Idle Power and Corresponding Blade Stored Thermal Energy in Each Stage.
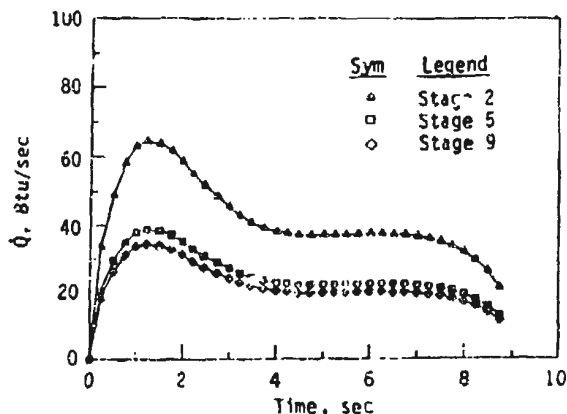

Figure 11 Typical Stage Heat Transfer Rates Based upon Experimental Results.

The model was operated to simulate operation at 70% speed with the throttle set such that a compressor instability would occur. The stage force lagging constant, τ, was set at a slightly lower value than the model-determined surge/stall boundary to ensure that surge would be the initial poststall event. (Smaller values of τ encourage a surge-like result

from the model.) A stage specific heat transfer was chosen for each stage based upon the calculated temperature distribution represented in Fig. 10. Heat-transfer rates were calculated from Eq. 6, and were brought to their maximum level exponentially over a time period of approximately one second, as was indicated experimentally (Fig. 11). The postulated heat-transfer distribution for the nine-stage compressor is illustrated in Fig. 12. Since the throttle was set such that an instability would occur, the heat-transfer rates are shown to be oscillating during the first second of the dynamic event because the compressor was experiencing surge during this period. However, once the stage heat-transfer rates had reached their maximum values, the compressor moved to the nonrecoverable state as illustrated in Fig. 13. Once the nonrecoverable state was reached, heat transfer rates reduced because of the reduction in overall airflow.
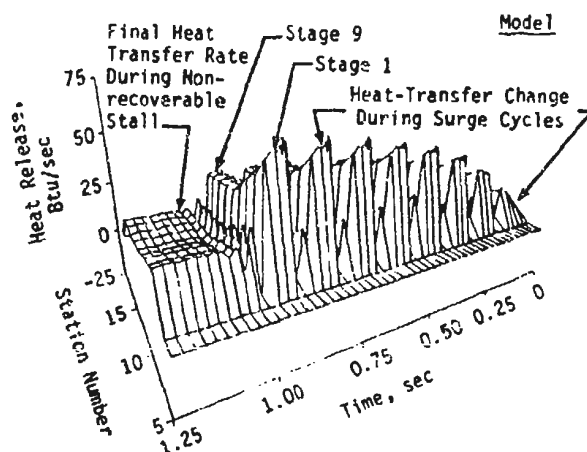
Figure 12 Heat Transfer Changes During Throttle Induced Surge Cycles of a Nine-Stage High Pressure Compressor at 70% Speed.
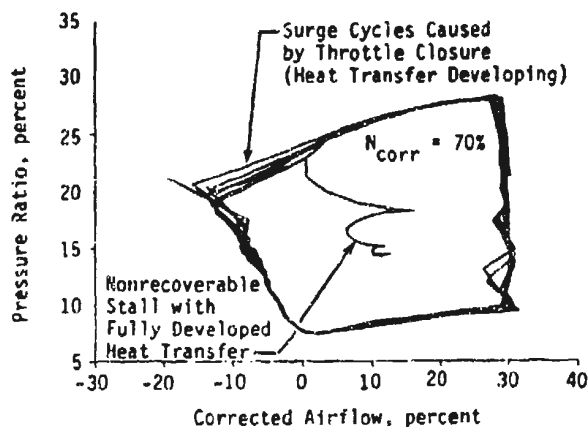
Figure 13 Effect of Compressor Heat Transfer (blade to gas path) on Poststall Behavior, Nine-Stage HPC at 70% Speed.

This study assumed that a compressor instability will occur during a bodie maneuver and the model was configured to favor this result. Even if such were not the case, the results from the model indicated that, because of the heat transfer generated within the compressor at time of throttle readvance,

the compression system may be more likely to enter the non-recoverable state (rotating stall) when the system is near the surge/rotating stall boundary.

Effect of Tip Casing Treatment on Post-Stall Behavior (Three-Stage Model)

Once a particular compression system is designed and built, the performance and stability behavior are fixed within certain limits. There are only a limited number of external changes that can be made to improve either performance or stability. If these changes cannot produce the desired result, certain internal or blade changes such as camber, stagger, tip clearance or tip casing treatment can be made which improve performance and stability.

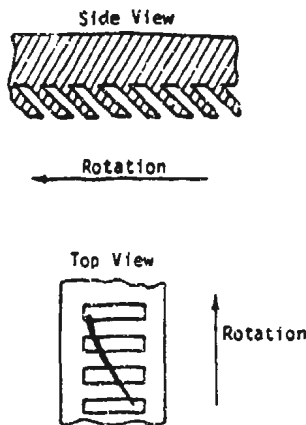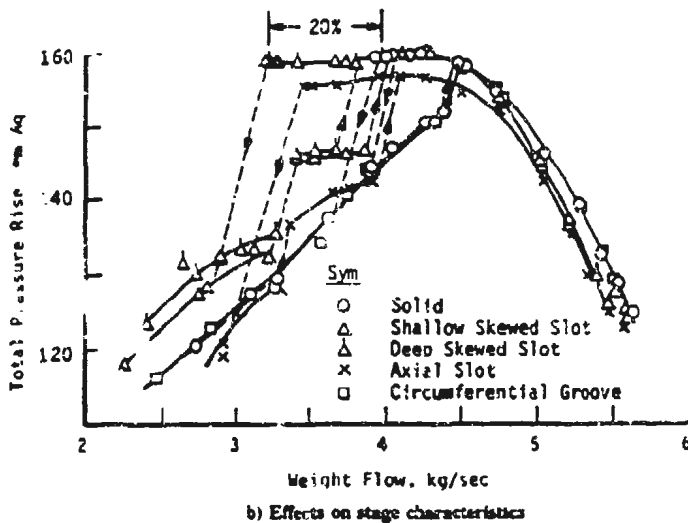a) Tip treatment modification—Deep skewed slot insert

b) Effects on stage characteristics

Figure 14 Possible Tip Treatment Modification and Its Effect on Stage Characteristics.

A possible change that will be considered is the effect of tip-casing treatment. Takata and Tsukuda, [23] utilizing a low-speed compressor rig, investigated the effects of tip-casing treatment on the performance of a single rotor row. Of the several types of treatment investigated, it was found that a deep-skewed slot tip treatment most improved the stage characteristics. Presented in Fig. 14 is the deep-skewed slot modification and the observed effect on stage performance. Although stage pressure rise is not increased by this tech-

nique, the amount of airflow reduction necessary for stall to occur was extended by 20%, providing more stall margin.. In addition, a portion of the rotating stall characteristic was presented, which indicated a higher average pressure level during rotating stall.
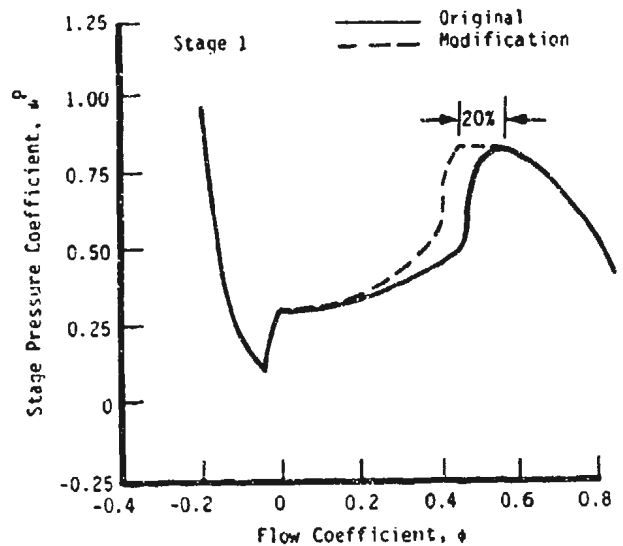
Figure 15 Postulated Stage Pressure Characteristic Modification as a Result of Tip Treatment.
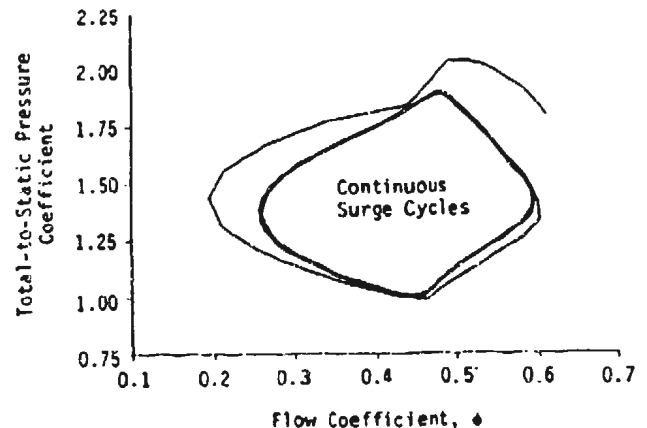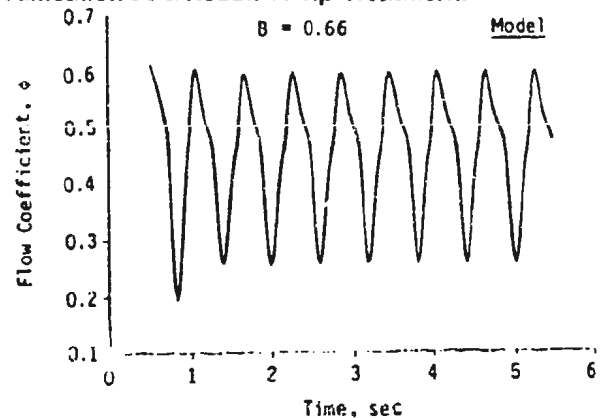
Figure 16 Model Prediction of the Effect of First Stage Tip Treatment on Poststall Behavior: B = 0.65.

To evaluate the effect of such a modification on compression system poststall behavior, the three-stage, low-speed model

was chosen for study. A low-speed condition (Fig. 5) was chosen for which rotating stall was the end result. During these studies, all variables (B parameter, force lagging constant τ, speed and plenum configuration) were held constant except for the changes in the quasi-steady characteristics described below.

Presented in Fig. 15 is a postulated first-stage pressure characteristic with stall margin improvement based upon the results of the deep-skewed tip-casing treatment. The maximum stall point pressure rise is extended for a 20% reduction in airflow, effectively increasing the stall margin for the first stage. The rotating stall characteristic is assumed to be similar to the original shape, but at a higher pressure, as was indicated experimentally. With this change to the first stage only, the modeled compression system exhibited continuous surge cycles, rather than rotating stall, as illustrated in Fig. 16. When similar changes were made to the second and third stages individually, the results were nearly identical. However, when changes to all three stages were incorporated, the compression system resisted the stall condition altogether at the throttle setting which had previously caused instability.

TEN STAGE COMPRESSOR MODEL

The techniques of dynamic modeling find one of their most useful applications in the detailed study of stage behavior and interactions in multistage compressors. A ten-stage compression system was tested in the Compressor Research Facility (CRF) of Wright-Patterson Air Force Base [25]. The detailed interstage measurements obtained are ideal for comparison with results from the dynamic model.

The compressor used in the CRF test program was a high-speed, 10-stage, axial-flow compressor assembled from hardware obtained from a modern, high-performance aircraft gas turbine engine. Compressor design parameters include a pressure ratio of 8.3, corrected mass flow of 54.44 lbm/sec, and corrected speed of 16,913 rpm. The rig was instrumented to obtain total and static pressures, and total temperatures at various inlet, interstage, and exit measurement planes. Compressor measurement plane locations and stage definition are shown in Fig. 17. As mentioned in an earlier section, for the purpose of analysis, a stage is defined as stator-rotor, since interstage instrumentation was located on the stator leading edges. A complete description of the test facility, test compressor, compressor instrumentation, specialized test procedures, and data acquisition is contained in Refs. 24 and 25.

Time-averaged pressure and temperature measurements were used to calculate unstalled and in-stall steady-state stage characteristics required as model input. The in-stall mass flow rate was determined from measurements obtained with a venturi located downstream of the compressor exit. Additionally, time-averaged pressure and temperature measurements obtained at the compressor inlet and exit were used to model the boundary conditions. Both time-averaged and close-coupled (transducer close as physically possible to pressure port) pressure measurements were used for comparison with model simulations. Although the high-response measurements were not directly used in this effort, they were used by Copenhaver [24], in part to verify that the close-coupled

data accurately represented the pressure history resulting from a post-stall transient.
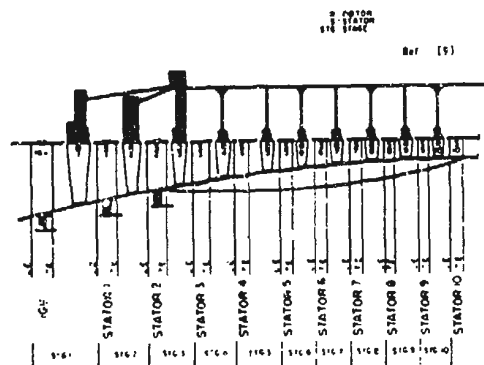
Figure 17 CRF Test Compressor Measurement Plane Location and Stage Definition.

Copenhaver performed a detailed analysis of the test data to examine stage effects on compressor in-stall performance and recoverability. Specifically, the analysis was aimed at offering explanations for the high hysteresis levels observed during the test and indicated in the data. Ideas for reducing the hysteresis were also proposed. The results and conclusions from that analysis pertinent to the current effort are summarized below:

  1. The first three stages of the test compressor did not operate in full-span rotating stall after overall compressor stall occurred.
  2. Choking is likely in the unblocked portion of the tenth stage rotor while the compressor is operating in rotating stall.
  3. Compressor in-stall hysteresis is prolonged due to choking of the rear stages during rotating stall.
  4. Stage matching has a significant effect on multistage compressor in-stall performance and recoverability.

Stage-by-Stage Model

For the model study, the compressor rig geometry (control volumes) and experimentally-determined stage performance characteristics were used. The resulting control volume geometry is shown in Fig. 18. Initially, unstalled performance comparisons were made at numerous speeds to ensure accurate simulation of speedline shape, stall point, etc. Once steady-state performance was verified, the model was exercised to simulate post-stall events (surge or rotating stall). By matching the experimental boundary conditions, model simulations were shown to accurately represent overall and individual stage steady-state, transient, and quasi-steady measured performance. The majority of model simulations were run at or near the compressor's rotating stall/surge boundary speed (78.5% design corrected speed). The post-stall simulations demonstrated the importance of the time lag constant, τ, in determining which event (stall or surge) would occur.
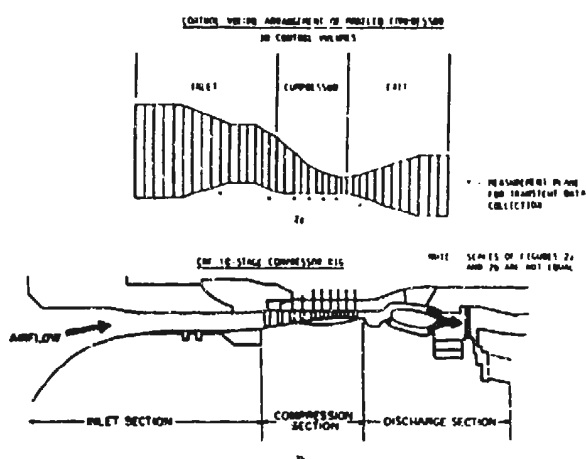
Figure 18 Control Volume Representation of Ten Stage Compressor.

The present requirement to use experimental results to determine correct value of τ (or any other model parameter) does not invalidate the usefulness of the model as an analysis aid. Once an initial value for τ is determined, it can be left unchanged. As a result, the effect of various design changes or other system parameters on model simulations can be examined. In the present investigation, τ was used to calibrate the model at the stall/surge boundary. The model was repeatedly exercised at 78.5% speed until a τ boundary of 0.028 seconds was determined. Once determined, τ was held constant (along with all other model parameters), and the model was run at 82.0% speed. Fig. 19 displays the results of these runs, and demonstrates the model's ability to simulate the compressor's stall/surge boundary. The value of τ was held at a constant value (0.028) throughout all the model simulations/predictions.
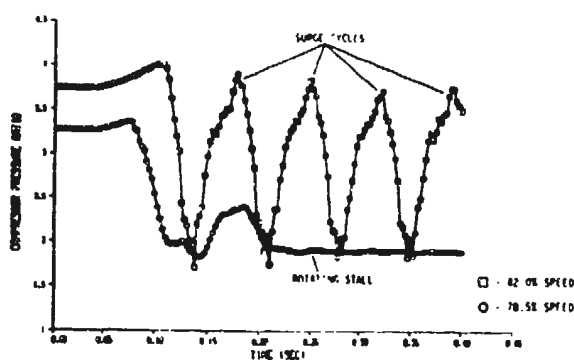
Figure 19 Model Simulation of Experimentally-Determined Rotating Stall/Surge Boundary.

Model prediction of a rotating stall event is shown in Figs. 20 and 21, along with the experimentally-determined performance for the same event. Figure 20 demonstrates overall performance comparison, while Fig. 21 shows interstage comparisons. Both plots were produced from the results of the same model run, namely, a 78.5% corrected speed simulation. The model was supplied with steady and dynamic boundary conditions that were consistent with the experimental conditions. The model simulation was started away from the stall point because of numerical oscillations associated with the start of a model run. Figure 20 demonstrates the model's ability to accurately simulate overall compressor stalling features. These features include stall point, transient drop in performance (including the initial surge-like behavior), and final, average in-stall performance.
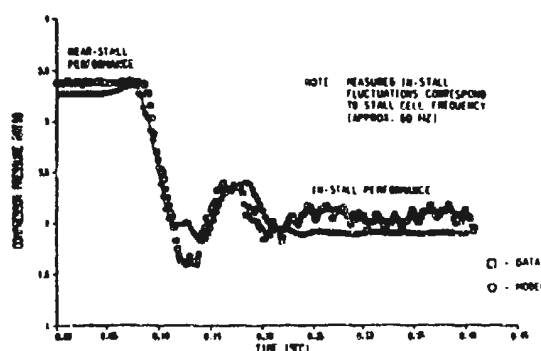
Figure 20 Model Simulation of Overall Rotating Stall Performance and Comparison with Data.

Figure 21 displays similar agreement on an interstage basis. In a flow-averaged sense, model-predicted overall and interstage steady and transient behavior agreed well with the measured performance.
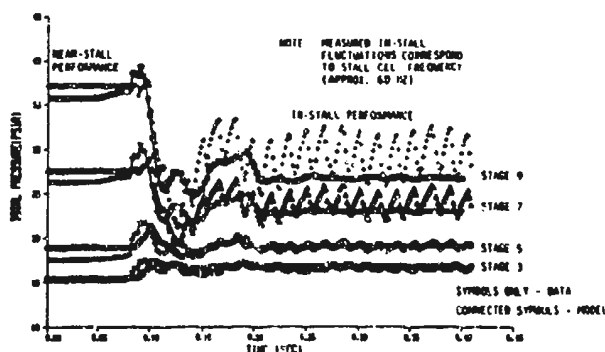
Figure 21 Model Simulation of Interstage Rotating Stall Performance and Comparison with Data.

Of particular interest in Fig. 21 is the apparent increase in average performance of the front stages of the compressor once rotating stall developed. The back stages (4-10) exhibited an expected drop in performance associated with a stage operating in rotating stall. The apparent mismatch between stages three and four is the basis for model predictions concerned with improving compressor recoverability.

The ability of the model to simulate the extensive hysteresis exhibited by the compressor at the stall/surge boundary speed of special interest. This ability was made possible through a modification to the model allowing the addition of double-valued stage characteristics (double-valued in terms of flow coefficient). As shown in Fig. 22, the model is able to accurately represent the hysteresis, and thus the poor recovery behavior exhibited by the compressor rig when operating below

its stall/surge boundary speed. The simulation is a result of decreasing the throttling function by 15 percent (as was the case for the simulation described in the preceding paragraphs), holding long enough to establish steady, in-stall performance, and then increasing the throttling function 35 percent. This is shown graphically in Fig. 22. As indicated in the plot, the model does not predict recovery from stall as the "throttle" is opened well beyond its initial stall inception value.

Model Predictions For Improved Recoverability

As previously noted, results from the CRF test indicated extensive compressor in-stall hysteresis at 78.5% design corrected speed. Subsequent data analysis yielded important conclusions concerning the influence of stage performance effects on the recovery of the test compressor from rotating stall [24]. The stage-by-stage model presented has been shown to accurately represent the compressor transient and quasi-steady, in-stall measured performance (Figs. 20 and 21), as well as the extensive hysteresis described above (Fig. 22). The excellent agreement between model simulations and experimentally-determined performance served to both validate the application of the modeling technique to the CRF compressor rig, and increased the level of confidence placed in model predictions.
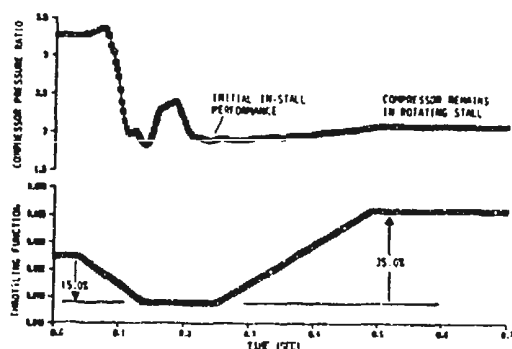

Figure 22 Model Simulation of Experimentally-Determined Compressor Recovery Hysteresis.

Both model and experimental results indicated that at 78.5% design corrected speed, the front stages of the compressor may remain unstalled while the compressor exhibits rotating stall behavior (the first three stages generate a higher time-averaged pressure rise once the compressor is in stall). In addition, the poor recovery behavior (extensive hysteresis) exhibited once the compressor is in stall appeared to be a result of flow blockage of the rear stages. As discussed in detail in Ref. 24, the prolonged in-stall hysteresis is likely due to choking in the unblocked portion of the tenth stage rotor (note the negative pressure coefficients and negative slope of the in-stall characteristic of the tenth stage as shown in Fig. 24). Thus, the hysteresis level can be reduced if the latter stage flow blockage can be reduced or eliminated, improving recoverability.

Model investigations for improved compressor recovery behavior involved reducing the in-stall hysteresis by taking actions that reduced or eliminated the rear stage blockage. These actions included enlarging the rear stage flowpath or

adding a bleed outflow downstream of the middle stages. Modifications to actual stage geometry are represented as changes in stage characteristics. Enlarging stage flowpath area, either through variable vanes or changes to hub/tip geometry, increases the flow capacity of that stage, and results in a shift of its characteristic in the direction of increasing flow. Thus, in order to investigate the effects of an enlarged rear stage flowpath, the tenth stage characteristic was arbitrarily translated by a positive four-hundredths of a flow coefficient (shown in Fig. 24). No attempt was made to change the level of the characteristic; the stall and in-stall pressure coefficients of stage ten remained unchanged.
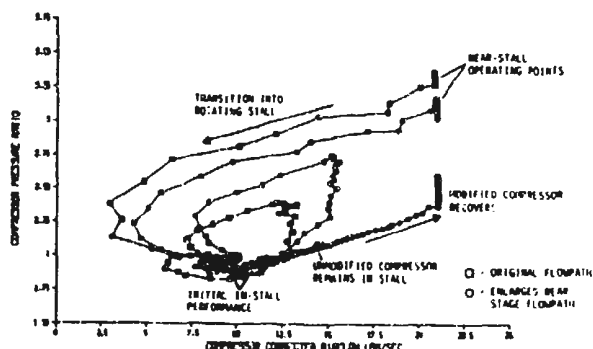
Figure 23 Overall Compressor Map Showing Predicted Improved Recovery Behavior due to Enlarged Rear Stage Flowpath.
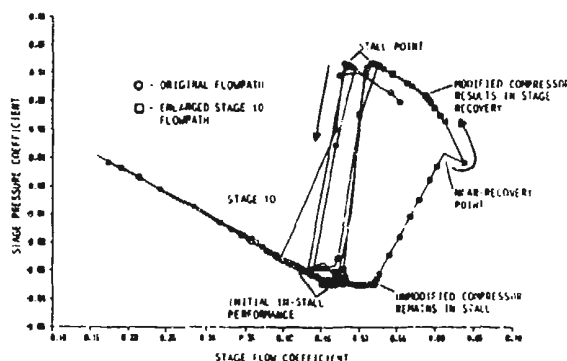
Figure 24 Effect of Enlarged Rear Stage Flowpath on Stage Performance.

Figure 23 demonstrates the improved compressor recovery behavior predicted by the model as a result of the enlarged tenth stage flowpath simulation. The initiation of and subsequent recovery from rotating stall for the "modified" compressor was achieved via the model throttling function through settings identical to those shown in Fig. 22. As shown in Fig. 23, the modified compressor stalls at a slightly higher mass flow rate and lower pressure ratio than does the original compressor. It appears that the increased flowpath resulted in a reduction of the original in-stall aerodynamic blockage extent. The blockage reduction resulted in a higher average in-stall mass flow rate for the modified compressor, and thus improved the ability of the compressor to return to unstalled operation, as shown in Fig. 23. The improved compressor recovery behavior was not without performance penalties. The approximate five percent reduction in stall

pressure ratio indicated in Fig. 23 also produces a loss in stall margin.

Examination of the differences in stage ten performance for the original and modified compressors offers insight into the improved recovery behavior of the enlarged flowpath case. As shown in Fig. 24, the shift of the tenth stage characteristic redistributes the stage loading so that during unstalled operation, the tenth stage is more highly loaded for a given flow coefficient. By enlarging the rear stage flowpath, the stability limit for stage ten occurs at a higher stage flow coefficient. The resulting change in stage matching produces overall compressor stall at a slightly higher mass flow rate and lower pressure ratio than the original compressor (Fig. 23). Further, it appears that the modified stage matching results in decreased levels of aerodynamic blockage when the compressor is in rotating stall. In doing so, initial in-stall stage average mass flow is increased and stage recovery behavior is improved.

In addition to the enlarged flowpath studies, model recovery investigations were performed to investigate the use of interstage bleed flow. The modeling technique here treats bleed flow and its effects as additional source terms in the conservation equations (Eq. 1).

Results from both the model simulations and data analysis suggest that the effectiveness of interstage bleed on compressor recoverability is dependent on bleed location. The results of two model predictions involving interstage bleed are presented in Figs. 25 and 26. In both cases, rotating stall was initiated through the use of the model throttling function. To examine bleed effects, the value of the throttling function was left unchanged once rotating stall had developed. Other than bleed location, the model runs were identical. As shown in the two figures, the model predicts that the rear stage blockage can be essentially eliminated if a 3.0 lbm/sec bleed outflow (15% of the unstalled mass flow) is applied at the entrance of the tenth stage. The result is compressor recovery from rotating stall. The same amount of bleed applied upstream of the middle stages (Fig. 26) does not result in recovery; however, the overall compressor in-stall performance is increased. This apparent dependence of compressor recoverability on bleed location was also demonstrated through the use of a dynamic component-by-component turbofan engine model [27].
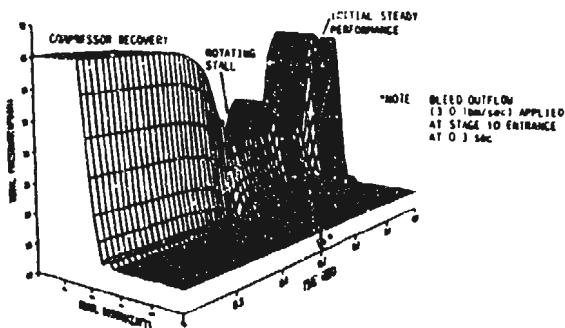
Figure 25 Predicted Compressor Recovery Resulting From Stage 10 Bleed Outflow.
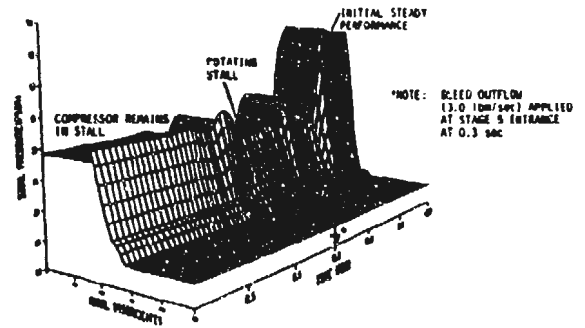
Figure 26 Stall Related Prediction Resulting From Stage 5 Bleed Outflow.

As was done for the increased flowpath study, an examination of stage behavior was performed in an attempt to gain further insight into the effects of interstage bleed on compressor recoverability. Stage dynamic behavior was examined through the use of a dynamic pressure coefficient, obtained by applying a time lag to the stage steady-state forces. Consistent with the observation that of the front stages of the compressor rig remained unstalled with the compressor
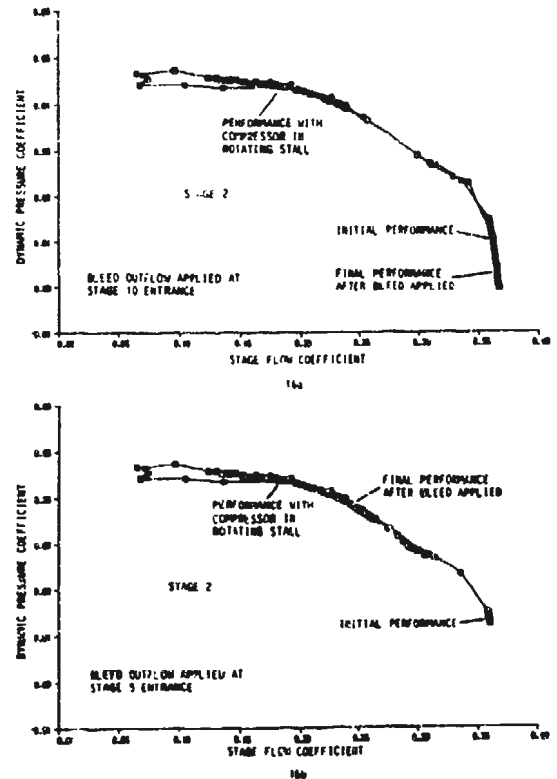
Figure 27 Effect of Bleed Flow Location on Stage 2 Dynamic Behavior.

operating in rotating stall, the dynamic behavior of the front stages does not significantly deviate from steady performance (Fig. 27). Note that when the bleed is applied downstream (Fig. 27a), the front stages return to higher flow levels indicative of unstalled operation (recovery). Figure 28 demonstrates the dependence of stage recovery behavior on bleed

location. Bleeding downstream of the stalled middle stages increases the axial velocity, thus reducing the blade angle of attack and unstalling these stages (Fig. 28a). Applying the same amount of bleed upstream of the middle stages does not result in recovery of the latter stages (Fig. 28b). Stalled stages, and therefore the compressor, receive little recovery benefit from a bleed outflow applied upstream of the stalled stages.
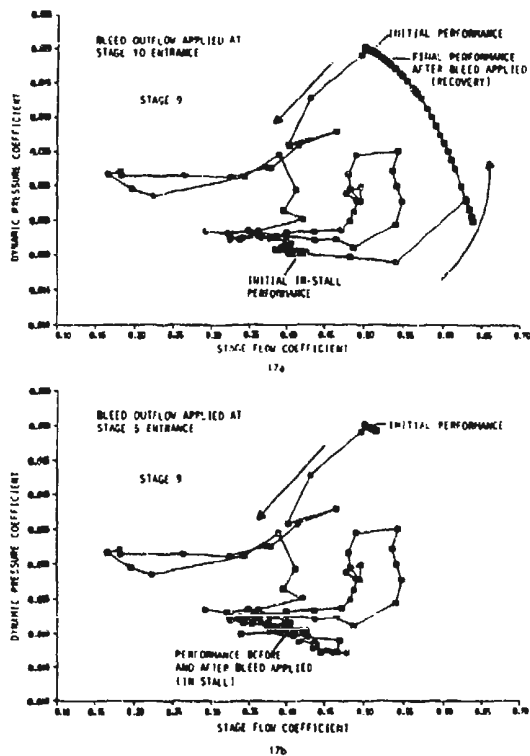
Figure 28 Effect of Bleed Flow Location on Stage 9 Dynamic Behavior.

The following conclusions were based on the combined results of the compressor rig test and model predictions:

1. The improved recovery predictions presented here were made possible by the stage-by-stage compressible model. The following observations are offered:

    a. Analysis of individual stage behavior during transient events such as surge or rotating stall can be performed. This analysis resulted in a more quantitative understanding of post-stall, interstage fluid mechanics in multistage axial-flow compressors.
    b. The effects of design changes to a stage or stages on model-predicted overall and interstage performance can be examined.
    c. The physical features of the modeled compressor were retained. Control volume size is governed by actual stage geometry.
    d. The usefulness of a stage-by-stage model of this type extends beyond the obvious stall/recovery investigations.

The model's ability to provide information that is very difficult or costly to measure is a true asset. For example, in this effort, the dynamic behavior of individual stages was examined in detail (Figs. 27 and 28), and then actions were studied to alter the behavior resulting in a more recoverable compressor.

The choice of a stage-by-stage model or a lumped control volume representation is dependent on the application. For example, an overall model would be appropriate for a recovery investigation involving overall compressor behavior or studies related to system parameters (discharge volume, compressor length, etc.). However, a detailed investigation involving interstage changes would require a stage-by-stage model.

2. The effect of the actions taken on compressor recoverability was dependent on axial location (i.e., bleeding upstream of the middle stages did not result in compressor recovery). As such, the actions point to the importance of stage matching on compressor stalled behavior, and its influence on recoverability. Highly unloaded front stages may result in an extension of the compressor starting problem (front-stage stall, rear-stage choke) into stages downstream. Specifically, the front stages may remain unstalled while the compressor exhibits stalled behavior [24]. If this is the case, actions known to improve compressor starting may improve recovery behavior, but only if they are applied downstream of the stalled stages.

3. The extension of compressor test results, as was done in this study, represents one of the primary uses of a model of this type. The following extensions have been identified, and represent only a sample set:

    a. Study of velocity and/or Mach number profiles within the machine.
    b. Throttle ramp rate studies, both in and out of stall.
    c. Stall margin studies, including the graphical representation of the path of each stage toward stall as the flow is reduced.
    d. Introduction of pressure and/or temperature pulses anywhere in the machine; study of the effect of slow or fast temperature changes.
    e. Study of the effects of inlet resistance (distortion-producing device), combustion, and gas path heat transfer on compression system operation.

COMPRESSOR STAGE CHARACTERISTICS

As has been seen in the previous examples, detailed stage-by-stage dynamic models require stage characteristics for the entire flow range spanning near-design flows, rotating stall, and reversed flow (Fig. 29). The characteristics used were either taken from the modeled experiment, or estimated for ranges where the experimental values were not available. It is, of course, desirable to predict stage characteristics from design information for a complete simulation prior to an experiment. The following material summarizes results of a recent effort [28] to develop a stage characteristic prediction method.

STAGE MODEL THEORY

The elementary axial-flow compressor stage mean-line analysis principles for forward, unstalled flow are well-known. This type of analysis assumes incompressible, inviscid flow through a single stage and uses empirical correla-

tions to estimate the pressure losses and flow deviation in each blade row. The classical correlations are given by Lieblein [29] and Carter [30], respectively, for unstalled operation. Methods for prediction of in-stall and reversed-flow stage performance have not previously been developed.
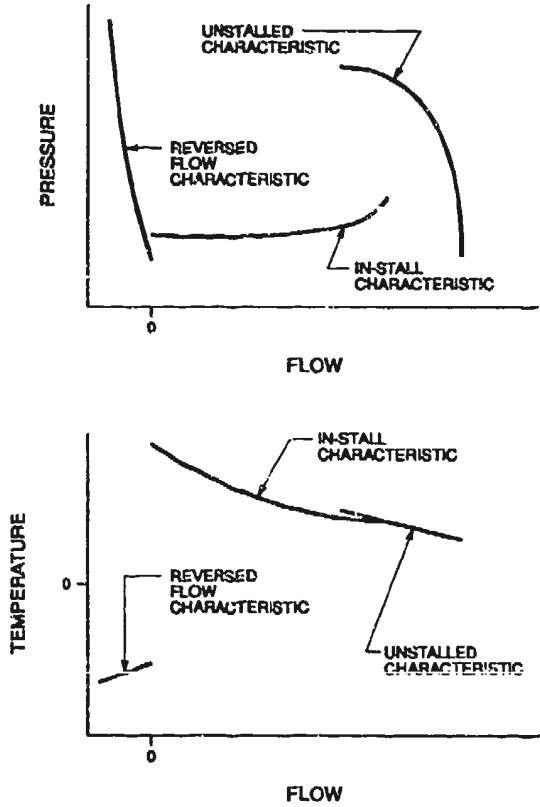
Figure 29 Full-Range Compressor Stage Characteristic.

Unstalled Forward Flow
A typical compressor stage and the flow angles associated with forward flow are shown in Fig. 30. Using the moment of momentum equation for this geometry, Euler's turbine equation gives the stage temperature rise.

$$\frac{\Delta T_0}{T_{01}} = \frac{T_{02}-T_{01}}{T_{01}} = \frac{U^2}{c_p T_{01}}\left[1-\frac{V_{x1}}{U}\left(\frac{V_{x2}}{V_{x1}}\tan\beta_2+\tan\alpha_1\right)\right] \quad (7)$$

For incompressible flow, the total pressure rise for the stage is related to the total temperature rise and the blade row pressure losses by

$$P_{02}-P_{01}=\rho c_p\Delta T_0-(\Delta P_{0R}+\Delta P_{0S}) \quad (8)$$

For incompressible flow, the total pressure losses are related to the cascade loss parameters by

$$\bar{\omega}_R=\frac{\Delta P_{0R}}{\rho W_1^2/2} \text{ and } \bar{\omega}_s=\frac{\Delta P_{0S}}{\rho V_2^2/2}. \quad (9)$$

For incompressible flow, the stage efficiency is given by

$$\eta=1-\frac{\Delta P_{0R}+\Delta P_{0S}}{\rho c_p\Delta T_0} \quad (10)$$
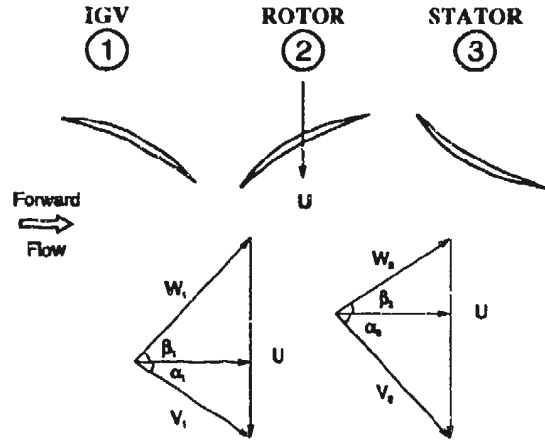
Figure 30 Mean Radius Section of a Compressor Stage in Forward Flow Operations.

Since the angles in Eq. 7 are flow angles and the pressure losses cannot be calculated directly, approximations for the deviation angle and loss coefficients must be made.

To estimate the flow exit angle in the unstalled, forward flow regime, the model uses Carter's correlation, which is for near-design operation. Because the deviation does not change significantly until the blade stalls, this angle is assumed to be constant.

$$\beta_2-\beta_2'=\frac{m\theta}{\sqrt{\sigma}} \quad (11)$$

where m is obtained from the reference.

The blade losses are calculated as the sum of profile, annulus and secondary losses. The profile losses are given by Lieblein [29] and the annulus and secondary losses are given by Dixon [31] as follows.

$$\bar{\omega}_p=2\sigma\frac{\cos^2\beta_1}{\cos^3\beta_2}\left(\frac{\theta^*}{c}\right)_2\left[\frac{\frac{2H_2}{3H_2-1}}{\left[1-\left(\frac{\theta^*}{c}\right)_2\frac{\sigma H_2}{\cos\beta_2'}\right]^3}\right] \quad (12)$$

$$\bar{\omega}_a=0.02\sigma\left(\frac{c}{H}\right)\frac{\cos^2\beta_1}{\cos^3\beta_m} \quad (13)$$

$$\bar{\omega}_s=\frac{0.072}{\sigma}\frac{\cos^2\beta_1}{\cos\beta_m}(\tan\beta_1-\tan\beta_2)^2 \quad (14)$$

where $\tan\beta_m=\frac{(\tan\beta_1+\tan\beta_2)}{2}.$

Stalled Forward Flow
For in-stall, forward flow operation, the flow is assumed to separate from the blade leading edge, as shown in Fig. 31, and the approximation of Moses and Thomason [32] is used to

predict the fully mixed flow angle and loss coefficient. The determination of the jet exit angle, β_2, is based on additional empiricism and is discussed later. The jet velocity ratio is given by

$$\frac{V_2}{V_1} = \frac{-b \pm \sqrt{b^2 - 4ac}}{2a} \qquad (15)$$

where

$$a = 1 + \frac{0.15\sigma}{\cos\beta_1} \quad b = \frac{-2\cos\beta_1\cos\delta}{\cos\gamma} \quad c = \frac{2\cos\beta_1\cos\alpha}{\cos\gamma} - 1$$

To give meaningful results, only the positive result in Eq. 15 is used.
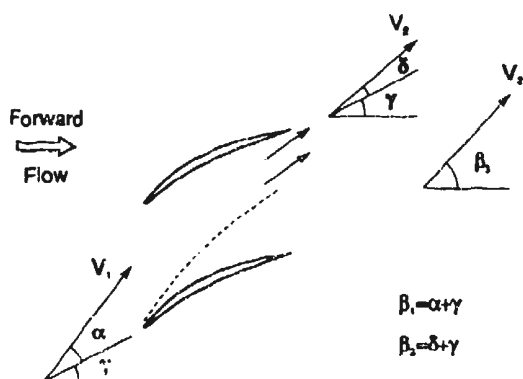
Figure 31 Compressor Cascade Geometry and Nomenclature for Stalled Operation.

The fully mixed flow angle and loss coefficient are given by

$$\tan\beta_3 = \frac{V_2\sin\beta_2}{V_1\cos\beta_1} \qquad (16)$$

$$\bar{\omega} = \frac{P_{01} - P_{03}}{\rho V_1^2 / 2}$$

$$= (1 + \frac{0.15\sigma}{\cos\beta_1})\frac{V_2^2}{V_1^2} + 2\cos\beta_1\left(\cos\beta_1 - \frac{V_2}{V_1}\cos\beta_2\right) - \frac{\cos^2\beta_1}{\cos^2\beta_3} \qquad (17)$$

Because the profile losses for a stalled blade row are much larger than the annulus and secondary losses, the latter are ignored in this flow regime.

Reversed Flow

A typical compressor stage and the flow angles associated with reversed flow are shown in Fig. 32. The development of the basic stage performance equations is a direct extension of that presented previously, with the subscripts changed to reflect the direction of flow. Using the moment of momentum equation for this geometry, Euler's turbine equation gives the stage temperature rise.

$$\frac{\Delta T_0}{T_{02}} = \frac{T_{02} - T_{01}}{T_{02}} = \frac{-U^2}{c_p T_{02}}\left[1 - \frac{V_{x1}}{U}\left(\frac{V_{x2}}{V_{x1}}\tan\alpha_2 + \tan\beta_1\right)\right] \quad (18)$$

It should be noted that the compressor does work on the fluid in the direction of flow, increasing its temperature in that direction. When the compressor is operating in reversed flow, the temperature at station 1 is greater than at station 2 and the result in Eq. 18 is negative. The flow angle, β_1, is assumed to be the blade metal angle as suggested by Turner and Sparkes [33] and by Koff and Greitzer [34].
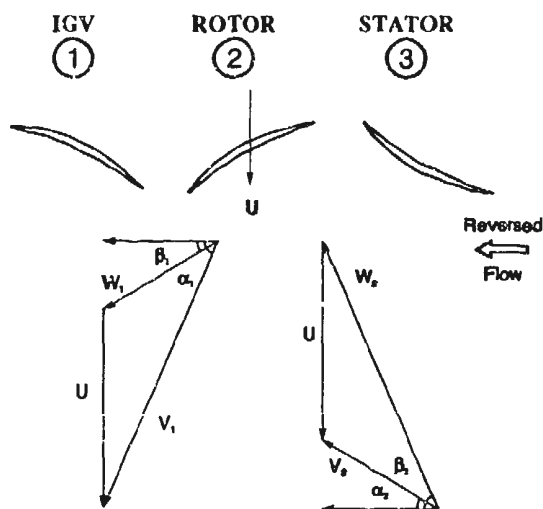
Figure 32 Mean Radius Section of a Compressor Stage in Reversed-Flow Operation.

For incompressible flow in the reversed direction, the pressure losses are *added* in Eq. 19 because they are positive in the direction of flow, which is from station 2 to station 1.

$$P_{02} - P_{01} = \rho c_p \Delta T_0 + (\Delta P_{0R} + \Delta P_{0S}) \qquad (19)$$

In a cascade experiment to study reversed flow, Cameal [35] showed that losses in the reversed-flow region, when non-dimensionalized by wheel speed, collapse onto a single parabola as shown in Fig. 33. While the data for reversed-flow losses were derived from cascade tests, it is possible to express the results in terms of wheel speed for a rotating cascade. Although the loss curve for one stagger angle diverges from the others at reversed flow coefficients less than -0.25, the region of typical compressor operation is $V_x/U \ge -0.25$, even during a deep surge cycle. The implication of this result is that the reversed-flow losses are reasonably approximated as a function of mass flow only, independent of flow angle, solidity, blade shape, and other flow details. A parabola fit to the five coincident curves of Cameal's data is used to determine the blade row losses as a function of mass flow, and this result is used in Eq. 19 to calculate the stage pressure rise.
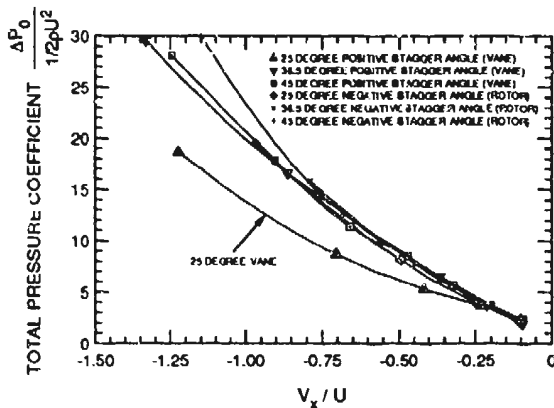
Figure 33 Corrected Pressure Losses in a Reversed-Flow Compressor Cascade.

Gamache [10] noted that the last stage stator in reversed flow functions in the same manner as the IGV during forward flow. The flow enters the blade row with a small angle of attack and is turned from the axial direction, accelerating the flow like a nozzle. Gamache measured a negligible pressure loss across this blade row in reversed-flow operation, so the model neglects the losses for the last stator of the compressor when operating in reversed flow.

The stage efficiency is not a meaningful number in reversed flow because the large pressure losses in the reversed flow analog of Equation (10) and the use of correction factors discussed in a later section often make the result fall outside of the bounds of $0 \leq \eta \leq 1$.

EMPIRICAL OBSERVATIONS AND ADDITIONS

Although the present model is based on fundamental fluid mechanics and experiments, some empirical additions have been necessary to achieve the desired agreement with measured characteristics. These additions were based on logical extensions of the published literature.

Criteria Used For Stall Inception

Yocum [36] reported the angle of incidence at which flow separation would occur in a test cascade to be 8°. Longley and Hynes [37] reported that a stage operating as part of a multistage compressor can remain unstalled at flows much lower than the isolated clean-flow stall point. It has been suggested that the pumping action of the downstream stages tends to prevent upstream flow separation. In an attempt to model this effect, the angle of incidence at which separation occurs is assumed to be the sum of the isolated stall incidence (8°) and a correction for the location of the stage in a multistage environment, which leads to the following expression for stalling incidence.

$$i_{stall} = 8° + a\Delta i \qquad (20)$$

where $\quad a = \dfrac{current\ stage\# - 1}{total\ \#\ stages - 1} \qquad \Delta i = i_{first\ stage \atop stall} - 8°$

The value used for the first stage stalling incidence was obtained from the first stage of the 3-stage compressor tested by Gamache [10], which stalled at 16° angle of incidence. If it is assumed that this result is generally applicable, the bounds on the incidence angle for separation are $8° \leq i_{stall} \leq 16°$, with 8° used for the last stage and 16° used for the first stage of a modeled compressor. This correlation was applied to all stages modeled and reported here.

When a blade row stalls, the flow at the trailing edge consists of a high velocity jet near the pressure surface and a separated, recirculating region near the suction surface. It is expected that the wake will not have sufficient time to mix to a uniform condition before reaching the downstream blade row and that the recirculating region will be sufficient to initiate stall of the downstream row. For this reason, the model assumes that when the rotor stalls, the downstream stator stalls as well.

Stalled-Flow Jet Exit Angle

The reasoning used to determine the stalled flow jet exit angle is similar to that presented in the previous section. The approximation of Moses and Thomason [32] suggests that the flow leaves the trailing edge at approximately the stagger angle. The present author suggests that the pumping action of the downstream stages, which delays the onset of stall in the upstream stages, tends to reduce the extent of separation once stall occurs.

The jet angle is assumed to be the sum of the trailing edge blade angle and a correction for the location of the stage in a multistage environment, which suggests the following correlation for the jet exit angle.

$$\beta_2 = \beta'_2 + a(\beta'_2 - \gamma) \qquad (21)$$

where $\quad a = \dfrac{current\ stage\# - 1}{total\ \#\ stages - 1}$

The resulting bounds on the exit jet angle are $\beta'_2 \leq \beta_2 \leq \gamma$, with the lower bound of β'_2 being used for the first stage and γ for the last stage.

Recovery Hysteresis

It is well-known that a compressor will not recover from stall until the mass flow is increased to a value greater than that which existed when stall was initiated, but the extent of the hysteresis that will be present is not well understood. The present model predicts the stage performance in the region where the characteristics are double valued, but does not attempt to calculate the extent of the hysteresis. To include this effect in the model, the stalled flow calculations are begun with an incidence of 6° before stall inception. This selected amount of hysteresis is considered reasonable based on experience of the author, but cannot be calculated by any present theory. Because the stalled calculations involve solving the quadratic in Eq.15, solution is not possible for all incidence angles and not all of the predicted stage characteristics presented below show the full 6° of hysteresis.

Reversed-Flow Pressure Prediction

The flow field in a compressor operating in annulus reversed flow is not well understood, as there has been little research performed in this flow regime. The present model predicts reversed-flow performance with reference to the experiments of Carneal [35] and Eq. 19, with an empirical correction in the form of Eq. 22 to improve agreement with experiments.

$$P_{02} - P_{01} = a_1 \rho c_p \Delta T_0 + a_2 (\Delta P_{0R} + \Delta P_{0S}) + a_3 \qquad (22)$$

where

$$a_1 = 0.31$$
$$a_2 = 1.33$$
$$a_3 = 0.20$$

By use of the performance of the first stage of the compressor tested by Gamache [10], the values for the coefficients in the above equation were obtained and were used in all predictions presented. It should be noted that at this time there is no theory to predict these coefficients.

ASSEMBLY INTO A WIDE RANGE PREDICTION MODEL

A full-range stage performance computer model (FULRANGE) was developed as an assembly of the methods discussed in the previous sections. To implement the model over the range of mass flow coefficients in the forward flow regime, the relative flow angle at the rotor inlet is varied from zero angle of attack to zero flow (relative flow angle is 90°) in one degree increments and the appropriate flow calculation is applied. To generate the reversed-flow characteristics, the model increments the mass flow index, V_x/U, by a fixed (negative) amount and the reversed-flow calculations are performed.

The information required by the model to predict stage performance is the rotor and stator mean-radius geometry, as summarized in Table 1.

Table 1 FULRANGE model input parameters.

rotor blade leading edge angle
rotor blade trailing edge angle
rotor blade stagger angle
rotor blade mean radius
number of rotor blades
rotor blade chord
rotor blade span
rotor blade thickness/chord ratio
IGV or (upstream) stator exit flow angle
stator blade leading edge angle

stator blade trailing edge angle
stator blade stagger angle
stator blade mean radius
number of stator blades
stator blade chord
stator blade span
stator blade thickness/chord ratio
stage axial velocity ratio
location (stage number) of stage being modeled
number of stages in the machine being modeled

APPLICATION TO A LOW SPEED COMPRESSOR

To verify the accuracy of the FULRANGE technique, the model was used to predict the performance of the low-speed 3-stage rig [10]. This compressor had a constant flowpath annulus with 3 non-repeating stages; further details about this compressor can be found in the reference. For this machine, a stage was defined as a rotor and the downstream stator.

The predicted and measured pressure characteristics for this machine are presented in Figs. 34 through 36. The predicted characteristics showed very good qualitative agreement in the forward flow region and excellent agreement in the reversed-flow region. The prediction has the same curvature as the measured characteristic throughout the entire flow regime and has no unexplained discontinuities.
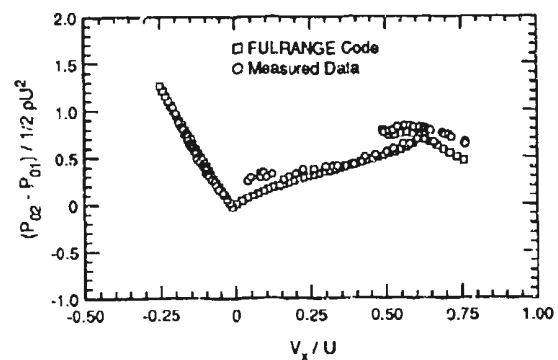
Figure 34 Three-Stage Test Compressor First Stage Pressure Characteristic.

For all 3 stages of this machine, the FULRANGE model predicted the flow coefficient, V_x/U, within 0.01 of the measured value for transition to abrupt stall. It should be noted that this difference between predicted and measured transition represents an error of less than 1° angle of incidence to the rotor.

The unstalled pressure prediction was within 0.15 of the measured values for the first and third stages, but the second

stage agreement was not as good. The unstalled prediction for the second stage was within 0.20 of the measured values.

For flow coefficients greater than 0.10, approximately 90% of the in-stall data were within 0.10 of the predicted pressure characteristic. The general shape of the predicted character-istic is the same for all stages, reaching a zero pressure rise at zero flow, while many compressors exhibit some positive pressure rise at zero flow. The mechanisms for this observed phenomenon are not currently understood.

The first stage reversed-flow pressure prediction is coincident with the measured characteristic, as would be expected (this was the one stage used to develop the correlation coeffi-cients). Application of the reversed-flow model to the second stage prediction yielded an essentially exact match to the characteristic. This supports the application of the results of Carneal [35], which indicated that both rotors and stators in reversed flow could be treated as nearly equal loss producers. For both of these stages, the slope of the characteristic is very steep. This is because the blade row losses in reversed flow are very large as shown in Fig. 33, and a large pressure is re-quired at station 3 as shown in Fig. 34, to force air through the stage.
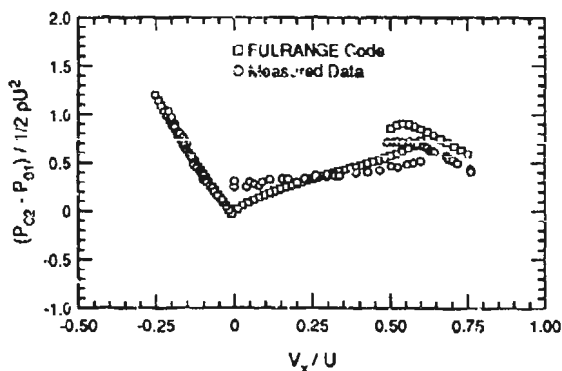
Figure 35 Three-Stage Test Compressor Second Stage Pressure Characteristic.
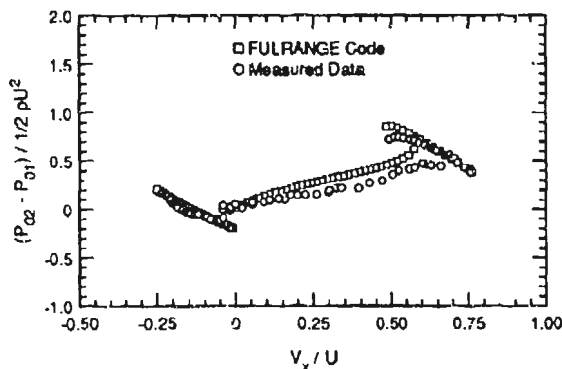
Figure 36 Three-Stage Test Compressor Third Stage Pressure Characteristic.

The reversed-flow pressure prediction for the third stage is within 0.07 of the corresponding measured values. The more nearly horizontal characteristic for this stage is the result of the last stator in reversed flow operating in the same manner as the IGV in forward flow. Because there are small pressure losses in the last stator row (as compared to the first two sta-tor rows), a smaller pressure at the stage exit will force flow backwards through this stage.

APPLICATION TO A HIGH SPEED COMPRESSOR

The FULRANGE code was used to model the performance of the 10-stage, high-speed compressor tested by Copenhaver [24,25]. This compressor was the high pressure compressor from a modern high-performance aircraft gas turbine engine and was tested at five speeds ranging from 49.8% to 78.5% of design corrected speed to investigate stalling and recovery behavior. For this range of corrected speeds, the variable vane schedule was fixed so there was no change in stage ge-ometry; the vanes open only at higher corrected speeds. Be-cause the present model assumes incompressible flow across a single stage, the predicted stage characteristics are inde-pendent of wheel speed and the measured data are presented without distinction of the speed at which they were obtained. The flow, pressure, and temperature coefficients plotted in these figures are defined as follows.

$$\phi = \frac{\left[\dfrac{\dot{m}\sqrt{T_0}}{P_0 A}\right][NC]}{0.5318} \qquad (23)$$

$$\psi^P = \left[PR^{\frac{\gamma-1}{\gamma}} - 1\right][NC]^2 \qquad (24)$$

$$\psi^T = [TR - 1][NC]^2 \qquad (25)$$

where

Before discussing the pressure and temperature characteris-tics, a comment regarding the flow coefficient predictions is in order. The model predicted the transition to stall within 2° angle of incidence to the rotor for all stages in the compres-sor. It is unknown whether this is the result of an underlying mechanism that is approximated but not yet understood, or whether this is a fortuitous coincidence.

Pressure Characteristic Predictions

The model consistently over-predicted the unstalled pressure coefficients for the first three stages by a significant amount, as shown in Figs. 37 and 38. The second stage characteristics are similar to those of the third stage and were omitted for brevity. The reasons for the significant disagreement in this area are not clearly understood at this time, but two theories are put forth.

For the low corrected speeds at which this compressor was tested, the IGV and first two stator rows were fully closed (large stagger angles, as measured from an axial reference). Under these conditions, the flow into the IGV is at a large angle of incidence and is turned significantly away from the axial direction. The large incidence is likely to cause

Figure 37 Ten-Stage Compressor: a) First Stage Pressure Characteristic; b) First Stage Temperature Characteristic.
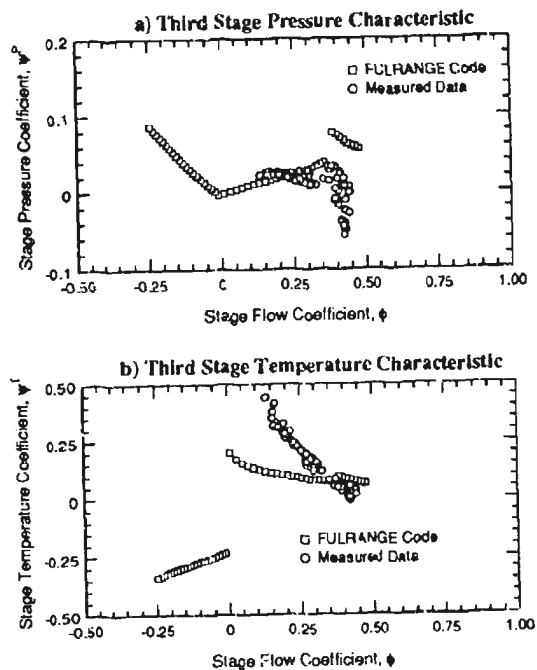
Figure 38 Ten-Stage Compressor: a) Third Stage Pressure Characteristic; b) Third Stage Temperature Characteristic.

separation from the IGV leading edge, causing large pressure losses and a large flow deviation angle. This situation is far from design-point IGV operation and the current model is unable to approximate the performance accurately. It is believed that a similar flow separation may occur in the stator rows of stages two and three, as well.

A second effect of the closed vanes is that the flow is accelerated significantly due to the reduction in apparent flow area. This area ratio is of sufficient magnitude to cause choking of the flow (even at moderately low mass flow), a phenomenon which the present (incompressible) model is not capable of predicting.

Based on the nearly vertical pressure characteristics for the second stage (not shown) and the third stage (Fig. 38), Copenhaver [24,25] concluded that choking existed in these stages. Because these stages appeared choked at high flow coefficients, and because of the negatively sloped pressure characteristics for the entire operating region, Copenhaver concluded that they were operating in a high-flow manner under all conditions. Based on the flow angles calculated by the FULRANGE model, it is suggested that the stages were operating in-stall when the mass flow was low enough to eliminate the choking. The fact that there is good agreement between the predicted in-stall pressure rise and the measured performance for the second and third stages would tend to support this idea.

The predicted and measured pressure performance of stages four through eight are very similar and the fifth stage characteristics shown in Fig. 39 is representative. The unstalled pressure predictions for these stages are nearly coincident with the actual data points. The in-stall predictions have the same slope and curvature as the measured characteristics, but are significantly lower in magnitude. It is believed that the under-prediction is a result of the modeling assumption of axisymmetrically stalled flow. Continuing work is addressing methods for improved modeling of the circumferential variations which exist in in-stall flows.

The qualitative agreement of the predicted and measured performance of the ninth stage is similar to that of the eighth and the tenth stages, and comparison is omitted for brevity.

Before discussing the operation of the tenth stage, it is instructive to look at the effect of density variation on stage performance. Under low speed conditions, the density increase across each stage is lower than the design value. The area reduction found in high speed, multi-stage compressors results in high axial velocities in the rear stages and can lead to choking.

The unstalled pressure prediction for the tenth stage agrees well with the measured data for flow coefficients less than 0.60, as shown in Fig. 40. At higher mass flows, the high velocity air at the stage entrance causes the pressure to *drop* and the stage performs like a turbine. When operated in-stall, the tenth stage was extracting work from the flow for all data points, with an apparent choking condition at a flow coefficient of 0.57. For these reasons, the predicted and measured performance were not close.

a) Fifth Stage Pressure Characteristic
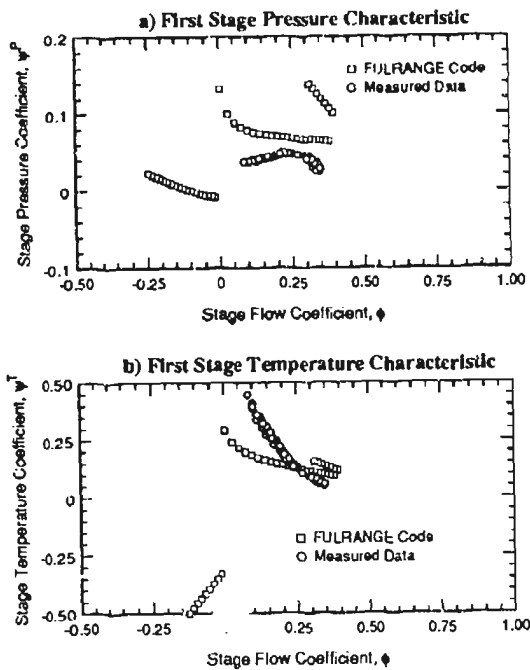

b) Fifth Stage Temperature Characteristic

Figure 39 Ten-Stage Compressor: a) Fifth Stage Pressure Characteristic; b) Fifth Stage Temperature Characteristic.

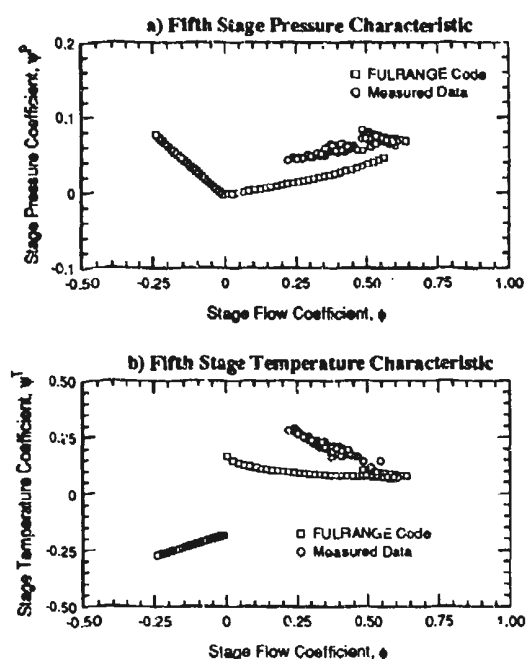## a) Tenth Stage Pressure Characteristic

b) Tenth Stage Temperature Characteristic
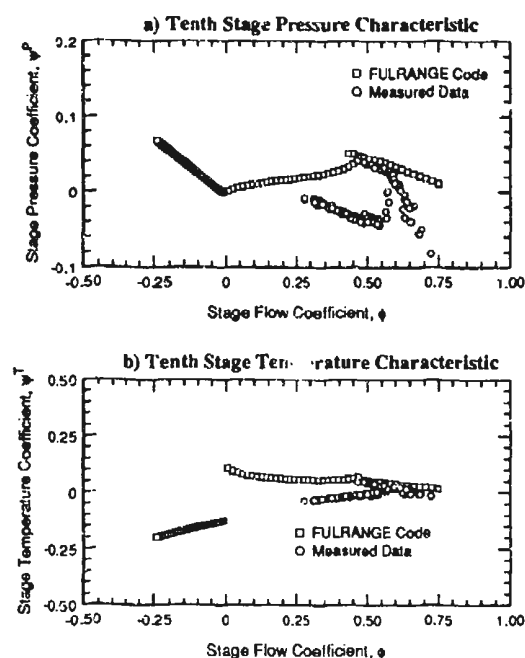
Figure 40 Ten-Stage Compressor: a) Tenth Stage Pressure Characteristic; b) Tenth Stage Temperature Characteristic.

Before discussing the reversed-flow pressure characteristics, it should be noted that the instrumentation placed on this compressor resulted in a stage being defined as a stator followed by a downstream rotor. There are two implications of

this stage definition for reversed-flow operation. The first implication is that there is no "last stage stator" for which the losses should be neglected, because the tenth stator is not part of a stage for which performance was measured; the tenth stage consists of stator 9 and rotor 10. The second implication is that the effect of the fully closed IGV and first two stators in reversed flow will only be seen in the first and second stages; stator 3 will control the flow angle into stage 2, stator 2 will control the flow angle into stage 1, and flow downstream of the IGV in reversed flow is outside of the compressor.

Because of the experimental difficulty of generating reversed flow in high-speed, high-pressure ratio compressors, no reversed-flow data were obtained. For this compressor, the quantitative predictions of the model are therefore unsupported.

For similar stage geometry's, Gamache [10] measured nearly identical performance in reversed flow. The last eight stages of the 10-stage compressor were geometrically similar, and the reversed-flow performance predictions for these stages are very similar. The model predicted a smaller (magnitude) slope of the reversed-flow pressure characteristic for the first two stages because the IGV and first two stators are closed to the flow path. This resulted in a larger relative flow angle into the first and second rotors and more work being done on the air in the reversed direction.

Temperature Characteristic Predictions
The unstalled temperature predictions for the first three stages are higher than the measured characteristics, but show good qualitative agreement. It is believed that the errors in calculating the flow angles leaving the IGV and first two stators (which were fully closed to the flow path) resulted in the calculation of more flow turning than actually occurred. The predicted in-stall temperature rise for these stages is approximately correct at stall inception, but at lower mass flow the measured temperature rise increases much more than the present model predicts. This is believed to be the result of the significant viscous heating which occurs at low flow rates in high speed compressors.

At this time, an interesting point can be made about the perceived inception of stall. In the unstalled region, both the FULRANGE predictions and the measured temperature rise show a linear characteristic with negative slope. It is clear from the first and fifth stage data that the temperature characteristic experiences a discontinuous change in slope and curvature at the inception of stall (as defined by the slope of the pressure characteristic) and this is confirmed by the model. Since the change in slope of the measured temperature characteristic is much more pronounced than that of the pressure curve for these stages, it is suggested that temperature performance may be a better indicator of the onset of progressive stall. In reference to the performance of the second and third stages, the temperature characteristics would indicate that at flow coefficients less than 0.30 and 0.33, respectively, these stages are operating in-stall.

The unstalled temperature prediction for the fourth through tenth stages showed excellent agreement with the measured

performance. A large fraction of the predictions are almost coincident with the data in this region. The in-stall predictions for the fourth and fifth stages show the same trend of under-predicted temperature rise at low mass flow that was shown by the first three stages, but this trend is less pronounced for the fourth stage.

The in-stall temperature predictions for the sixth through tenth stages are of the same form as for the first five stages (negatively sloped with positive concavity), but the measured characteristics are positively sloped and linear. The measured data often show a steady-state *drop* in temperature with an increase in pressure, which violates the second law of thermodynamics, for a portion of the stalled characteristic. Copenhaver [25] suggested that the indicated drop in temperature was the result of significant recirculating flow within the rotating stall cells. As the flow moved backwards through each stage, work was done on it and its temperature increased.

For all stages, the reversed-flow temperature prediction is positively sloped and linear. The slope of the temperature characteristic is larger for the first two stages than for the last eight. This is because the IGV and first two stators are fully closed to the flow path, creating a larger relative flow angle to the rotor and resulting in higher turning. There are currently no reversed-flow data for this compressor, so comparisons cannot be made.

Finally, all of the above predictions must be viewed as the result of an axisymmetric model. The model cannot presently account for two- and three-dimensional, non-uniform effects which may influence the flow field.

STAGE MODEL SUMMARY
The model was applied to a 10-stage high-speed compressor and mixed results were shown. There were effects of compressibility apparent in the forward stages which could not be captured by the current model. The predicted pressure characteristics showed very good agreement with the unstalled performance of the last five stages, although the tenth stage characteristics diverged at high mass flows. The in-stall prediction was positively sloped and similar for all stages, but the measured performance was dependent on the stage location; the measured slopes were positive for some stages and negative for others. The reversed-flow pressure characteristics are in good qualitative agreement with those of the low-speed compressor modeled, but no high-speed data exists in the open literature for this flow regime.

The unstalled temperature predictions for the first three stages showed the correct trends, but were larger than the measured performance; for the last seven stages, the agreement was excellent in this flow regime. At low flow rates, the model under-predicted the temperature rise for the first five stages by a substantial amount; it is believed that this is the effect of significant viscous heating which is not captured by the present model. The in-stall performance of the last five stages indicated a significant amount of recirculating flow in the rotating stall cells which could not be predicted by the steady-state, mean-line stage model.

As mentioned previously, the unstalled temperature predictions for the ninth and tenth stages were very close to the measured values, but the pressure characteristics did not show the same level of agreement. It is suggested that the stage losses, and hence the performance, are a function of the environment in which the stage is operated, as well as the aerodynamic design of the stage.

The stage temperature characteristic is essentially linear in the unstalled operating region, but has a discontinuous change in slope and curvature at the inception of progressive stall. Because a stage can operate in-stall with a negatively sloped pressure characteristic, it is suggested that the temperature characteristic might be a better indicator of stall inception.

When a stage stalls, it upsets the flow field downstream to a sufficient extent that it can drive the next downstream stage into stall, even if the downstream stage was operating away from its stall point. It is also possible that choking of a downstream stage can prevent upstream stages from operating at higher mass flows which might be attainable if the upstream stages were operated in isolation. For these reasons, it is suggested that there are certain points on the steady-state stage characteristics which cannot be reached in a multi-stage environment. This is complimentary to the conclusion that a stage operated in a multi-stage environment could operate unstalled at flows significantly below the isolated clean-flow stall point, as reported by Longley and Hynes [37].

COMPUTATIONAL CONSIDERATIONS
Dynamic Models obviously require computer solution, but an additional concern is added if the simulation is to be interactive. since the models are based on design features of the machinery, there are interesting possibilities for rapid assessment of design alternatives, prediction of test results, and study of dynamic behavior if the simulation can be executed rapidly. In multistage compressor simulations, it has been found that the typical dynamic model requires 300-500 times actual time for execution on fast computers; thus, a 0.1 second study of a compressor dynamic might require 50 seconds of computer time. Aside from the cost, this ratio essentially dictates that the simulation is a "batch" computer operation, and that results are studied after a file is created. The above possibilities for interactive use may be realized if the simulation occurs in "near-real-time". Considering the applications, we have defined "near-real-time" as within ten times the actual time simulated. This requirement obviously requires careful attention to efficient programming, and computer architecture in the sense of serial and parallel design.

With these requirements in mind, a near real-time dynamic compression system simulation has been developed. The following discussion is focused on the approach taken to handle the computational requirements of this task for both serial and parallel computer platforms. Important aspects of serial programming are identified that can have a dramatic effect on computational performance. The procedure followed to select the computational platform for this simulation is discussed, and a comparison of how different inter-processor communication schemes affect computational performance in parallel computers is presented. It is shown that efficient program execution demands that communication overhead be reduced as much as possible. This study shows that communication overhead can be reduced considerably by taking advantage of a concurrent communication and computation ap-

proach. The resulting simulation allows near-real-time performance which is "scalable". As the problem size grows, the simulation time can be maintained by simply adding additional parallel processing nodes.

Serial Code Optimization

When developing a computationally efficient computer model or simulation, it must be insured that only required operations are being used. Additionally, these operations should be completed in the most efficient way possible. To identify the cost of various operations, short code segments were developed and tested on an IBM 3090 series 300. Table 2 shows a relative comparison of various floating point operation costs in terms of execution time.

Based on the results in Table 2 the equivalent floating point operation count was determined for each operation type. This was done by normalizing the execution times with the assumption that an individual floating point addition is equivalent to a single floating point calculation. These results reflect the performance of fully optimized and vectorized code with the vector lengths shown. It should be noted here that each computer will have different performance values. Therefore, these specific numbers have no meaning except on the IBM 3090. However, a similar approach can be used on any computer platform. Therefore, this approach will allow improvement of existing computer codes. Additionally, while the specific performance values differ from computer to computer, the relative floating point performance for each type of operation appears to be fairly consistent from one computer to the next.

With the relative cost of each operation type identified, it is a simple matter to count the number of each operation type to determine the total number of floating point operations required for one simulation time step. This number is then used to determine the computational needs of the simulation and hence the computer requirements.

Table 2. Comparison of execution times for different types of floating point operations. Values represent microseconds of execution time on the IBM 3090 series 300.

	NoOpt	Full Optimization and Vectorization			
	NoVec	Vector Lengths			
Type of Operation	10000	10000	1000	100	50
a(i)=b(i)	5986	757	68	6	4
a(i)=b(i)*b(i)+b(i)	9088	1014	90	8	4
a(i)=b(i)*b(i)	7561	989	77	7	2
a(i)=b(i)/b(i)	11052	3713	368	34	18
a(i)=dsqrt(b(i))	29178	8823	923	140	97
a(i)=b(i)**b(i)	71524	19916	1966	205	126

The effectiveness of the compiler's optimizer was investigated. It was found that integer power operations (var**2) were not modified to be calculated as (var*var). Additionally, subroutines were not inserted as in-line code. While some compilers will carry out these types of operations, when writing code for use on many different platforms, it is prob-

ably more efficient to explicitly write the code to minimize computational effort without compiler intervention.

To reduce execution time in the original code, constants that were used in combination at multiple locations in the simulation were calculated once and only once at program initiation. All integer power operations were reduced to combined multiplies. Any division by a constant was converted to a multiply by the inverse constant, and all vectorization opportunities were used.

Because the solution method is based on an explicit algorithm, a time step on the order of 10^{-5} is required. Therefore, a one second simulation requires 100,000 individual predictor and corrector steps, and 200,000 individual thermodynamic property and force evaluations for each control volume. The overhead associated with these calls amounted to 15-20% of the overall program execution time. This overhead figure was determined through the use of an interactive debugger available on the IBM 3090. Because of the large overhead associated with these subroutine calls, many of these routines were rewritten as in-line code. To insure that the program could be readily maintained, numerous comments separated each code segment.

We investigated whether rewriting the simulation in "C" would improve simulation performance. As will be shown later, using "C" did not generally improve program execution speeds. However, we did see dramatic improvements in performance on the parallel computer based on the Transputer® processor. In general, "C" has much less overhead associated with function calls and therefore allowed the development of a much more supportable program without the overhead penalties seen in the FORTRAN version of the program.

Finally each section of the code was carefully scrutinized with emphasis on reducing operation count through different calculation approaches and elimination of unnecessary operations. The pay-back for this effort was an 80 percent reduction in serial code execution time. Serial code optimization is a very important process and should be completed before any parallel code development. Serial code optimization reduces the execution time of the code on all computer platforms. Additionally, using this approach, the benchmarks will compare computer performance as opposed to compiler performance.

Computer Selection Considerations

As stated earlier, by counting the floating point operations in each code segment, serial and parallel calculation requirements may be determined. Table 3 shows the number of floating point operations required by each segment of simulation code. The workload values have been combined into columns that represent the control volume types used in this simulation. At the bottom of each column is the total number of floating point operations required by each control volume type.

It should be noted that no time has been allotted for the communication processes that are necessary on parallel machines. Knowing the average time step which could be used, based on the Courant number, the required computational performance

for different types of computer platforms were determined and are shown in Table 4.

Table 3 Floating point operations required by each control volume type (one iteration time step).

Inlet CV	Duct CV	Blade CV	Exit CV
Evaluate BC (79flops)	Thermo (25flops)	Thermo (25flops)	Evaluate BC (79flops)
Pass Data Left(72Bytes)			
------------	Duct Calc (11flops)	Blade Calcs (148flops)	------------
Pass Data Right(72Bytes)			
Print Output			
Inlet Calcs (262flops) Outflow (167flops)	Diffusive Flux (24flops) Predictor (17flops) Thermo (25flops)	Diffusive Flux (24flops) Predictor (17flops) Thermo (25flops)	Diffusive Flux (24flops) Isen Nozzle (101flops) Outflow (167flops)
Pass Data Left(72Bytes)			
------------	Duct Calc (11flops)	Blade Calcs (148flops)	------------
Pass Data Right(72Bytes)			
------------	Corrector (23flops)	Corrector (23flops)	------------
Pass Data Right(72Bytes)			
------------	Antidiff Flux (23flops)	Antidiff Flux (23flops)	Antidiff Flux (23flops)
Pass Data Left(72Bytes)			
------------	Diffuse (7flops) Antidiffuse (7flops)	Diffuse (7flops) Antidiffuse (7flops)	Diffuse (7flops) Antidiffuse (7flops)
Total (341 flops)	Total (173 flops)	Total (447 flops)	Total (271 flops)

Table 4 Estimate of compressor simulation computational requirements when run on serial or parallel computers.

```
Assumptions:
    1) 50 Control Volumes
    2) 5x10^-5 sec/time step
    3) 3 compressor stages

Required Computational Speed:

    Real Time              1/10th Real Time
    200 MFLOPS (serial)    20  MFLOPS (serial)
    8.9 MFLOPS (parallel)  .89 MFLOPS (parallel)
```

Figure 41 illustrates the computational difference between serial and parallel processor solution approaches. In the compressor simulation problem, the finest grain distribution

of work is obtained by allocating a single control volume to each processing node.

From Figure 41 it is easy to see that the serial processor must do much more work than the individual processing nodes on the parallel computer. Also, the parallel computer solution more accurately reflects the events that are being modeled. Events occur throughout the compression system simultaneously. The parallel computer solution calculates these events like they occur in the physical system. As the problem size grows the execution time on the serial computer increases However, the parallel computer has the ability to maintain the execution time by simply adding additional processing nodes for larger problems.
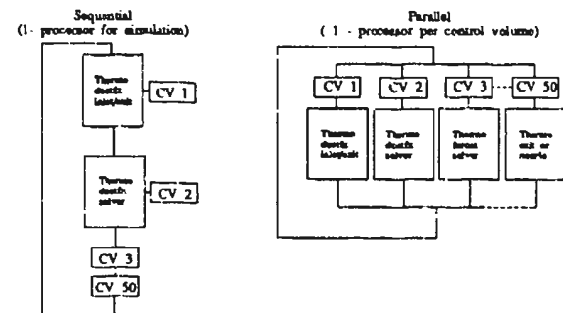
Figure 41 Comparison Between Serial and Parallel Computational Approaches.

Table 5 Differences in computational effort-per-processor for serial, SIMD, and MIMD computers.

```
Given:
    one(1)    Inlet control volume (ICV)
    n         Duct force control volumes (DFCV)
    m         Blade force control volumes (BFCV)
    one(1)    Exit control volume (ECV)

Required Computations/ time step for different
computer types:

Serial:  Flops = 1xICV+nxDFCV+mxBFCV+1xECV
SIMD:    Flops = 1xICV+1xDFCV+1xBFCV+1xECV
MIMD:    Flops = Max(ICV,DFCV,BFCV,ECV)
```

Table 5 extends Figure 41 by also illustrating the computational difference between the two major types of parallel computer architectures. As can be seen from this figure, the serial computer demands the largest work from its processor, the SIMD (Single instruction multiple data) computer reduces the serial workload considerably, and the MIMD (Multiple instruction multiple data) computer has the minimum workload for each processor. The major difference between these machines is in the way they execute computer instructions.

The SIMD computer requires that each processing node complete the same computer instruction at the same time. As long as every node in the simulation requires the same calcu-

lation, the SIMD approach works very well. However, if a node requires different calculations than the other processing nodes, the nodes that do not require that calculation must wait until the calculation has been completed before continuing with the work that they need to do. For problems that require different work on each processing node, the SIMD approach is not very efficient. If we take this to the extreme, a problem that requires every processing node to execute a different set of instructions would show no speedup over the serial machine because each node would have to wait for every other node to complete its work before it could continue. Fortunately most CFD type problems result in similar computations in each processing node.

The MIMD approach provides the most flexible computer solution for handling computational problems. MIMD computers allow each processing node to execute different instructions at the same time. Problems that have parallel solution opportunities but that also require different work in each processing node are best suited to application on MIMD computers. However, the MIMD approach also requires the largest amount of programming effort.

In order for a problem to be run efficiently on a MIMD computer, the computational workload must be evenly distributed between the available processing nodes. Also the communication between each processing node must be formally defined. If the communication is not properly implemented, the simulation will likely lead to a condition known as deadlock.

Deadlock occurs when a node can not continue to work because it is waiting for information from a neighboring node. If the neighboring node never delivers the message, the node that was to receive it ends up waiting forever. In a progressive fashion, adjacent nodes end up waiting for messages that are not delivered until all the processing nodes are waiting for messages that will never arrive. At this point the entire simulation has come to a halt. Care must be taken when programming MIMD computers to insure that deadlock does not occur. Deadlock is not as likely occur on SIMD computers because they synchronize the processing nodes through the use of the common instruction approach.

Results
Having completed the studies of serial code optimization, and computer selection/parallel processing considerations, a baseline simulation was run on different platforms to assess computer performance. A "small" simulation problem, modeling a compressor with three stages and 29 control volumes was chosen. All code improvements were incorporated in both FORTRAN and C code versions. In the case of the Transputer®, it was possible to implement the buffered message passing technique discussed earlier. Results are shown in Table 6.

For the computers tested, the fastest compute time was achieved with the IBM 3090 computer. In fact, this simulation required a time ratio of 10:1, which is in the range which we have defined for near-real-time simulations. The other serial machines tested required longer compute times. It should be noted, however, that the serial results are not

"scalable". A larger simulation problem will require more compute time.

The best results, for the parallel machines tested, were achieved with a Transputer®-based system. The Transputer® processor is designed for parallel computing, with four com

Table 6 Simulation execution time on various computer platforms.

Baseline: Three stage compressor (29CVs)
    1 sec simulation
    10,000 Iterations Time Step=.0001secs

SERIAL MACHINES	(FORTRAN)	(C)
IBM 3090 series 300 with vector facility	10.0 secs	
CONVEX C2	17.0 secs	
IBM RISC 6000 model 530	18.7 secs	19.0 secs
SILICON GRAPHICS 4D80GT	52.0 secs	53.0 secs
SUN model 330	90.0 secs	
INTEL i860 one processor	29.0 secs	
PARALLEL MACHINES		
NCUBE2 32 node machine		
one node	90.0 secs	
16 nodes	45.0 secs	
TRANSPUTER 25Mhz		
one node	259. sec	173. secs
5 nodes		86.6 secs
20 nodes		30.8 secs
20 nodes		15.2 sec

munication links for fine-grained message passing built into the processor chip. The Transputer® is capable of simultaneously communicating messages and calculating integer and floating point operations. Each processing node has the approximate performance of a 25Mhz 486 computer. During testing, we found that the Transputer®-based system did indeed handle message passing well, and that the individual node floating point performance was almost fast enough to allow near-real-time simulation of the modeled compression system. There is reason to believe that the Transputer®-based simulation will be "scalable", since more processors can be added for larger simulations. Disadvantages of the Transputer®-based system include, limited availability of hardware and software, increased user knowledge of the system is necessary, and the communication aspects of parallel computing can be complex.

GAS TURBINE DYNAMIC SIMULATIONS
Full gas turbine dynamic simulations are not, in principal, different from compressor simulations. Additional source terms representing combustor and turbine processes must be included. Provision must be made for variable speed and rotor inertia effects. The compressor simulations discussed thus far were for rig tests; that is, the speed was held constant. The matter of computational speed becomes even more important, as the simulation may involve fifty or more control volumes.

In the combustor, a variety of source terms may be important. consideration of diffuser and linear pressure loss, combustion-related pressure loss and efficiency, flammability limits, and reignition delay times are all required for a full range simulation. A turbine characteristic must be available. In the simulation, a power calculation between compressors and turbines must be performed to determine acceleration potential. To date, only one such study has been reported [39], but work by the author's research group is in progress to produce a dynamic engine model based on the methods outlined in this review.

SUMMARY AND CONCLUSIONS

Dynamic models of compressors and gas turbines are simulations of performance over the range of possible operation. As such, the models have use in design studies, examination of dynamic performance with the opportunity to study details of local flow behavior, test programs, and many other areas. Successful dynamic models require consideration of fluid mechanic modeling methods and computational methods. Parallel computation is well suited to dynamic simulation, representing the potential for development of complex engine models operating at near-real-time. Future developments will lead to multi-dimensional models of components and engines, with increasing simulation accuracy.

ACKNOWLEDGMENTS

References

1. Fishbach, L. H., and R. W. Koenig, "GENENG II - A Program for Calculating Design and Off-Design Performance of Two- and three-Spool Turbofans with as many as Three Nozzles," NASA TN D-6553, 1972.

2. Fishbach, L. H., and M. J. Caddy, "NNEP - The Navy/NASA Engine Program," NASA TM X-71857, 1975.

3. NASA TM-87033, July 1985.

4. Saravanamuttoo, H. I. H., and A. J. Fawke, "Simulation of Gas Turbine Dynamic Performance," ASME Paper 70-GT-23.

5. Davis, M. W. Jr., and W. F. O'Brien, "Stage-by-Stage Poststall Compression System Modeling Technique," AIAA Journal of Propulsion and Power, Vol. 7, No. 6, Nov-Dec 1991.

6. Greitzer, E. M., 1976, "Surge and Rotating Stall in Axial Compressors, Part I: Theoretical Compression System Model; Part II: Experimental Results and Comparison With Theory," ASME Journal of Engineering for Gas Turbines and Power, Vol. 98, No. 2, pp 190-217.

7. Day, I. J., "Axial Compressor Stall," Ph.D. Dissertation. Christ's College, Cambridge University, Cambridge, England, UK, 1976.

8. Burwell, A. E., and G. E. Patterson, "Dynamic Engine Behavior During Post Surge Operation of a Turbofan Engine," AIAA/SAE/ASME/ASEE 21st Joint Propulsion Conference, AIAA Paper 85-1430, Monterey, CA, July 8-10, 1985.

9. French, J. V., "Modeling Post-Stall Operation of Aircraft Gas Turbine Engines," AIAA/SAE/ASME/ASEE 21st Joint Propulsion Conference, AIAA Paper 85-1431, Monterey, CA, July 8-10, 1985.

10. Gamache, R. N., "Axial Compressor Reversed Flow Performance," Ph.D. Dissertation, Massachusetts Inst. of Technology, May 1985.

11. Kimzey, W. F., "An Analysis of the Influence of Some External Disturbances on the Aerodynamic Stability of Turbine Engine Axial Flow Fans and Compressors," Arnold Engineering Development Center TR-77-80 (AD-A043543), Arnold AFS, TN, Aug. 1977.

12. Davis, M. W., Jr., "A Stage-by-Stage Dual-Spool Compression System Modeling Technique," ASME Gas Turbine Conference, ASME Paper 82-GT-189, London, England, March 1982.

13. Tesch, W. A., and W. G., Steenken, "Blade Row Dynamic Digital Compressor Program, Vol. 1, J85, Clean Inlet Flow and Parallel Compressor Models," NASA CR-134978, Lewis Research Center, Cleveland, OH, March 1976.

14. Sugiyama, Y., Hamed, A., and W. Tabakoff, "A Study on the Mechanism of Compressor Surge Due to Inlet Pressure Disturbances," 16th Aerospace Sciences Meeting, AIAA Paper 78-246, Huntsville, AL, Jan. 1978.

15. Greitzer, E. M., "Surge and Rotating Stall in Axial Flow Compressors-Part I: Theoretical Compression System Model," ASME Journal of Engineering for Power, Vol. 98, April 1976, pp. 190-198.

16. Moore, F. K. and E. M. Greitzer, "A Theory of Post-Stall Transients in Axial Compression Systems: Part I-Development of Equations," 30th International Gas Turbine Conference, ASME Paper 85-GT-171, Houston, TX, March 1985.

17. Takata, H., and S. Nagano, "Nonlinear Analysis of Rotating Stall, " Journal of Engineering for Power, October 1972.

18. MacCormack, R. W., "The Effect of Viscosity in Hypervelocity Impact Cratering," AIAA Hypervelocity Impact Conference, AIAA Paper 69-354, Cincinnati, OH, April 30 - May 2, 1969.

19. Davis, M. W. Jr., "A Stage-by-Stage Post-Stall Compression System Modeling Technique: Methodology, Validation and Application," Ph.D. Dissertation, Virginia Polytechnic Inst. and State University, Dec. 1986.

20. Eastland, A. H. J., "Investigation of Compressor Performance in Rotating Stall: I--Facility Design and Construction and Initial Steady State Measurements," MIT Gas Turbine and Plasma Dynamics Lab. Rept. 164, June 1982.

21. MacCalum, H. R. L., and P. Pilidis, "The Prediction of Surge Margins During Gas Turbine Transients," ASME Gas Turbine Conference, ASME Paper 85-GT-208, Houston, TX, March 1985.

22. Crawford, R. A., and A. E. Burwell, "Quantitative Evaluation of Transient Heat Transfer on Axial Flow Compressor Stability," AIAA/SAE/ASME/ASEE 21st Joint Propulsion Conference, AIAA Paper 85-1352, Monterey, CA, July 1985.

23. Takata, H., and U. Tsukuda, "Stall Margin Improvement by Casing Treatment--Its Mechanism and Effectiveness," Journal of Engineering for Power, Jan. 1977.

24. Copenhaver, W. W., "Stage Effects on Stalling and Recovery of a High-speed 20-stage Axial-Flow Compressor," Ph.D. Dissertation, Iowa State University, October 1988.

25. Copenhaver, W. W., and T. H. Okiishi, "Rotating Stall Performance and Recoverability of a High-speed Ten-Stage

Axial-Flow Compressor," AIAA Paper No. 89-2684, July 1989.

26. Copenhaver, W. W., and C. J. Worland, "Acquisition of Unsteady Pressure Measurements from a High Speed Multi-Stage Compressor," ASME Paper No. 88-GT-189, June 1988.

27. Hopf, W. R., and W. G. Steenken, "Stall Recovery Control Strategy Methodology and Results," AIAA Paper No. AIAA-85-1433, July 1985.

28. Bloch, G. S., and W. F. O'Brien, "A Wide-Range Axial-Flow Compressor Stage Performance Model," 37th International Gas Turbine Conference, ASME, Cologne, Germany, June 1-4, 1992.

29. Lieblein, S., "Loss and Stall Analysis of Compressor Cascades," Trans. of the ASME, *Journal of Basic Engineering*, 1959, pp. 387-400.

30. Horlock J. H., *Axial Flow Compressors*, Robert E. Krieger Publishing Company, 1973.

31. Dixon, S. L., *Fluid Mechanics, Thermodynamics of Turbomachinery*, Pergammon Press, 1975.

32. Moses, H. L., and S. B. Thomason, "An Approximation for Fully Stalled Cascades," ASME *Journal of Turbomachinery*, 1986, pp. 188-189.

33. Turner, R. C., and D. W. Sparkes, "Complete Characteristics for a Single-Stage Axial-Flow Fan," Thermodynamics and Fluid Mechanics Convention, *Proceedings of the Institution of Mechanical Engineers*, Cambridge, England, 1964.

34. Koff, S. G., and E. M. Greitzer, "Axisymmetrically Stalled Flow Performance for Multistage Axial Compressors," ASME *Journal of Turbomachinery*, 1986, pp. 216-223.

35. Carneal, J. P., "Experimental Investigation of Reversed Flow in a Compressor Cascade," M.S. Thesis, Virginia Polytechnic Institute and State University, Blacksburg, VA, 1990.

36. Yocum, A. M., III, "An Experimental and Numerical Investigation of the Performance of Compressor Cascades with Stalled Flow," Ph.D. Dissertation, Virginia Polytechnic Institute and State University, Blacksburg, VA, 1988.

37. Longley, J. P., and T. P. Hynes, "Stability of Flow Through Multistage Axial Compressors," ASME *Journal of Turbomachinery*, 1990, pp. 126-132.

38. Graham, R. W., and E. C. Guentert, "Compressor Stall and Blade Vibration," Chapter XI of *Aerodynamic Design of Axial Flow Compressors*, Johnson, I. A., and Bullock, R. O., eds, NASA SP-36, 1965.

39. Sugiyama, Y., "Surge Transient Simulation in Turbo-Jet Engine," Doctoral Dissertation, University of Cincinnati, May 1984.

40. Boyer, K. M., and W. F. O'Brien, "Model Predictions for Improved Recoverability of a Multistage Compressor," AIAA Paper 89-2687, July 1989.

41. J. K. Harvell, and W. F. O'Brien, "Computational Considerations Associated with the Development of Near-Real-Time Dynamic Simulations for Propulsion Applications," AIAA Paper 92-0560, January 1992.

APPENDIX A

MacCormack Algorithm for Solution of Dynamic Model Equations.

Solution Method

The MacCormack predictor/corrector algorithm [18] is used to solve the system of equations described above.
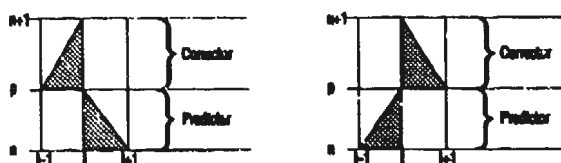
Figure A-1 Computational Molecule used for the MacCormack Algorithm.

Figure A-1 shows the computational molecule and Equations (A-1 - A-3) show the discretization of the quasi-one-dimensional Euler equations. Note that the order of differencing is alternated to insure that no bias is propagated into the solution from the boundary conditions.

Predictor

$$\bar{U}_i^P = \bar{U}_i^n - \frac{\Delta t}{\Delta x}\left(\bar{J}_{i+1}^n - \bar{J}_i^n\right) + \Delta t \bar{Q}_i^n \qquad (A-1)$$

Corrector

$$\bar{U}_i^c = \bar{U}_i^n - \frac{\Delta t}{\Delta x}\left(\bar{J}_i^P - \bar{J}_{i-1}^P\right) + \Delta t \bar{Q}_i^P \qquad (A-2)$$

New Time Step

$$U_i^{n+1} = \frac{1}{2}\left(\bar{U}_i^c + \bar{U}_i^P\right) \qquad (A-3)$$

where;

$$\bar{U} = \begin{bmatrix} \rho A \\ \rho A u \\ \rho A \left(e + u^2/2\right) \end{bmatrix}; \quad \bar{J} = \begin{bmatrix} \rho A u \\ \rho A u^2 + pA \\ \rho A u \left(e + p/\rho + u^2/2\right) \end{bmatrix};$$

$$\text{and} \quad \bar{Q} = \begin{bmatrix} -w_b \\ F_x \\ -H_b + SW + Q \end{bmatrix}$$

It has been shown that the axial area variation in compression systems can lead to numerical instabilities when solving this set of equations using the MacCormack approach [19]. The original stage-by-stage model was found to exhibit numerical instabilities when the area change from one control volume to the next exceeded approximately twenty percent. This restriction was found to inhibit the use of physical geometry for some compression systems. Therefore, the MacCormack algorithm was modified by applying the Flux Corrected Transport approach to the existing scheme. This approach was

found to stabilize the MacCormack scheme for all area variations considered.

Figure A-2 shows the computational process required to complete one time step of the modified stage-by-stage compressor simulation. Included in this flow chart are the communication processes that must occur when the simulation is run on a parallel computer. These communication processes are not explicitly required when the simulation is run on conventional serial or shared memory parallel computers.
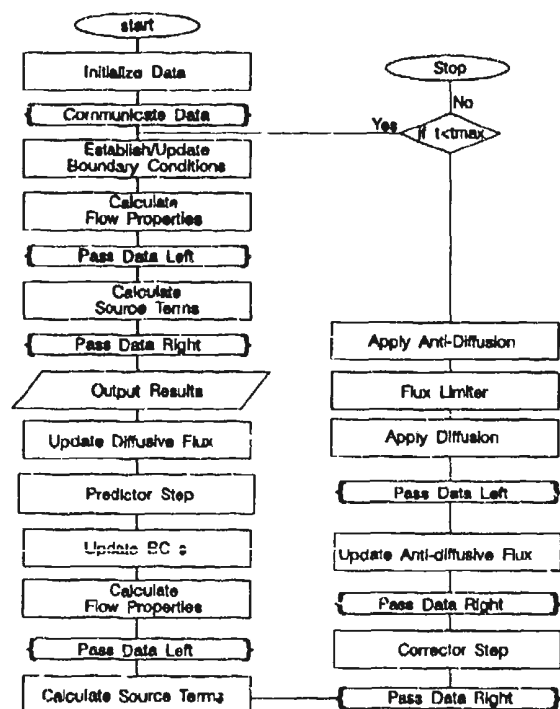
Figure A-2 Flow Chart Showing the Computational Process for the Stage-by-Stage Compression System Model.

Inlet Distortion Effects in Aircraft Propulsion System Integration

J. P. Longley
Whittle Laboratory, Cambridge University
Cambridge, England

E. M. Greitzer
Gas Turbine Laboratory, Massachusetts Institute of Technology
Cambridge, MA

92-20694

1. INTRODUCTION

This lecture presents a tutorial survey of inlet flow distortion effects on engine performance and stability. Inlet distortions in aero engines arise through a variety of causes. They can be essentially steady, due to non-axisymmetric intake duct geometry, or time varying, for example from flow separation off the lip of the inlet during maneuvers or shock-induced separation during supersonic flight. Whatever the cause, the result is generally a decrease in performance and, more importantly, a lessening of the stable flow range of the compressor.

Although the distortions encountered are generally three-dimensional, it is an extremely useful simplification to break them, at least conceptually, into radial and circumferential non-uniformities and approach each separately. Purely radial distortions can be treated by the methods that have been developed for designing compressors in nominally axisymmetric inlet flow, and this type of distortion will be only briefly discussed. Circumferential non-uniformities, however, introduce additional fluid dynamic features into the analysis of compressor behavior and often have the larger impact on performance and stability. The lecture thus concentrates mainly on the effects of steady circumferential inlet flow distortion.

We first consider the case of a square wave inlet total pressure non-uniformity in an idealized compression system. This example serves to explain many of the physical phenomena involved and is used in several of the subsequent sections as a background for introducing more general forms of inlet and engine compatibility problems, including temperature distortions and the fluid dynamic interaction between different compression system components. The final sections of the lecture discuss some recent developments in the theoretical modelling of inlet flow distortion problems, to illustrate the new insight that they can give, as well as areas for future work.

Aeroengine compressors, both with and without inlet distortion, exhibit two types of fluid dynamic instability, surge or rotating stall, and the occurrence of either of these marks the stability boundary beyond which the aeroengine cannot operate. Surge is characterized by periodic fluctuations of the mass flow through the compressor, often severe enough to cause temporary reversal of the flow. Rotating stall is a region of stalled flow, covering a significant fraction of the circumference, which propagates around the compressor annulus at speeds between 20-80% of rotor speed. Although there is considerable research interest in the development of these instabilities [1], [2], as well as the post-instability behavior [3], the primary interest here is how non-uniform flow affects the stability boundary. The material presented in the lecture thus introduces the fluid dynamic effects relevant to this specific topic, and the references cited should be consulted for supplementary information.

2. INLET DISTORTION FLUID DYNAMICS

2.1 Fundamentals of Compressor Behavior in Non-Uniform Flow

Many of the fundamental principles involved in the analysis of compressor operation in a steady, circumferentially non-uniform, flow field may be introduced by considering the case of two streams of different total pressure entering a compressor intake, with the flow approximated as low Mach number and radially uniform. The distortions of most interest as far as stability is concerned are those which occupy an appreciable fraction of the annulus, and the appropriate length scale for such non-uniformities is the radius of the machine. In the regions upstream and downstream of the compressor, therefore, the influence of viscous forces on the overall distortion velocity distribution are small and can generally be neglected. If so, the total pressure is a convected quantity and the total pressure distribution at the compressor inlet face will be the same as that far upstream. The particular form that we consider is a
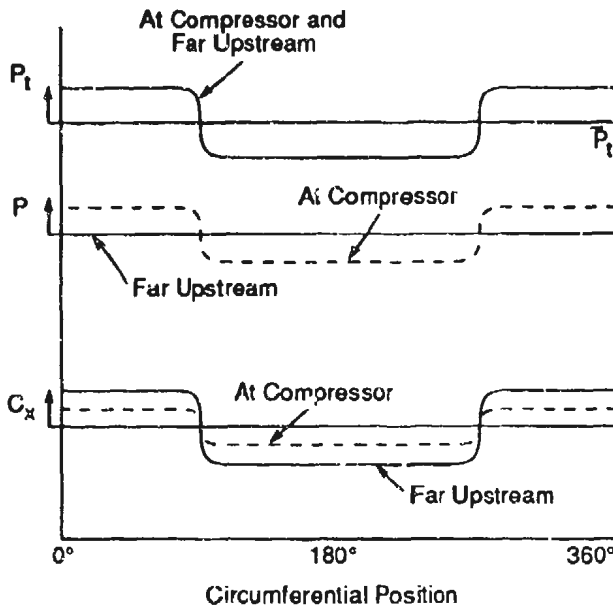
Figure 1: Total pressure, static pressure, and axial velocity distributions at a far upstream station and at the compressor inlet.

square wave with, for simplicity, equal circumferential extents of high and low total pressure regions, as shown in the top part of Figure 1.

At the compressor exit, the flow angle from the last row of stator vanes can be approximated as uniform around the circumference of the machine. If the exit duct is straight and of constant area and the flow can be considered two-dimensional, the condition of uniform exit angle implies that the static pressure at the compressor exit will also be uniform. (More detailed discussion of the conditions under which this is true is given by Mazzawy [4], and Greitzer and Griswold [5].)

With conditions of uniform exit static pressure and two streams of different inlet total pressure, the compressor can be viewed conceptually as *two compressors in parallel*, pumping from two streams with different inlet total pressures to a common static pressure. Implicit in this description is the restriction that negligible circumferential flow, from one of the streams to the other, exists within the compressor. Because the circumferential length scales are large compared to the axial gaps in an aeroengine compressor (the latter might be roughly one-third the blade chord), the axial length available for such redistribution even in a multistage compressor is small, and neglect of the cross flows within the compressor is generally a very good approximation [6], [7]. Put another way, with closely spaced compressor blading any mass flow non-uniformity at the compressor inlet will also be present at the compressor exit, because there is little opportunity for further redistribution within the compressor. It can be noted, however, that since the cir-

cumferential static pressure gradients are greatest at the front of the compressor, if any significant internal flow redistribution does exist, it is likely to occur within the first few stages [8].

These ideas, plus the assumption that each of the two streams (i.e. each of the two compressors in parallel) will operate at a point on the uniform flow compressor characteristic appropriate to the local mass flow, allow a description of the behavior of the compressor in the distorted flow which is shown in Figure 2a. The figure shows the compressor pressure rise, ψ_{TS}, in terms of exit static pressure minus inlet total pressure, non-dimensionalized by ρU^2, where ρ is density and U is the mean wheel speed, versus flow coefficient, $\phi = C_x/U$. The solid curve corresponds to the uniform flow performance characteristic and the local operating points with inlet distortion are indicated by the symbols.

Several important aspects of the inlet distortion problem are shown in the figure. First, the mean pressure rise is below that which would be achieved at the same mean mass flow, as indicated by the quantity $\Delta\psi$, which denotes the distance below the axisymmetric flow characteristic. Second, the different parts of the compressor annulus operate at different points on the characteristic. Since the exit static pressure is the same for both
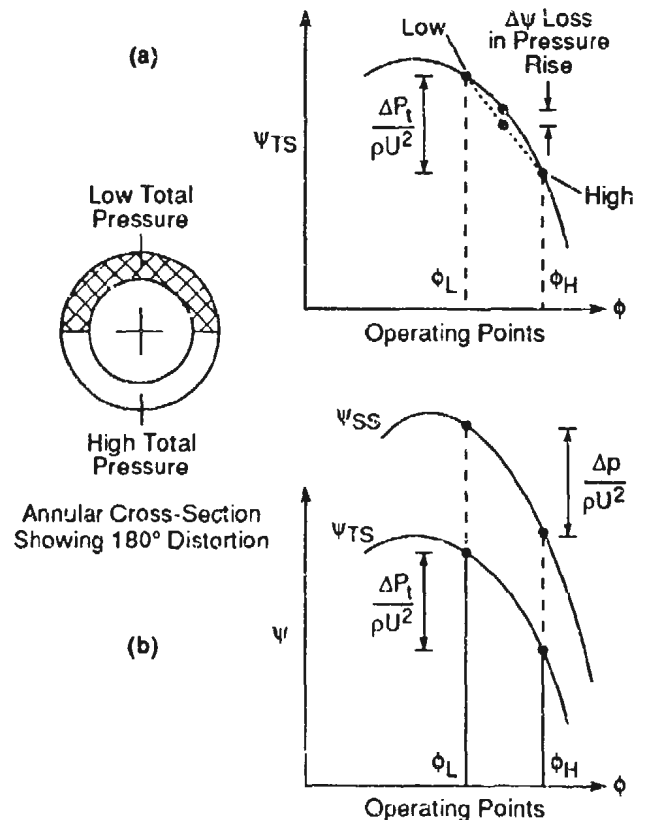

Figure 2: Basic parallel compressor model for compressor response to circumferential total pressure distortion.

streams, the difference in level between the pressure rise in each stream must be given by the difference in the inlet stagnation pressure. The lower inlet total pressure stream operates with a higher pressure rise, nearer to the stability boundary for uniform flow. Although the mean operating point may not be close to the stability boundary, a sizeable region of the compressor annulus can be operating at a flow equal to or below the boundary value, and it might be expected that instability could be initiated at a higher annulus average mass flow than with axisymmetric flow. This is one of the assumptions in the basic model, namely that the distorted flow stability limit is reached when the operating point for the low total pressure stream reaches the uniform flow stability limit.

The above approach to analyzing compressor performance in non-uniform flow is usually referred to as the "parallel compressor model". While it is overly simplified, it gives qualitative, and for some aspects quantitative, guidelines about compressor behavior in inlet flow distortion [7], and is a useful framework for understanding many trends seen with this type of flow. In the next several sections, we use the basic model to discuss several of the important features associated with circumferential flow distortion; later in the lecture, we describe how this model can be extended to deal with other fluid dynamic effects.

2.2 Upstream Flow Redistribution

Upstream of the compressor there will be a re-distribution of flow due to the upstream static pressure field which the compressor generates when operating in non-uniform flow. The flow redistribution is illustrated by the lower part of Figure 1, where the axial velocity distortion at the compressor is smaller than that far upstream. An explanation is obtained by considering the parallel compressor model in terms of the static-to-static pressure rise characteristic. The two operating points (for the high and low flow regions) can be transferred onto a static to static pressure rise characteristic, ψ_{SS}, in

Figure 2b. There is a difference in the compressor inlet static pressure because the the exit static pressures are equal. Far upstream of the compressor, however, the static pressure is uniform. The change in the static pressure from far upstream to inlet implies, as given by Bernoulli's equation, a change in axial velocity between these two stations. The effect of the upstream reaction is thus to decrease the axial velocity non-uniformity compared with the far upstream value.

The axial scale over which the upstream flow re-distribution takes place is also of interest. For low speed flows, small amplitude departures from a uniform static pressure obey Laplace's equation (i.e., $\nabla^2 p' = 0$, where p', the static pressure non-uniformity, is a function of axial position, x, and circumferential position, θ). There is no intrinsic length scale in this equation, and the axial length scale will thus be set by the circumferential length scale. The circumferential length scale can be regarded as being associated with the largest amplitude spatial (i.e.,θ) Fourier component of the distortion. For the distortions that have the largest effect on stability and performance, this is generally the first harmonic, and the relevant length scale is thus the radius of the machine.

The structure of the solutions to Laplace's equation imply that the amplitude of the static pressure variation, $|p'|$, will decay with axial distance according to: $|p'| \propto \exp[-2\pi(x-x_{ref})/R]$, where x_{ref} is a station (say the inlet of the compressor) at which the static pressure is referenced, and R is the mean radius of the machine. In accord with this idea, Figure 3 [9] presents experimental measurements of the static pressure variations upstream of a compressor with a distortion created by a screen of 180 degree circumferential extent. The figure shows the amplitude of the static pressure variation versus axial
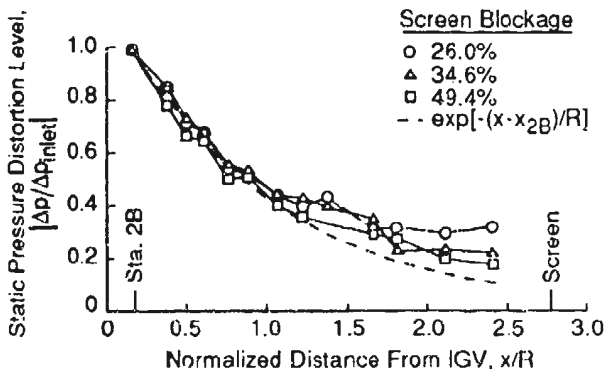
Figure 3: Variation of static pressure with distance upstream of an axial compressor; 180 degree inlet total pressure distortion [9].
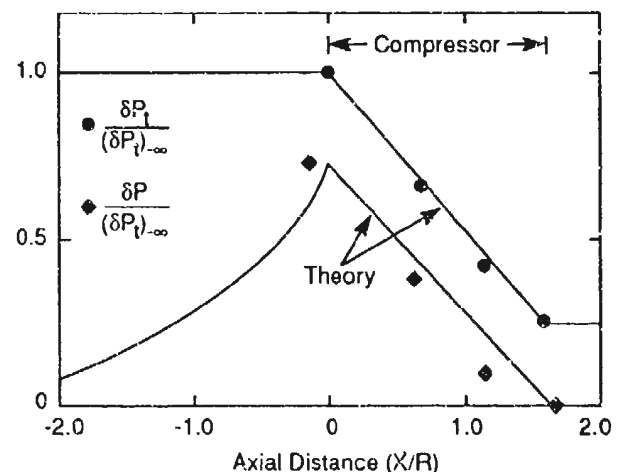
Figure 4: Overall variation of static and total pressure upstream and through three stage compressor [7].
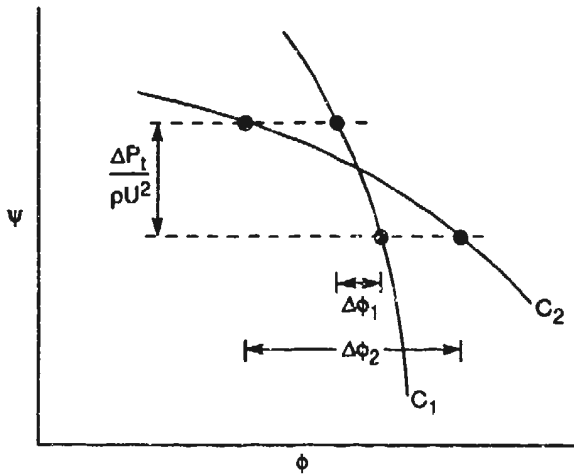
Figure 5: Increased compressor characteristic slope implies increased distortion attenuation.

position, with an exponential curve also shown. It can be seen that the static pressure is maximum at the compressor and decays in accord with the considerations that have been sketched out. The overall behavior of the total and static pressures upstream and through a compressor are thus as shown in Figure 4 [7], which presents experimental and theoretical results for a three stage low speed compressor.

2.3 Distortion Attenuation

Although the static pressure at the exit of the compressor can often be regarded as uniform, exit total pressure cannot, since the two streams have different velocities. The exit non-uniformity is experienced by any downstream aeroengine components, and the distortion attenuation, i.e., the ratio of the exit total pressure distortion amplitude to that at inlet, is of interest. The size of the exit total pressure non-uniformity is determined by the difference between the exit velocity in the high and low flow streams. The flow velocities in the two streams are set by the shape of the total-to-static pressure rise characteristic, as shown in Figure 5. The steeper the compressor characteristics the greater the distortion attenuation, as indicated in the figure. For the same total pressure distortion the velocity non-uniformity at the compressor is less for the steeper compressor characteristic, C_1, than for the flatter one, C_2.

2.4 Parallel Compressor Model for High-Speed Compressors

In the description given of the parallel compressor model it was assumed that the flow was low Mach Number. The uniform flow compressor characteristic was therefore expressed as pressure rise ψ against flow coefficient ϕ. However, the basic ideas can also be applied to flows in which compressibility effects are important. For these situations the performance is expressed in terms of pressure ratio versus "corrected
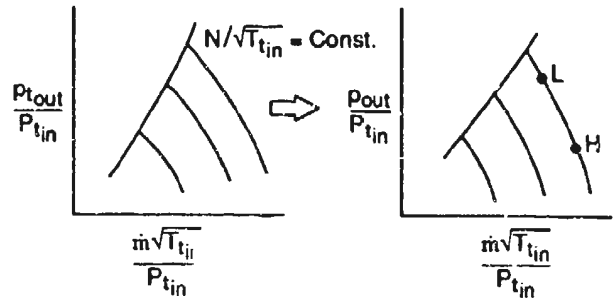
Figure 6: Parallel compressor model for high speed compressors.

flow" (mass flow function, $\dot{m}\sqrt{c_p T_t}/P_t$) for different values of the "corrected speed", $N/\sqrt{T_t}$. Figure 6 shows a compressor map expressed in the form of total pressure ratio versus corrected flow and the corresponding representation in terms of the ratio of exit static pressure to inlet total pressure. Using this latter representation, similar arguments as for the low speed case can be given concerning the two operating points, the distortion attenuation, and the onset of instability. It is in this compressible flow format that the model is generally used. Note that the model now also gives a statement about the effect of total temperature distortion, as indicated in Figure 7. For a total temperature distortion with no total pressure distortion, the two operating points (of the hot and cold streams) will be at two different corrected speeds, but the same pressure ratio. The hot stream is at a lower corrected speed, closer to the stall point, and the compressor suffers a decrease in stable flow range. Physically this occurs because the fluid on the hot side is less dense, and to have the same overall pressure rise the aerodynamic loading $[(\Delta p_{blade\ row})/(\frac{1}{2}\rho W_{inlet}^2)]$, say, must be higher for the individual blade rows.
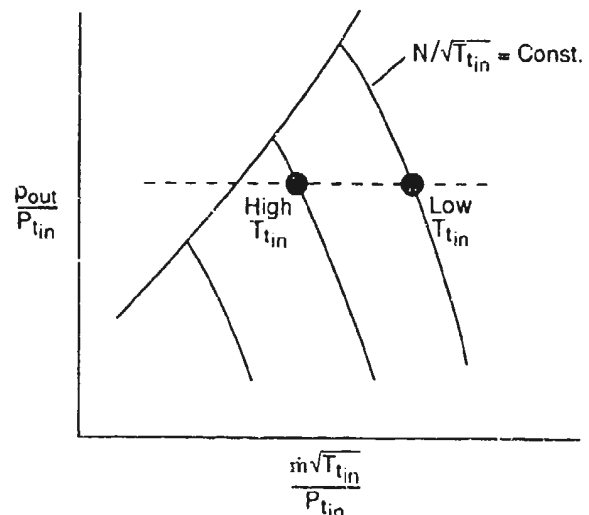
Figure 7: Compressor response to inlet total temperature distortion.

2.5 Differential Work Input and Generation of Exit Temperature Distortion

The above shows that compressors with steep characteristics will create nearly uniform inlet flow and thus nearly 100% distortion attenuation in terms of the total pressure field. However the greater pressure rise in the low flow region necessitates a greater work input and hence a higher total temperature at exit. Downstream of the compressor there is thus a total temperature distortion, which is imposed on the downstream components.

2.6 Summary of Results for the Basic Parallel Compressor Model

The parallel compressor model can give qualitative insight into several important features of the behavior of compressors operating with inlet flow distortion. Those illustrated include: decreased stable flow range with distortion, decreased pressure rise capability, upstream redistribution of the flow, the role of the speedline slope in setting distortion attenuation, and the production of total temperature distortion due to a variation in inlet flow coefficient. Of these, the one that is most important is the first, and the simple assumption made in the parallel compressor model concerning the stability boundary does not give an adequate quantitative prediction of the loss in stable flow range with inlet distortion.

To obtain improved descriptions of the stall point, several different approaches have been taken, at varying levels of empiricism. The first is empirical correlation of the loss in stall margin, which forms the subject of the next section. The second is the extension of the basic model to include multiple streams, effects of flow unsteadiness, as well as fluid dynamic interaction with other components. These will be described in the following section. The most recent approaches are rigorous hydrodynamic stability analyses of the distorted flow, and these are described in the final section.

3. EMPIRICAL CORRELATIONS FOR THE LOSS IN STABILITY WITH INLET DISTORTION

We begin by discussing some of the empirical correlations that have been developed to assess the effect of a given inlet distortion on the stability boundary of a compressor. Only a short description of the methods will be given because the intent is to focus on procedures rather than the details. In this general context, however, several documents are worthy of note. Two are publications of the S-16 Committee of the Society of Automotive Engineers: Aerospace Recommended Practice, ARP1420 and the associated Aerospace Information Report AIR1419. These give guidelines for treatment of the effects of total pressure distortion on engine stability. The two recent reviews of the subject by Williams [10], [11], as well as that by Steenken [12] are also informative and useful, not only for discussion of the correlations but for an overall review of the existing methodology for engine stability assessment.

In correlating the effects of non-uniform flow two main questions have had to be addressed. First, how does one define the change in the stability boundary. Second, how can a complex distribution of inlet total pressure be reduced to a workable distortion index.

3.1 Loss of Surge Margin

The movement of the compressor stability boundary is generally referred to as the loss of surge margin (although the fluid dynamic instability may in fact be rotating stall). With an inlet distortion present, the compressor operating point, mean mass flow and pressure rise, may be plotted to give the compressor map and the stability boundary for that distortion pattern. Quantifying the relationship between the uniform flow stability boundary and that for distorted flow may be done in a number of ways. There are two methods that are often used:

(i) Loss of pressure rise at constant speed. The change in the pressure rise at instability is expressed as a fraction of the uniform flow pressure rise for the compressor operating at constant speed.

(ii) Loss of pressure rise at constant mass flow. Here the speed of the compressor is varied so that the stability limit is at the same mass flow for uniform and distorted conditions. This is illustrated in Figure 8 [10].

Other definitions may also be used, for example that described by Cumpsty [13], which is in terms of the exit corrected mass flow and is thus related to the actual downstream throttle area. The important point is that the
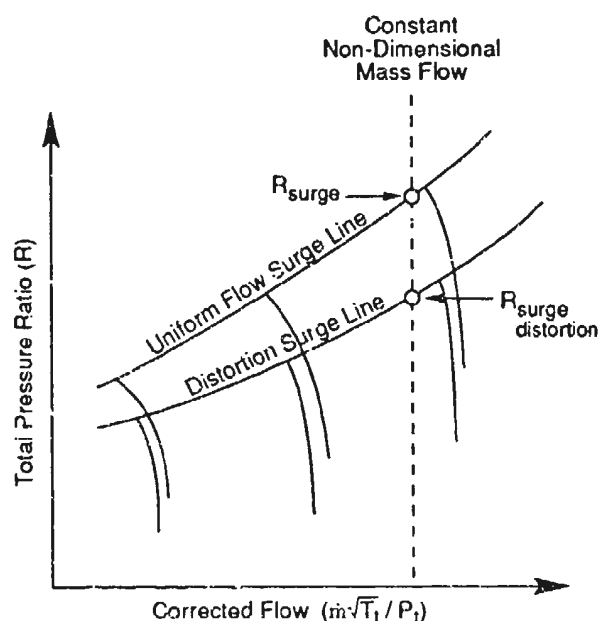

Figure 8: One definition of surge margin decrease; loss in pressure ratio at constant mass flow.

relationship between the different definitions depends upon the shape of the performance characteristics of the compressor concerned. As illustration, the above two definitions are identical for compressors which have vertical pressure rise mass flow characteristics but are different for any non-vertical slope.

3.2 General Trends in Compressor Response to Inlet Distortion

The distribution of the inlet total pressure is usually measured at an aerodynamic interface plane (AIP) which is approximately a radius upstream of the compressor face. Distortion indices are calculated by reducing the measured distribution of inlet total pressure, $P_t(\theta,r)$, to a group of numbers which reflect those aspects of the inlet distortion which affects compressor performance. The general trends of compressor performance with different
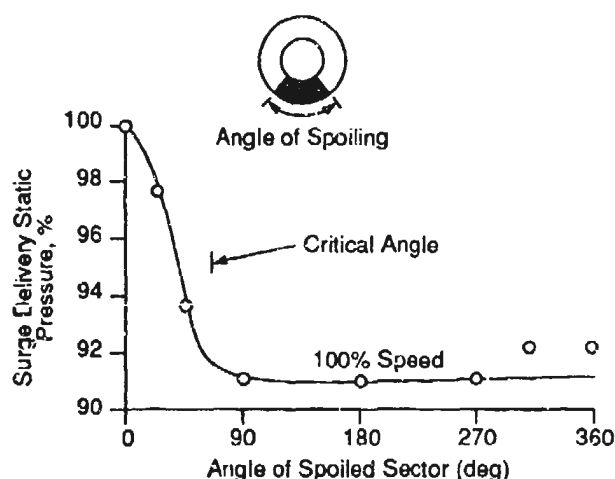
(a) Effect of Spoiled Sector Width
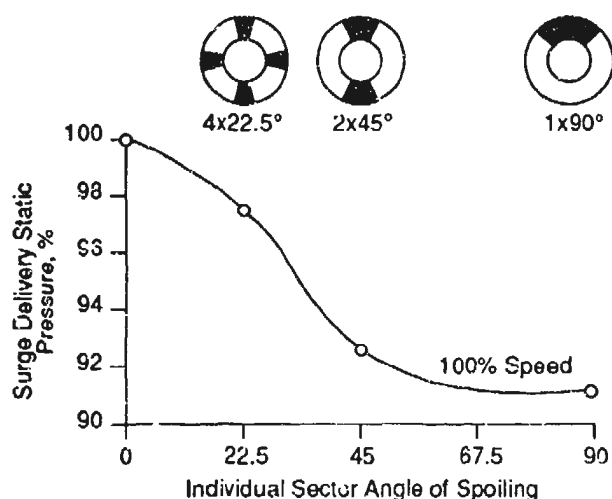
(b) Contiguous Spoiled Sector Width Is Important

Figure 9: Effect of: a) circumferential distortion sector angle, and b) number of sectors, on surge pressure ratio [14].

inlet distortions are illustrated in the series of experiments undertaken by Reid [14], which are presented in Figure 9. The figure shows the compressor delivery pressure at the surge line, for different types of distortions. Two aspects may be identified:

(i) As the angular width of the spoiled sector (low inlet total pressure) is increased there is a width above which there is little change in the exit static pressure (Figure 9a). This width is often referred to as the critical sector angle, θ_{crit}.

(ii) Holding the total angular extent of the distortion screen fixed, the effect of sub-dividing it into different numbers of equal sections is shown in Figure 9b. The greatest effect on the loss of peak pressure rise is observed when there is only one region. This suggests that the longer length scale, lower circumferential harmonics, are the most important.

3.3 Specific Forms of the Correlation Parameters

Many methods have been developed and refined for evaluating distortion indices based on experimental observations similar to those described above. Here, only two will be described both of which emphases the severity of the distortion in terms of the size of the total pressure region which is below the average inlet value. For simplicity, the distortion will be assumed to have a singe lobe and to be uniform in the radial direction (extensions for these will be introduced later).

"K" series Distortion Indices
$$\theta_{ext} = \text{width of total region below the average } (\overline{P_t}|_{360°})$$

$$K = \frac{\overline{P_t}|_{360°} - \overline{P_t}|_{\theta_{ext}}}{\frac{1}{2}\rho C_x^2}$$

This is a two parameter method with correlations defined in terms of θ_{ext} and K.

$DC(\theta_{crit})$ Distortion Indices
The concept of the critical sector angle, θ_{crit}, may be used to define an alternate distortion index:

$$DC(\theta_{crit}) = \frac{\overline{P_t}|_{360°} - \overline{P_t}|_{\text{worst } \theta_{crit}}}{\frac{1}{2}\rho C_x^2}$$

An example for $\theta_{crit} = 60$ is shown in Figure 10.

The above two definitions are included to illustrate the general approach taken in reducing a circumferentially non-uniform inlet total pressure distribution to a distortion index. These indices are not unique (hence the important role of AIR1419 in setting out a common approach), but can often be related to each other through

$$DC(60)_{overall} = \frac{\bar{P}_t - (P_t)_{min\ 60}}{\bar{q}}$$
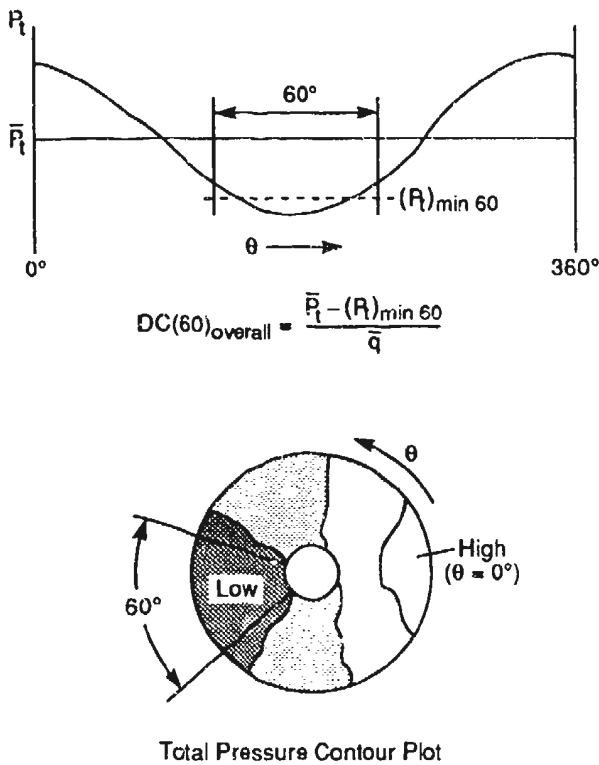
Total Pressure Contour Plot

Figure 10: Definition of $DC(\theta_{crit})$ parameter for inlet total pressure distortion [10].

conversion formulae. The above $DC(\theta_{crit})$ and K series may be approximately related by:

$$DC(\theta_{crit}) \approx \frac{\theta_{ext}}{\theta_{crit}} K, \quad \theta_{ext} < \theta_{crit}$$

$$DC(\theta_{crit}) \approx K, \quad \theta_{ext} \geq \theta_{crit}$$

Approaches based upon the above have been successful in correlating inlet distortion effects. The loss of surge margin has been found to be approximately proportional to the size of the distortion index, and a compressor sensitivity may be defined thus:

Sensitivity = loss of surge margin / $DC(\theta_{crit})$

Modifications are made to the above definitions for cases where there are more than one region below the mean value. If the regions are close together, set by an empirical constant, the two regions are analyzed as if they were one. For distortions with regions relatively far apart the worst one is taken and a multiplicative factor is used [11].

Many distortions of interest involve radial variations in the total pressure and refinements to the above methods have evolved. The simplest one is to radially average the flow and then consider only the resulting circumferential pattern. More complicated extensions involve dividing the annulus into several rings of equal area and analyzing the circumferential pattern in each ring and the radial variation of these patterns. The loss of surge margin is then assumed to be the linear superposition of the effects of the circumferential distortion in each ring and a contribution depending on the difference between the ring average and annulus average inlet total pressure.

4. MODELS FOR DISTORTION TOLERANCE AND TRANSFER

Conceptually there are two parts to the modelling of inlet distortion problems. First, the compressor performance for a given inlet distortion and operating point (mass flow and pressure rise) must be predicted. Second, a method or criterion is needed to determine whether or not this operating point with distortion has crossed the stability boundary. The models which have been developed may be, loosely, split into those which have resulted from empirical observations and those based on simplifying assumptions which allow theoretical analysis.

4.1 Parallel Compressor Model with θ_{crit} Concept

The basic form of the parallel compressor model assumes that the stability boundary of the compression system occurs when the portion of the annulus operating with the low inlet total pressure reaches the uniform flow stability limit. Using this approach, the mean operating point at instability is a weighted average of the low flow sector operating at the uniform flow stability boundary, and the high flow sector operating at a point $\Delta P_t/\rho U^2$ lower. Therefore, the loss in surge margin predicted by the basic parallel compressor model may be represented as a straight line on Figure 11. The greatest loss in surge margin occurs with the narrowest spoiled
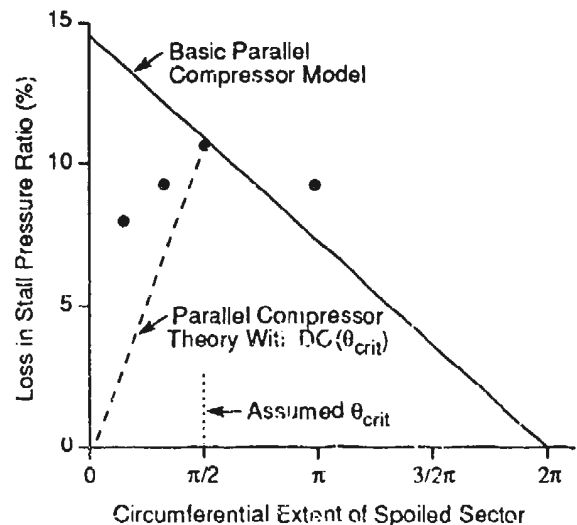

Figure 11: Prediction of loss in surge margin using parallel compressor analysis plus $DC(\theta_{crit})$ concept [10].
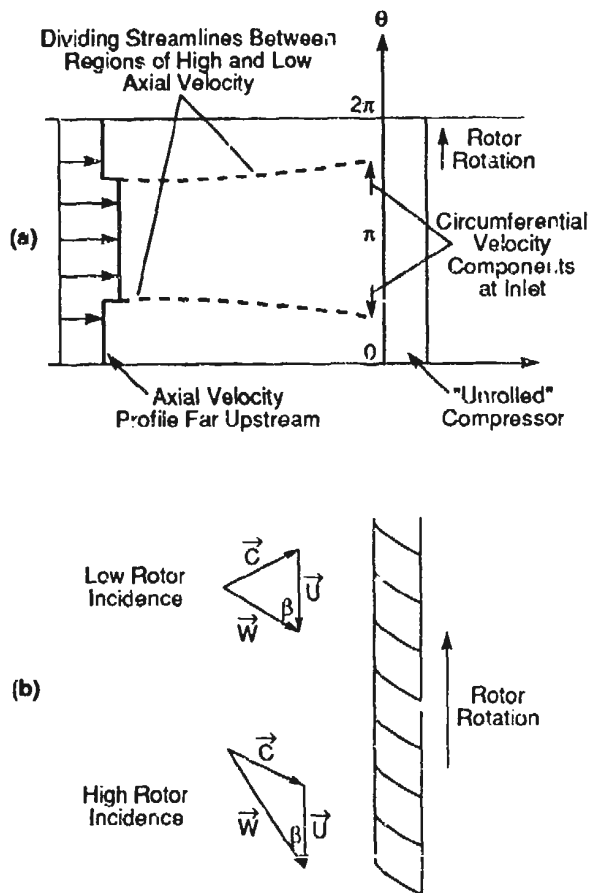
Figure 12: Flow angle variation at compressor inlet due to upstream flow redistribution [4].

sector inlet distortion. In the light of experimental observations like those of Reid [14], the prediction of the large loss for a narrow spoiled sector is inadequate, and modified forms of the parallel compressor model have been developed to overcome this weakness.

The concept of a critical sector angle may be included within the parallel compressor model by specifying that the maximum loss in surge margin occurs when the spoiled sector width is θ_{crit}. For inlet distortions which are narrower than θ_{crit} the loss of surge margin is set to be proportional to $\theta_{extent}/\theta_{crit}$, as indicated by the dashed line in Figure 11. This approach is a useful one [10], and is linked to the empirical $DC(\theta_{crit})$ correlation described above. In terms of the stability criterion, the critical sector angle concept means that instability occurs when some weighted average of the low and high flow sectors reaches the uniform flow stability boundary. The implication is that it is possible for a small portion of the compressor annulus to operate beyond the usual, or natural, stability boundary provided that there is enough of the annulus operating on the stable side to maintain overall stability.

4.2 Multiple Segment Parallel Compressor Model

The modelling of non-uniform flow through a compressor may be undertaken using more than two idealized operating points. In the multiple segment parallel compressor model the annulus is split into a number of segments of equal circumferential width [4]. In a manner similar to the simple parallel compressor model, the operating point of each segment is determined by the local inlet total pressure and the local exit static pressure and the overall performance is the average of the individual segments. These models can also account for fluid dynamic effects that are not present in the basic model. For example the upstream flow redistribution brings about an asymmetric inlet angle and relative dynamic pressure, as shown in Figure 12a and 12b. Inclusion of this feature can give considerably better agreement with data, as evidenced in Figure 13. In the same paper, Mazzawy also describes some of the non-steady flow phenomena associated with rotor blades passing through non-uniform flow, which have been shown to be important in determining the inlet distortion tolerance of a compressor. Two important observations made by Mazzawy are:

(i) The idealized operating point of each segment does not necessarily match the corresponding operating point in uniform flow conditions.

(ii) The individual blade row performances may extend beyond the stability boundary in undistorted flow.

4.3 Linearized Distortion Transfer Calculations

The parallel compressor model can be viewed as a method for calculating the non-uniform flow through the compression system, the stability of which is then assessed using the critical sector angle concept. Theor-
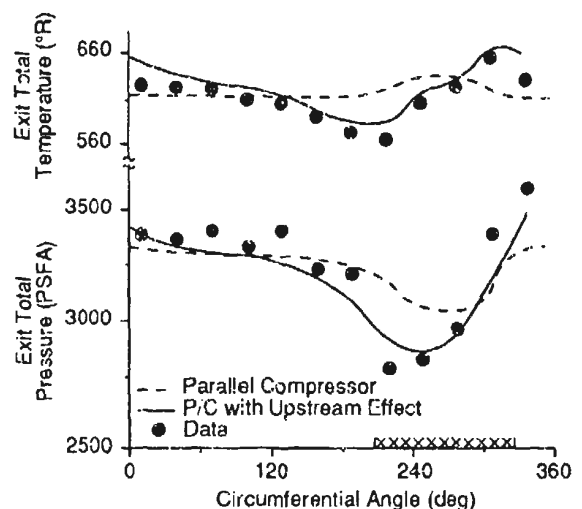

Figure 13: Effect of upstream angle and dynamic pressure variation on compressor response to inlet [4].

etical models for calculating the non-uniform flow through a compressor have been developed with the aim of replacing or improving the parallel compressor model predictions. Some of these rely on a linearized approach where the flow non-uniformity is considered to be sufficiently small in amplitude to ignore non-linear effects.

The advantage of a linearized approach is that many different fluid dynamic effects, for example non-steady blade losses, non-steady blade deviation and the flow redistribution in the gaps between the blade rows, may be easily included with little conceptual difficulty. Advanced forms of these models are those developed by Hynes [15] and Kodama [16]. These are useful for examining distortion transfer and for understanding different physical effects. For example, they have been used to explore the possible benefits to be gained through use of asymmetric vane stagger in attenuating inlet distortion [17]. It is to be emphasized, however, that a linearized approach is fundamentally unable to predict changes in stability margin.

5. OTHER TYPES OF FLOW NON-UNIFORMITIES

This lecture so far has been concerned with inlet total pressure distortions, but other flow non-uniformities also affect stability and performance. We now examine some examples of this broader class of distortions.

5.1 Temperature Distortions
A non-uniform temperature distribution may arise through various causes, for example from ingestion of hot gases in VSTOL aircraft or from a non-uniform total pressure distortion in an upstream compressor which causes a temperature distortion for the downstream compressor. Total temperature non-uniformities are similar to total pressure ones as they are convected quantities and so, conceptually, may be analyzed by using the parallel compressor approach as described in Section 2.4. Correlative procedures, similar to those for total pressure distortions, have also been developed using temperature distortion indices, TC(120) (see [10]), and the effects of combined temperature and pressure distortions have also been addressed.

5.2 Inlet Swirl Distortions
An inadequacy of defining the inlet flow into a compressor in terms of P_t and T_t is that it does not include the effects of swirl in the inlet flow field. There may be bulk swirl due to the generation of streamwise vorticity when an inlet shear non-uniformity is turned in a bifurcated duct geometry. This swirl can load or unload the compressor, depending on the direction relative to that of the rotor rotation. In addition the effect of swirl and of inlet distortion appear to interact in a nonlinear manner in that the effect of combined swirl and distortion is considerably more severe than might be inferred from simple addition of the effect of swirl plus the effect of distortion.
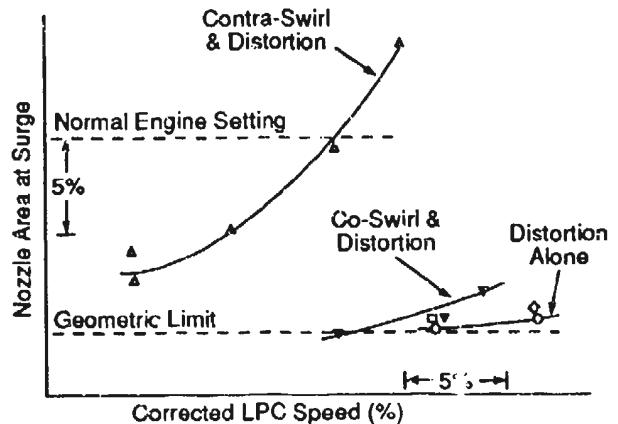
Figure 14: Effect of inlet swirl and total pressure distortion on compressor instability [10].

Some indication of the strong combined effect of swirl and distortion are given in Figure 14, from Williams [11]. The figure shows the fan nozzle area at surge, with smaller areas upward, plotted versus fan speed for three cases: total pressure distortion alone, distortion with swirl and rotation aligned (co-rotation) and swirl and rotation opposed (contra-rotation).

Regions of localized swirl can also be generated either due to upstream flow field redistribution (as in Figure 12a), secondary flow effects in the endwalls, or due to inlet vortex problems. Correlative procedures for these types of distortion are currently areas of research interest, and one approach has been to relate the compressor performance in terms of the relative inlet flow angle onto the first rotor row [18].

5.3 Inlet Duct Geometry and Back Pressure Distortions
In many cases aeroengines are "buried" within the body of the aircraft and long curved intake ducts, which often include variable geometry and bleeds to control the shock system, are necessary. The development of the boundary layers along these duct walls can be affected by the intake shock (causing thickening and possible separation of the boundary layers) or, if the duct is highly curved the associated static pressure gradients can generate secondary flow which concentrates the boundary layer material into localized regions. The total pressure distribution at the engine face can thus be highly non-uniform.

The development of the flow within the intake duct can be substantially changed by the presence of the aeroengine. This has been demonstrated by Hodder [19] who investigated the development of flow separation in an intake when operating at incidence, with and without the engine. As shown in Figure 15, without engine, at 30° incidence there was a large region of low total pressure flow due to separation. With an engine present,

Incidence = 30°
Without Engine Interaction

Incidence = 35°
With Engine Interaction
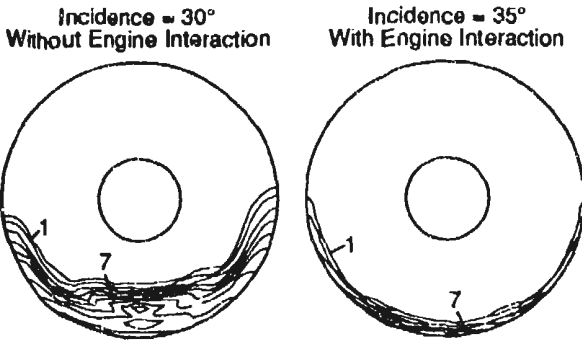
Figure 15: Effect of engine presence on total pressure distribution in a short pitot inlet [19].

even at a larger incidence of 35°, the region of low total pressure fluid was much smaller because the compressor acts to equalize the velocities and the size of the separated flow (low inlet total pressure) region thus shrinks in size. (The actual loss in total pressure was similar in both cases.) It is thus important to ensure that the correct component interaction is included when undertaking both experimental and theoretical work.

The flow path through an aeroengine can be obstructed by mechanical constraints such as support vanes behind the outlet guide vanes in a bypass duct. The blockage due to these support vanes causes the flow to redistribute upstream of them, and if they are sufficiently large then a non-uniform flow can exist at the outlet of the upstream component. Although not specifically an inlet distortion, this type of flow non-uniformity should be mentioned because it can excite blade vibrations, generate high noise levels and reduce fan performance. The analysis of such distortions has been undertaken using linearized analyses [20], singularity methods [21], [22], and also by finite difference methods [23]. For example, investigations have been made into using non-axisymmetric outlet guide vanes to reduce the upstream influence of the support strut [22].

6. COMPONENT COUPLING WITH CIRCUMFERENTIAL DISTORTION

In the above it has been assumed that distortion and propulsion integration assessment may be done component by component. However, the length scale of flows with circumferential distortion is the mean radius, and this can be large compared to the distance between components. Therefore, with distortion, components can interact much more strongly than in an axisymmetric flow. The fluid dynamic interaction between individual components may involve steady or unsteady flow. An example of unsteady flow interaction is the evolution of a rotating stall cell which can take the form of the growth of a small amplitude, but long wavelength, circumferential disturbance. Hence the time development of a stall cell and therefore the stability limit for nomi-

nally uniform flow can be affected by the presence of upstream or downstream components [24].

6.1 General Effects of Downstream Components on Distorted Flow Compressor Performance

The coupling that can occur in circumferential distortion was initially examined quantitatively for passive components such as downstream diffusers and nozzles [5], and discussion of this forms a useful introduction to the topic. Suppose: 1) there were a diffuser downstream of the compressor, rather than a constant area duct, and, 2) the diffuser was short enough so a "parallel diffuser" view of the flow in the high and low total pressure streams could be invoked. Such a situation is shown schematically in Figure 16. In the diffuser, the low total pressure (low velocity) stream produces a lower static pressure rise than the high total pressure (high velocity) stream (Figure 16b). The static pressure at the compressor exit, in the low total pressure region, is thus higher than in the high total pressure region, since the static pressure is uniform at the *diffuser exit*. The converse situation would occur for a downstream nozzle, where the

(a)

$(P_t)_H$ →

$(P_t)_L < (P_t)_H$

ρ = constant
at diffuser exit

Compressor   Diffuser

Throttle

Collector

(b)

$(p_1)_{low}$

$(P_1)_{high}$

p_2 = constant

①   ②

One-Dimensional Ideal Flow

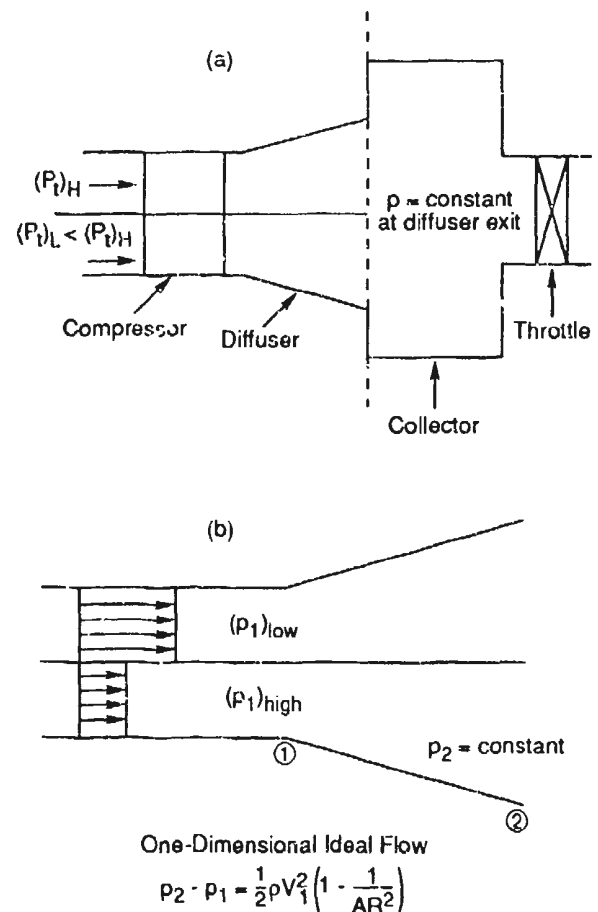$$p_2 - p_1 = \frac{1}{2}\rho V_1^2\left(1 - \frac{1}{AR^2}\right)$$

Figure 16: Parallel diffuser model for compressor-component coupling effects; a) parallel diffusers, b) non-uniform flow in a parallel diffuser.

low velocity stream would have a lower static pressure at the compressor exit. Although the parallel diffuser concept is clearly a crude approximation, detailed computations of the asymmetric flow in diffusers which examine this effect quantitatively bear out the qualitative validity of this explanation.

One implication of the presence of the downstream component is indicated in Figure 17, which relates to operation in distorted flow for a compressor with a constant area downstream annulus, with an exit diffuser, and with an exit nozzle. For the same mean flow and inlet total pressure distortion, the local working points of the compressor, as given by the parallel compressor model, can be strongly affected by the downstream component. In particular, the low flow side is pushed nearer to stall by the presence of the diffuser. Although the arguments presented are not by any means conclusive, it is nevertheless found that a downstream diffuser can indeed provide a destabilizing influence.

A more quantitative view of this phenomena is shown in Figure 18 which gives data and computations for the circumferentially distorted flow downstream of a three-stage compressor, which was run with an exit diffuser, an exit nozzle, and a constant area annulus [25]. The mean flow and inlet total pressure distortion was the same for all three tests. As suggested by the physical arguments given above, the static pressure non-uniformity at the compressor exit is in phase with the total pressure distortion for the nozzle, out of phase for the nozzle, and virtually zero for the constant area annulus.

Figure 18: Effect of downstream components on static pressure distortion at exit of three-stage compressor: a) theory, b) experiment [25].

The referenced papers include other predictions and measurements of the overall distortion attenuation, the behavior of the total and static pressure within the compressor, and the quantitative definition of the strength of the coupling for a given distortion. In regard to this last issue, it can be noted that the different spatial harmonics of the circumferential distortion experience different degrees of coupling because the ratio of axial distance between component and the wavelength of the harmonic will differ. It is the low spatial harmonics that show the strongest effects, hence the emphasis on large extent distortions.

6.2 Multi-Spool Component Coupling

More recent investigations of compressor-component coupling in distorted flow have focused on the coupling between the different spools in multi-stage engines. The type of interaction considered can be discussed in the context of flow through a two-spool aeroengine (high and low pressure compressors), with a square wave inlet total pressure distortion. If the compressors were far apart (several radii) the static pressure at the exit of the low pressure compressor would be uniform, even though the downstream high-pressure compressor would create a static pressure field ahead of it. If the distance between the two compressors were reduced to a level typical of practice, however, the static pressure field ahead of the downstream compressor would be seen at

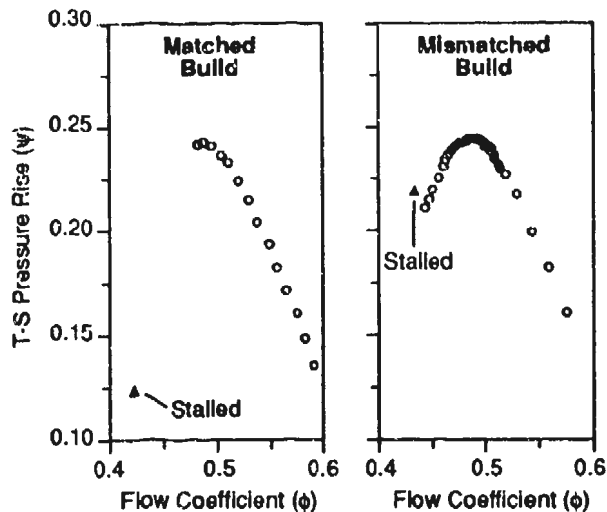Figure 17: Effect of downstream components on compressor performance with inlet distortion.

the exit of the upstream compressor and would affect its performance.

Ham & Williams [20] examined this steady flow interaction and developed a "coupling number" which related the influence of the downstream component on the size of the non-uniformity at the exit of the upstream component. The coupling number CN was defined as

$$CN = \frac{\Delta P_{t2}(\ell) - \Delta P_{t2}(\infty)}{\Delta P_{t2}(0) - \Delta P_{t2}(\infty)}$$

where $\Delta P_{t2}(x)$ is the amplitude of the total pressure distortion at the exit of the upstream component when there is an axial distance x between the upstream and downstream components. The value $x = \ell$ corresponds to the actual distance between the two components, whereas $x = 0$ and ∞ relate to zero and far apart spacing respectively. The coupling number varies between 0, representing no static pressure field interaction ($x = \infty$), and 1, where the two components abut ($x = 0$) and there is a strong static pressure interaction. Higher values of the coupling number correspond to instances where the presence of the downstream component reduces the distortion attenuation across the upstream one. In terms of the parallel compressor concept, the two operating points for the upstream compressor are closer together (higher CN) so there is a decreased loss in upstream compressor surge margin.

The analysis of Ham and Williams [20] was based upon a linearized approach to the modelling of the compressor behavior, but it gave insights into the differences between distortion tolerance of the low pressure com-

Figure 20: Effect of vane chord on static pressure distortion [20].

pressor when tested in isolation against that when tested in the aeroengine with a downstream high pressure compressor. Figure 19 gives the predicted surge lines for a two-spool system, assuming that no coupling exists between the compressors as well as that assuming that the compressors are 100% coupled (no spacing between high and low compressors). Experimental measurements are also shown, and these clearly indicate the effect of the compressor coupling on the engine stability limit.

Analysis of the flow coupling between two compressors becomes more complex when there are vanes in the duct. This problem was also considered by Ham and Williams [20] (and theoretically by Hynes [26]). As might be expected, the vanes reduce the circumferential flow redistribution between the two compressors and therefore increase the coupling (effectively making the duct shorter). Results of computations and measurements showing this effect are given in Figure 20, which shows how the ratio of duct entry to exit static pressure ratio increases as the eight vanes fill a greater percentage of the duct length.

6.3 Non-Steady Flow Interaction

Components in a compression system have also been shown to influence each other in a non steady-flow manner. Longley and Hynes [27] demonstrated that the uniform flow stability boundary of a single stage research compressor was significantly affected by the presence of different downstream components. In particular, as shown in Figure 21, the stage was able to be stabilized past its nominal stall point (matched build) when the two stages downstream of it were restaggered to a lower flow coefficient (mismatched build). This behavior can be explained on the basis of the interaction of long wavelength, small amplitude disturbances which would

Figure 19: Distortion tolerance for different amounts of coupling between compressors; - - - - prediction for 100% coupling, —— prediction for 75% coupling, ·········· prediction for zero coupling, • data [20].

Figure 21: Comparison of research stage performance for different downstream components [27].

Figure 22: Effect of distortion rotation rate on compressor stall onset [29].

grow into rotating stall, but which are suppressed by the presence of stable downstream compressor stages. Measurements of the time resolved flow in the compressor, within the stabilized regime, indicated that there was an increase in flow unsteadiness but no coherence that would suggest the presence of either part or full span rotating stall.

6.4 Radial Coupling
Component coupling has also been suggested to depend on the radial interaction in low hub-to-tip ratio compressors. Lambie [28] investigated a core compressor, fan and bypass duct geometry and found that the stability boundary (as a function of bypass ratio and mass flow) depended on the axial distance between the core compressor and fan. The explanation given for the change in the stability boundary was that the core compressor was sufficiently stable to inhibit the development of flow instability in the hub region of the fan and hence allowed a greater operating range. An analysis which puts this on a firm quantitative footing, however, has yet to be developed.

6.5 Rotating Distortion
A further aspect related to component coupling is the response to a rotating distortion pattern. Such a flow could arise from an upstream compressor in rotating stall generating a non-uniform total pressure profile at the downstream compressor. This situation has been experimentally investigated by Ludwig et al. [29] who showed that the stability boundary of a compressor strongly depended on the frequency at which the distortion rotated. As seen in Figure 22, for their geometry, co-rotational distortions at approximately 50% of rotor speed were the most damaging with respect to loss in stable flow range.
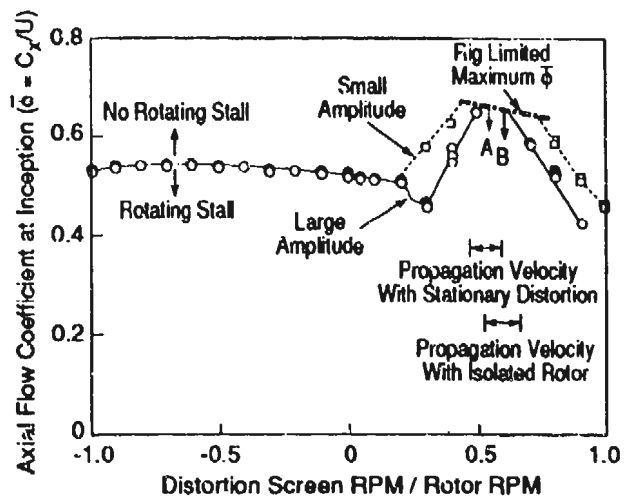
7. RECENT DEVELOPMENTS IN MODELLING COMPRESSOR RESPONSE TO INLET DISTORTION

In the methods described above, the assessment of when instability will occur requires some type of empirical input. One goal, therefore, is to reduce the level of empiricism and place such assessments on a more rigorous theoretical footing. In this section we describe an approach aimed at doing this within the framework of hydrodynamic stability analysis.

7.1 Hydrodynamic Stability Analysis of Distorted Flow Compressor Behavior
A flow field is considered to be stable if any small disturbance decays in time. The stability boundary thus occurs where conditions are such that an initially small flow perturbation can grow into a large amplitude disturbance. Mathematically this question can be examined by considering the time dependent equations which determine the compressor flow field and solving for the temporal development of the most general flow disturbance.

A theoretical model for analyzing the effects of a total pressure inlet distortion in low-speed high hub-to-tip ratio compressors was developed by Hynes & Greitzer [30], (following the earlier work of Moore [31]). The analysis proceeds in two steps. The first is the solution of the (non-linear) distortion transfer through the compressor for a time independent flow. This yields a steady-state background flow, non-uniform around the circumference, whose stability is then examined as the second step. The stability of the flow is assessed by linearizing about this non-uniform background solution and determining the time development of the most general flow disturbance. The existence of any disturbance

which would grow in time indicates the occurrence of a flow instability at that compressor operating point.

The analysis, including the pseudo-spectral computation procedures for the mean flow and the structure of the perturbation modes, is described in some detail in the referenced paper, and some illustrative results only are presented here. In contrast to other distortion analyses, not only the compressor and the exit conditions must be considered, but also the rest of the compression system. This is because the general unsteady perturbation is not necessarily confined to the compressor, but may include motion in the plenum and downstream ducts. Put another way, a stability analysis for a uniform flow would yield modes that were purely sinusoidal (zeroth spatial harmonic, first spatial harmonic, second spatial harmonic, etc.) in the circumferential direction. Hence the small amplitude compressor type modes (the asymmetric perturbations) would not be coupled to the compression system mode (the axisymmetric zeroth order disturbance). With a non-uniform inlet flow, however, each of the modes now has a spatial structure that is rich in harmonics, so that there is a coupling between disturbances that propagate round the compressor annulus and variations in the mean flow. Essentially, the annulus averaged flow changes in response to the movement of small amplitude circumferential disturbances in and out of phase with the background steady flow non-uniformity.

The wave structure (around the compressor annulus) predicted for the case with inlet distortion is shown in Figure 23. The axes in the figure are circumferential position and axial velocity perturbation against time. It can be seen that the wave shape changes as the waves move in and out of the shadow of the distortion screen. This behavior was subsequently verified by Longley [27] in a three-stage compressor, as seen in Figure 24, which shows the measured and predicted amplitudes of the unsteady perturbation versus circumferential position for a compressor with inlet total pressure distortion. The

Figure 24: Amplitude of unsteady axial velocity perturbation versus circumferential poistion for low speed multistage compressor with inlet total pressure distortion [34].

magnitude of the unsteadiness can be seen to vary strongly around the circumference, evidence of the effect of local conditions on disturbance amplification and decay.

A more global result is that the model gives good correlation for the empirically derived $DC(\theta_{crit})$ parameter, as seen in Figure 25. Further, the trends shown by the model are in agreement with the type of behavior described earlier in Figure 9; distortions of small circumferential extent have little effect on stability and sectoring a given total angle of distortion also causes reduced effect. Based on the parametric studies carried out, Hynes and Greitzer [30] suggested that the stability boundary of the compression system could be approximated as the condition for a zero mean slope of the compressor characteristic around the annulus:

$$\text{mean slope} = \frac{1}{2\pi} \int \frac{d\psi}{d\phi} \, d\theta$$

This has been referred to as the IMS (Integrated Mean Slope) criterion and supports the idea that instability does not occur when an operating point reaches the clean flow stability boundary but when there is a balance
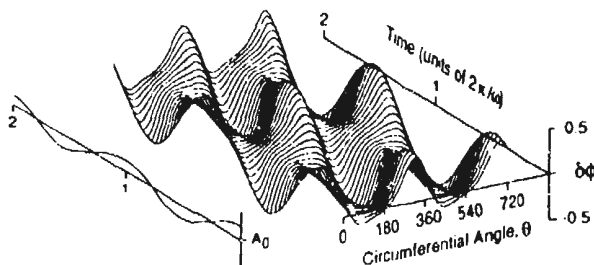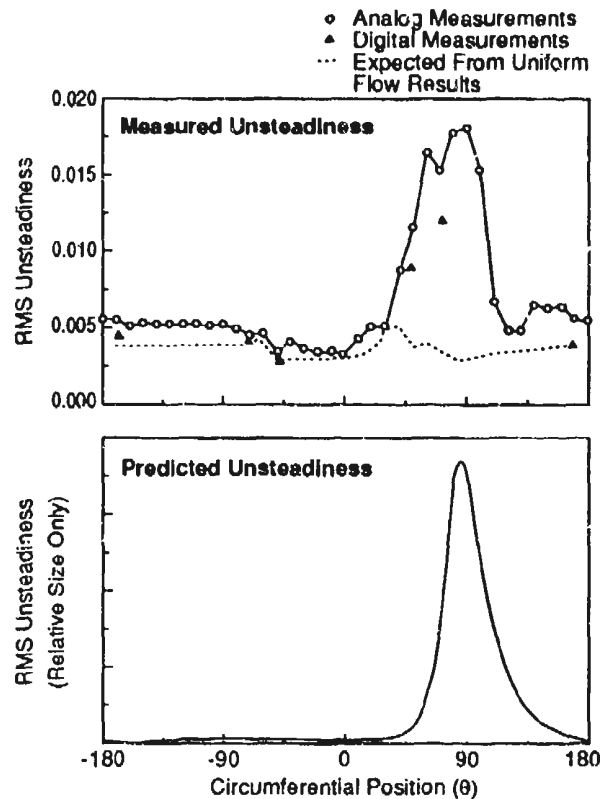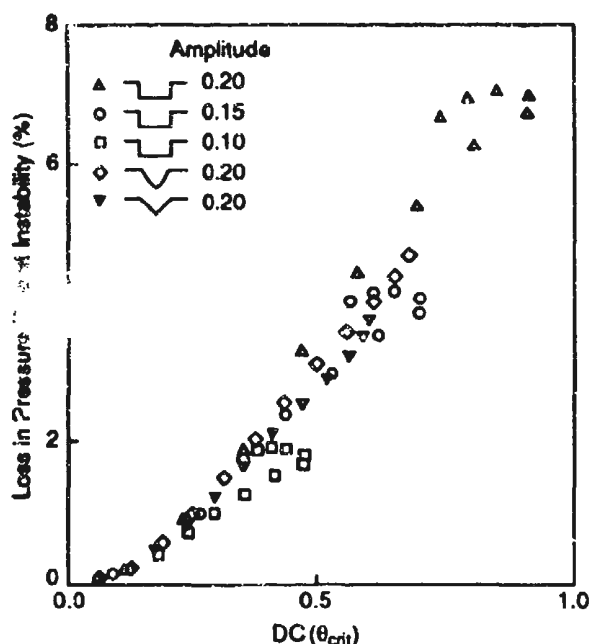

Figure 23: Structure of compressor inlet axial velocity perturbation with inlet distortion; axial velocity versus circumferential position at different times. A_0 denotes annulus averaged mass flow fluctuation. Distortion of $\Delta P_t/\rho U^2 = 0.2$ from $\theta = 120°$ to $240°$ [32].

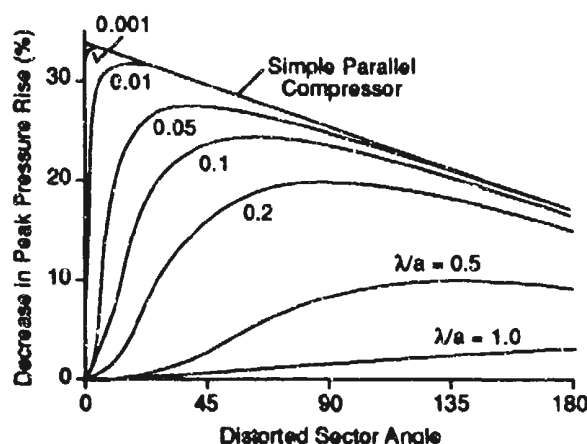Figure 25: Loss in stability margin versus $DC(\theta_{crit})$ [30].

Figure 26: Effect of compressor parameter λ/a on decrease in peak pressure rise; computations based on criterion of zero integrated mean slope (IMS) at instability point and parabolic compressor characteristic [32].

between the extents of the unfavorable and favorable compressor operation. (The zero slope is the theoretical prediction for the instability point in uniform flow.)

The theory has also been applied to rotating distortions, referred to earlier in Section 6.5. The calculations show that there is an increased effect on stability when the rotation speed of the distortion is near the propagation velocity of the naturally occurring perturbations (the eigenmodes of the compressor/compression system) in the compressor annulus [32]. Experiments on a low speed multistage compressor confirming the basic phenomena predicted by the model are reported by Plumley [33].

7.2 Connections with the Parallel Compressor Model
The IMS stability criterion has been applied by Chue et al. [32] to the case of a square wave inlet distortion and the results are shown in Figure 26. The stability analysis reduces to a form very similar to the modified parallel compressor model (Figure 11), with the critical sector angle a function of the non-dimensional quantity λ/a. The parameter λ is defined by

$$\lambda = \sum_{\substack{\text{rotor} \\ \text{rows}}} \frac{\text{axial blade chord}}{R \times \cos^2 (\text{stagger})}$$

and represents the inertia of the fluid in the rotor passages, and $1/a$ is proportional to the curvature of the compressor characteristic at the peak. Williams [10] has applied these ideas to the prediction of θ_{crit} for a num-

ber of different multistage compressors, with the encouraging results shown in Figure 27.

In summary, the theoretical model appears to be in accord with a large body of experimental data, and can be used to give insight in a number of situations. The main reason for this is the inclusion within the model of non-steady fluid dynamic features of the coupling between high and low flow regions of the compressor annulus. Further results of computations, the application to the case of increased stability degradation due to rotating distortions, and comments on the regimes of applicability of the IMS criterion, are given by Chue et al. [32] and Longley [8], [34].

8. SOME COMMENTS ON FUTURE REQUIREMENTS FOR COMPRESSOR MODELS

The models described above provide explanations for many aspects of compressor behavior in non-uniform flow. The new theoretical approaches have suggested various fluid dynamic phenomena, which in turn have led to improved predicative ability. At present, however, the theoretical models are primarily for low Mach number and high hub-to-tip ratio compressors, and this section reviews the ways in which these approaches are being extended.

Inlet distortion problems are, in general, three-dimensional and can involve significant radial flows in low hub-to-tip ratio compressors. These types of non-uniform flow problems were initially investigated using linearized approaches [6], [35], though the restrictions on the formal solutions limited the insight they provided. The availability of reliable three-dimensional computation solution methods has renewed the research into
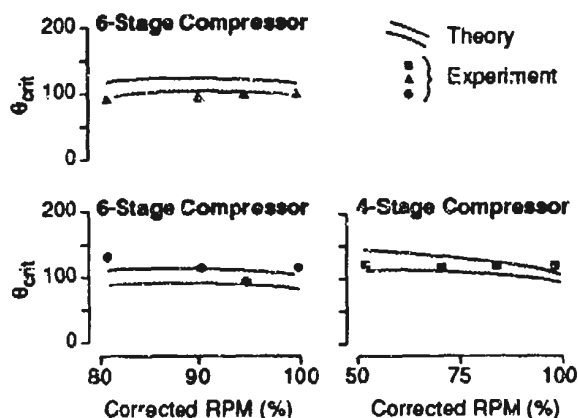
Figure 27: Predicted and experimental critical sector angles [10].

these problems. The general approach is to solve the three-dimensional flow upstream of the compressor using a standard Euler or Navier-Stokes solver and then applying a compressor like boundary condition at the aeroengine location to generate the appropriate upstream flow field redistribution. Problems currently being addressed are the interaction between the nacelle and fan in bypass engines, inlet vortex generated distortions, and hot gas reingestion in VSTOL aircraft.

High Mach number flows, where compressibility effects can be important, are only just being investigated from the point of view of the effects of inlet distortion on compressor stability. For high-speed compressors, linearized distortion transfer (LINEARB) and the analysis of the uniform flow stability [36] have both been carried out. These techniques can be combined to provide a compressible form of the rigorous inlet distortion stability model that was described for low speed flow in Section 7.

9. SUMMARY AND CONCLUSIONS

It is interesting to put the present lecture in perspective by comparing the topics discussed with those described in a previous AGARD Lecture Series (LS72, 1974), which dealt with inlet distortion effects on engine stability. Substantial progress has been made since then on several levels. First, the empirical methods have now been given a wider degree of commonality (AIR1419). Second, many aspects which had not been dealt with at that time have now been sorted out. These include, among others: 1) the development of methods to deal with many different streams of different total pressure so that a more detailed description of the circumferential flow distortion can be carried out; 2) the assessment of the effects of temperature distortion and of combined temperature and pressure distortion; 3) the theoretical and experimental studies of compressor-component cou-

pling; and 4) the development of three-dimensional computational procedures to deal directly with the effects of inlet geometry on fan distortion. Third, the development of a rigorous stability analysis of compressor behavior in distorted flow has so far yielded results that are encouraging, at least qualitatively, and have provided insight into situations such as the effect of distortion extent, which were not available before. This theoretical analysis can build on the first two aspects in showing which fluid dynamic effects are important and in analyzing a wider range of problems. It offers much potential for the development of methods for dealing with many aspects of inlet distortion which are currently beyond predictive capabilities.

10. ACKNOWLEDGEMENTS

11. REFERENCES

1. McDougall, N.M., Cumpsty, N.A., Hynes, T.P., 1990, "Stall Inception in Axial Compressors", *J. of Turbomachinery*, 112, pp. 116-125.

2. Day, I.J., 1991, "Stall Inception in Axial Flow Compressors", ASME Paper 91-GT-86.

3. Day, I.J., 1991, "Axial Compressor Performance During Surge", presented at Tenth ISABE International Symposium on Air Breathing Propulsion, Nottingham, England.

4. Mazzawy, R.S., 1977, "Multiple Segment Parallel Compressor Model for Circumferential Flow Distortion" *ASME J. Engineering for Power*, 99, pp. 288-296.

5. Greitzer, E.M. and Griswold, H.R., 1976, "Compressor-Diffuser Interaction with Circumferential Flow Distortion", *J. Mechanical Engineering Science*, 18, pp. 25-39.

6. Dunham, J., 1965, "Asymmetric Flows in Axial Flow Compressor", *Institution of Mechanical*

Engineers Mechanical Engineering Monograph Number 3.

7. Stenning, A.H., 1980, "Inlet Distortion Effects in Axial Compressors" *ASME J. Fluids Engineering.* 102, pp.7-13.

8. Longley, J.P., 1990, "Measured and Predicted Effects of Inlet Distortion on Axial Compressors," ASME Paper 90-GT-214.

9. Soeder, R.H., and Bobula, C.A., 1979, "Effect of Steady-State Pressure Distortion on Flow Characteristics Entering a Turbofan Engine", NASA TM-79134.

10. Williams, D.D., 1987 "Review of Current Knowledge of Engine Response to Distorted Inflow Conditions", in AGARD CP-400, Engine Response to Distorted Inflow Condition.

11. Williams, D.D., 1992, "Engine Compatibility" to appear as Chapter 3 in *Practical Intake Design,* Seddon, J., and Goldsmith, E.L., eds., Blackwell Scientific Publications.

12. Steenken, W.G, 1989, "Engine Operability", Ch. 6 in Aircraft Propulsion Systems Technology and Design, Oates, G., ed., AIAA Education Series.

13. Cumpsty, N.A., 1989, *Compressor Aerodynamics,* Longman Scientific and Technical Publishers, Essex, England.

14. Reid, C., 1969, "The Response of Axial Flow Compressors to Intake Flow Distortion", ASME Paper, 69-GT-29.

15. LINEARA & LINEARB, "Linearised, Two-Dimensional, Actuator Disk and Semi-Actuator Disk Computer Codes," Rolls-Royce.

16. Kodama, H., 1986, "Performance of Axial Compressor With Non-Uniform Exit Static Pressure," *Trans. ASME,* 108, pp. 76-81.

17. Chen, G-T., Greitzer, E.M., and Epstein, A.H., 1987, "Enhancing Compressor Distortion Tolerance by Asymmetric Stator Control", AIAA Paper 87-2093.

18. Pazur, W., Fottner, L., 1990, "The Influence of Inlet Swirl Distortions on the Performance of a Jet Propulsion Two-Stage Axial Compressor," ASME Paper 90-GT-147.

19. Hodder, B.K., 1981, "An Investigation of Engine Influence on Inlet Performance", NASA CR-166136.

20. Ham, C.J. and Williams D.D., 1983, "Some Applications of Actuator and Semi-Actuator Disk Theory to the Problem of Intake/Engine Compatibility", presented at JSME Tokyo Gas Turbine Conference, Paper 83-Tokyo-IGTC-50.

21. Barber, T.J. and Weingold, H.D., 1978, "Vibratory Forcing Functions Produced by Non-Uniform Cascades", *ASME J. Engineering for Power,* 100, pp 82-88.

22. Kodama, H. and Nagano, S., 1988, "Potential Pressure Field by Stator/Downstream Strut Interaction", ASME Paper 88-GT-54.

23. Giles, M.B., 1990, Personal Communication.

24. Greitzer, E.M., 1981, "The Stability of Pumping Systems" *ASME Journal of Fluids Engineering.* 103, pp 193-243.

25. Greitzer, E.M.., Fulkerson, D.A., Mazzawy, R.S., 1978, "Flow Field Coupling Between Compression System Components in Asymmetric Flow", *ASME J. Engineering for Power,* 100, pp. 66-72.

26. Hynes, T.P., 1983, Personal Communication.

27. Longley, J.P., Hynes, T.P., 1990, "Stability of Flow Through Multistage Compressors", *ASME J. Turbomachiner.,* 112, pp. 126-132.

28. Lambie, D., 1989, "Inlet Distortion and Turbofan Engines", Ph.D. Thesis, Engineering Department, Cambridge University.

29. Ludwig, G.R., Nenni, J.P., Arendt, R.H., 1973, "Investigation of Rotating Stall in Axial Flow Compressors and Development of a Prototype Stall Control System", Technical Report USAF-APL-TR-73-45.

30. Hynes, T.P. and Greitzer, E.M., 1987 "A Method for Assessing Effects of Inlet Flow Distortion on Compressor Stability", *ASME J. Turbomachinery,* 109, pp. 371-379.

31. Moore, F.K., 1984, "A Theory of Rotating Stall of Multistage Compressors, Parts I-III" *ASME J. Engineering for Gas Turbines and Power,* 106, pp. 313-336..

32. Chue, R., Hynes, T.P., Greitzer, E.M., Tan, C.S., Longley, J.P., 1989, "Calculations of Inlet Distortion Induced Compressor Flow Field Instability", *International Journal of Heat and Fluid Flow,* 10, pp. 211-223.

33. Plumley, R.M., 1990, "Unsteady Compressor Distortion Response and Compressor Instability," M.S. Thesis, Department of Aeronautics and Astronautics, Massachusetts Institute of Technology.

34. Longley, J.P., 1988, "Inlet Distortion and Compressor Stability", Ph.D. Thesis, Engineering Department, Cambridge University.

35. Hawthorne, W.R., McCune, J.E., Mitchell, N.A., and Tan, C.S., 1978, "Non-Axisymmetric Flow through Annular Actuator Disks: Inlet Distortion Problem", *ASME J. Engineering for Power*, 100.

36. Bonnaure, L.P., 1991, "Modelling High Speed Multistage Compressor Stability", M.S. Thesis, Department of Aeronautics and Astronautics, Massachusetts Institute of Technology.

AD-P007 896

92-20695

CALCULATION OF INSTALLATION EFFECTS WITHIN PERFORMANCE COMPUTER PROGRAMS

J. Kurzke
MTU München GmbH
Performance Department ETL
Postfach
8000 München
Germany

SUMMARY

Gasturbine engine components as compressors, burners and turbines are usually tested on rigs prior to installation into an engine. In the engine, the component behaviour is different due to a variety of reasons. The installation effects are caused by small geometrical differences due to nonrepresentative rig operating temperatures and pressures, by different gas properties and Reynolds numbers and by radial as well as circumferential temperature and pressure profiles at the inlet to the component. For highly accurate performance predictions these rig-to-engine effects have to be taken into account.

Traditionally the term "installation" is also used for describing all the differences in engine operation and behaviour between testbed and aircraft. Intake and afterbody drag, power offtake and bleed as well as intake pressure losses and inlet flow distortion have significant impact on airflow, thrust, specific fuel consumption and compressor stability. Using modern performance synthesis programs all these effects can be simulated reasonably well.

LIST OF SYMBOLS

A_8	nozzle throat area
A_9	nozzle exit area
DC_{60}	distortion coefficient
f	factor
F_g	gross thrust
H	specific work
ISA	international standard atmosphere
k	constant
L	characteristic length
M	Mach number
n	exponent
N	spool speed
OTDF	overall temperature distribution factor
P	total pressure
P_s	static pressure
pol	polytropic
PW	power
R	gas constant
Re	Reynolds number
ref	reference
RNI	Reynolds number index
RTDF	radial temperature distribution factor
SFC	specific fuel consumption
sm	surge margin
T	total temperature
T_s	static temperature
V	velocity
W	mass flow
war	water-air-ratio
β	auxiliary coordinate
δ	corrected pressure P/101325Pa
η	efficiency
θ	corrected temperature T/288.15K
κ	isentropic exponent
μ	dynamic viscosity
μ_0	dynamic viscosity for T=273K
ν	kinematic viscosity

1. INTRODUCTION

A performance calculation computer program is sometimes also called a "synthesis" program, because performance is synthesized from lots of ingredients. Those ingredients are the components of the engine like compressors, turbines, burners, ducts and nozzles.

The behaviour of the components is described by their characteristics. In case of a compressor for example the characteristic is the compressor map with pressure ratio plotted over corrected flow for several values of corrected speed. Efficiency contours can be plotted in the same map.

In a simple synthesis program the component characteristics are used as calculated or measured on a rig whithout applying any corrections. That however does not result in very accurate results. To match such a model to measured data from an engine test sometimes socalled "fiddle factors" are used. That are factors used either within the model or applied to the results for which no physical justification is available. Models with fiddle factors are rather easy to produce, but they are not suited to predict the performance of an engine for other operating conditions than those for which the fiddle factors are defined. They are also not suited to study the effect of component modifications.

For accurate performance synthesis one needs to make corrections to the component characteristics which take into account any difference between the in-engine operating conditions and the conditions for which the characteristic originally was set up.

This paper attempts to give a more or less complete summary of all rig-to-engine effects. Introducing these effects into the performance model should minimize the need for "fiddle factors" and thus provide the best performance synthesis model of an engine.

The discussion of the installation effects starts with rig-to-engine effects for components. Under this heading both geometrical and aero-thermodynamical differences between component rig tests and component operating conditions in the engine are discussed.

In the second part the integration of the components into the overall engine performance computer program is described. Here those effects are dealt with, which cannot be allocated to a single component.

2. RIG-TO-ENGINE EFFECTS FOR COMPONENTS

A rig-to-engine effect is anything which is different between component behaviour during a rig test and while operating in the engine. Note that there can be a true difference in behaviour between rig and engine or it can only look like a difference. The latter can happen when the instrumentation is not identical between both vehicles. Another reason could be, that temperature readings are not properly (i.e. both static and dynamic) calibrated.
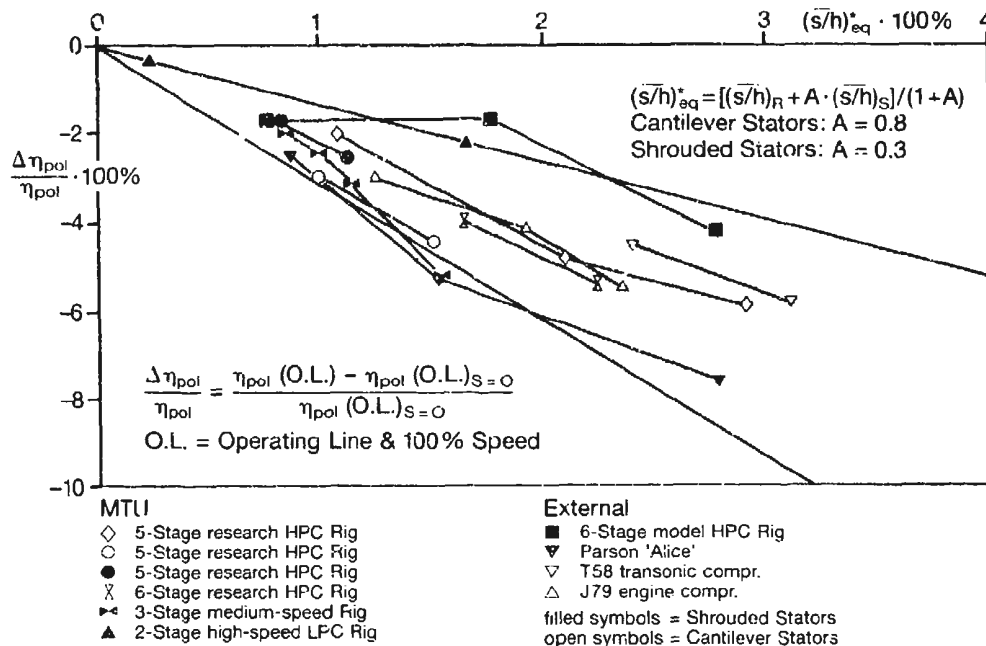
$$(\bar{s}/h)^*_{eq}=[(\bar{s}/h)_R + A \cdot (\bar{s}/h)_S]/(1+A)$$
Cantilever Stators: A = 0.8
Shrouded Stators: A = 0.3

$$\frac{\Delta \eta_{pol}}{\eta_{pol}} = \frac{\eta_{pol}(O.L.) - \eta_{pol}(O.L.)_{S=O}}{\eta_{pol}(O.L.)_{S=O}}$$

O.L. = Operating Line & 100% Speed

MTU
◇ 5-Stage research HPC Rig
○ 5-Stage research HPC Rig
● 5-Stage research HPC Rig
X 6-Stage research HPC Rig
⋈ 3-Stage medium-speed Rig
▲ 2-Stage high-speed LPC Rig

External
■ 6-Stage model HPC Rig
▼ Parson 'Alice'
▽ T58 transonic compr.
△ J79 engine compr.

filled symbols = Shrouded Stators
open symbols = Cantilever Stators

Fig. 1: Efficiency Loss in Multistage Axial Flow Compressors Due to Tip Clearance

Instrumentation problems are outside the scope of this paper. However they must not be forgotten when small effects are being discussed.

2.1 Geometrical Component Differences Rig-to-Engine
When there are geometrical differences between rig and engine then corrections to the rig results have to be applied. The type of correction and how it is to be applied depends on the change of the flow pattern due to the geometrical difference.

2.1.1 Tip Clearance
The impact of tip clearance on compressor and turbine behaviour is so severe, that every effort is made to minimize it during engine operation. That can be done to a limited amount by passive means, i.e. an optimal thermal match of static and rotating parts. An active clearance control (ACC) system is used on all new big civil engines: Cold air is blown onto the casing during steady state operation. The casing shrinks and thus running tip clearance is minimized. For a correct simulation of an engine with active clearance control one needs to model the change in tip clearance and its effects on the component behaviour.

Tip clearance can affect both flow capacity and efficiency of turbomachines. In case of compressors also the surge pressure ratio will change with tip clearance.

In figures 1 and 2 (taken from reference [1]) the impact of tip clearance on efficiency is shown for compressors and turbines. These figures shall give only an impression about the magnitude of the effect. The total effect of tip clearance depends on the operating conditions. In principle the whole characteristic will be modified by an increase in tip clearance. An example is given in figure 3.

Running tip clearance for a specific design depends on build clearances (production tolerances, squeeze film behaviour), thermal expansion and centrifugal forces. Thermal expansion of rotors and casings are generally different between rig and engine. In addition to these axisymmetrical effects casing ovalization due to external forces (thrust loads, gyroscopic forces etc.) causes locally increased tip clearance.

There are two types of rigs: specific development rigs and engine parts rigs. Development rigs are heavy designs with lots of additional instrumentation and features not available in the engine. For example on compressors there are stators adjustable during the rig test which are not planned to be variable on the engine.

Engine parts rigs are built from engine parts - as the name says. However the surroundings of the component in the engine cannot be simulated during the rig test. High pressure compressors in bypass engines will have quite different heat transfer to the bypass when operating in the engine. There will be a flow of varying temperature with speed on the outside of the compressor while on the rig there is no flow around the compressor casing. This causes a difference in tip clearance behaviour when the speed is changing. An example for this effect is shown in figure 4.

2.1.2 Blade Untwist
Compressor blades are twisted to comply best with the increasing circumferential speed from hub to tip. Centrifugal stresses tend to untwist the blades during operation if this is not prevented at least partly by snubbers. In case of snubberless blades this untwist is taken into account during the mechanical blade design.

Blade untwist has an impact mostly on flow but also on efficiency of compressors with low hub-tip ratios. At a given corrected speed the mechanical speed will vary with inlet temperature significantly. Imagine a fighter engine which has to operate at high altitude, low Mach number with an inlet temperature of say $T_2=240$ K at low altitude and high ambient temperatures with $T_2=380$K. At the same corrected speed the mechanical speeds can be calculated from

$$\frac{N_1}{\sqrt{240K}} = \frac{N_2}{\sqrt{380K}}$$

or $N_1 = 0.8 * N_2$. That means, that the centrifugal forces are at low inlet temperature only about 64% of those at high inlet temperature. Figure 5 shows the untwist of a snubberless fan blade from low to full speed.
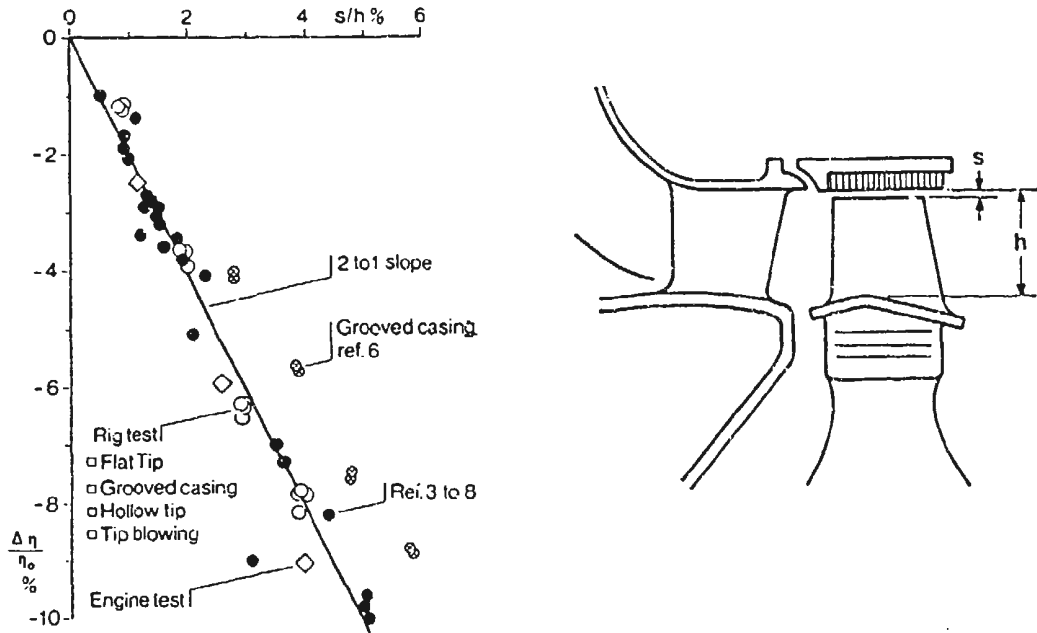
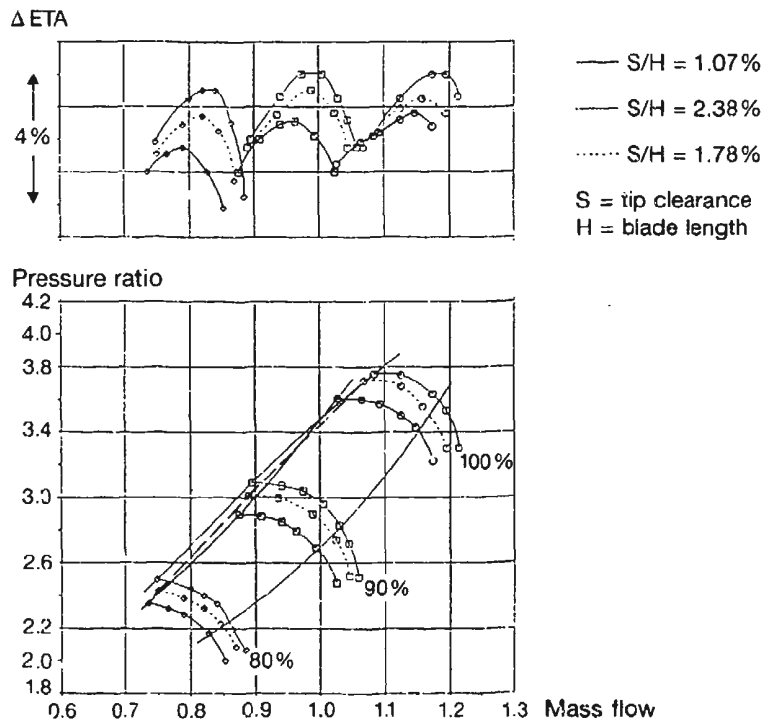**Fig. 2: Effects of Tip Clearance on the Efficiency of Single Stage Shroudless Turbines [1].**

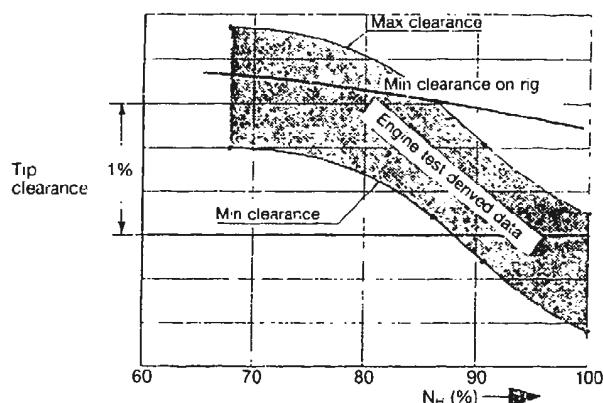**Fig. 3: Effects of Tip Clearance on Compressor Characteristics**

Fig. 4: Comparison of Tip Clearance Changes with Speed on Rig and in Engine

For the first rotor the untwist effect is the biggest - because it has the longest blades. The effect of blade untwist is similar to the effect of staggering. In figure 6 a typical result of restaggering the first rotor by 1 degree can be seen: At high corrected speeds the flow is much more increased than at low corrected speeds. Furthermore there is a significant change in efficiency.
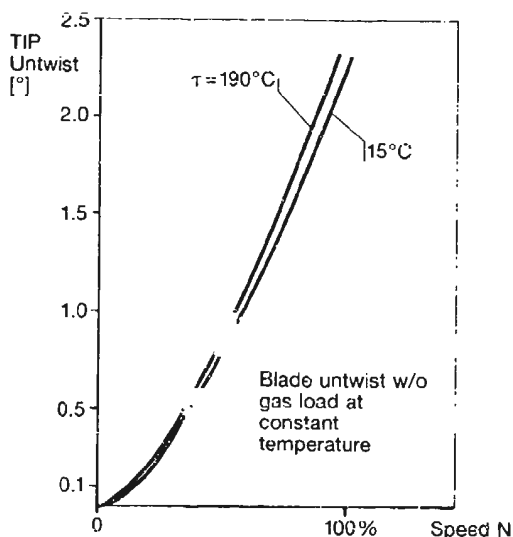

Fig. 5: Blade Untwist of a Snubberless Wide Chord Fan

2.1.3 Thermal Expansion

Some remarks about thermal expansion have already been made. Obviously during cold flow turbine rig tests using engine parts the difference in thermal expansion between engine and rig is most pronounced. Turbine throat area will be smaller during cold flow tests, the correction can be a simple factor on flow. The aerodynamic similarity of the flow is retained.

2.1.4 Bleed Offtake

In compressors we have often interstage bleed offtake. The internal flow of the compressor is affected by the ammount of bleed taken off. Changing the amount of bleed is equivalent to changing the annulus of the compressor, thus it is a modified compressor geometry.

If during the rig test there is less bleed than on the engine then the last stages will operate at higher flow and thus with more distance to last stage surge. For an accurate synthesis model it may be necessary to use different compressor maps if the amount of interstage bleed (in percentage from compressor inlet flow) is variable during engine operation.
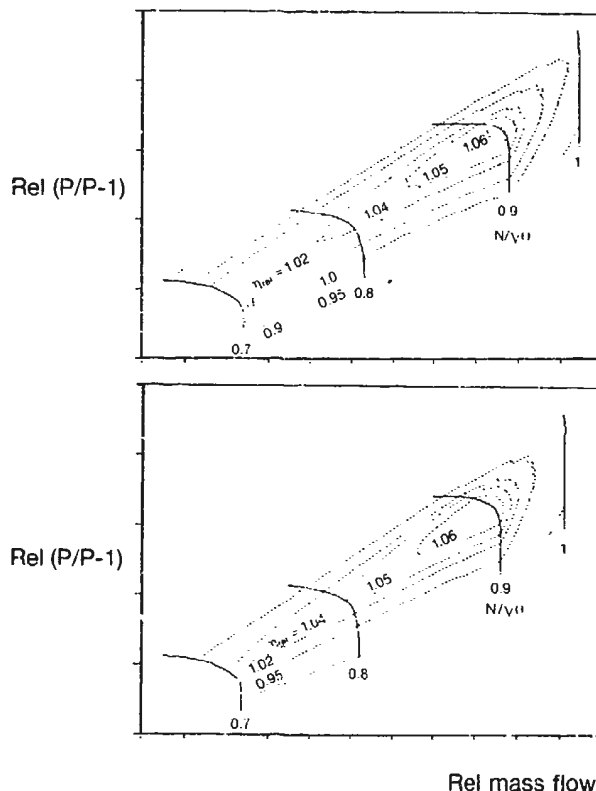

Rel mass flow

Fig. 6: Effect of 1° Restagger of the First Rotor on the Compressor Characteristic

2.1.5 Cooling Air Injection

The cooling air injection in turbines can be regarded as a geometrical difference in the flow boundaries between rig and engine.

On cold flow turbine rigs the cooling air injection cannot be simulated correctly. Even if there is cooling flow simulation at all the cooling air temperature is often not in the same relation to the hot gas temperature as in the engine. In case of correct simulation of cooling air pressures the cooling air Mach numbers will be o.k., however the absolute velocities and thus the relation between the momentum of the cooling flow and the main flow is different.

Nevertheless - the effect of cooling air injection on turbine efficiciency has to be taken from rig tests.

Cooling air injection will also have an influence on the flow capacity of the turbine. It can happen, that on the rig the stator is defining the turbine capacity and in the engine the cooling air injection causes the rotor to choke before the stator. This leads to an increasing flow capacity with decreasing turbine corrected speed.

2.2 Aero-Thermodynamic Differences

The data measured on rigs cannot directly be used as an input into engine simulations. Component characteristics based on the laws of similarity are used for this purpose.

Full similarity of the flow between any two tests implies:

o   geometric similarity (dimensional ratios = constant)

o   kinematic similarity (velocity ratios = constant)

o   dynamic similarity (ratio of forces = constant)

Provided that Reynolds number, gas constant and isentropic exponent are the same full similarity is achieved for a given turbomachine when Mach numbers are the same. The component characteristics for turbomachines are based primarily on the Mach number similarity. Characteristics measured on a rig are exactly valid only for the Reynolds numbers, the gas constant and the isentropic exponent encountered during the test.

2.2.1 Gas Properties
In the engine the isentropic exponent can be quite different to the rig test value, especially for turbines. The gas constant may be also not the same. There are three reasons for that:

o   the isentropic exponent for dry air varies with temperature

o   burning a fuel in dry air results in decreasing isentropic exponent with increasing fuel-air-ratio. The gas constant does not change very much in case of the normal hydrogen-carbon fuels.

o   water vapor in the air has an impact on isentropic exponent. The gas constant is also dependent on humidity.

2.2.1.1 Temperature, Pressure and Fuel-Air-Ratio
The standard procedure for performance calculations is, to use gas properties as a function of temperature and fuel-air ratio. The gas constant is often used with a fixed value in case of dry air.

In reality the gas properties are also dependent on pressure. However in the normal operating range of aircraft gasturbines the effect of pressure is small and usually neglected.

Only in case of combustors and reheat systems the pressure level is important: because of dissociation the heat release of burning fuel is dependent on pressure, especially near to stoechiometric fuel-air-ratios.
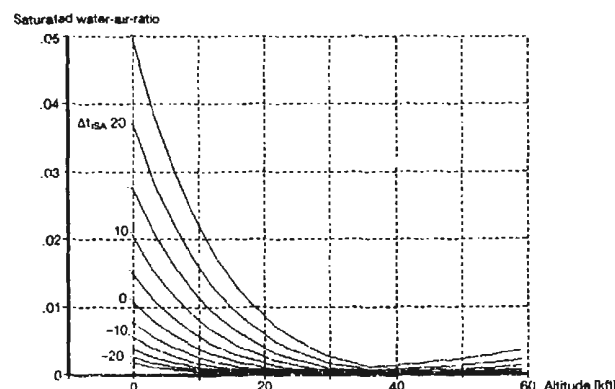
2.2.1.2 Humidity
Water can be in the air as vapor, as liquid or as ice. Here we deal only with the vapor content. Phase changes as for example condensation shocks are outside of the scope of this paper.

In figure 7 the water-air-ratio of saturated air is shown as a function of altitude and temperature. The latter is expressed as deviation from the ISA temperature. One can see, that at low altitude and temperatures above ISA a significant amount of water can be in the air.

It is recommended to take the effect on performance into account when the actual humidity level - which is lower than the saturated value shown in figure 7 - exceeds approximately 0.005 in water-air-ratio.

Be careful during tests in an altitude test facility (ATF)! The impression from figure 7, that one can forget about humidity effects at altitudes above 20 kft is misleading. In front of the engine there will be stagnation temperature and pressure, not the ambient conditions being simulated. Therefore the air can hold much more water, see figure 8.

How much water is in the air in a real test depends obviously on the outside air conditions. The maximum amount of water in the outside air can be taken from figure 7. (Read the figure for the altitude of the ATF location and the actual outside air temperature). The relative humidity measured on the day gives then the real water-air-ratio of the airstream entering the ATF.
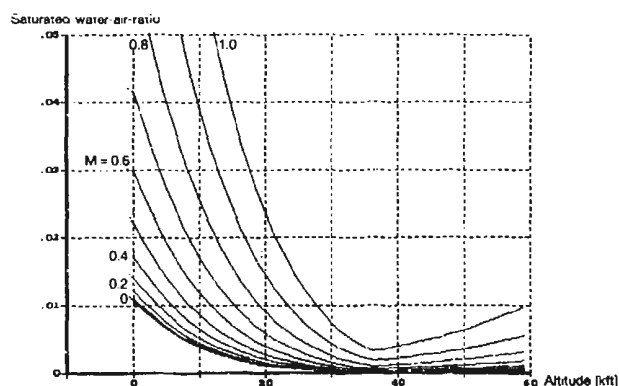
Fig. 8:   Water-Air-Ratio for Saturated Conditions during ATF Tests as Function of Altitude and Simulated Flight Mach Number

When the saturated water-air-ratio from figure 8 is lower than the water-air-ratio of the outside air then condensation will take place in the ATF machinery and the air in front of the engine will contain water droplets or ice. This causes on one side measurement problems - icing of probes - and on the other side a nontypical behaviour of the engine. The water evaporates during the compression in the engine and thus reduces compressor work. Thrust and SFC taken from such a test are not representative for an engine operating on an aircraft.

To avoid this the condensed water or the ice particles need to be separated out in the ATF downstream of the cooler respectively expansion turbine.

Fig. 7:   Water-Air-Ratio for Saturated Conditions as Function of Altitude and Deviation from ISA

3. CALCULATION OF COMPONENT PERFORMANCE

As already mentioned in the introduction one does not get the best engine simulation if the component characteristics are used directly as calculated or measured on a rig. Corrections for deviating gas properties are necessary. Additionally the characteristics have to be prepared for the use in a computer in a suitable format.

3.1 Compressors

3.1.1 Basic Procedure
Compressor performance as measured on the rig is normally presented in form of a characteristic with pressure ratio versus corrected flow $W*\sqrt{T}/P$ with corrected speed $N/\sqrt{T}$ as parameter. Efficiency contours complete the map.

Such a map is valid only for a gas with the same isentropic exponent as during the rig test. For correct performance calculations it is necessary to take into account the variation of the isentropic exponent with temperature and - if applicable - with water-air-ratio.

Unfortunately it is not possible to achieve full flow similarity with changing isentropic exponent, an approximation must be found. Let's define map correction factors based on Mach number similarity: in case of speed this factor is defined as

$$f = \frac{(N/\sqrt{T})_{true}}{(N/\sqrt{T})_{map}} = \frac{(N/\sqrt{T})_1}{(N/\sqrt{T})_0}$$

For Mach number similarity we have to achieve the same Mach Number for two different isentropic exponents. Note that this is possible *either* at the inlet *or* at the outlet of the turbomachine. We are concentrating now on the inlet conditions and request:

$$N/\sqrt{\kappa_1 R_1 T_{s1}} = N/\sqrt{\kappa_0 R_0 T_{s0}}$$

Using basic gasdynamic relationship. gives for the speed correction factor:

$$f_N = \sqrt{\frac{\kappa_1 R_1}{\kappa_0 R_0} \times \frac{(1 + \frac{\kappa_0 - 1}{2} M^2)}{(1 + \frac{\kappa_1 - 1}{2} M^2)}}$$

This factor is cumbersome to work with because of the Mach number term. It is common practice to neglect the term in brackets which is equivalent to setting the Mach number to zero. The error made by doing this can be read from figure 9. There as an example the water-air-ratio is varied between 0 and 0.03. 3% water in the air leads to a decrease in isentropic exponent by 0.28%.

A similar procedure leads to the definition of a flow correction factor f_W:

$$f_W = \sqrt{\frac{\kappa_1 R_0}{\kappa_0 R_1} \times \frac{(1 + \frac{\kappa_0 - 1}{2} M^2)^{\frac{\kappa_0 + 1}{2(\kappa_0 - 1)}}}{(1 + \frac{\kappa_1 - 1}{2} M^2)^{\frac{\kappa_1 + 1}{2(\kappa_1 - 1)}}}}$$

Again the Mach number term is often neglected, the consequence is only a small error, see figure 10.

For efficiency no correction factor can be derived from theory. Since full similarity cannot be achieved, the flow field will be changed by a change in isentropic exponent. Remember, that

for example shock wave angles are dependent on isentropic exponent. The impact of a changed isentropic exponent on efficiency is generally regarded as negligible.
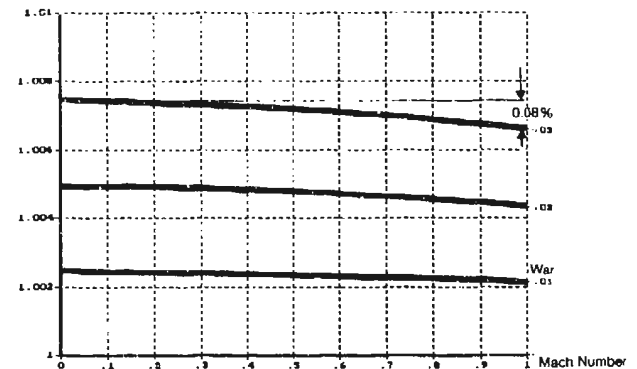

Fig. 9: Speed Correction Factor as Function of Water-Air-Ratio and Mach Number

Pressure ratio needs also a correction for varying isentropic exponent. The procedure is, to evaluate specific work from the data in the rig map, correct it for the new isentropic exponent and then recalculate the pressure ratio using the map efficiency.

The correction factor for specific work can be directly derived from the speed correction factor: Since specific work is proportional to speed², the specific work correction factor is the square of the speed correction factor.

As mentioned above, the correction procedure described is based on Mach number similarity at compressor inlet only. To check the influence of this simplification two compressor maps were calculated with different inlet temperature - which implies different isentropic exponents throughout the compressor. Then the correction factors derived above were applied to one of the maps. The corrected values were checked against the other map: the lineup between the data is not satisfying. Applying the factors overestimates the effect. More work is needed to develop an improved correction method.
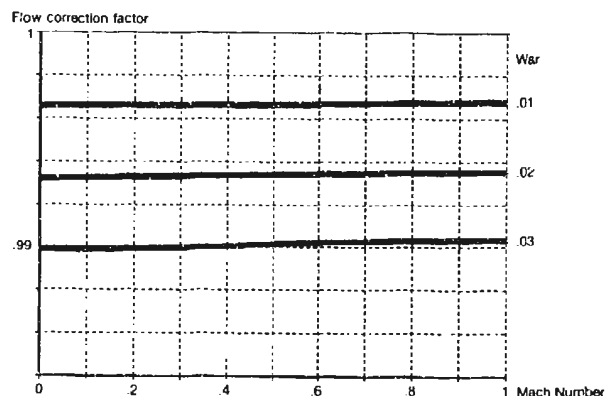

Fig. 10: Flow Correction Factor as Function of Water-Air-Ratio and Mach Number

3.1.2 Compressor Map Format
Sometimes it is tried to describe compressor maps by mathematical formulas, for example polynominals. This procedure will always need some compromises and thus a pseudo rig-to-engine effect is introduced which can easily be avoided.

From experience the best way of preparing compressor maps for use in the computer 's, to draw manually smooth lines through the measured data and check them carefully for consistency. If necessary, additional lines can be interpolated or extrapolated. Only by this procedure one has full control, no outlier in your measured data can introduce unwanted effects.

By the way - drawing manually does not necessarily mean the use of pencil and ruler. The job can be done for example with a special drawing program on the computer.

The standard compressor map format - where pressure ratio is plotted over mass flow with speed as parameter - is not directly suited for performance calculations. This is because from a given speed and mass flow one cannot read in all cases an unambiguous pressure ratio - that happens when the speed line is vertical. It is also not possible to use pressure ratio and speed as input - one could get two answers.

Fig. 11: Compressor Map with Auxiliary Coordinates

The solution is, to introduce some type of auxiliary coordinates ("β-lines") as shown for example in figure 11. These coordinates give always unambiguous intersections with the speed lines. Thus a given combination of speed and β fixes pressure ratio, mass flow and efficiency.

Together with the map the reference inlet temperature and pressure should be stored in the computer. From the actual compressor inlet conditions the speed correction factor discussed above can be calculated. Then the map is read using the map speed and β. For the reference inlet conditions specific work is calculated and then corrected to the actual inlet conditions. After that the pressure ratio can be calculated. The mass flow read from the map has also to be corrected as described in the preceding chapter.

A special case are maps for low pressure compressors of bypass engines. They have to be taken from a rig where both the core and the bypass stream can be throttled independently from each other.

The correct way to describe the behaviour of such a compressor would be, to measure on the rig a complete set of maps with bypass ratio as parameter. That is expensive and therefore such maps are normally not available.

Often only two maps are used: one for the core and one for the bypass stream. This can be done in two ways:

In the first approach - which is often applied with high bypass engines - there are two independent maps. In the alternative method pressure ratio and efficiency of both streams are plotted over the total mass flow, not over the individual mass flows as in the first approach. This calculation method is used mostly for low bypass engines as for example the RB199 or the EJ200.

In both approaches the impact of bypass ratio on compressor performance is only implicitly taken into account. It is important, to set up the two maps for bypass ratios as near to the real engine operating conditions as possible. If the bypass ratio is assumed constant throughout the map, then the description of the compressor is barely adequate for precise performance calculations. It is better, to assign to each speed line in the map a bypass ratio.

Rather good accuracy can be achieved when bypass ratio is not only varied with speed but also with pressure ratio. In tendency, bypass ratio will decrease with increasing speed and with increasing pressure ratio on a typical turbofan engine.

With all those simplified approaches one cannot describe exactly the compressor. Bypass ratio will be different between rig and engine, a pseudo rig-to-engine effect is introduced by a too simple compressor map representation.

By the way, if tip clearance corrections are required these should be applied only to the bypass map. Reynolds number corrections can also be different for both streams.

3.2 Turbines

3.2.1 Basic Procedure
Especially in case of highly cooled gas generator turbines it is very important to have identical efficiency definitions for both rig and engine. Detailed bookkeeping for all the cooling and leakage flows is necessary. Often it is assumed, that cooling air injected upstream of the turbine inlet nozzle guide vane throat does do work while the rest is - performance wise - bypassing the rotor.

The rotor blade cooling air is often pumped by a coverplate attached to the rotor disk. This coverplate operates as a radial compressor, which obviously needs a certain work input. Some - but not all - of the work put into the cooling air will be regained.

Sometimes work consumed by the coverplate is simulated separately, sometimes the effect of cooling air pumping is included in the efficiency definition. Whichever efficiency definition is used - it should be exactly the same for rig and engine. Otherwise one gets a rig-to-engine effect which in reality doesn't exist.

The basic procedure for taking into account a change in isentropic exponent is equivalent to the procedure for compressors described above. However when simplified versions of the correction factors are used then they are derived from the exact value by assuming sonic flow instead of M=0 as in case of compressors.

The magnitude of the isentropic exponent corrections are not negligible when the turbine map is taken from a cold flow rig. Changing the turbine inlet conditions from for example [T_1=400K, dry air] to [T_1=1700K, combustion gases with fuel-air-ratio = 0.023] results in a speed correction factor of 0.939 (sonic flow assumed).

The corresponding mass flow correction factor is 0.972. By chance the mass flow decrease is in the same order of magnitude as the thermal expansion of the turbine throat area. The flow changes approximately cancel each other and therefore often no mass flow correction is applied to the cold flow rig results.

3.2.2 Turbine Map Format
There are several formats in use for turbine maps. The input parameters for reading the map are often speed $N/\sqrt{T}$ and specific work H/T. In the normal operating range of a turbine these inputs are unambiguous and allow to read corrected flow and efficiency.

However there are problems with this turbine map format. Have a look on figure 12: While at high speed the efficiency is changing only moderately with specific work this is not the case at low speeds. There efficiency changes much more with specific work H/T than at high speed. For a precise numerical presentation of the map one needs small steps in H/T and therefore quite a lot of breakpoints.

To use many breakpoints on a speed line is not sufficient. If not enough speed lines are stored, then the interpolation error for efficiency can be significant, see figure 13.
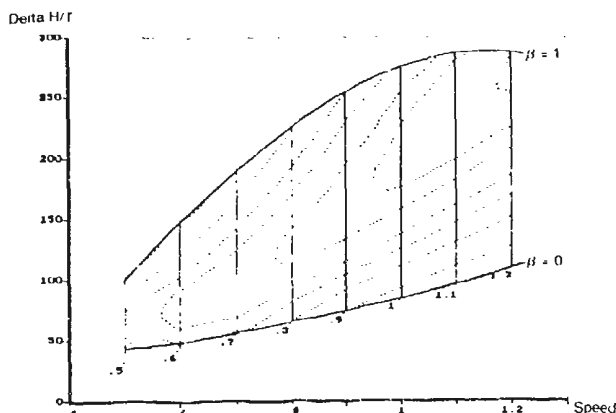
Fig. 12: Example for a Turbine Map

The problems described can be avoided by introducing auxiliary ß coordinates similar to those in case of compressors. Both the maximum and the minimum specific work of the turbine are stored as oneparametric functions of speed. The lower specific work is assigned by definition to ß=0, the higher one to ß=1. Then any other point within the map can be addressed by a value of ß between 0 and 1 and its speed.

By this it is achieved, that the sharp efficiency changes with specific work at low speeds are described properly without using an excessive number of breakpoints in areas where efficiency is changing only marginally.

At the same time only meaningful data are stored, no points with specific work above the turbine maximum capability are necessary to fill an array completely.

If it is made sure that the efficiency maximum is approximately at constant ß, then the interpolation error is minimized.

The format described up to now is not suitable for all turbines for the following reason: If one increases for example on a turbine rig at constant $N/\sqrt{T}$ the pressure ratio starting from a low value, then specific work will increase up to a maximum value. After achieving that maximum it can happen, that with further increasing pressure ratio specific work drops slightly - that depends on the special turbine design. As soon as in the turbine exit annulus sonic flow is reached, any further increase in pressure ratio has no effect on specific work.

In such a case for a given specific work there can be two solutions for reading the map or no solution at all.

Storing the turbine map in a different format avoids this difficulty. Instead of efficiency the isentropic specific work H_{is}/T is stored and used to read the real specific work. H_{is}/T can be tabulated up to sufficiently high values, the turbine maximum specific work can be described exactly.

Note that this format is especially suited for free turbines where instead of the work required to drive a compressor the pressure ratio is given.

In case the turbine is followed by a duct and the duct losses are dependent from flow angle then it is necessary to complete the

turbine map representation by a map of exit flow angles. This is simple since the turbine exit flow angle is directly coupled to its operating point.

3.3 Burners and Reheat Systems

Rig tests for burners are often done with less than nominal pressure. The consequences are bigger dissociation effects than compared to in engine operation. In proper performance synthesis programs this is taken into account, additional rig-to-engine corrections are normally not required.
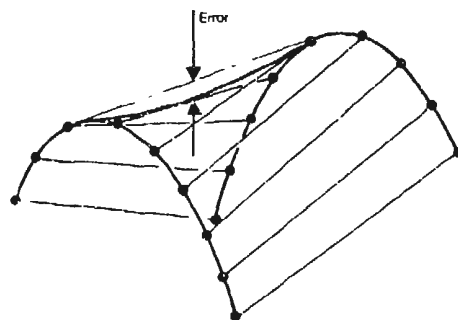
Fig. 13: Linear Interpolation Error

In case of reheat systems however the situation is more difficult. The simulation of the gas composition of the turbine exit flow needs special care. If this flow is simply heated by a conventional kerosine burner, then the fuel-air-ratio required to achieve a given temperature is significantly lower than the fuel-air-ratio at low pressure turbine exit in the engine.

In the engine the fuel is burned in the combustor, but after that the turbines are cooling the gases down. The oxygen content of the hot gases in the engine is much less than on the rig in case there only a simple heater is used for the turbine exit flow simulation.

Obviously a reheat rig without correct simulation of the oxygen content in the inlet flow is of limited value. If more oxygen is available, then more fuel can be burned. The fuel injection system cannot be properly optimized on such a rig.

To produce the correct oxygen content it is possible to inject water in the simulated turbine exit stream. This gives a significant improvement of the simulation quality, however the circumferential and radial oxygen distribution found in the engine cannot be simulated exactly.

Since the oxygen distribution on the rig will always deviate from the one found on the engine there are differences in efficiency between both vehicles to be expected. Note that the ideal case of stoichiometric combustion is achieved only, when each drop of fuel finds exactly the right amount of oxygen it needs.

As in case of gas generator turbines it is necessary to have identical definitions for reheat efficiency and fuel-air-ratios on both rig and engine. Also the method of deriving efficiency should be the same when comparing rig and engine results. On the rig efficiency can be analysed from gas sampling or by using an assumed nozzle discharge coefficient. On the engine gas sampling normally is not used, however engine thrust measurement allows to use an additional efficiency analysis method. Murphy's law implies, that you never will get the same answer for different analysis methods applied to the same set of measured data. Nevertheless one should always try to understand the reasons for the differences.

The operating conditions of the reheat system need also to be described properly. Note that for burning the Mach number similarity is of no importance. Burner loading parameters are more appropriate to describe the physics.

3.4 Nozzles

With respect to performance calculations nozzles are fairly simple components compared for example to turbomachines. In spite of that some rig-to-engine effects must be mentioned.

Often nozzle tests are done in reduced scale using model nozzles. When the nozzle inlet temperature and pressure were uniform during those tests as in case of reference [2] then care should be taken when the results are used within performance synthesis.

Pressure and temperature profiles at nozzle inlet - which are quite pronounced on mixed flow turbofans - can change both thrust and discharge coefficients, see references [3] to [5].

One can try to model the nonuniform flow through the nozzle, see for example reference [5]. The standard approach however is to use mixing efficiency. Three nozzle flows are calculated:

o   fully mixed flow
o   core flow (hot stream)
o   bypass flow (cold stream)

Each of the three streams is expanded from its total pressure to ambient conditions. Since each stream has got a different nozzle pressure ratio also the individual discharge and thrust coefficients can be different - that depends on pressure ratio.

The most relevant result of the calculation is the gross thrust which is calculated from

$$F_g = \eta_{mix} \ast F_{g,mixed} + (1 - \eta_{mix}) \ast (F_{g,cold} + F_{g,hot})$$

This type of nozzle modelling is rather crude, it aims primarily at the calculation of thrust. The effect of the radial nozzle inlet temperature and pressure distributions on discharge coefficient is only a by-product.

A second problem with model tests of nozzles is the mostly nonexistent simulation of nozzle leakage. In case of variable nozzles - as required for reheated engines - there is some leakage through the slots between the nozzle petals. Its amount depends on local pressure ratio between inside the nozzle and the surrounding pressure.

For convergent nozzles the leakage is always from inside to outside of the nozzle. Convergent-divergent nozzles when operated at low pressure ratios behave differently: around and downstream of the throat the static pressure inside the nozzle can be significantly lower than ambient pressure. The consequence is, that there is a "negative leakage": air from outside is sucked into the nozzle.

This has an effect on both discharge and thrust coefficient. While con/di nozzle model tests (without leakage in either direction) show the discharge coefficient being only dependent on primary petal angle and not on pressure ratio this does not hold with leakage. With leakage through the divergent petals the nozzle can have a discharge coefficient which is more similar to that of a convergent nozzle.

The effect of negative nozzle leakage can be beneficial for thrust in case the geometrical nozzle area ratio A_9/A_8 is too big for the operating pressure ratio. By sucking air through the divergent petals the effective area ratio is reduced, overexpansion avoided or less pronounced and the thrust coefficient will be bigger than the one measured on nozzle models without leakage.

4. REYNOLDS NUMBER CORRECTIONS

As already mentioned above, the characteristics used for turbomachines are only valid for a certain Reynolds number niveau. When changing Reynolds number there will be an effect on both mass flow and efficiency and in case of compressors also on the surgeline. So correction factors to the maps have to be applied.

4.1 Compressors

A summary of Reynolds number effects on axial compressor performance including empirical correlations can be found in [6]. In spite of the fact that this paper was published more than 20 years ago it is still being widely used for project assessments. Some important conclusions are summarized in the following.

With Reynolds number the characteristics of a compressor will change. Basically the shape of the speedlines will remain the same, but shifted towards lower mass flow and pressure ratio when Reynolds number is lowered, see figure 14.
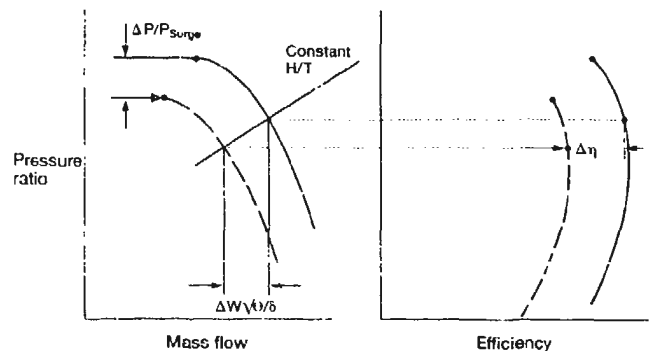
Fig. 14: Reynolds Number Effect on Compressor Performance

To define a correlation between both characteristics one has to define equivalent points. It is a good choice, to use points with the same specific work. Then the mean velocity triangles will have the same shape.

Correction factors for flow and efficiency can be derived from experiments. For each point in the characteristics the pressure ratio can be recalculated from specific work and the corrected efficiency value.

Note that also the surgeline is affected by Reynolds number level. The basic phenomenon however is different as compared to the efficiency and the flow shift. Those are caused by the increase in losses with decreasing Reynolds number. The surgeline shift however is connected to a reduced operating range of the cascades. Therefore a different correlation should be used as compared to the efficiency and mass flow shift, the assumption of constant specific work is not applicable in this case.

From the empirical data taken both from cascades, single and multistage axial compressors it is concluded in [6], that the best empirical approach to describe the effect of Reynolds number on efficiency is, that the polytropic efficiency changes with Reynolds number exponentially:

$$(1 - \eta_{pol}) = kRe^{-n}$$

Generally the impact of Reynolds number on mass flow is less pronounced. As a rule of thumb, the change of mass flow is half of the change of efficiency.

Values for k and n depend on the specific design of the compressor and also on the Reynolds number level. As described in [7] there are three different regimes which can be connected to the boundary layer condition. Figure 15 taken from this reference describes the phenomena.
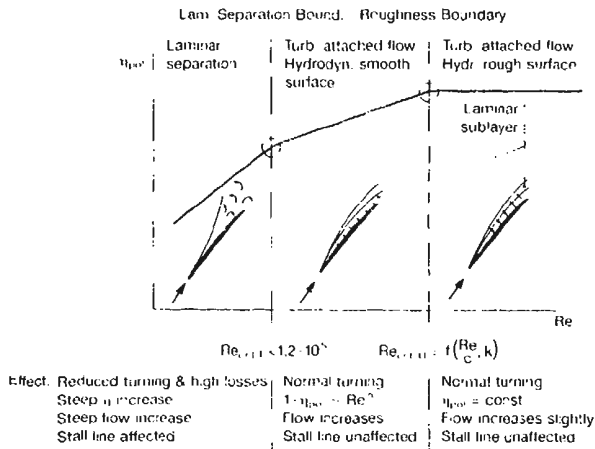

Lam Separation Bound. Roughness Boundary

| Laminar separation | Turb. attached flow Hydrodyn. smooth surface | Turb. attached flow Hydr. rough surface |

Laminar sublayer

$Re_{crit} \sim 1.2 \cdot 10^5$ $Re_{crit} = f\left(\frac{Re}{c}, k\right)$

Effect. Reduced turning & high losses	Normal turning	Normal turning
Steep η increase	$\eta \sim Re^n$	$\eta \sim const$
Steep flow increase	Flow increases	Flow increases slightly
Stall line affected	Stall line unaffected	Stall line unaffected

Fig. 15: Effect of Boundary Layer Condition on Compressor Behaviour [7]

For application of Reynolds corrections it is a good idea to use instead of absolute Reynolds numbers a Reynolds number index RNI:

$$RNI = \frac{Re}{Re_{ref}}$$

Reynolds number is defined as

$$Re = \frac{V*L}{\nu} = \frac{V*L*P_s}{\mu*R*T_s}$$

This can be expanded:

$$Re = L * \frac{V}{\sqrt{\kappa*R*T_s}} * \sqrt{\frac{T}{T_s}} * \frac{P_s}{P} * \frac{P}{\sqrt{T}*\mu}$$

The dynamic viscosity μ kann be approximated for the temperature range of compressors by

$$\mu = \mu_0 * \left(\frac{T}{273K}\right)^{0.75}$$

For fixed Mach number, gas constant and isentropic exponent the Reynolds number index is:

$$RNI = \frac{P/P_{ref}}{(\eta T_{ref})^{1.25}}$$

The correlations established in [6] were derived from data taken in the vicinity of the design operating conditions. Performance calculations however have to cover the full range of speeds and inlet conditons. A procedure is needed to correct the component characteristics not only near to design operating conditions but everywhere.

It is not appropriate simply to correct efficiency and mass flow read from the map by applying a simple factor. Note that within a compressor map the Reynolds number is not constant but obviously varying considerably with speed.

Imagine an example where the upper critical Reynolds number - above which efficiency is constant, see figure 15 - is at 80% corrected speed for reference inlet conditions. No efficiency correction is required at and above that speed. Let's assume now an increased inlet pressure: the Reynolds numbers throughout the compressor map will increase. The upper critical Reynolds number will be achieved already at say 60% corrected speed. Now efficiency is unaffected by Reynolds number at and above 60%. Using a correction procedure depending only on RNI but not on corrected speed would give the wrong answer.

Therefore the Reynolds correction applied to turbomachinery maps has to be done in two steps: firstly the Reynolds number effect hidden in the characteristic has to be calculated using $RNI = N/\sqrt{T}/(N/\sqrt{T})_{Design}$. In the second step a revised RNI is used which takes both $N/\sqrt{T}$ and the changed inlet conditions into account. Only the net effect of both steps is applied to the values read from the characteristics.

In case of Reynolds correction of the surgeline the procedure is simpler: One stores in the computer several surgelines in terms of pressure ratio over mass flow with RNI (derived from compressor inlet conditions only) as a parameter.

4.2 Turbines
Reynolds number effects are also existent in turbines. The basic correction procedure to be applied to turbine maps is essentially the same as in case of compressors.

The Reynolds number index for turbines depends on pressure and temperature according to

$$RNI = \frac{P/P_{ref}}{(\eta T_{ref})^{1.15}}$$

The exponent is matched to the normal operating range of turbines. It reflects the change in viscosity with temperature which is dependent on temperature level - therefore the exponent is different to that shown above for compressors.

Turbine maps can be valid for constant inlet Reynolds number or for constant exit Reynolds number - that depends on the rig test conditions. Often on the rig the air is expanded against ambient pressure; the map from such a test has fairly constant exit Reynolds number.

4.3 Ducts
Duct losses can increase sharply below a critical Reynolds number. This can be important in bypass ducts which are fairly long channels. The critical Reynolds number and the magnitude of the effect can be derived from theory or analyzed from ATF data. Sometimes also model tests are used to measure the duct loss characteristics.

5. FLOW DISTORTION EFFECTS ON COMPONENTS

Only the first compressor of an engine can operate without inlet flow distortion - and that only while the uninstalled engine is running on a testbed. Installed in an aircraft often there are more or less severe pressure nonuniformities at the engine face. In some cases, for example during thrust reverser operation also the engine inlet temperature is not uniform.

The downstream compressors see besides a pressure distortion also a temperature distortion. At burner inlet there can be some swirl and a radial temperature profile of 2 to 3%. In the turbines the inlet temperature varies widely both circumferentially and radially. Mixer inlet conditions are also not uniform, nor the pressures and temperatures at nozzle inlet.

In the following the effects of flow distortion on component performance is discussed.

5.1 Compressors
It is very difficult to predict the stability limits of compressors even for clean inlet flow. Distortion obviously aggravates the problem. The lecture presented by Professor Greitzer has already introduced into the subject from a specialists point of view.

The presently most appropriate method to simulate flow distortion effects within performance synthesis programs is the parallel compressor theory. If used in conjunction with empirical corrections this can be a valuable tool for the prediction of both stability and performance with distorted inlet flow.

than the other. The distance of the points increases with increasing distortion coefficient DC_{60}.

When the operating point in the distorted sector is on the surgeline, then the basic parallel compressor theory states, that the stability limit of the compression system has been reached.

The mean operating point of the compressor with distortion is calculated as a mass average. With the shape of speed lines as shown in the figure above the distorted speed line will always give a lower mass flow and a lower pressure ratio than the undistorted speed line. This is in line with measurements. However, when the speed line is vertical - which is typical for overspeed conditions of modern low pressure compressors - then the parallel compressor model will also produce vertical speed lines. This is not in line with measurements.

5.1.2 Empirical Corrections
There are other - more important - discrepancies between the measured characteristics and the one calculated using the parallel compressor theory. Firstly, the calculated surgeline is mostly lower than the measured surgeline. Thus the model is conservative. Secondly, the calculated efficiency is overestimated in the part of the map near to the surgeline.

Fig. 16: Compressor Operating Points from Parallel Compressor Theory
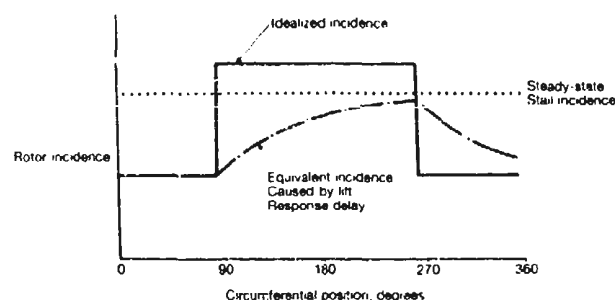
Fig. 17: Effect of Lift Response Delay on Apparent Rotor Stall [8]

5.1.1 Parallel Compressor Theory
The engine intake especially in case of a fighter aircraft produces a quite complex total pressure distribution. This distribution is described within the parallel compressor theory in a rather crude way by two streams with different, but uniform pressure. Both streams are filling a sector of the stream tube. This simplified pressure field is characterized by a distortion coefficient. For the example, that in a 60° sector there is the total pressure lower than average, the distortion coefficient is called DC_{60} and is defined as

$$DC_{60} = \frac{P_{mean} - P_{60^\circ\ sector}}{(P - P_s)_{mean}}$$

Now it is assumed, that there are two compressors working in parallel. They have both the same characteristics - the one measured on the rig for undistorted flow. One of the theoretical compressors has a flow capacity of 60°/360° = 1/6, the other one has 5/6 of the real compressor's capacity.

Further assumptions are, that there is no mass transfer between both compressors and that downstream of the compressor exit there is circumferentially a static pressure balance.
These assumptions lead to two different operating points in the characteristic (figure 16). They are on the same speed line, the operating point of the distorted sector is nearer to the surgeline

5.1.2.1 Surgeline
An explanation for the better distortion tolerance found in tests is described in [8]. There the behaviour of single stage axial compressors was studied.

What happens to the flow when the rotor periodically passes regions with low and high inlet pressure? When the rotor passes from the undistorted to the distorted sector the incidence is increased suddenly because the parallel compressor theory implies a step change in inlet flow conditions. The flow field is not able to adjust itself immediately, there is a delay in response. Figure 17 taken from [8] illustrates this.

It is known from tests with single airfoils that for a short time a much higher incidence can be tolerated than for steady state conditions. The shorter the time, the more the steady state limit can be exceeded. Transfering this observation to a compressor means: there is a dynamic surgeline which is higher than the steady state surgeline.

For a given compressor the time needed for the rotor blade to pass through the distorted sector depends only on the sector angle and speed. An empirical correction for the surgeline to be applied to the parallel compressor theory can be defined. The operating point in the distorted sector is allowed to move beyond the steady state surgeline by

$$\Delta sm = \frac{P/P_{dyn.surgeline}}{P/P_{steadystatesurgeline}} = f(sectorangle, speed)$$

As mentioned above, the theory described in [8] was developed for single stage compressors. On multistage machines the theory must be applied with care, especially if one tries to predict a surgeline shift without having any rig test evidence.

However, from analysis of rig test data from two multistage compressors (3 respectively 5 stages) - which need not necessarily be representative for other compressors - it was found, that the influence of speed was within measurement scatter. The dynamic surgeline shift varied with sector angle only as shown in figure 18.
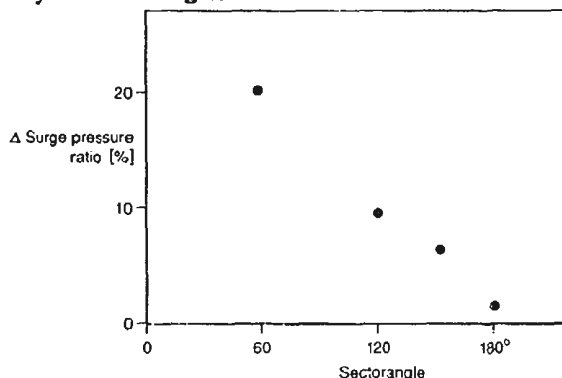
Fig. 18: Dynamic Surgeline Shift Analyzed from Rig Tests

5.1.2.2 Efficiency
As already stated, the parallel compressor model does not result in correct efficiency numbers in a region near to the surgeline, measured efficiency is lower. This phenomenon can also be correlated with dynamic exceedance of the surgeline.

From test analysis of the same compressors mentioned above it was found, that the parallel compressor model gives reasonable answers as long as the distorted sector operates in the characteristics on a point below the steady state surgeline. As soon as the steady state surgeline is dynamically exceeded, the measured efficiencies are lower than the calculated ones. That means, that the transient exceedance of the surgeline does not cause compressor surge, but it increases significantly the losses.

An empirical correction to the parallel compressor theory can bring theory in line with measurements. In the distorted sector efficiency is decremented by

$$\Delta \eta_{distortedsector} = f(sectorangle, speed)$$

To apply the modified parallel compressor theory one needs to read from the steady state characteristics data above the surgeline. That means, the map has to be extrapolated. This is rather easy when instead of efficiency specific work is extrapolated. The latter is fairly linear in a wide part of the map.

The empirical correction of surgeline and efficiency allows to better simulate the behaviour of a compressor, from which measured data both for clean and distorted inlet flow are available. Care should be taken before such empirical corrections are used for compressors which have not yet been rig tested.

5.1.3 Inlet Swirl
Long, S-shaped inlet ducts like those on the Tornado aircraft can produce at the engine face a swirling flow. One of the engines sees flow rotation in the same direction as the fan (co-

rotation), the other engine is in a more difficult situation. The counter-rotating flow effectively increases the incidence of the first rotor (the RB199 has got no inlet guide vanes) and drives the fan towards surge.

The impact of inlet swirl on the compressor characteristic and its surge line is best tested on a rig. In performance calculations several compressor maps with swirl angle as parameter can be used. An alternative is, to apply rig test derived influence coefficients to a map valid for clean intake flow.

5.2 Turbines

On a turbine rig the temperature distribution both radially and circumferentially is uniform. In the engine however the burner produces a nonuniform temperature profile.

The circumferential differences can be even bigger when the engine operates with distorted inlet flow. As mentioned above, a pressure distortion at the engine face is transformed to a temperature distortion at the burner inlet. The burner outlet temperature distribution will therefore be also affected by the distorted engine inlet flow.

5.2.1 Effect of Burner Exit Temperature Distribution
The temperature distribution at the combuster outlet can be described by the Radial Temperature Distribution Factor (RTDF) and by the Overall Temperature Distribution Factor (OTDF). Those factors are defined as

$$RTDF = \frac{T_{max,radial} - T_{mean}}{\Delta T_{Burner}}$$

$$OTDF = \frac{T_{max} - T_{mean}}{\Delta T_{Burner}}$$

While a turbine can be designed for the radial temperature profile it is not practical to design for a circumferential temperature distribution.

The circumferential temperature differences can be quite large. A value of OTDF=25% - which is not exotic for a modern gasturbine - results in circumferential temperature variations from peak to peak of up to 500K!

To estimate the effect of these temperature differences one can use a parallel turbine theory. As in case of the parallel compressor theory it is assumed, that two machines with identical characteristics are working in parallel.

At the inlet of both turbines the pressure is the same, but the inlet temperatures are different. Corrected speed is also different. How can we find the operating points in the turbine map?

Within a performance cycle calculation the total power output of the two turbines is defined by the power requirement of the compressor to be driven. Total mass flow is known also from upstream components when the parallel turbine calculation starts.

For the turbine exit conditions there are two possibilities:

o   The turbine is expanding into a duct where equal static pressure can be assumed.

o   A further turbine is following directly. Corrected turbine exit flow must be the same for both turbines operating in parallel.

In both cases the parallel turbine model gives very similar operating conditions in the turbine map, see figure 19.

With increasing OTDF the two operating conditions are moving away from each other. The mass averaged efficiency is dropping slightly (figure 20).
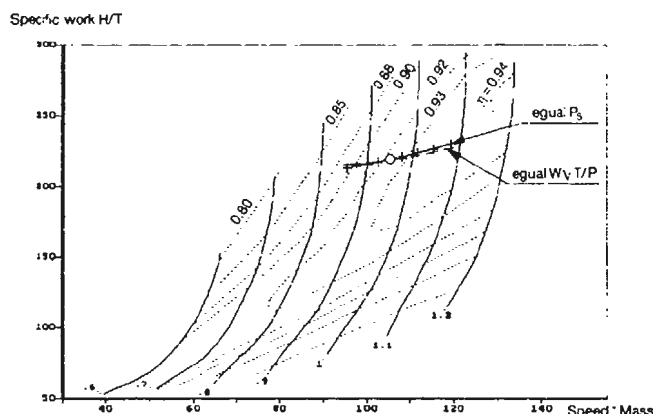
Fig. 19: Turbine Operating Points from Parallel Turbine Theory

Downstream of the turbine there is a flow angle difference between the cold and the hot sector which is proportional to the OTDF (figure 21). This effect can cause downstream of the turbine losses for example if there is an incidence sensitive exhaust guide vane.

The parallel turbine model answers also the question: what happens with OTDF while the flow is passing the turbine? In the example shown in the previous figures the difference between peak and mean temperature is approximately 10% lower at turbine exit. The relationship between $OTDF_{inlet}$ and $OTDF_{exit}$ is linear. Note however that mixing during the expansion process will reduce OTDF additionally.
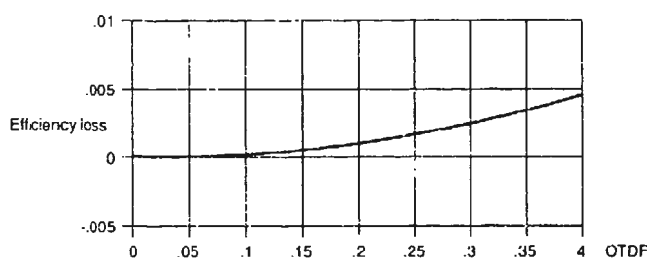
Fig. 20: Efficiency Loss Due to Inlet Temperature Distortion OTDF

5.2.2 Effect of Inlet Flow Distortion

The temperature distortion at the compressor exit caused by engine inlet pressure distortions does not exceed OTDF=2-3% even in extreme cases. Assuming a circumferentially uniform fuel distribution leads however to a nonuniform fuel-air-ratio distribution and therefore to an increased OTDF at combustor exit.

6. INTEGRATION OF COMPONENTS INTO THE PERFORMANCE SYNTHESIS PROGRAM

The preceding chapters have dealt with rig-to-engine effects for components. In the performance calculation program their characteristics and the necessary corrections for rig-to-engine

effects are combined and the overall performance is synthesized. The result of the calculation is an operating point for each component, temperatures and pressures throughout the engine, spool speeds and - last but not least - thrust and specific fuel consumption.

6.¹ Modular Performance Synthesis

How does a modern performance synthesis program work? There is in practice a quite different approach u . as compared to the one described by Professor Saravanamuttoo in the preceeding lectures. Before discussing the merits of each synthesis method let us first describe the structure of modern performance synthesis programs.

A rather comprehensive overview over the historical development of those programs in general is given in [9].
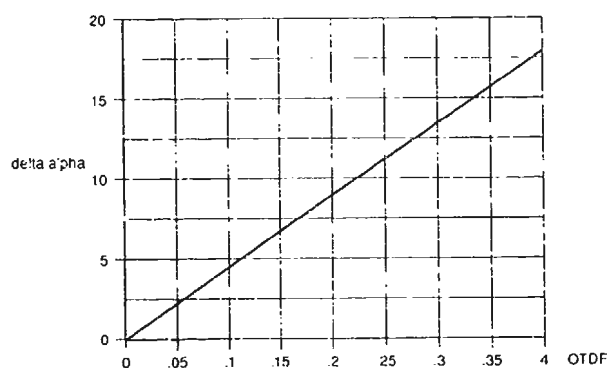
Fig. 21: Turbine Exit Flow Angle Variation Due to Inlet Temperature Distortion

6.1.1 Program Structure

6.1.1.1 The Problem

The task is, to calculate both design and off design performance for a wide variety of engine types. For each engine type one needs a specific way of calculation - you certainly remember from Professor Saravanamuttos lectures. One can attempt to write a program which can deal with a preselected number of cycles, that was done for example by NASA, see references [10] to [12] and also in the previous version of the MTU performance synthesis program.

However engineers are very inventive. There are new ideas about the best simulation of component performance as well as new cycles. In the last years for example we at MTU had to deal with performance calculations for the following engine types:

o   turbojets
o   gasgenerators
o   turbofans
             two- and three spools
             mixed and unmixed
             with and without reheat
             convergent and con/di nozzle
o   turboprops
o   propfans
             single rotating
             counter rotating
o   turboshafts
             without and with heatexchanger
o   variable cycle engines
o   ramjets
o   turbojet - turbofan - rocket combinations
o   closed cycles
o   use of alternative fuels (e.g. in hypersonic vehicles)
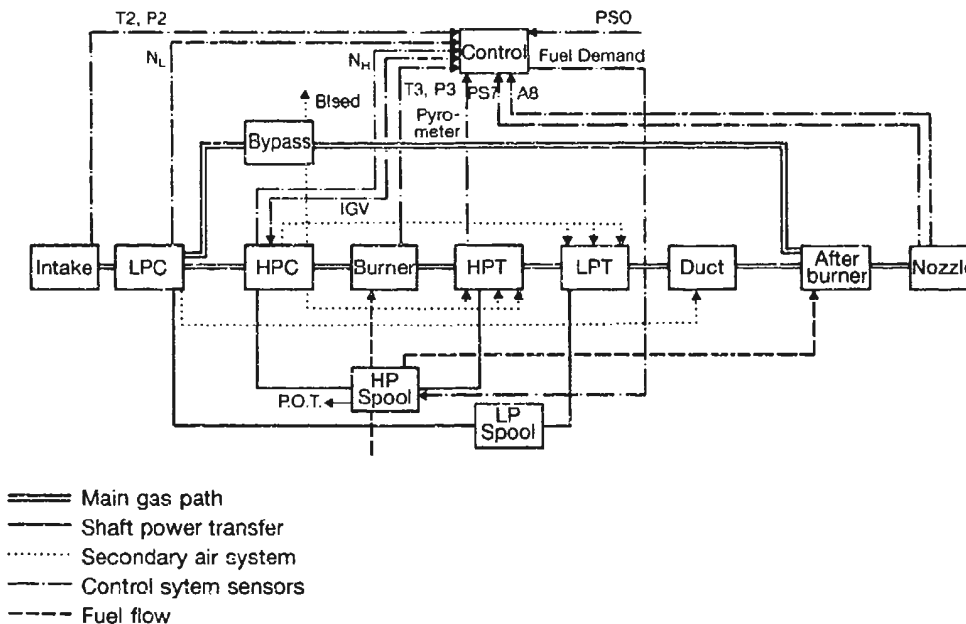
Fig. 22: Modular Performance Synthesis Structure for a Mixed Flo/Turbofan

There is no realistic chance to write a conventional program which covers all the cycles. The program logic and structure would be very complicated and any program modification would be timeconsuming and prone to errors. Note that a program is never finished in practice - with the exception of programs which are no longer in use. For performance programs the only requirement which does not change is the requirement for program changes.

6.1.1.2 Possible Solutions

There are two ways out of the dilemma: One is, to write specific programs for each type of engine. As far as possible for all of those individual programs the same set of subroutines is used. The drawback of this method is, that the modifications of the steadily increasing number of programs becomes more and more expensive.

The way chosen at MTU is the modular approach. In the MOdular Performance Synthesis program "MOPS" each engine component is represented by a program module. The user of the program selects the required modules for his cycle and writes down, how they are connected with each other. The program has some similarity with the Navy NASA Engine Program NNEP, see references [9] and [13].

There are "thermodynamic" modules which make up the main flow path through the engine. Such a module - representing for example a compressor - has standardized inlet and exit stations where mass flow, total temperature and pressure, effective area and the fluid properties like fuel-air-ratio are stored. The standardization makes sure, that all modules can be connected in arbitrary sequence.

What happens internally in a module is dependent on the module properties - in principle the input data for the module like compressor maps, Reynolds correction factors etc. The modular calculation results are also stored as properties of the module.

Besides the main gas flow there are other connections between modules. Compressors are delivering cooling air to turbines, they require shaft power and the variable guide vanes need to know from the control module, how they are positioned. Those connections between modules are also standardized and can be connected in any reasonable way.

Besides the thermodynamic modules there are others representing for example the control system or a shaft including possibly a gearbox.

A special module calculates overall engine quantities like thrust and specific fuel consumption. This module is able to read out properties from other modules - which is forbidden for other modules.

In figure 22 a graphical representation of the module connections for a mixed turbofan is shown as an example.

All modules are programmed fully independent from each other. Within the module the nomenclature can be selected fully free, conflicts with other modules are made impossible by the following data structure:

The module properties are addressed in the data input and output by their "first name" - which is identical to the FORTRAN name in the module program list - and their "second name" - a two letter combination which stands for the module. Thus for example ETA HC is the efficiency of a high pressure compressor and ETA HT is the efficiency of a high pressure turbine.

The nomenclature used within the modules follows closely the SAE rules layed down in [14]. That makes sure, that the program code is readable also for non-programmers. Having at least 50% of the program listing as comments is an additional help.

Of course there is also a user's manual for the program available. However it describes only the basic principles and gives general advice. Experiences shows, that one is never able to produce an user's manual which is up-to-date in every detail. The only program description which is 100% correct is the program listing itself.

6.1.2 Finding Valid Solutions

When all the modules are programmed individually, how are then valid engine operating points found where mass flow continuity and power balance between all components is achieved?

An iterative procedure is used and the task is dealt with as a pure mathematical problem. Let us describe the iteration necessary for the example of a simple turbojet:

Take compressor spool speed as given. The compressor operating point is then estimated by fixing a value for the auxiliary coordinate β. With given compressor inlet conditions everything within the compressor module can be calculated.

Burner inlet conditions are known now. Burner exit temperature or fuel flow is again estimated, the turbine inlet conditions are thus clear. For the turbine module the shaft power requirement is known from the compressor and the gearbox calculations. The turbine map coordinates corrected speed $N/\sqrt{T_4}$ and corrected specific work H/T_4 are now known.

From the turbine characteristics one reads efficiency and corrected flow $W_4\sqrt{T_4}/P_4$. Since both the compressor operating point and burner temperature were only estimated values the map corrected flow will not be in line with the turbine inlet corrected flow as long as the iteration has not yet converged. The deviation between both corrected flows is called an error - the "turbine flow error".

The turbine calculation is completed within the program module using the data read from the characteristic, the error mentioned above is reported to a driver routine but otherwise ignored.

In our simple example directly after the turbine a convergent nozzle shall follow. Here a second error will be detected: The turbine exit total pressure will not be the one required to pass the turbine exit flow through the nozzle. Let's call this error the "nozzle pressure error".

We have found two errors in the calculation and we have estimated two variables - compressor β and T_4. We need now an algorithm to manipulate our estimated values such, that both errors are simultaneously below a certain limit.
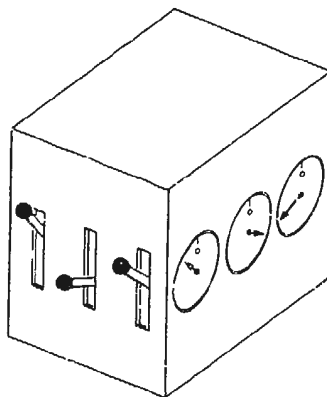
Fig. 23: A "Black Box" Model for the Iteration Procedure

How this algorithm works in detail is not important to the performance engineer. This is a purely mathematical problem. Obviously we want rapid convergence, but more important is, that the module internal calculations remain fully independent from the iteration algorithm. Only then we have the freedom to describe the physics in any way deemed necessary.

Within MOPS there is a complete isolation of the iteration algorithm from the module calculations. Any input quantity into a module can be a variable of the iteration. The corresponding errors are for standard calculations built into the modules; they can also be defined by program input.

For the mathematical algorithm the engine model (consisting of several program modules) is like a "black box". Attached to the box there is for each variable a lever. Moving a lever is equivalent to modifying a variable.

When a lever is moved, then something happens within the box. To the outside world the only visible thing is, that on instruments attached to the box one or more indicators are moving. In fact, the instruments are indicating the errors found during the calculation, see figure 23.

There is the trivial case when each lever is directly connected to one single instrument. Then it is easy to adjust the variables in the way, that all error readings are zero.

Within performance calculation programs however the situation is more difficult: changing one variable results in modified instrument readings for several errors at the same time! Remember our simple example: when the estimate for the compressor operating point is changed by modifying β then both the "turbine flow error" and the "nozzle pressure error" will change.

What is a suitable strategy for finding quickly the lever positions where all instruments are indicating zero? One way is, to move each lever independently a little bit and observe the indicators. The lever must be put back to its previous position. After all these test movements (one for each lever) one can conclude a combination of lever movements which will result in reading zero for all instruments - assuming linear relationships between lever movements and instrument readings. Since in reality the relationships are nonlinear, the instrument readings for the new lever positions will not be exactly zero, but certainly much smaller than before.

There are powerful algorithms readily available which can cope with the problem. One of those is for example described in [9]. We at MTU are using an algorithm taken from the commercially available mathematical library MINPACK and have made good experiences with it.

It is not always easy for the user of a modular performance synthesis program like MOPS to select the relevant variables and to define the corresponding errors properly. It happens, that variables are selected which don't change any of the errors. Then the mathematical algorithm has no chance to find a solution. Sometimes - for example with excessive power offtake at altitude - no solution exists. Also the existence of two solutions can confuse the algorithm.

6.1.3 Comparison with Simplified Performance Synthesis

Setting up a working iteration scheme - that is a proper selection of variables and errors - requires a physical understanding of the engine to be simulated. Here comes the point where we need the thoughts presented by Professor Saravanamutto in the preceeding lectures. The way to use a performance computer program successfully needs the understanding of the nondimensional engine behaviour.

Applying the rig-to-engine effects described in main chapter 2 gives the required accuracy of the results. Within a limited range of parameters however the engine will still behave as described by schoolbook science. If in a specific example that should not apply - check your computer result carefully!

A computer program is a tool to produce numbers, but it is not very well suited to teach physics. The user of a performance program needs to understand what he is doing - otherwise he never can be sure that the printed result is correct and not the consequence of an input error. One never can make a program foolproof, especially not a big program with an practically unlimited number of input options!

7.ENGINE INSTALLATION EFFECTS

Let us now come to some results from performance synthesis. In the following chapters those engine installation effects are dealt with, which can not be attributed to a specific component alone. Also problems of interaction between components will be discussed.

7.1 Thrust-Drag-Bookkeeping

On a testbed as used by the engine manufacturer often the thrust is measured without any power offtake and bleed. The measured value is corrected for testbed specific effects; as a result one gets uninstalled engine thrust.

Installed into an aircraft the thrust will be different for a variety of reasons. There is an intake pressure loss, at the engine face pressure is lower than ram total pressure. Shaft power is taken off to drive a generator. Bleed air is used for cabin pressurization.

Even if one corrects for all the effects mentioned - which is rather straightforward with a synthesis program matched to test data - one does not get the thrust value needed by airframers for flight performance calculations.

For those calculations a clearly defined bookkeeping of all forces acting on the aircraft is required. Forces produced by the engine must be separated from drag and lift.

This is not a trivial task because the flow field around the aircraft is affected by the engine mass flow and the nozzle exhaust conditions. With variable intakes, boundary layer bleeds etc. found on supersonic fighter aircraft the bookkeeping can be quite complicated. In the following only the two most important elements are discussed briefly: spillage drag and afterbody drag.
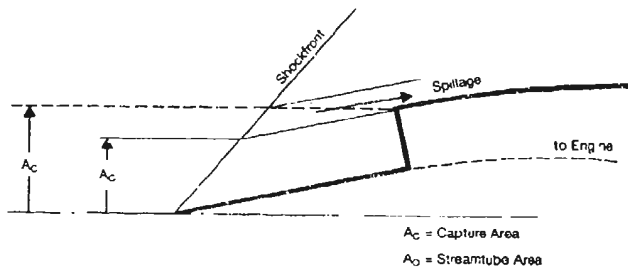
Fig. 24: Spillage Around an Intake

7.1.1 Intake Forces

One can define a reference condition where the engine mass flow is optimally matched to the intake. The streamtube of the engine air is just of the same size as the intake area, see figure 24.

When the engine is throttled back, its mass flow goes down. The approaching streamtube is now smaller than the intake area. When compared to the reference condition described above there is some air bypassing the intake. This causes the socalled "spillage drag".

7.1.2 Afterbody Forces

On a fighter aircraft with reheated engines the exhaust nozzle is variable. The external flowfield around the afterbody of the aircraft is quite different between dry and reheat operation. When the nozzle is closed the boattail angle is big and there is a danger of flow separation. Even without flow separation the drag is bigger than during reheated operation when the nozzle external fairing is of more or less cylindrical shape.

When optimizing the control laws for an engine one can get quite different results for installed and uninstalled conditions. For installed conditions the optimum SFC requires a bigger nozzle area than for uninstalled conditions. The reason for that is, that both spillage and afterbody drag are decreasing with increasing engine mass flow.

7.2 Power Offtake and Bleed Effects

7.2.1 Power Offtake

It is no problem at all to simulate the effect of power offtake within a performance synthesis program. One should however be aware, that taking off a fixed power can have quite different effects on the cycle - that depends on engine inlet conditions. Corrected power offtake is $PW/(\delta*\sqrt{\theta})$, thus for example at flight condition 50000ft/M=0.7 one can take only 14% of the power available at ISA sea level static.

Since however aircraft power demand is an approximately constant absolute power, at 50000ft/M=0.7 the corrected power offtake is 7 times as big as at sea level. Such a power offtake has a severe effect on the cycle: the operating point in the high pressure compressor is moving towards lower spool speed and in direction of the surgeline. While at sea level power offtake is limited by mechanical restrictions within the gearbox, at high altitude it is limited by the compressor stability boundary.

From this considerations it can be concluded, that for performance calculations at high altitude the power consumption of the engine gearbox and the accessories attached to it need to be better simulated than just with a constant mechanical efficiency of the high pressure spool.

Power requirements for the different fuel pumps are dependent on fuel flow and speed. Bearing and gearbox losses vary with speed, but also with oil temperature. The latter can be controlled by the thermal management system within the FADEC (=Full Authority Digital Engine Control) which switches between fuel cooled and air cooled oil coolers.
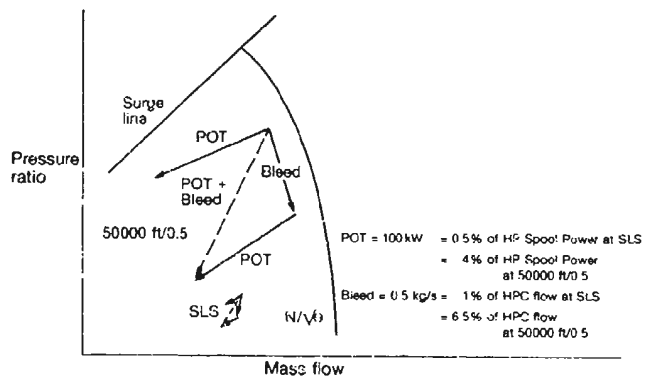
Fig. 25: Power Offtake and Bleed Effects on High Pressure Compressor Operating Points at Sea Level and at Altitude

7.2.2 Bleed Air for Aircraft Purposes

The bleed air used for aircraft cabin pressurization alleviates the compressor stability problem, but weakens the cycle. Again the bleed air requirement in terms of kg/s is fairly independent from flight conditions, the effect on the cycle is much more severe at altitude.

In figure 25 the impact of both power offtake and bleed is shown in a high pressure compressor map for sea level and

altitude. The absolute amount of bleed respectively power offtake is the same for both flight conditions.

In case the bleed air is taken not from the exit of the compressor but as an interstage bleed then for precise calculations the change of the compressor characteristic has to be modelled as already mentioned in chapter 2.1.4.

The total temperature at the offtake port can be calculated from the relative work consumed up to the relevant stage. Note that near to the wall the total temperature is higher than average and adjust the relative work accordingly! The total pressure at the bleed port can be calculated by using a somewhat lower polytropic efficiency than that of the main stream.

Bleed air pressure and temperature are important for the aircraft designers. There are both maximum and minimum limits for the pressure and sometimes there is also a not-to-exceed bleed air temperature. On modern civil engines it can be necessary, to have two customer bleed air offtakes which are switchable: at idle compressor exit bleed is used, at max climb rating an interstage bleed port.

Bleed air conditions at aircraft/engine interface have to be calculated with sufficient care. The local pressure - where the air is taken off - is dependent on the specific design, it is seldom the total pressure. The pressure losses within the bleed manifold and pipe system are very much mass flow dependent.

Temperature calculation for the bleed air has also to start at the offtake position. There is some mass flow dependent temperature change when the bleed air pipe is cooled by the bypass air flow.

7.3 Intake Losses and Flow Distribution

7.3.1 Pressure Losses
Total pressure losses of an intake with fixed geometry are dependent on flight Mach number, corrected airflow, angle of attack, angle of sideslip and Reynolds number. In case of intakes with variable geometry of course the position of the ramps and boundary layer bleeds have to be taken into account.

Extensive test series are required to find out the loss characteristics and the optimum control laws for the variable geometry of an intake. This is done by the airframers. Within the engine companies often only the most important parameters - which are Mach number and corrected flow - are simulated.

When the aircraft intake is operated near to its maximum flow capacity then it produces high intake pressure losses and at the same time severe flow distortion.

7.3.2 Flow Distribution
While it is rather straightforward to calculate the effect of mean intake total pressure loss on engine performance this is not the case for maldistributed flow.

The most simple case is a pure radial pressure distribution. For bypass engines one takes then just different inlet pressures for both streams. For such engines different characteristics for inner and outer flow are used anyway.

For a description of a pure circumferential pressure distribution the distortion coefficient can be used. The empirically corrected parallel compressor model is suited to do the performance calculations.

Pure bulk swirl effects can be taken into account by use of several fan characteristics and interpolating between them over swirl angle.

The prediction of the effect of a real distorted inlet flow with both radial and circumferential pressure distribution - combined with bulk swirl and possibly a component of twin swirl - cannot be handled within a performance program. This needs compressor characteristics derived from rig test experience.

May be one can find a simplified description of the measured stability, but the prediction of engine behaviour in case of complex flow distortion is very difficult.

7.4 Effect of Inlet Flow Distortion on Stability and Performance
It is advantageous to include a simple distortion calculation model into the performance synthesis program. This allows to find out critical operation conditions for a specific aircraft / engine combination. The distortion level is a complex function of aircraft flight condition (Mach number, angles of attack and sideslip) and engine corrected flow.

The most critical point within the operating envelope can be at high altitude, low Mach number with moderate flow distortion, heavy power offtake and no bleed. It can however also be at low altitude, with heavy flow distortion due to high aircraft angles of attack and sideslip and fast acceleration of the engine up to high corrected speeds.

7.4.1 Parallel Compressor Model Integrated into the Performance Synthesis Program
In the component chapter it was shown, that one can model both stability limit and efficiency level of a compressor with distorted inlet flow. There is no problem to integrate the empirically corrected parallel compressor theory into the performance synthesis.

7.4.1.1 Interaction Effects between Components
In the engine however there are phenomena which were not yet discussed. The parallel compressor theory uses the assumption, that there is static pressure balance downstream of the compressor. This assumption is not justified in case of the inner fan flow of bypass engines. The struts in the intermediate casing will prevent the adjustment of the streamlines which is necessary for static pressure balance.

The phenomenon is called spool coupling. A theory which describes it is presented in reference [15]. A subroutine based on this reference was written by our specialists for unsteady aerodynamics and is used in the MTU synthesis program for the description of spool coupling effects.

There can be also another spool coupling effect in an engine. On the early RB199 engine it happened, that when the fan was operated on a high running line (but still below the surge line) it caused the high pressure compressor (HPC) to surge. The HPC surged in spite of the fact, that its operating line was well below the rig measured surge line.

The full explanation for that is reported in reference [16]. Basically the fan had local flow detachment in the hub region at its exit and this caused a severe flow distortion for the intermediate compressor - which could cope with it. The HPC however could not tolerate the distortion and surged.

While an effect like the one just described can hardly be predicted there is another interaction effect between compressors which is automatically handled by the parallel compressor model when integrated into the synthesis program. The inlet pressure distortion is transfered by the fan into an inlet temperature distortion for the high pressure compressor. Thus at the inlet of the HPC each sector has its own inlet temperature and pressure. In the characteristic the two operating points are no longer on the same speedline as in case of the fan.

The effect of inlet temperature distortion is discussed in reference [17], there also experimental results are included.

7.4.1.2 Iteration Scheme for a Bypass Engine with Circumferential Inlet Flow Distortion
In chapter 6.1.2 the very simple iteration scheme applicable to a turbojet was discussed. Now a more complex example is

dealt with: a mixed flow turbofan with inlet distortion operated at max dry rating.

Max dry rating is an ambiguous definition: dependent on flight condition, power offtake and bleed it can be a maximum N_L, $N_L/\sqrt{\theta}$, N_H, $N_H/\sqrt{\theta}$, P_3, T_3 or a turbine temperature limiter. When starting the calculation one does not know, which of the various limiters will be active. Therefore both spool speeds have to be estimated at the beginning of the iteration, they are the first two variables in the iteration scheme.

Due to the distorted inlet flow there are two operating points to be found in the fan characteristics. That means, that we have to estimate two values for the auxiliary coordinate β. Also for the high pressure compressor there are two β's to be estimated.

We need further to estimate bypass ratios for both the spoiled sector and the unspoiled sector and the fuel flow.

Now we have estimated alltogether 9 variables. There must be exactly 9 conditions (prior convergence: errors) taken into account during the calculation. Those are:

1. circumferential static pressure balance in the bypass channel
2. circumferential static pressure balance in the combustion chamber
3. high pressure compressor flow must be in line with map value (unspoiled sector)
4. high pressure compressor flow must be in line with map value (spoiled sector)
5. high pressure turbine flow must be in line with map value
6. low pressure turbine flow must be in line with map value
7. static pressure balance between core and bypass stream at bypass exit
8. nozzle total pressure must be in line with the required one to pass the flow through the given area.
9. the engine shall run at max dry rating

The last condition is a special one: there are deviations from all limiters to be calculated. The errors have to be defined such, that a limiter exceedance is expressed as a *positive* error. Then all deviations from the limiter settings are checked and the biggest one is introduced in the iteration scheme.

It may happen, that during the iteration the active limiter switches from for example N_L to a turbine temperature limit. But that is no problem for the mathematical routine which drives the 9 variables towards the solution. After convergence one of the limiter errors is just 0 - that is the active limiter. All the other errors are smaller, no other limiter is violated.

Normally it takes between 15 and 25 passes through all module calculations until convergence is achieved. For our present model of the EJ200 engine that means approximately 1 CPU second on our IBM NAS/EX100 mainframe computer.

8. FLIGHT PERFORMANCE CALCULATION

Who uses performance computer programs and for which purpose?

Engine manufacturers are mainly interested in the operating conditions of the engine components. During development it has also to be found out, which component is responsible for performance shortfalls and how the components are matched together in the best way.

Aircraft manufacturers are interested in the aircraft performance in terms of achievable turn rates, specific excess power, mission fuel consumption and so on. For that purpose they need programs (also called computer decks) which calculate installed engine performance.

There are detailed requirements for such programs laid down in reference [18]. In principle a foolproof program is requested:

for any input a reasonable answer should be given. To produce such a computer deck is quite challenging.

The computer decks produced at MTU are specific versions of our standard synthesis program MOPS. All the description of the physics is exactly the same for both versions, only input and output routines are different. By this approach we accumulate a lot of experience with the program for a specific engine model during our daily work. We see it as the best way to produce as reliable customer decks as possible.

In spite of all the success we had in the past with the computer decks for various military and civil engine projects we are quite aware, that one can neither produce an absolute faultfree nor a real foolproof program: Fools are just too inventive!

References:

[1] Hourmouziadis, J. and Albrecht, G.
An Integrated Aero/Mechanical Performance Approach to High Technology Turbine Design
AGARD CP 421
May 1987

[2] Grey, R.E. and Wilsted, H.D.
Performance of Conical Jet Nozzles in Terms of Flow and Velocity Coefficients
NACA Technical Note No. 1757, 1948

[3] Wehofer, S. and Matz, R.J.
Turbine Engine Exhaust Nozzle Performance
AIAA Paper 73-1303, 1973

[4] Groothoff, C.C.
Influence of Jet Parameters: Nozzle Thrust and Discharge Coefficients
in: AGARDograph No. 208, 1974

[5] L'Ecuyer, M.R. Morrison, J.J and Mallett, W.E.
Correlation of Turbofan Engine Thrust Performance with Compound Nozzle Flow Theory
Journal of Aircraft July 1971

[6] Wassell, A.B.
Reynolds Number Effects in Axial Compressors
Jounal of Engineering for Power
April 1968

[7] Schäffler, A.
Experimental and Analytical Investigation of the Effects of Reynolds Number and Blade Surface Roughness on Multistage Axial Flow Compressors
ASME Paper 79-GT-2, 1979

[8] Korn, J.A.
Estimated Effect of Circumferential Distortion on Axial Compressor Using Parallel Compressor Theory and Dynamic Stall Delay
AIAA Paper No. 74-233

[9] Fishbach, L.H.
Computer Simulation of Engine Systems
NASA TM 79290 1980

[10] Koenig, R.W. and Fishbach, L.H.
GENENG - A Program for Calculating Design and Off-Design Performance for Turbojet and Turbofan Engines
NASA TN D-6552, 1972

[11]   Fishbach, L.H. and Koenig, R.W.
        GENENG II - A Program for Calculating Design and
        Off-Design Performance of Two- and Three-Spool
        Turbofans with as Many as Three Nozzles
        NASA TN D-6553, 1972

[12]   Sellers, J.F. and Daniele, C.J.
        DYNGEN - A Program for Calculating Steady State
        and Transient Performance of Turbojet and Turbofan
        Engines
        NASA TN D-7901, 1975

[13]   Fishbach, L.H. and Gordon,S.
        NNEPEQ - Chemical Equilibrium Version of the
        Navy/NASA Engine Program
        ASME Paper 88-GT-314 1988

[14]   Anonym
        Gas   Turbine   Engine   Performance   Station
        Identification and Nomenclature
        Aerospace Recommended Practice ARP755A
        Society of Automotive Engineers, Inc. 1974

[15]   Ham, C.J. and Williams, D.D.
        Some Applications of Actuator and Semi-Actuator
        Disk Theory to the Problem of Intake/Engine
        Compatibility
        Tokyo International Gas Turbine Congress 1983
        Paper 83-TOKYO-IGTC-50

[16]   Schäffler, A. and Miatt, D.C.
        Experimental Evaluation of Heavy Fan-High-Pressure
        Compressor Interaction in a Three-Shaft Engine:
        Part I - Experimental Setup and Results
        Part II - Analysis of Distortion and Fan Loading
        ASME Papers 85-GT-173 and 85-GT-222, 1985

[17]   Biesiadny, T.J. et alii
        Summary of Investigations of Engine Response to
        Distorted Inlet Conditions
        NASA TM 87317, 1986

[18]   Anonym
        Gas Turbine Engine Steady State Performance
        Presentation for Digital Computer Programs
        Aerospace Standard AS681E
        Society of Automotive Engineers, Inc. 1982

DYNAMIC CONTROL OF AERODYNAMIC INSTABILITIES
IN GAS TURBINE ENGINES

E. M. Greitzer, A. H. Epstein, G. R. Guenette, D. L. Gysling, J. Haynes,
G. J. Hendricks, J. Paduano, J. S. Simon, L. Valavani

Gas Turbine Laboratory, Massachusetts Institute of Technology
Cambridge, Massachusetts, 02139 USA

AD-P007 897

ABSTRACT

This lecture discusses the use of closed loop control at
the component level to enhance the performance of gas
turbine engines. The general theme is the suppression of
flow instabilities (rotating stall and surge) through use of
feedback, either actively or by means of the aerome-
chanical coupling provided by tailored structures. The
basic concepts that underlie active control of turboma-
chinery instability, and their experimental demonstra-
tion, are first described for a centrifugal compressor. It
is shown that the mechanism for stabilization is associat-
ed with damping of unsteady perturbations in the com-
pression system, and the steady-state performance can
thus remain virtually unaltered. Control of instability
using a tailored structure is then discussed, along with
experimental results illustrating the flow range extension
achievable using this technique. A considerably more
complex problem is presented by active control of rotat-
ing stall where the multi-dimensional features mean that
distributed sensing and actuation are required. In addi-
tion, there are basic questions concerning unsteady fluid
mechanics; these imply the need to resolve issues con-
nected with identification of suitable signals as well as
with definition of appropriate wave launchers for imple-
menting the feedback. These issues are discussed and
the results of initial successful demonstrations of active
control of rotating stall in a single-stage and a three-
stage axial compressor are presented. The lecture con-
cludes with suggestions for future research on dynamic
control of gas turbine engines.

NOMENCLATURE

a	speed of sound
A	area
$\hat{A}_T$	non-dimensional throttle area
B	dimensionless ratio of compliance to inertia $\left(= (U/2a)\sqrt{V_p/L_cA_c}\right)$
C_x	axial velocity
L_c	equivalent compressor length

m	mass of moveable plenum wall
M	Mach number
Q	frequency ratio (Eq. (6))
s	complex variable
T	throttle characteristic
U	rotor tip speed
V	plenum volume
W	aeroelastic coupling parameter (Eq. (5))
Z	proportional feedback gain
$\delta(\ )$	perturbation quantity
α	disturbance growth rate ($e^{\alpha t}$)
ζ	damping ratio
ρ	density
τ	dimensionless time
ϕ	flow coefficient (= C_x/U)
ψ	pressure coefficient
ω	frequency

Subscripts

c	compressor
p	plenum
o	ambient conditions
H	Helmholtz frequency
n	n^{th} spatial mode
T	throttle

1. INTRODUCTION

The continuing microelectronic revolution opens new
doors to the designer of fluid and mechanical systems
who can now consider replacing basically open-loop
devices with ones employing integrated electronic feed-
back control at relatively low cost. This engineering
approach is fundamentally different from the traditional
one that emphasized simplicity, but the potential for
increased performance, functionality, maintainability,
and lowered development costs has made integrated
control machines attractive in a number of applications.
Many of these are flight critical in the sense that mal-
function of the control system could result in loss of the
vehicle, requiring extreme confidence in the control sys-
tem.

The application described here is the use of integrated feedback control to improve the performance of pumps and compressors by increasing the stability of the machine through suppression of surge and rotating stall. These aerodynamic instabilities are intrinsic to a wide variety of turbomachines, and often stand as absolute limits to their performance. Increased stability gives potential for increases in machine performance, operating range and pressure rise.

Because of its importance, stall and surge control have been under investigation for a number of years. The schemes investigated, however, relied on finite movements lowering the operating point, so that the nominal surge line was not crossed. The present approach is fundamentally different in that:

a)   it is aimed at suppressing the instabilities through active control, allowing stable compressor operation in a previously unstable (and thus forbidden), high-performance region, and

b)   it operates on small amplitude disturbances, thus requiring relatively little control power.

The approach is illustrated conceptually on the compressor map shown in Fig. 1. Point A represents a conventional operating point without control and point B a new operating point in the region (shaded) stabilized by active flowfield control past the "natural" stall line.

In this lecture, we discuss strategies for using the type of approach described to control a broad class of turbomachinery instabilities. Rotating stall is one such example, in which small disturbances evolve into a finite amplitude limit cycle, where the strength of this "rotating stall cell" is set by nonlinear effects [1]. Surge, which is a more global system instability, is another example [2], [3].

The basic ideas underlying active control of turbomachinery instability are presented in the next section with reference to a particular situation: surge control in centrifugal compressors. It is shown that the mechanism for stabilization is associated with the damping of unsteady perturbations in the compression system, and that the stabilization process may leave the steady-state performance virtually unaltered. The control of instability using a tailored structure as the feedback mechanism is then discussed. Following this, an evaluation is carried out of a number of possible schemes for practical application.

A more complex implementation problem is presented by the control of rotating stall which is a multi-dimensional (rather than one-dimensional) instability, so that distributed sensing and actuation are required. Basic questions arise concerning the fluid mechanics of the unsteady disturbances, the identification of suitable sig-

nals, and the definition of appropriate wave launchers for implementing the feedback. These issues are discussed and experimental results concerning the active control of rotating stall in a single-stage and a three-stage axial compressor are presented. The lecture concludes with suggestions concerning unanswered questions and areas of future research on dynamic control of gas turbine engines.

Two points can be remarked on at the outset. First, the field of active control of complex fluid systems is new and rapidly evolving, and the present document is thus very much a snapshot of this evolution rather than a retrospective survey of a mature area. Second, although the lecture predominantly describes work conducted at MIT, care is taken to point out those areas in which there are either alternative approaches to the problem or where differences in interpretation and/or philosophy occur.

2. ACTIVE CONTROL OF COMPRESSOR SURGE

It is useful to introduce the ideas in a specific context, namely control of compression system surge. The basic model developed for this situation provides an instructive example for discussing the different aspects of the problem. There has been much work carried out on what is termed surge control, and discussions of different available techniques have been given by Boyce et al. [4], Ludwig and Nenni [5], and Staroselsky and Ladin [6]. The approach here is fundamentally different because it is based on effecting changes in the unsteady system response, i.e., the system dynamics, rather than the steady-state behavior. More specifically, existing surge control schemes act by effectively lowering the
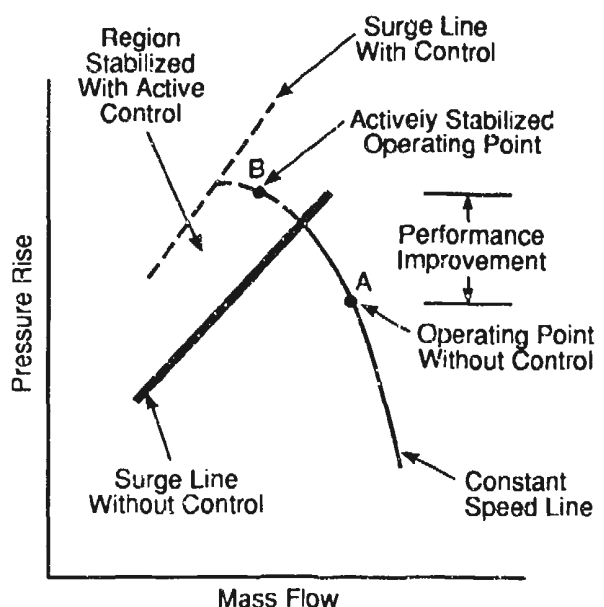
Fig. 1:   The intent of active compressor stabilization is to move the surge line to lower mass flow.

operating line once some steady-state, near-surge operating condition is reached or detected. In contrast, the present approach uses active control to enhance the stability of the compression system, effectively moving the surge line.

The conceptual basis for the active control scheme is that the nonlinear limit cycle oscillations characterizing surge start as small amplitude disturbances. We monitor these disturbances and feed back a signal derived from them into an actuator or actuators. The combination of compressor, sensors, processors, and actuators (i.e., of compressor plus controller) constitutes a new machine with different stability properties from the compressor alone; these can be exploited to enhance the stable flow range.

2.1 System Modeling

Lumped parameter system models have been used by many authors to examine instability inception in both axial and centrifugal compression systems, e.g., Emmons et al. [7], Greitzer [8], and Ffowcs Williams and Huang [9], and there is no need to enter into a detailed description here.

The basic system representation is shown in Fig. 2a, and incorporates the following assumptions: one-dimensional, incompressible flow in the compressor duct; compressor considered as a quasi-steady actuator disk; plenum pressure is spatially uniform but varying in time and flow velocity is negligible; throttle behavior is quasi-steady.

We are interested in the question of whether small perturbations will grow or decay. A linearized description of the departures from an arbitrary equilibrium point can thus be adopted, with all quantities expressed in a Taylor series about this equilibrium point (e.g., Greitzer [8]). Carrying out this step and writing the resulting equations in non-dimensional form, the temporal (τ) behavior of the *perturbations* in non-dimensional plenum pressure rise ($\delta\psi$) and non-dimensional mass flow (or flow coefficient) ($\delta\phi$) can then be described as:

$$\frac{d\delta\phi}{d\tau} = B\left[\left(\frac{d\psi_c}{d\phi}\right)\delta\phi - \delta\psi\right] \tag{1a}$$

$$\frac{d\delta\psi}{d\tau} = \frac{1}{B}\left[\delta\phi - \frac{1}{\left(\frac{dT}{d\phi}\right)}\delta\psi\right] \tag{1b}$$

for the system without active control. Equation (1a) expresses a one-dimensional momentum balance in the compressor duct where the quantity ($d\psi_c/d\phi$) is the slope of the compressor characteristic, evaluated at the equilibrium operating point. Equation (1b) represents a mass balance for the plenum with the term ($dT/d\phi$) representing the slope of the throttle pressure-drop characteristic. [The compressor characteristic, ψ_c, gives the non-
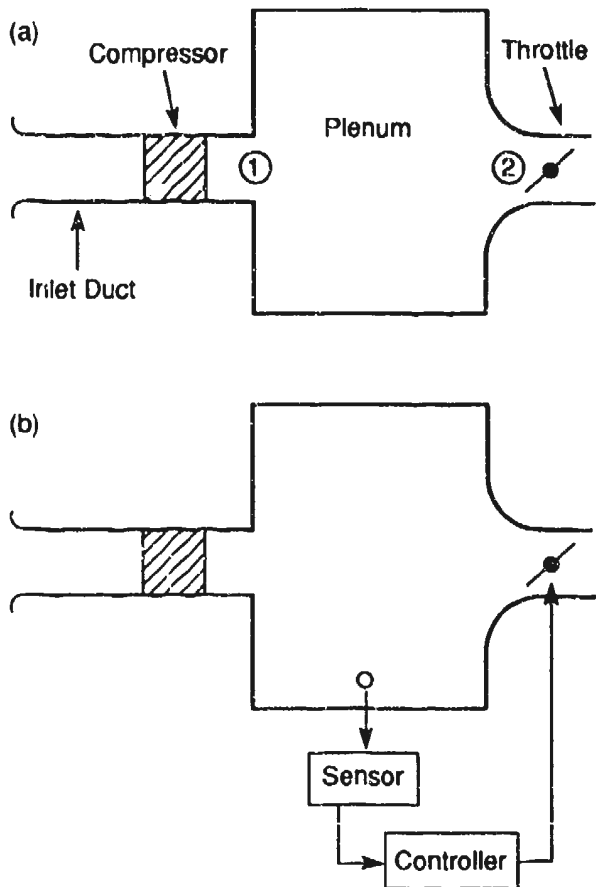
Fig. 2: Lumped parameter compression system: (a) no control; (b) controlled system with sensor in plenum and throttle actuator.

dimensional compressor pressure rise as a function of the flow coefficient, ϕ, and the throttle characteristic, T, represents the throttle pressure drop.] The non-dimensional quantity B, defined as $(U/2a)\sqrt{V_p/L_cA_c}$, which can be regarded as a measure of the ratio of plenum compliance to duct inertia, is of considerable importance in determining control effectiveness.

2.2 Feedback Stabilization

For feedback stabilization, one measures the system output, compares it with some desired reference level, determines the error and computes an input signal (command to some actuator) based on this error to drive the error to zero. If this can be successfully accomplished, the system output will be maintained close to the desired value which normally implies that the system is stable. The relationship between the system error signal and the actuator command is called the control law, and may be dynamic (involving differential equations) or static (involving only algebraic relationships). In this section we will use the simplest control law, a proportional relation between input and output, subsequent sections will discuss the impact of the form of the control law.

To describe an actively controlled system, we must therefore account for the influence of actuators on system performance, represent sensor measurements, and incorporate a feedback law. Each choice of sensor-actuator pair, when coupled to the control law, results in a distinct dynamical system. We illustrate the derivation of the characteristic equation for one particular system only and present results for the other systems.

Suppose a pressure probe in the plenum is used as the sensor and a valve which modulates the throttle area is selected for the actuator (as indicated in Fig. 2b). The equations that describe the dynamics of the system are now (1a) plus

$$\frac{d\delta\psi}{dt} = \frac{\delta\phi}{B} - \frac{1}{B\left(\frac{T}{\phi}\right)_{\widehat{A}_T}}\delta\psi + \frac{\left(\frac{T}{\widehat{A}_T}\right)_\phi}{B\left(\frac{T}{\phi}\right)_{\widehat{A}_T}}\delta A_T \quad (2)$$

$\widehat{A}_T$ is a non-dimensional control valve area, and $(\partial T/\partial \widehat{A}_T)_\phi$ is the derivative of the characteristic curve of valve pressure rise versus valve area. Comparison with Eq. (1b) shows that the original system has been modified by the introduction of the control term which involves $\delta\widehat{A}_T$ in Eq. (2).

Equations (1a) and (2) do not yet define the system dynamic behavior because the relation between the throttle area perturbation is not linked to the pressure rise or mass flow perturbations. Specifying this relation defines the throttle control law. In this initial discussion, we take the relation to be the simple proportionality, expressed in Eq. (3):

$$\frac{\delta\widehat{A}_T}{\widehat{A}_T} = Z\,\delta\psi \quad (3)$$

where Z is constant, relating sensed pressure perturbations and instantaneous valve area. Inserting Eq. (3) into the system Eqs. (1a) and (2) produces two coupled equations for $\delta\phi$ and $\delta\psi$, with solutions of the form e^{st}. The characteristic equation for s is given by:

$$s^2 + s\left[\frac{1}{B}\left(\frac{1-\left(\frac{T}{\widehat{A}_T}\right)_\phi \widehat{A}_T Z}{\left(\frac{T}{\phi}\right)_{\widehat{A}_T}}\right) - B\left(\frac{d\psi_c}{d\phi}\right)\right]$$

$$+ \left[1 - \frac{\left(\frac{d\psi_c}{d\phi}\right)}{\left(\frac{T}{\phi}\right)_{\widehat{A}_T}}\left(1 - \left(\frac{T}{\widehat{A}_T}\right)_\phi \widehat{A}_T Z\right)\right] = 0$$

$$(4)$$

Equation (4) is the equation of a damped harmonic oscillator, with the damping positive or negative depending on compressor operating point. The primary role of the active control is to modify the damping term (note the presence of the parameter Z) in the equation, increasing the stability of the oscillatory system.

2.3 Some Results From System Modelling Studies.
From the system model one can extract several general trends pertaining to the control scheme described so far. For this scheme, the control effectiveness decreases as either or both the B-parameter and the slope of the compressor characteristic increase, as illustrated in Fig. 3. The figure shows the value of gain (Z) needed to stabilize a compressor operating with given compressor slope, as a function of B-parameter. As described in the paper by Pinsley et al. [10], which gives a physical argument for this limitation, the maximum slope of compressor characteristic at which stabilization can be achieved is equal to 1/B.

The reason for the decreased effectiveness with increase in B-parameter is connected to the overall decrease in stability that occurs as B increases. This is well known, and has been amply discussed in the literature (e.g., Greitzer [8]). Larger B implies a more compliant system, which means that the unsteady flow through the throttle is less coupled to the unsteady flow through the compressor. Control strategies using a downstream throttle would therefore be expected to lose effectiveness. We return to this point when we discuss evaluation of the strategies for practical situations.

2.4 Initial Experiments on Surge Control
Based on the analytical results, experiments were carried out using a small centrifugal turbocharger (Holset 1D).
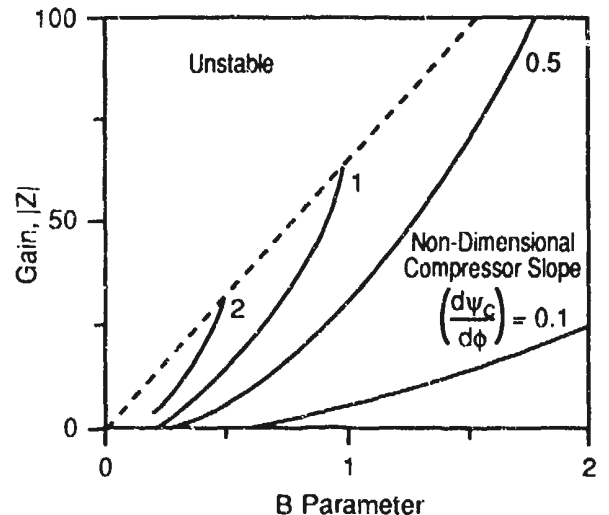
Fig. 3: Gain required to stabilize the compression system increases with increasing B and compressor slope ($d\psi_c/d\phi$).
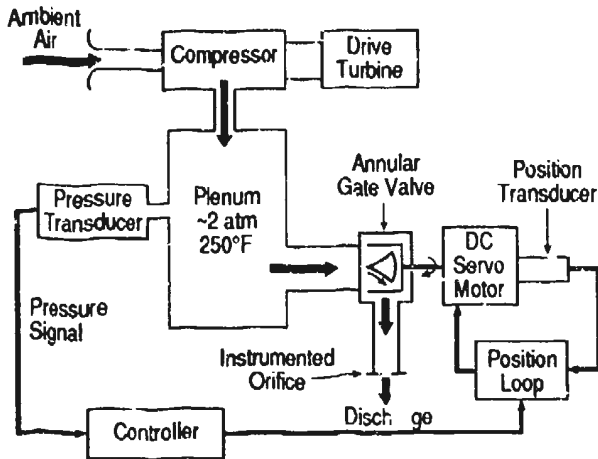
Fig. 4:   Experimental setup of actively stabilized cen-
          trifugal compressor [10].

Fig. 5:   Speedline indicating time mean operating
          points with and without control [10].

Impeller tip diameter at outlet was 5.5 cm, with the max-
imum compressor speed investigated 110K rpm. A
schematic of the facility is shown in Fig. 4; more detail
is given by Pinsley et al. [10].

The exit throttle was a rotary gate valve mounted at the
plenum exit. Valve opening was set by rotating a ported
inner sleeve relative to outer stationary ports, and valve
angular position was measured with a rotary variable
differential transformer angular displacement transducer.
The control valve was actuated by a low inertia D.C. ser-
vomotor. Inertias of the motor and valve rotors were
kept small to maximize frequency response, which was
flat to 80 Hz.

The most basic task of the controller is to shift the surge
onset point to lower mass flow. This behavior is shown
in Fig. 5 for a speedline at 90K rpm. There is roughly a
25% change in the instability onset flow. Also, the time
mean pressure rise in surge (the open squares) is roughly
20% lower than the controlled values at the same mass
flow.

Investigations were carried out over a range of speeds
and B-parameters and the overall conclusions can be
summarized as follows: The active control stabilized the
system at flows below the natural surge point, the com-
pressor pressure rise in controlled operation remained
near the pre-surge level, the control effectiveness
decreased as B increases, and the position of the surge
line "knee" was a function of B.

Time-resolved measurements were also conducted to
examine the perturbations prior to and during large
amplitude surge. The pressure fluctuations along the
90K speedline with and without control are shown in
Fig. 6. The letters correspond to the points marked on
the time mean characteristic in Fig. 5. The suppression
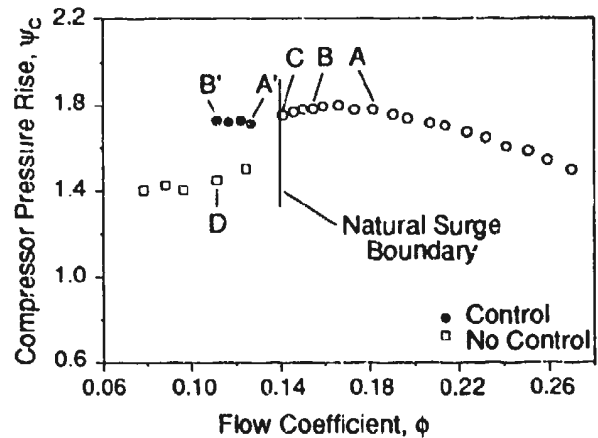
of the oscillations when the control is applied is evident.
An alternative way to view the effect of control on pres-
sure fluctuations in the system is to examine the peak
amplitudes as a function of flow. This is shown in Fig.
7. With control, the amplitude is suppressed at flow
coefficients below the natural surge value to a level
below that of mild surge. Even when surge can no
longer be avoided, the peak amplitude of the fluctuations
remains lower than the level without control.

The transient behavior of the system when the control is
turned on or off is also of interest as a measure of con-
trol effectiveness. Figure 8 shows non-dimensional
fluctuations in valve area and plenum pressure, as well
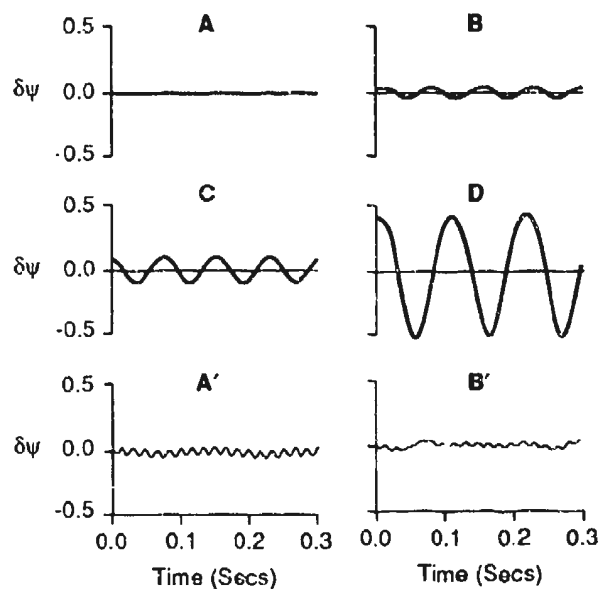
Fig. 6:   Time-resolved compressor performance without
          control at points A-D and A', B', as indicated in
          Fig. 5 [10].
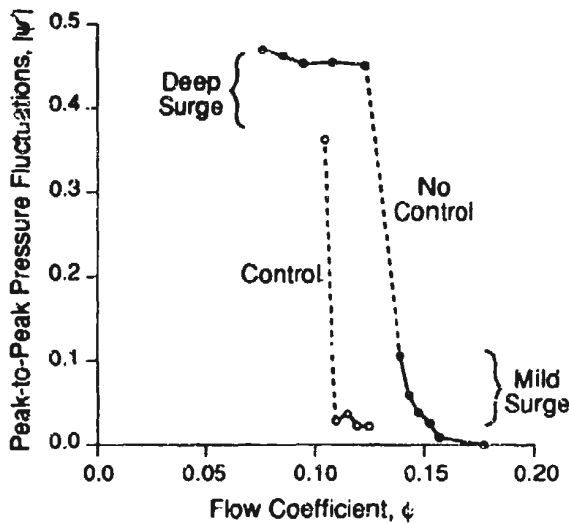
Fig. 7: Reduction in amplitude of peak pressure fluctuations with feedback control; mild surge and deep surge [10].

Fig. 8: Transient behavior of system initially in deep surge during controller turn-on [10].

...ariations in compressor mass flow during a transient ...om deep surge with the controller off, to stable operation with the controller on. (This figure can be compared with Fig. 15 of Ref. [9].) In the figure, time is given in dimensional form to show the actual temporal characteristics of the valve action. At t = 1.03 seconds, the controller is switched on at a previously set controller gain and phase. The controller captures the surge fluctuations within one to two surge cycle periods, even though the system is operating in a highly nonlinear regime. Although implementation of the controller shifted the time-averaged operating point along a constant throttle line, the stabilized operating point remained within the flow range where surge was encountered with no control.

2.5 Summary of Initial Investigation of Active Control
The experiments reported demonstrate that active control can be an effective means of suppression of centrifugal compressor surge. We emphasize that the strategy described is by no means optimal and other strategies are examined in Section 4. The results presented subsequently also point up the dependence on sensor and actuator position, which are issues that must be taken into account when deciding methods of practical implementation.

3. DYNAMIC SURGE CONTROL USING TAILORED STRUCTURES

Another new approach to stabilization is via the use of tailored structural properties, i.e., modifying the dynamic response through aeromechanical interaction so that the system stability is increased. Such an approach was investigated by Gysling et al. [11], who used a movable

plenum wall as a mass-spring-damper system, driven by unsteady pressure perturbations in the plenum. A sketch of the overall configuration is shown in Fig. 9. The aeroelastic coupling (between the wall and the compression system) allowed the damper on the moving wall to dissipate mechanical energy associated with flow disturbances, thereby suppressing surge.

3.1 Non-dimensional Parameters
The detailed analysis is presented by Gysling et al. [11]. The degree of suppression depends on matching the structural and system fluid dynamics and there are four non-dimensional parameters, in addition to B, that feature in this interaction.
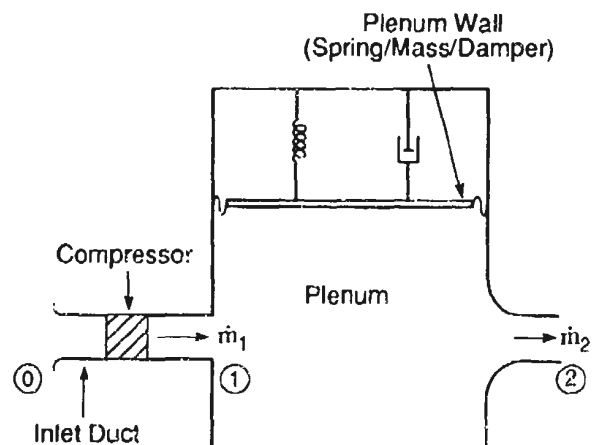
Fig. 9: Schematic of moveable plenum wall compression system [11].

The *tip Mach number* (based on plenum conditions) is defined as:

$$\text{Tip Mach number} = U/a_{plenum}. \qquad (5)$$

The tip Mach number enters as a measure of the effect of wall motion on the mass balance in the plenum. (It does not appear explicitly for a fixed wall configuration.) The pressure and mass flow fluctuations are functions of tip Mach number (they scale as M^2 at low speed), but the wall motion is not. In this problem the Mach number is a measure of the aerodynamic - structural coupling, rather than a representation of the importance of compressibility.

The parameters W, ζ, and Q determine the wall dynamic characteristics relative to the unsteady behavior of the basic (rigid wall) compression system. *W is an aeroelastic coupling parameter* defined as

$$W = \frac{\rho_0 A_p^2 L_c^2}{m V_p} \qquad (6)$$

This parameter determines the degree to which the wall responds to pressure fluctuations in the plenum. Increasing W implies a greater wall response.

ζ is the *critical damping ratio* of the plenum wall mass-spring-damper system, corrected to remain independent of compressor operating conditions, and is defined as

$$\zeta = \frac{c}{2m\,\omega_p}\sqrt{\frac{\rho_p}{\rho_0}} \qquad (7)$$

Q defines the *ratio of natural frequencies* for the wall mass-spring-damper system and for the fixed wall compression system (the Helmholtz frequency), also corrected to be independent of compressor operating point.
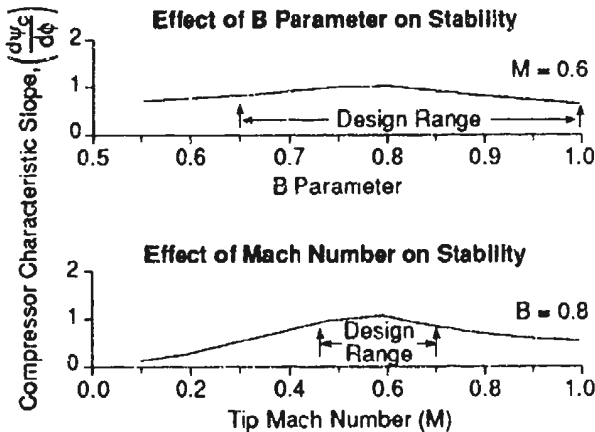
$$Q = \frac{\omega_p}{\omega_H}\sqrt{\frac{\rho_p}{\rho_0}} \qquad (8)$$

3.2 Summary of Model Results for Dynamic Structural Control

Linear and nonlinear computation of the system dynamics have been carried out and are reported by Gysling et al. [11]. Two representative calculations are shown in Fig. 10 which presents the maximum stable compressor slope that can be achieved as a function of B-parameter and Mach number. The important result is that the peak is not a sharp one, and the scheme should work over a range of conditions, i.e. it need not be re-tuned for each operating condition.

3.3 Experiments on Control of Surge Using Tailored Structures

A small turbocharger facility, sketched in Fig. 11, was used to assess the concepts described. Several different ways to implement the control scheme were reviewed. The wall had to be capable of withstanding large steady state and transient pressure loading, yet respond to small amplitude perturbations in plenum pressure. A rigid piston and an aerodynamic spring were determined to be practical solutions to these constraints. The rigid piston was mounted on a shaft, guided by linear bearings, and allowed to float between the main plenum and an auxiliary plenum. A small diameter tube connected the two plenums so they were isolated for high frequency pressure disturbances (i.e. surge oscillations), but steady state pressures were able to equalize. A viscous dash pot was used for the damping.

The compressor was operated at corrected speeds from 60 to 100K rpm, corresponding to B-parameters of 0.65 to 1.0. It was of interest to operate with the moveable plenum wall in optimized as well as non-optimized configuration, and speedlines were recorded with various levels of wall damping.

Fig. 10: Independent effects of B-parameter and tip Mach number on maximum compressor characteristic slope for stable operation [11].
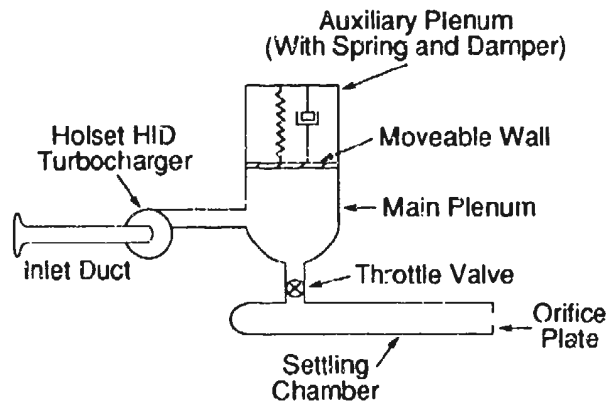
Fig. 11: Schematic of experimental facility for investigation of dynamic structural control.
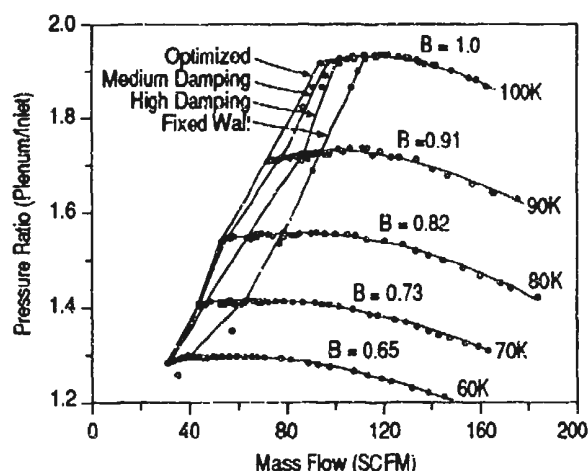
Fig. 12: Compressor map showing increase in stable flow region due to tailored structure for three values of damping; damping values $\zeta = 1.5$, 2.25, 3.0, other parameters at optimized values [11].

Fig. 13: Predicted and measured stability limits with dynamic structural control [11].

The steady state compressor performance map for the three moveable wall configurations and the fixed wall system, is shown in Fig. 12. The steady state pressure ratio is unaffected by the presence of the moving wall in the stable flow range of the fixed wall system, but the surge line is moved to the left markedly. The degree of surge suppression achieved is dependent on the moveable wall control parameters, as predicted; the optimized configuration performed the best, with the performance of the other two configurations decreasing as one moved farther from optimum.

Figure 13 shows predicted and experimental surge lines for rigid wall and for the optimized system. The predicted surge line is based on the linear instability point, and the experimental surge line is defined as the onset of deep surge (i.e. reverse flow); this also marked the points at which the time-mean pressure ratio dropped sharply. The compressor characteristics used were a third order polynomial curve fit of the speedlines measured by Pinsley [12].

3.4 Summary of Results for Dynamic Control Using Tailored Structure

Dynamic control using tailored structure was effective in suppressing centrifugal compressor surge; the surge line was shifted roughly 25% in flow over a significant portion of the corrected speed range examined. The effectiveness of surge suppression is function of a set of non-dimensional parameters which govern the aeroelastic coupling of the wall to the compression system dynamics. The scheme was robust, suppressing surge over a wide range of operating conditions with no adjustment to the parameters. Tailored structural damping of aeroelastic instability was also demonstrated to

lead to suppression of existing, (highly nonlinear), surge cycles. For the configuration investigated, the nominal limit cycle wall motion in the stabilized region was roughly 0.1% of plenum volume, with frequencies near the Helmholtz frequency. Pressure fluctuations in the stabilized region were on the order of 0.5% of the mean pressure rise of the compressor.

4. EVALUATION OF DIFFERENT APPROACHES TO ACTIVE COMPRESSOR SURGE STABILIZATION

4.1 Discussion of Practical Limits to Control

Selection of sensor and actuator type and location is a critical factor in determining the effectiveness and practicality of an active stabilization system. A methodology to compare different implementation alternatives, as well as a comparison for a number of candidate strategies has been examined by Simon et al. [13]. The general problem of actuator/sensor selection has been considered by a number of researchers in other applications (see, for example, Norris and Skelton [14]; Schmitendorf [15]; Muller and Weber [16]). These provide comparisons based upon somewhat abstractly defined performance indices, whereas the paper by Simon et al. [13] makes quantitative comparisons more closely related to the turbomachinery community. The active control systems studied were ones that might be implemented in various gas turbine systems.

Figure 14 shows schematically the types of actuators and sensors considered. The results of the analysis, the specific transfer functions and a description of the limitations of compressor flow range increase with *proportional control*, are given in in the paper.

The analytical results indicated that ability to stabilize the system depends strongly on proper pairing of actua-
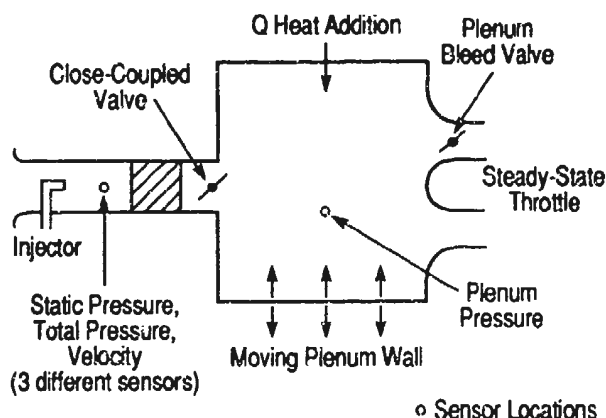
Fig. 14: Schematic of actuators and sensors evaluated [13].

tor and sensor, as well as on the values of the system parameters, particularly the compressor slope and B-parameter. The systems considered, however, had idealized controllers, and it is necessary to include bandwidth limitations and actuator constraints (for example, servo dynamics and stops) which are encountered in any physical realization. As a matter of definition, by actuator we refer here to the entire actuation *system* including the flow train element (e.g. the valve), the motor that drives it, and any included feedback elements.

Bandwidth limitations may be imposed by sensors, processor, actuator, or some combination of the three. System bandwidth may also need to be constrained to maintain stability if unmodelled dynamics are present. The lags introduced by finite bandwidth generally result in reduced control effectiveness, although to some degree, they can be compensated for by use of a control law more sophisticated than proportional control.

Another constraint on control effectiveness is introduced by bounds on actuator influence. For example, valve areas can only be modulated between 0 and 100% (i.e. the valve must be somewhere between full open and full closed).

4.2 Sensor and Actuator Pairs
Five actuators and four sensors (Fig. 14) were studied as representative of a diverse set of implementation options. The actuators were:
1) injection in the compressor duct;
2) close-coupled control valve;
3) plenum bleed valve;
4) plenum heat addition; and
5) a movable plenum wall.

The sensors were:
1) compressor duct mass flow;
2) plenum pressure;
3) compressor face static pressure; and
4) compressor face total pressure.

All twenty pairings of the five actuators and four sensors were evaluated with a proportional control law. Such a comparison provides two useful results. One is the identification of actuator-sensor pairs which provide stabilization over a significant range of system parameters using the simplest possible control law. In addition, for those pairs with significant stabilization, the required gain gives a measure of the combined effectiveness of this choice of sensing and actuating locations.

In view of the preceding discussion of bandwidth and actuator limitations, two constraints were imposed. First, the allowable magnitude of the normalized proportional gain was limited to be no more than twenty. Second, the bandwidth of the feedback loop was limited by modeling a two-pole, low pass Butterworth filter in the feedback path. The filter can be given various physical interpretations such as probe dynamics, amplifier dynamics or actuator dynamics, but whatever the interpretation, insertion of the filter insures that the feedback path has finite bandwidth, a constraint which will always exist in practice. The study was carried out with the cutoff frequency of this filter maintained at ten time the Hemholtz frequency of the system.

The figure of merit used to assess the actuator-sensor pairs was to examine the stability boundaries in a compressor slope versus B parameter plane. Preliminary studies showed that these two parameters have a dominant effect on system stability. It is more relevant to quantify the stabilization that can be achieved in terms of compressor slope rather than in terms of change in mass flow at stall.

With the four sensors studied, and proportional control, the close-coupled valve and injector emerged as the most promising actuators. A further question to address, however, is whether the type of compensation or choice of sensors would affect this conclusion, and optimal control theory was used to address this. The actuators were thus compared based upon their minimal required RMS (root mean square) response to persistent broadband disturbance, while maintaining system stability. This comparison is independent of choice of sensor, because it is assumed that the state of the system is known at all times. Further, the comparison is based upon the minimal possible RMS amplitude, and hence there is no question as to whether a particular actuator would perform better if another control law were used. In this sense, the comparison is also independent of the control law.

4.3 Quantitative Results of the Control Scheme Evaluations
The results of the calculations are summarized in Fig. 15, which shows stability boundaries for the twenty actuator-sensor pairs. The figure is broken into four plots, one for each sensor. Within each plot, the five
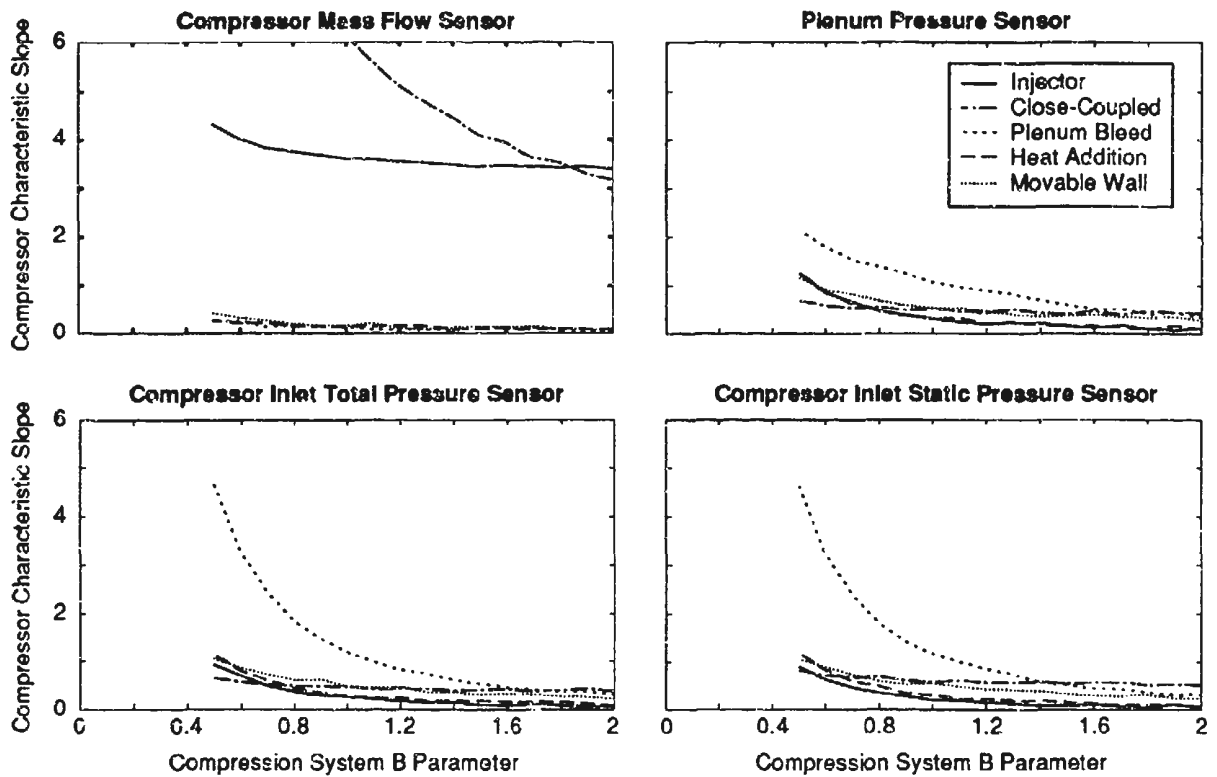
Fig. 15: Influence of sensor and actuator selection on maximum stabilized compressor characteristic slope, for a bandwidth and gain-limited system [13].

curves indicate the different actuators. The region below and to the left of any given line is the region in which stabilization can be achieved. In the upper left hand plot, for example, all the region to the left of the dash-dot line represents the range of compressor slope and B-parameter in which the combination of compressor mass flow sensor and close-coupled valve is capable of suppressing the instability.

Several general conclusions can be drawn from the computations:

a) Control becomes more difficult as the compressor slope and B-parameter increase, with the maximum stable slope decreasing with increasing B.

b) Only the actuators located in the compressor duct, which act upon the compressor duct momentum (injector and close-coupled control valve), are capable of stabilization at steep slopes over the full range of B.

c) Plenum heat addition gives little or no stability.

d) In general, there is no best sensor independent of the actuator.

A more specific conclusion is given by the comparison

of the results with the mass flow sensor to those achieved with other sensor locations. As B reaches a value of roughly unity, the ability of all the pairs to stabilize the system becomes small, except for the close-coupled valve and the injector which use mass flow sensing . Thus, both actuator position and sensor position are important.

4.4 Effect of Control System Bandwidth

The study of the sensor-actuator pairs was carried out using a fixed value of control system bandwidth (ω_c) ten times the compression system Helmholtz frequency (ω_H). The influence of controller bandwidth on the stabilization process was therefore also examined. Figure 16 shows the changes in instability onset that occur with different controller bandwidths for conditions corresponding to the close-coupled control valve, with feedback on mass flow and a B-parameter of 2. In the figure, the horizontal axis is the controller gain, and the vertical axis is the compressor characteristic slope at instability. Curves are shown for values of ω_c/ω_H from 1.0 to 100, representing extremes of this ratio, and it is evident that controller bandwidth strongly influences the range of stabilization that can be achieved.

Other results are given in the referenced paper but the overall conclusions of the control evaluations are as follows:
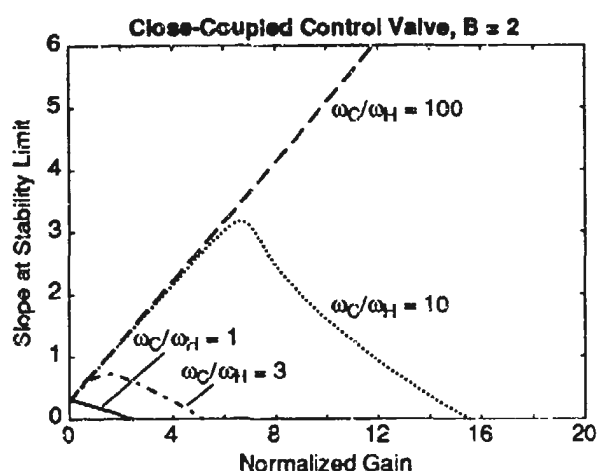
Fig. 16: Influence of normalized control system band-
width (ω_C/ω_H) on feedback gain required and
compressor slope at instability onset; close-cou-
pled control valve [13].

- Proper choice of actuator and sensor is an important
  part of the overall design of a surge stabilization
  system.
- Mass flow measurement with either a close-coupled
  valve or an injector for actuation are the most
  promising approaches of these evaluated.
- Fuel modulation is not a promising candidate for
  practical ranges of system parameters.
- Characterization of compression system disturbance
  sources is important for determining the require-
  ments for active control schemes.
- Steep slopes and large B parameters make control
  more difficult.
- Actuator bandwidth can be an important constraint
  in many practical implementations.

5. ROTATING STALL

The higher order modes of instability in compression
systems have to do with *rotating stall*. As analyzed by
Moore and Greitzer [1], for example, one view is that
the stability of the compressor is tied to the growth of an
(initially small amplitude) wave of axial velocity which
travels about the circumference of the compressor. If
the wave decays (i.e. its damping is greater than zero),
then the flow in the compressor is stable, whereas if the
wave grows (wave damping negative), the flow in the
compressor is unstable. In a multistage axial flow com-
pressor it is critical to control rotating stall as this can
act as a "trigger" for the more global instability. In par-
ticular, *control of surge only does not appear to be a
useful effort if one is targeting at increasing the stable
flow range of multistage aircraft engine compressors at
or near design speed.*

5.1 Travelling Wave Behavior and Rotating Stall Inception

A prediction of this model useful for present purposes is
that rotating waves should be present at low amplitude
prior to stall. McDougall [17], [18] has identified these
waves in a low speed, single-stage compressor, and
Garnier et al. [19] observed them in both a single- and a
three-stage low speed compressor, and in a three-stage
high speed compressor. The waves were often evident
long (ten to one hundred rotor revolutions) before stall.
It was found that the waves grew smoothly into rotating
stall, without large discontinuities in phase or ampli-
tude, and that the wave growth rate agreed with the theo-
ry of Moore and Greitzer [1]. Further, the
measurements showed how the wave damping, and thus
the instantaneous compressor stability, could be extract-
ed from real time measurements of the rotating wave.

In Garnier's experiments, an array of hot wires or pres-
sure probes were used to look for small amplitude trav-
elling waves. During the experiments, the compressor
operation was first maintained close to stall and then the
throttle closed very slowly, so that the machine would
stall within 10 - 20 seconds. Data were taken during this
entire period from the eight hot wires about the com-
pressor annulus.

Figure 17 shows the time history of the axial velocity as
measured by a single sensor during a stall transient. The
period of a rotor revolution is used as the unit of time,
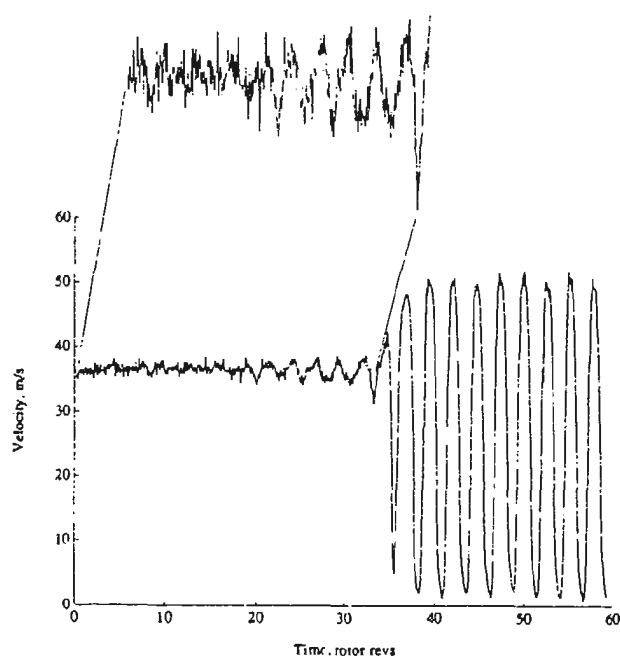
Fig. 17: Time history of axial velocity from a single hot
wire positioned upstream of the single-stage
compressor; the machine is in rotating stall after
a time of 35 rotor revolutions [19].
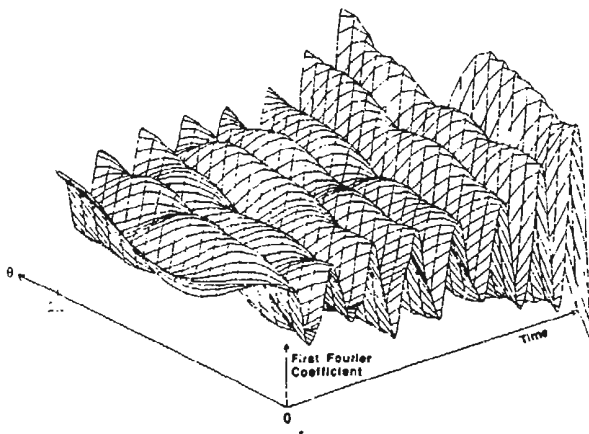
Fig. 18: Measured first harmonic behavior at stall onset [19].

Fig. 20: Time evolution of the first harmonic of the axial velocity in the three-stage compressor during the inception of rotating stall [19].

since this is a characteristic time scale for the phenomena. As can be seen, the prestall fluctuations have a small amplitude compared to the rotating stall itself, during which the velocity fluctuations are greater than 100 percent of the prestall mean velocity. From the eight wires, the first Fourier coefficient of the travelling wave perturbation could be extracted and two views of this are shown in Figs. 18 and 19.

Figure 18 presents a three-dimensional representation of the axial velocity component during the last 20 revolutions before stall. Figure 19 shows the phase angle of the travelling wave for both first and second spatial Fourier harmonics. The slopes of these lines in Fig. 19 are the speeds at which the harmonics of the waves travel around the compressor annulus, which is unwrapped in the figure so that 2π radians is one trip around. This

coarse scale is used deliberately to show the overall trend. The key point is that phase speed of the first harmonic of the traveling waves is essentially constant and readily discernible for almost 90 rotor revolutions before the stall.

The present model of compressor transient behavior describes the evolution of the traveling wave system in the compressor and should be capable of quantitatively predicting the growth of the waves. Comparison of model prediction with experimental measurement for the three-stage low-speed compressor (Fig. 20) shows good agreement. (The initial conditions for the model are not known, and the zero time reference for the data and the calculation are arbitrary.)

In addition to low speed experiments, Garnier [19] also reports results from a high speed compressor. In this case also, using static pressure transducers, a travelling wave could be clearly seen.

Garnier also used the wave behavior to obtain the damping ratio, i.e. how close the system is to instability onset. On the basis of the machines he examined, two low-speed and one high-speed compressor, the conclusions were:

a) Small-amplitude (less than 5 percent of the stall amplitude) waves can be discerned traveling about the compressor annulus at close to the rotating stall speed for 10 or more revolutions prior to the onset of rotating stall.

b) The waves grow into a fully developed rotating stall without apparent sharp changes in either phase or amplitude.

c) The behavior was similar in both the high and low-

Fig. 19: Time history of the phase of first and second spatial Fourier harmonics measured upstream of a low speed, three-stage compressor [19].

speed compressors, except the first spatial harmonic was the strongest in the low-speed machines and the second in the high-speed.

d) In multistage compressors, the pre-stall waves are clearest in the stage that stalls first.
e) Inlet distortion reduces the period during which the pre-stall waves were discerned.

5.2 A caveat on Travelling Wave Behavior

Although Garnier's results are encouraging, it should be noted that there have been several compressor builds examined in which the pre-stall waves were not seen, as is discussed in some depth by Day [2], [20]. In these situations, local regions of strongly retarded flow were first seen, rotating at roughly 70% of rotor speed. These grew in circumferential extent and decreased in angular velocity, eventually evolving to rotating stall cells with a speed roughly half of the initial value. The reason for the two types of behavior is not known at present, and it appears that this is an important area to pursue.

6. ACTIVE CONTROL OF ROTATING STALL

The basic concept that has been used in active control of rotating stall is to measure the wave pattern in a compressor and generate a circumferentially propagating disturbance, based on the measurements, so as to damp the growth of the naturally occurring waves. In the particular implementation described herein, shown schematically in Fig. 21 and in more detail in Fig. 22, individual vanes in an upstream blade row are oscillated to create the travelling wave velocity disturbance. The flow which the upstream sensors and the downstream blade rows see is a combination of both the naturally occurring instability waves and the imposed control disturbances. As such, the combination of compressor and controller is a different machine than the original compressor, with different dynamic behavior and different stability.
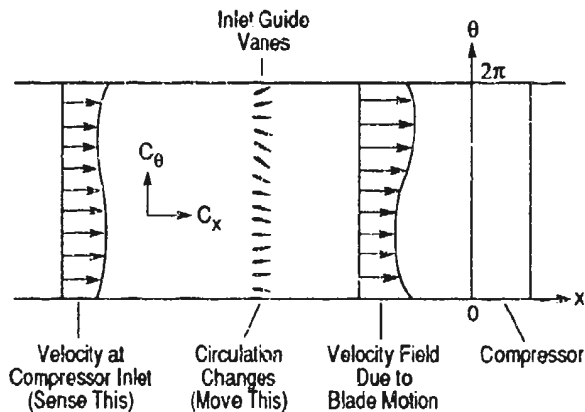
6.1 Design of an Experimental Facility for Active Stall Control

The first use of this approach to active control of rotating stall was reported by Paduano et al. [21]. A theoretical framework for the control was developed and, based on this, experiments were carried out in a single stage research compressor. The apparatus can be considered to consist of four sections: the compressor instrumentation for wave sensing, actuators for wave launching, and a signal processor (controller).

The sensors used were eight hot wires evenly spaced about the circumference of the compressor, 0.5 compressor radii upstream of the rotor leading edge, positioned at mid-span and oriented so as to measure axial velocity. The axial position was chosen to filter the higher harmonic components of the disturbances generated by the compressor (the decay rate is like $e^{-nx/R}$, where x is upstream distance, n is disturbance harmonic number, and R is the mean radius of the compressor) and reduce the likelihood of spatial aliasing of the signal. The axial location of the sensors was important in determining the signal to noise ratio of the rotating wave measurements; this question was studied by Garnier et al. [19], who showed the ratio to be largest upstream of the stage compared to within or downstream of the compressor.

Although there are many ways to generate the required travelling waves in an axial compressor, for this initial demonstration, oscillating the IGV's was chosen on the basis of minimum technical risk. As described by Paduano et al. [21], different airfoil shapes and number were examined, with the eventual configuration adopted being twelve untwisted oscillating airfoils with an aspect ratio of 0.9 and a solidity of 0.6 (Fig. 22). The complete actuation system has a frequency response of 80 Hz (approximately eight times the fundamental rotating stall frequency) at plus or minus ten degrees of airfoil yaw.

Proportional control was used for the experiments; at each instant in time, the nth spatial mode of the IGV stagger angle perturbation is set to be directly propor-

Fig. 21: Conceptual control scheme using "wiggly" inlet guide vanes to generate circumferential travelling waves (axial distances not to scale).
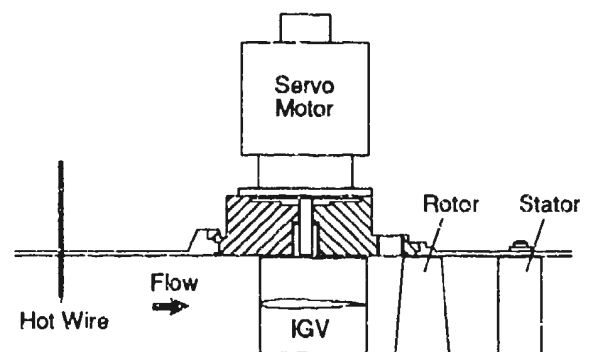
Fig. 22: Compressor flow path showing actuated inlet guide vanes.

tional to the nth mode of the measured local velocity perturbation. The complete control loop consisted of the following steps. First, the sensor signals are digitized. A discrete Fourier transform is taken of the eight sensor readings. The first, second and/or third discrete Fourier coefficients are then multiplied by (predetermined) complex feedback gains. Next, an inverse Fourier transform is taken which converts the modal feedback signals into individual blade commands. These, in turn, are sent to the individual digital motor controllers. Additional housekeeping is also performed to store information for post-test analysis, limit the motor currents and excursions (for mechanical protection), and correct for any accumulated digital errors.

The controller hardware selection is set by CPU speed requirements (main rotating stall control loop and individual blade position control loops), I/O bandwidth (sensor signals in, blade positions out, storage for post-test analysis), operating system overhead, and cost. The final selection was a commercial 25 MHz 80486 PC with co-processor. The D.C. servo motors were controlled individually by commercial digital motion control boards. Using position feedback from optical encoders on the motors, each motor controller consisted

of a digital proportional, integral, derivative (PID) controller operating at 2000 Hz. The entire control loop was run at a 500 Hz repetition rate. Motor power was provided by 350-watt D.C. servo amplifiers. The hardware is shown in Fig. 23.

6.2 Open Loop Compressor Response

The inputs and outputs characterizing the fluid system of interest (the compressor and associated flow in the annular region) are the twelve inlet guide vane angles (inputs) and the eight hot wires that give the axial velocity distribution (outputs). It might appear that a multiple input-multiple output control is required, however, because the disturbances of interest are of small amplitude, the system behavior can be taken as linear. The spatial distribution of the input and output perturbations (or indeed of any flow perturbations) can thus be expressed as a sum of spatial Fourier components, each with its own phase velocity and damping. This allows us to treat disturbances on a harmonic-by-harmonic basis, and reduces the input-output relationship to single input-single output terms, an enormous practical simplification.

An important (although *not necessary*) concept in the present approach is the connection between rotating stall
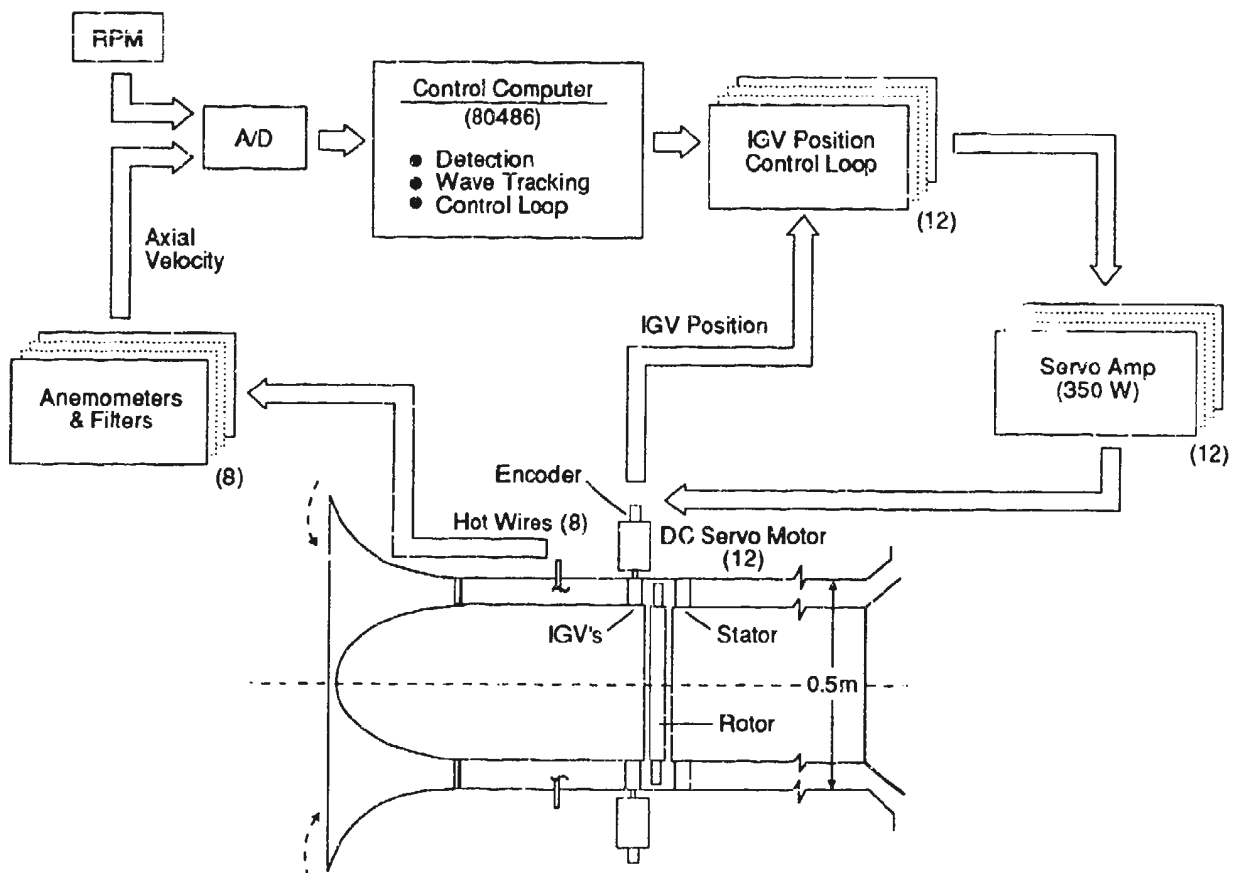
Fig. 23: Hardware component of actively stabilized axial flow compressor [21].
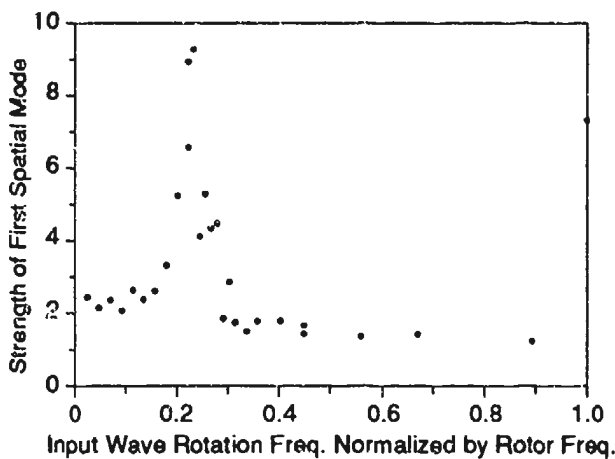
Fig. 24: Measured open loop response of the first spatial mode of the compressor to a 10° IGV stagger rotating sine wave excitation[21].

and travelling wave type of disturbances in the compressor annulus; wave damping and compressor damping are equivalent and determine whether the flow is stable. At the neutral stability point, the damping of disturbances is zero, and close to this point the damping should be small. The measurements given by Garnier et al. [19] show this. At a compressor operating point near stall, the flow in the annulus should behave like a lightly damped system, i.e., should exhibit a resonance peak when driven by an external disturbance. The width of the peak is a measure of the damping.

The sine wave response of the compressor was measured by propagating a 10 degree sinusoidal IGV angle distribution around the circumference at speeds ranging from 0.05 to 1.75 of rotor rotational speed. Figure 24 shows the magnitude of the first spatial Fourier coeffi-
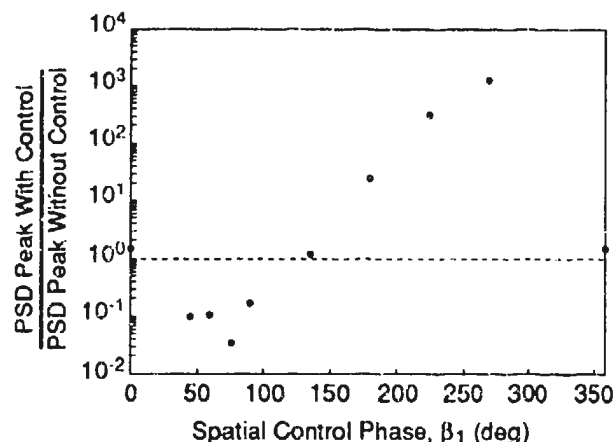
Fig. 25: Influence of feedback control phase angle (β_1) on the strength of the first spatial mode of the flow in the compressor at $\phi = 0.475$ [21].
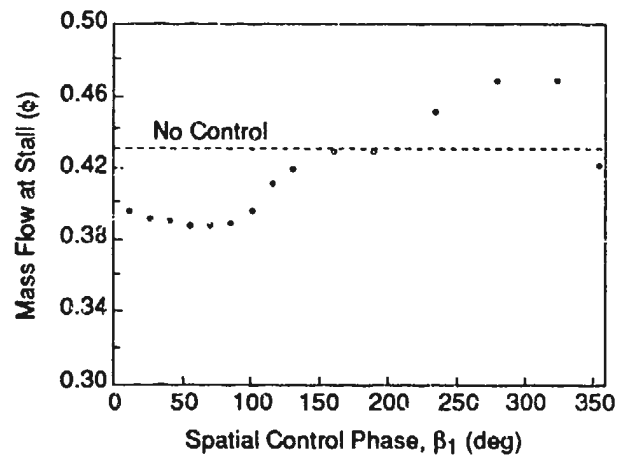
Fig. 26: Influence of feedback control phase angle (β_1) on the flow coefficient at which the compressor goes into rotating stall [21].

cient, as a percentage of the mean flow coefficient, as a function of input wave rotation frequency, i.e. the transfer function for the first spatial mode. The peak response to the forcing sine wave is seen to be at 23% of the rotor rotation frequency. This is close to the frequency observed for the small amplitude waves without forcing (20%) and for the fully developed rotating stall (19%).

6.3 Closed Loop Experiments - Rotating Stall Stabilization of the First Fourier Mode
The open loop experiments described above are of interest in elucidating the basic structure of the disturbance field in the compressor annulus, but the principal aim is suppressing rotating stall using closed loop control. The control scheme used was of the form

$$[\delta(\text{stagger angle})_{IGV}]_n = Z_n \, \delta(\text{axial velocity})_n \quad (9)$$

where Z_n, the control parameter is given by $Z_n = R_n \exp(i\beta_n)$, with R_n a feedback amplitude and β_n a spatial phase lag for the nth mode. The influence of controller phase at fixed gain on the wave amplitude ratio was experimentally evaluated, at a near stall point, for phase shifts between 0° and 360°, as shown in Fig. 25. For phases between 0° and 150°, the waves are attenuated, while the waves are amplified for phase angles between 160° and 350°. The maximum attenuation was found near 75°, and the maximum amplification near 275°. Between 290° and 345°, the flow was unstable and rotating stall occurred.

If wave stability is equivalent to compressor stability, then compressor stability should be enhanced for control phases at which the waves are attenuated and should be decreased when the waves are amplified. This is indeed the case as illustrated in Fig. 26. Here, the flow coefficient (ϕ) at which the compressor goes into rotating stall

as the compressor throttle is very slowly closed ($d\phi/dt = 2 \times 10^{-5}$/rotor revolution) is shown as a function of controller phase angle (β_n). Depending upon the phase, the control changes the stalling flow coefficient by more than plus or minus ten percent. Comparison of Figs. 25 and 26 emphasizes the connection between wave damping and rotating stall. Rotating stall is suppressed when the waves are damped and is promoted when the waves are amplified.

6.4 Time-Resolved Compressor Behavior and Travelling Wave Mode Content

Noting that wave stabilization changes the average flow coefficient at which stall occurs, it is instructive to look at the time evolution measured by a single sensor, both with control off and with control on. Figure 27 shows that with no control (Fig. 27a), the rotating stall grows quite slowly. With control of the first spatial mode (Fig. 27b), stall occurs at a lower flow coefficient, and the signal changes in character. The growth rate is faster and, more importantly, the disturbance with control has twice the frequency of the no control case. This is due to the primary disturbance now being the second spatial mode (two lobed stall).

Since the second spatial mode appeared predominant when the first mode was under control, the former was controlled as well. The effect of simultaneous control of the first two spatial modes on compressor stalling pressure rise is shown in Fig. 28. With both modes under control, the compressor does not stall until a flow coefficient of $\phi = 0.35$, a 20% increase in operating range over the no control case. Examination of the time behavior of the Fourier coefficients as the compressor throttle is slowly closed show a more complex behavior than that described for first-mode-only control, but the third spatial Fourier coefficient is discernable as an
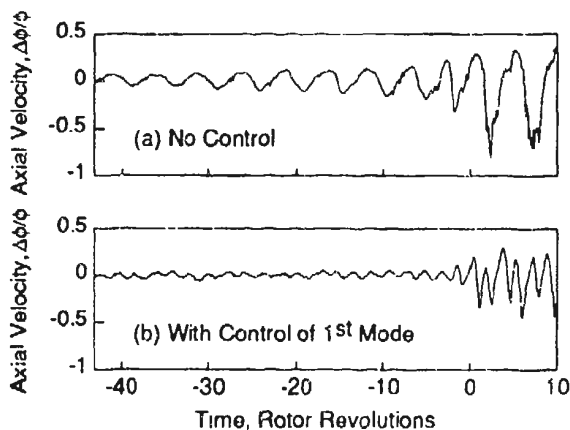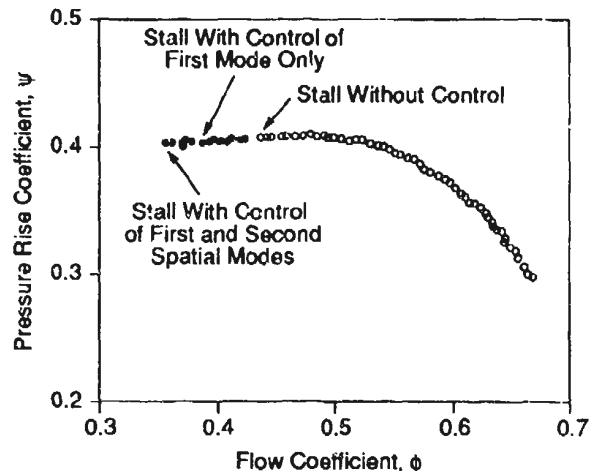
Fig. 28: Compressor characteristic but with active control of first and second spatial modes [21].

important contributor to stall inception. Indeed, stabilization of this mode along with modes 1 and 2, yields a further 3-5% increase in operating range.

6.5 System Identification

The measurements presented are for a compressor with simple proportional control law. There are many analytical tools now available to design more sophisticated control schemes, but the success of the control design is based in no small part on the fidelity of the system model assumed for the compressor. There is also interest in understanding more about the compressor fluid mechanics. Paduano et al. [22] thus describe the use of the apparatus assembled for the active control experiment to establish the dynamic response of the compressor by directly measuring its transfer function.

Section 6.2 and Fig. 24 describe the response of the single-stage compressor to rotating wave input on the IGVs. This compressor response can be put into a more complete form and compared to the structure of the fluid dynamic model by plotting the p͏ ͏ͺd magnitude (Bode diagram) of the transfer function between the first Fourier coefficient of the IGV motion and the first Fourier coefficient of the resulting axial velocity perturbations. Based on the modeling described in Paduano et al. [21], the system behavior is expected to be that of a second order system. A linear regression type fit [23] to the data is thus shown in Fig. 29. The model structure is justified from fluid mechanical considerations, and it can be seen that the experimental behavior is accurately described by the model. This type of fit could be obtained using any one of several types of IGV inputs: rotating waves, stationary waves with oscillating amplitudes, and stationary waves with random amplitudes. As would be expected in a linear system, the input-output behavior is unaffected by such variations in the character

Fig. 27: The influence of control on the time history of a single sensor as the throttle is slowly closed to stall the compressor [21].
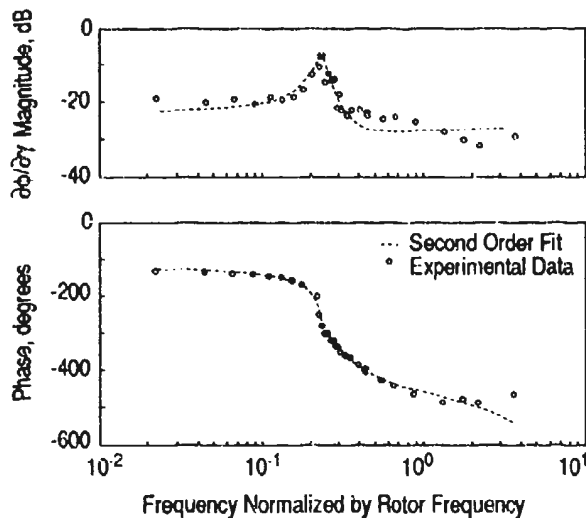
Fig. 29: Bode plot showing response of the compressor to a sine wave forcing excitation at $\phi = 0.475$ [21].

of the input, and the fit of the second order model to the measurements is consistently accurate. In summary, the fidelity of the model fit indicates that the structure of the fluid model is appropriate for the compressor examined.

Figure 29 presents results for the dynamics of the single-stage compressor at a particular flow coefficient, but the unique configuration of the compressor makes similar data obtainable over a wide range of flow coefficients. Because the wave dynamics can be directly forced by the IGVs, the system's response can be deduced under conditions which are not normally conducive to identification, for example beyond the uncontrolled stall point. In compressors which are not equipped for stabilization, identification of the linearized dynamics beyond the stall point is impossible; the system is unstable, and operates in rotating stall. Even in the compressor discussed here, which can operate in previously unreachable regions using active control, identification is difficult, but Paduano et al. [22] discuss a procedure which allows the compressor's innate dynamics to be deduced from experimental data.

The dynamics of the compressors under study have been thoroughly characterized over a large range of compressor operating points and provide a new data set for comparison to theoretical techniques. Of primary interest from a fluid mechanic viewpoint are the rotation rate and growth (or decay) rate (damping factor) of small-amplitude sinusoidal waves in the compressor. Although stall-cell rotation rate has often been used as a gauge of the predictive accuracy of theoretical techniques the small-amplitude wave behavior can differ from the fully developed state, and it is the former that is critical, especially if control laws are being designed.

The *growth rate* of the rotating waves, on the other hand, is a relatively new measure of the nearness to instability of the compressor.

6.6 Initial Results for Active Control of a Multistage Compressor

The type of experiments described have also been carried out on a low speed three-stage compressor, retrofitted with a similar set of moving guide vanes. The results are analogous, with an eight percent reduction of the mass flow at stall obtained. Further, the same system identification techniques and software are applicable to both compressors.

Figures 30 and 31 show the results of an extensive set of identification experiments on the 3-stage compressor [24]. In the figures the wave propagation rate (Fig. 30) and the growth (or decay) rate (Fig. 31) are plotted for the first three disturbance modes. At flow coefficients below the natural stall point (denoted in Fig. 31), the growth rates are positive, indicating that the system is unstable. Identification at these flow coefficients must be conducted under closed-loop operation, and this type of data has previously not been available.

The compressor stall point can be identified based on the growth rate parameter. For instance, under no control, rotating stall occurs at $\phi = 0.46$. Referring to Fig. 31, this is approximately the flow coefficient at which the first mode becomes unstable. Under first mode control, rotating stall then occurs at roughly the flow coefficient at which the second mode becomes unstable. Finally, under control of the first and second modes, it appears that the third mode is at least partially responsible for stall.
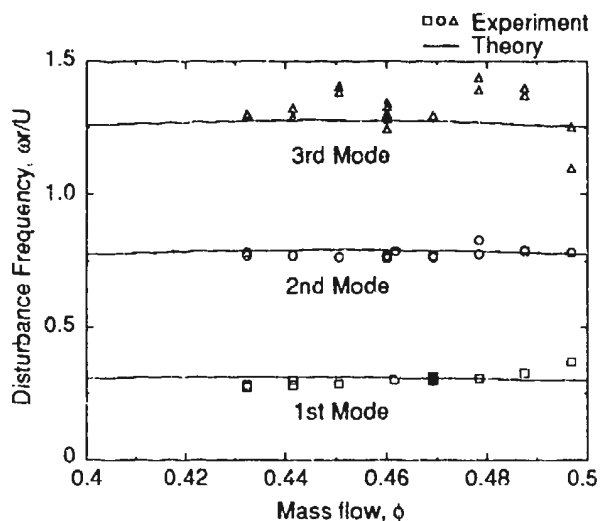
Fig. 30: Disturbance wave frequency for first three modes; three-stage axial compressor [24].
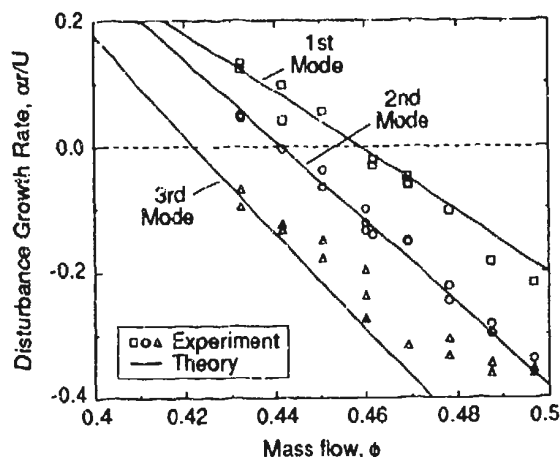
Fig. 31: Disturbance growth rate for first three modes; three-stage axial compressor [24].

Also shown in the two figures are the results of a theoretical model of the compressor dynamics, based on a simple extension of the Moore and Greitzer [1] theory to include an unsteady loss response in the compressor blade passages. With correct choice of the single parameter representing this effect the theoretical model is able to match the entire set of data trends. Although additional measurements of unsteady compressor behavior are needed to assess this conclusion in more depth, the data show that the theory characterizes the evolution of unsteady perturbations as well as provides a framework about which identification and control experiments can be built.

6.7 Dynamic Control of Rotating Stall Using Structural Feedback

The concept of using unsteady feedback to stabilize rotating stall is not limited to active control techniques. Calculations indicate that the rotating stall dynamics of a compression system can also be modified using structural feedback, and the analytical studies have resulted in several promising strategies. In these, additional aeroelastic dynamics are introduced to the basic compression system to modify its aerodynamic stability.

To illustrate the basic principles, consider a hypothetical control strategy in which the variable inlet guide vanes used in the active control experiment were replaced with flexible vanes. The latter would introduce an aeroelastic feedback loop into the compression system; flow perturbations cause the vanes to deflect, which in turn, modifies the flow perturbations. Tuning the structural dynamic properties of the vanes is equivalent to adjusting the gain and phase of the control law.

Conceptually, active control and structural feedback strategies are similar, in that they both use feedback to increase the stability of a dynamical system. The imple-

mentation, however, may be fundamentally different. The active control strategies employed to date have used modal based control schemes, where the rotating disturbance is decomposed into Fourier components and each component is controlled individually. The structural feedback schemes, on the other hand, lend themselves to "local implementation" in which local control action is determined by local information. Overall stability is achieved by making the flow field locally stable at all points around the annulus. Since local instability is a prerequisite for the more global, modal instability, local control may be an approach with wide applicability for stabilizing compression systems.

7. DISCUSSION OF ACTIVE CONTROL OF ROTATING STALL AND RECOMMENDATIONS FOR FUTURE WORK

7.1 Implications of the Overall Results so Far

Several important points emerge from the experiments that have been carried out. First is the demonstration that it is possible to actively control rotating stall in an axial flow compressor and obtain a useful extension in compressor operating range. In this, it can be noted that one series of experiments has been conducted on a multistage compressor that was designed by an engine manufacturer; the compressor parameters are in a range of general interest. Second, the experiments emphasize the link between low amplitude circumferentially propagating disturbances prior to stall and fully developed rotating stall; when the disturbances are suppressed, rotating stall is prevented. Third is that a strong connection has been made between the measurements and the theoretical description of the evolution of small disturbances to rotating stall.

An additional point concerns the utility of the compressor plus controller for basic research on unsteady flow in compressors. The controlled compressor provides a unique vehicle to examine many aspects of the dynamic behavior of compressors that were heretofore inaccessible. Examples of this are the first-of-the-kind data concerning the mode structure that was presented in Fig. 30 and 31, in particular the system identification under closed loop control in a naturally unstable region. Viewed in this regard, the active control allows completely new, and much deeper, investigations of fundamental stall inception flow physics than previously, with the potential for shedding new light on a long standing, but not well understood, problem.

Finally, we note that there have been other approaches to the active control of rotating stall and compression system instability. The experiments reported by Day are based not on sensing the modal structure, but rather on detecting more localized, but large amplitude, flow non-uniformities [20]. The actuators used were discrete jets at the outer diameter of the compressor. Examinations of alternative strategies for the control of multistage

compressor instabilities have also been carried out by Harris and Spang [25], Hosny et al. [26], and Badmus et al. [27], which can be consulted for further details.

7.2 Some Unanswered Questions: Areas to be Addressed

The initial attempts to control rotating stall in axial compressors have yielded very positive results so far, but there are still many questions that remain. In this section, we note several research topics that are fruitful to pursue.

- Control Law Modification

The control law used in the experiments reported herein is quite simple. Effort is now being spent on the design of more sophisticated controllers, and this can be useful in two ways: first, in extending compressor performance and, second, in elucidating the details of the dynamic behavior of the compression system.

- Generality of Results

There is also a need to establish the generality of the observed behavior. The wave behavior exploited in this control scheme has been found on several low and high speed compressors [18], [19], although some other machines do not appear to exhibit small amplitude waves (or at least they cannot be sensed) prior to stall [2], [3]. It is emphasized, however, and discussed further below, that *active control of compressor instabilities is not dependent on the existence of the waves*. It would be of considerable interest to reconcile quantitatively the two sets of circumstances, preferably with a first principles fluid dynamic model. This would enhance the range of applicability of the predictions of compressor behavior with control.

- Extension to Flows with Inlet Distortion

Another critical item is the extension of the ideas to flows with inlet distortion. It is often the case that the reason for the instability is the presence of an inlet distortion. The nature of the disturbance structure in this type of flow is fundamentally different from that with uniform inlet conditions [28], and relatively little work has been done yet on this topic.

- Extension to Compressible Flow Regime.

Extension of the analysis to the compressible flow regime has started [29] and should be pursued vigorously. Data for this regime are currently sparse, and obtaining the type of unsteady measurements that are needed is also an item of high interest.

- Optimization of Actuation and Sensor Strategies

Determining the most useful (practical) actuation schemes is a key item that influences both effectiveness of control and complexity and difficulty of implementation. The question is really on two levels: first what are the most useful fluid dynamic perturbations that one can have, and second, how one actually creates that type of

disturbance, i.e., how one links the disturbance to the actuator.

- Dynamic Compressor Behavior

The use of compressor facilities with active control provides a new diagnostic tool for the examination of basic unsteady fluid dynamics associated with stall onset. The ability to probe the compressor response in a way that was not possible before should be vigorously pursued.

- Use of Structural Feedback for Control of Rotating Stall

The use of tailored structure as an approach for controlling rotating stall should also be pursued. This is not only of interest from a technological point of view, but the results obtained from a scheme based on local sensing and actuation should also be useful for giving insight into the basic mechanism of stabilization in a general sense.

7.3 Interdisciplinary Nature of the Research

Finally, the interdisciplinary nature of the research can be commented on. The work described has been successful due to the combined efforts of both compressor and controls engineers, and it has been challenging for both specialties. In the past several years, considerable time, as well as considerable intellectual effort, has been spent learning how to talk across disciplinary boundaries, but the results so far appear to be well worth it.

8. ACKNOWLEDGMENTS

9. REFERENCES

1. Moore, F.K., Greitzer, E.M., 1986, "A Theory of Post-Stall Transients in Axial Compressors: Part I – Development of the Equations," *ASME Journal of Engineering for Gas Turbines and Power*, Vol. 108, pp. 68-76.

2. Day, I.J., 1991, "Stall Inception in Axial Flow Compressors," ASME Paper 91-GT-86.

3. Day, I.J., 1991, "Axial Compressor Performance During Surge," presented at Tenth ISABE International Symposium on Air Breathing Propulsion, Nottingham, England.

4. Boyce, M.P., et al., 1983, "Tutorial Session on Practical Approach to Surge and Surge Control Systems," in *Proceedings of the Twelfth Turbomachinery Symposium*, Texas A&M University Turbomachinery Laboratories.

5. Ludwig, G.R., Nenni, J.P., 1980, "Tests of an Improved Rotating Stall Control System on a J-85 Turbojet Engine," ASME Paper 80-GT-17.

6. Staroselsky, N., Ladin, L., 1979, "Improved Surge Control for Centrifugal Compressors," *Chemical Engineering*, pp. 175-184.

7. Emmons, H.W., Pearson, C.E., Grant, H.P., 1955, "Surge and Stall Propagation," *Trans. ASME*, Vol. 77, pp. 455-469.

8. Greitzer, E.M., 1981, "The Stability of Pumping Systems – The 1980 Freeman Scholar Lecture," *ASME Journal of Fluids Engineering*, Vol. 103, pp. 193-242.

9. Ffowcs Williams, F.E., Huang, X., 1989, "Active Stabilization of Compressor Surge," *Journal of Fluid Mechanics*, Vol. 204, pp. 245-262.

10. Pinsley, J.E., Guenette, G.R., Epstein, A.H., Greitzer, E.M., 1991, "Active Stabilization of Centrifugal Compressor Surge," *Journal of Turbomachinery*, Vol. 113, pp. 723-732.

11. Gysling, D.L., Dugundji, J., Greitzer, E.M., Epstein, A.H., 1991, "Dynamic Control of Centrifugal Compressor Surge Using Tailored Structures," *Journal of Turbomachinery*, Vol. 113, No. 4, pp. 710-722.

12. Pinsley, J.E., 1988, "Active Control of Centrifugal Compressor Surge," M.S. Thesis, Department of Aeronautics and Astronautics, MIT.

13. Simon, J.S., Valavani, L., Epstein, A.H., Greitzer, E.M., "Evaluation of Approaches to Active Compressor Surge Stabilization," to be presented at 1992 ASME Turbo Expo, Cologne, Germany.

14. Norris, G.A., Skelton, R.E., 1989, "Selection of Dynamic Sensors and Actuators in the Control of Linear Systems," *Journal of Dynamic Systems, Measurement and Control*, Vol.111, pp. 389-397.

15. Schmitendorf, W.E., 1984, "An Exact Expression for Computing the Degree of Controllability," *Journal of Guidance*, Vol. 7, No. 4, pp. 502-504.

16. Muller, P.C., Weber, H.I., 1972, "Analysis and Optimization of Certain Qualities of Controllability and Observability for Linear Dynamical Systems," *Automatica*, Vol. 8, No. 3, pp. 237-246.

17. McDougall, N.M., 1988, "Stall Inception in Axial Compressors," Ph.D. Thesis, Cambridge University.

18. McDougall, N.M., Cumpsty, N.A., Hynes, T.P., 1990, "Stall Inception in Axial Compressors," *Trans. ASME*, Vol. 112, pp. 116-125.

19. Garnier, V.H., Epstein, A.H., Greitzer, E.M., 1991, "Rotating Waves as a Stall Inception Indication in Axial Compressors," *Journal of Turbomachinery*, Vol. 113, pp. 290-301.

20. Day, I.J., 1991, "Active Suppression of Rotating Stall and Surge in Axial Compressors," ASME Paper 91-GT-87.

21. Paduano, J., Epstein, A.H., Longley, J.P., Valavani, L., Greitzer, E.M., Guenette, G.R., 1991, "Active Control of Rotating Stall in a Low Speed Axial Compressor," ASME Paper 91-GT-88.

22. Paduano, J., Valavani, L., Epstein, A.H., 1991, "Parameter Identification of Compressor Dynamics During Closed-Loop Operation," *Proc. of the Auto. Control Conference*, pp. 2379-2385.

23. Lamaire, R.O., 1987, "Robust Time and Frequency Domain Estimation Methods in Adaptive Control," Ph.D. Thesis, Department of Electrical Engineering and Computer Science, MIT.

24. Haynes, J.M., 1992, "Active Control of Rotating Stall in a Three-Stage Axial Compressor," M.S. Thesis, Department of Mechanical Engineering, MIT.

25. Harris, L.P., and Spang, H.A., 1991, "Compressor Modelling and Active Control of Stall/Surge", pre-

sented at 1991 American Control Conference,
Boston, MA.

26. Hosny, W.M., Leventhal, L., and Steenken, W.G,
    1991, "Active Stabilization of Multistage Axial-
    Compressor Aerodynamic System Instabilities",
    ASME paper 91-GT-403.

27. Badmus, O.O., Nett, C.N., and Schork, F.J., 1991,
    "An Integrated Full-Range Surge Control/Rotating
    Stall Avoidance Compressor Control System,"
    Proc. of the Auto. Control Conference.

28. Chue, R., Hynes, T.P., Greitzer, E.M., Tan, C.S.,
    Longley, J.P., 1989, "Calculations of Inlet
    Distortion Induced Compressor Flow Field
    Instability", *International Journal of Heat and
    Fluid Flow*, Vol. 10, pp. 211-223.

29. Bonnaure, L., 1991, "Modelling High Speed
    Multistage Compressor Stability," M.S. Thesis,
    Department of Aeronautics and Astronautics, MIT.

ENGINE PERFORMANCE AND HEALTH MONITORING MODELS USING STEADY STATE AND TRANSIENT PREDICTION METHODS

B.D. MacIsaac
GasTOPS Ltd.
1011 Polytek Street
Gloucester, Ontario, Canada, K1J 9J3

SUMMARY

This lecture note discusses the role of computer modelling in the design, development and validation of a performance monitoring system. The basic requirements of an engine health monitoring system are discussed in the context of the user environment.

A form of model based on stage characteristics provides the basis for describing engine measurements. Faults are modelled in accordance with empirical data obtained from tests conducted at the stage level.

The model is used to investigate various parameters that provide unambiguous identification of the fault in question. Fault libraries have been developed for field use.

LIST OF SYMBOLS

A	-	Area
CDP	-	Compressor Delivery Pressure
EGT	-	Exhaust Gas Temperature
EPR	-	Engine Pressure Ratio
F	-	Thrust
FS	-	Fault Severity level
k	-	Fault Severity factor
N_1	-	Fan Rotor Speed
N_2	-	H.P. Rotor Speed
T	-	Temperature
U	-	Blade Speed
V_a	-	Axial Velocity
VEN	-	Variable Exhaust Nozzle
W_f	-	Fuel Flow
W	-	Air Flow
ϵ	-	Tip Clearance Ratio
θ	-	Non-dimensional Temperature, T/T_{ref}
δ	-	Non-dimensional Pressure P/P_{ref}
ϕ	-	Stage Flow Coefficient $\left(\frac{V_a}{U}\right)$
ζ	-	Stage Temperature rise coefficient $\left(\frac{Cp\Delta T}{U^2}\right)$
ψ	-	Stage Pressure rise coefficient $(\eta\cdot\zeta)$
η	-	Stage Efficiency

INTRODUCTION

Life cycle costs have emerged as a primary factor in the design of gas turbine powerplants. The recognition of repairs/rebuilds and lost availability as major recurring costs suggests that some means of getting more usefulness from the engine is in order [1].

The concept of on-condition repair and maintenance has emerged as a common ownership philosophy for both military and industrial equipment. Such a philosophy can only be put into practice if the tools to accurately assess engine condition can be assured. Furthermore, these tools must be tailored to the needs and capabilities of the personnel who must use them.

The complexity of modern engines is such that no single failure or degradation mode can be described as dominant. While a number of failure modes such a Low Cycle Fatigue (LCF) are purely mechanical phenomena, a great many others directly affect engine performance and are best diagnosed through performance measurements.

The analysis of performance data has remained vexingly complex. if one considers the typical military fighter engine with at least two and often three elements of controllable variable geometry in addition to control of fuel, it becomes apparent that old simple rules of thumb in diagnosis will not apply. This state of affairs suggests that analytical methods must be sought to provide a more systematic approach to engine fault diagnosis.

This lecture note describes the application of computer modelling of gas turbines to the development of static and dynamic monitoring techniques applicable to modern gas turbines.

THE RIGOUR OF PRACTICAL REQUIREMENTS

Computer models are little more than useful tools in the process of developing a product or system. The form of the model is as variable as the questions that need to be answered during the course of the development. It is therefore useful to examine the practical requirements of a comprehensive engine monitoring system. From this examination, it will be apparent what type of models are required for design/development of a working EHM system.

The User Environment

The user environment is shown in schematic form in Figure 1. Each provide an opportunity for the use of EHM methods but each have unique and different requirements.

The flight line (Figure 1-a) is primarily the domain of the aircraft/engine technician. It is organized around the concept of the quick fix. Engine designs make every effort to make line replaceable units (LRU's) accessible and easy to change. In this environment, the technician is compelled to work with

some combination of pilot reported problems and whatever recorded limit exceedances or alarms are available. The latter implies that the aircraft has been fitted with a flight recorder which is usually the case for modern aircraft.

Time is of the essence at the flight line; the technician typically has only one or two hours in which to effect a repair and put the airplane back into service.

Based on available information, backed up with on-wing inspections, the technician makes a preliminary diagnosis and proceeds to conduct whatever tests he deems necessary to substantiate his hypothesis. It is also common practice to simply begin by changing a suspect LRU. This is followed by on-wing tests and if successful, the aircraft is released to fly. If unsuccessful, the technician may elect to replace another LRU and try again or he may elect to replace the entire engine and send it to the engine repair shop for more involved repair. In either case, the flight line actions trigger demands on spares supply and consume engine life in the process of on-wing tests.

From an EHM requirements viewpoint, a number of things are clear:

- Unless the diagnosis is quite unambiguous, the flight line repair is a haphazard process with very poor success rates in the diagnosis.

- Diagnosis must be quick and very convenient to the technician. The technician is not an engineer.

- Diagnosis must focus on those problems for which exchanging an LRU will effect a repair or else clearly indicate the need for engine removal.

The engine repair shop (Figure 1-b) is, in effect, a nearby garage which provides a service to the flight line. This service consists of stripping the engines and replacing life expired components (scheduled repairs) and dealing with all engines removed from the aircraft because a quick fix could not be effected at the flight line (unscheduled repairs).

Management of the engine repair shop is judged on its ability to complete repairs in a timely manner. This, in turn, is quite dependent on a timely flow of the right spare parts at the right time. Bearing in mind the very high cost of spares, this translates to "just in time", spares management. Clearly the key to success in this endeavour is accurate prediction of the workload and type of work in the engine shop.

Prediction of spares requirements for the scheduled repairs is predicated on accurate records of engine utilization. Whether these data are based on flying hours or more sophisticated life utilization algorithms is immaterial; the manager of the engine repair shop can make accurate predictions of this component of his workload by knowing the flying schedule and the method of life accounting. He can then order spares and schedule his personnel accordingly.

The unscheduled engine repairs can represent 50% or more of the engine repair shop workload. Without adequate means of assessment/prediction, this workload will appear quite suddenly (often in successive waves) and will make major demands on spares inventory and on personnel. It is evident, therefore, that some means of providing early warning of the arrival of unscheduled engines would have a very substantial impact on the entire range of concerns of the engine repair shop.

From an EHM requirements viewpoint, the engine repair shop is quite different from the flight line.

- The time frames of concern are substantially longer, making parameter trending very useful.

- A more sophisticated level of diagnosis is possible with the support of engineering personnel.

- Proper data management offers a feedforward information loop to the flight line.

- The essence of EHM at the engine repair shop is proper planning of resources.

The engine test cell (Figure 1-c) is an expensive facility provided for the primary purpose of ensuring safety. The engine undergoes a "pass-off" test which checks the engine in accordance with the repair level. Modern practice includes the possibility of on-wing tests, thus the test facility is often shared between the flight line and the engine repair shop.

Since the express purpose of the tests is to ensure flight safety, two major aspects of engine operation are examined. First, the mechanical integrity of the engine is established. This includes, possible hydraulic leaks, loose bolts and vibration levels. Secondly, the static and dynamic performance of the engine is examined. These tests consist of establishing throttle settings and/or manoeuvers and recording speeds, pressures, temperatures, etc. for purposes of comparison with acceptable standards of performance.

During the course of the tests, allowable control adjustments are made and the engine is retested. If the engine passes all tests, it is declared "ready for Installation". If, however, it fails and subsequent adjustments (e.g.

variable geometry) do not cause it to fall within acceptable limits, it must be partially or completely stripped and reworked.

The engine test itself is quite straight forward. Analysis of the data follows the normal practice recommended by the manufacturer; however, the diagnosis used in current test cells is little better than that available on the flight line. The requirements for diagnostic techniques in the test cell is self-evident.

- Test cells provide a larger complement of engine measurements than most flight recorders.

- Diagnosis requirements are similar to those for the flight line progressing from simple adjustments through the replacement of LRU's while the engine is on test.

- Test cell diagnosis can and should progress to fault identification deep within the engine. It can help to eliminate unnecessary testing and direct attention to repairs.

- Data obtained during engine test will provide quantitative assessment of available engine margins. These data are important in establishing a first estimate of when the engine will next need work and for what cause.

SYSTEMS OVERVIEW OF EHM

The foregoing discussion suggests that there are a number of distinct users of EHM within any organization. Each has different requirements for diagnostics and each have different levels of training.

Figure 2 provides an overview of a typical EHM system. It assumes the existence of an onboard data recorder and it further assumes that this data recorder offers the opportunity to transfer records to a ground component of the system. In addition, the overview presented in Figure 2 suggests that both static and dynamic data are recorded depending on the circumstances of the event. Diagnostics must, therefore, be provided for both static and dynamic situations.

The reader should note that in a complete EHM system, there will inevitably be linkages to other technologies including vibration and oil analysis. In addition, some elements of the system must be completely portable while others are inevitably of fixed location. It is beyond the scope of this lecture note to discuss the wider requirements of complete EHM systems; however, the reader should be aware of the more important aspects of system design in order to place performance diagnosis in its proper context.

Fundamentals of Successful Diagnosis

Any review of the field of EHM will quickly yield more than a few case studies of EHM systems which can only be described as failures. (see for example, Ref. 2) The reasons cited range from frequent and troublesome failures of electronics through to incomplete systems which provide ample opportunity to view engine data but little or no useful insight into their interpretation.

In the practical world of engine support, a system designer must ultimately satisfy the engine technicians. These men and women have no patience with systems that do not provide them with a useful tool. Thus there are really only two major ingredients for success in this endeavour:

a) a user friendly software package that can implement the concepts in use and

b) a proven fault identification system.

The former requirement recognizes that most technicians are not specifically interested in computers and will use them only if they provide an advantage. The latter requirement reflects the inevitable impatience of this same group with systems which provide wrong answers.

Why Modelling is Essential

There are essentially two primary factors that suggest that computer modelling techniques are the only practical approach to the development of reliable diagnostic techniques. These are:

a) system complexity
b) time

In any discussion of system complexity, it is worthwhile drawing an analogy with control systems development. An engine control system will typically consist of about 15-20 sensors and 2-4 actuators for a modern engine. Including engine start-up and limit exceedance protection, the complete control package will comprise 40-50 interrelated functions for which design tools are well developed. The control systems engineering community pioneered the development and application of computer modelling techniques to better understand and to control the dynamics of the jet engine. These models were restricted to healthy engines but provided the basis for control design.

A modern EHM system relies on the same sensor suite as the control with perhaps a few additional measurements such as fuel flow. The process of diagnosis is expected to segregate parameter deviations dictated by control actions from those dictated by engine degradation and simultaneously distinguish between

faulty engines and faulty control units. Does this not suggest at least a doubling of system complexity? Does this not suggest that the same models used to understand engine behaviour for control design purposes will be useful (with suitable enhancements) to design diagnostic algorithms? The author believes that the answer to both these questions is affirmative and further suggests that any other method for EHM design will prove inadequate.

The second major reason that computer modelling methods are essential to the successful development of diagnostic algorithms is time. To put this argument in perspective the following partial list of engine faults is offered:

- fouling
- blade surface changes
- tip clearance changes
- seal leakage changes
- foreign object damage
- variable geometry misrigging
- variable geometry linkage wear
- bleed valve leakage
- turbine area changes
- turbine blade profile changes
- corrosion/erosion
- thermal damage

The job at hand is to provide a method of recognizing, with minimum ambiguity, the existence of any one of these faults through the typical measurement suite available on a modern engine.

Now, the current achievable unscheduled removal rates for new military engines is in the vicinity of 2.5/1000 hrs. These numbers reflect all causes whether substantiated or not. Statistical analysis suggests that, at current flying rates, one would require at least 10-15 years of dedicated effort to collect sufficient data to even establish an accurate data base of engine measurement for each engine fault. In addition, to relate the measurement deviations to actual cause will require an engine teardown for each situation encountered. It is emphasized that these data do not form a diagnostic algorithm; they merely provide a basis upon which to begin the process of designing one. The complexity of the analysis remains to be dealt with!

THE FAULT MODELLING CONCEPT

General Approach

The earliest performance monitoring systems focused on fuel burn for the power and/or thrust delivered. Trending of these data were initially tried without reference to operating conditions and it was quickly found that the scatter associated with measurements of this type lead to little useful information. Gradually other gas path performance parameters began to be used as a means of inferring changes in machinery that would result in an increase in fuel burned. In general there was a recognition of the complexity of the interrelationships between the various engine measurements and there was a gradual emergence of a number of ways of analyzing these measurements to obtain performance information.

The linear analysis method, generally attributed to Hamilton Standard [3] was dependent on the Taylor Series expansion of the governing equations describing the performance of a gas turbine. The first derivatives of this expansion were evaluated at a specific operating point or in a specific operating range and these derivatives were generally referred to as fault coefficients.

The method relied on the measurement of specific performance parameters referred to as "deltas" and the use of the fault coefficients to obtain the deviations in other parameters of interest in the engine. It has never been published what the method of decision making was with respect to the interpretation of these changes; however, the system fielded recommended specific maintenance actions.

Considerable effort was expended in the linear analysis approach to data verification and smoothing with the obvious result that the system would have difficulty in coping with abrupt changes in the measurements. It is now well recognized that abrupt changes can take place in the performance of an engine as a consequence of a specific fault.

The linear analysis approach gradually gave way to a non-linear analysis such as Saravanamuttoo [4] in which matching type calculations were used to compute the various gas path parameters. This method resulted in an array of measured and computed differences with the primary advantage that the method could handle abrupt changes in measurements caused by operational damage. The method also required a smaller measurement suite than the linear method in order to complete the analysis. Fault matrices were formed to relate specific "critical engine parameters" to the available measurements. The published fault matrices were based on assumptions about the relationship between operational damage and component level performance changes. These assumptions were, unfortunately, based on little more than a gut feel about what might happen to the performance of a component in a damaged state.

In general the non-linear method was a sound approach to the problem of performance analysis but the lack of a substantiated fault matrix made its application impossible, except by a highly trained performance engineer.

Criticism of published performance analysis methods centers on the habit of

making assumptions about the fault and its effect. Assumptions appeared to be driven by the lack of performance data supporting physical evidence of a fault. A number of major operators had undertaken fault implantation programs (US Army, US Navy) with quite limited success. These efforts did not seem to be supported by analytical tools which would direct a fault implantation program nor did there appear to be any systematic attempt to use analysis for data interpretation.

Examination of the methods of aero-thermodynamic modelling of gas turbines over several decades indicated that the component based model had become a standard practice. Furthermore, the method was well validated. Although the technique required component performance maps which are considered proprietary, most investigations of parametric changes to these components have been published in the form of stage data. It was therefore hypothesized that:

(1) methods could be developed to allow synthesis of specific component performance maps from generalized stage data.

(2) stage data could be modified to accurately represent engine faults.

(3) a computer model based on these data could be used to accurately predict measurements from a specific engine which exhibited these faults.

(4) It would then be possible to assess/design fault recognition parameters in a systematic manner.

The overall concept is as shown in Figure 3.

DEVELOPMENT OF BASIC MODEL

The conventional component based model of the gas turbine relies upon the availability of component maps or characteristics. The calculation then proceeds to "match" all engine components by establishing the operating point on each map which will satisfy the laws of conservation of energy and mass throughout the machine. Such a model provides quite detailed information about the performance of the engine and, with suitable models of controls, can be used to study both the static and dynamic behaviour of the engine. However, direct use of the model in this form to study an engine in a degraded condition leads inevitably to speculation as to the effect of the damage on the component map in question.

Examination of any list of common engine faults (see previous section) suggests that:

a) Most, if not all, of the damage modes relate to quite specific changes in only one or two blade rows of the turbomachinery.

b) Some damage modes such as tip clearance changes and seal leakage changes have been well recorded by industry. Many others are observed during overhaul but little is known about their effect on the component characteristic.

c) Damage mode data which does exist is almost always in the form of stage data; not in the form of component map changes and/or effects on engine measurements.

The above suggests that the logical starting point in building up a component based model of an engine which is intended as a tool for EHM system design is the stage data and not the overall component data.

Estimation of Stage Characteristics

The methods developed by GasTOPS Ltd. for estimation of stage characteristics have been published elsewhere [5, 6] and will be reviewed here for completeness. Only the compressor characteristics will be considered.

In general, the performance of any compressor stage can be presented in non-dimensional form as shown in Figure 4. Such data are particular to a specific design; however, by selecting a reference condition (usually the point of maximum efficiency), it was found that these data could be generalized to a very great extent. Figure 5 shows data collected from a number of sources for which a mean curve has been established. A similar generalized efficiency curve is shown in Figure 6.

If the individual performance characteristics of each axial compressor stage are known, overall compressor performance over a range of rotational speeds and mass flows can be estimated by a stage stacking procedure which is well established in the industry [7, 8, 9].

However, in general, the individuals stage characteristics are not known and it becomes necessary to estimate them by using the operating line data to establish the reference conditions for the generalized data shown in Figures 5 and 6. The calculation scheme is shown in Figure 7.

As mentioned previously, once the stage data has been estimated, the overall component map can be determined for all values of rotational speed and flows of interest. Figure 8 shows the results of this estimation process as applied to the F404-CE-400 fan module.

Overall Engine Model

Much has been published on the structure of complete component based models (see for example References 10, 11, 12). The general form is similar in all circumstances and is shown for the F404-FE-400

engine in Figure 9. The reader should note that this type of calculation is set up so that differences in shaft torque and intercomponent flows are used to form a function which is to be driven to zero.

the model is to be restricted to static performance, a minimization search algorithm can be used to establish the engine parameters which will produce a minimum (zero) value of the function. Under this scheme, intermediate calculations are of no interest other than as a basis for the next parameter guess.

If the model is to be used to examine the dynamic performance of the engine, the various differences in torque and flows are used to form derivatives of speeds and pressures. Under this scheme, the derivatives are passed to a suitable integration algorithm and each successive calculation results in another time step, thus producing a time trace of the overall engine dynamic performance.

For this purpose, control inputs must either be presented as time histories or the entire control system must be modelled in enough detail to provide correct inputs to the engine model.

Control Systems Models

A fundamental underlying concept in the development of component based gas turbine models is the ability to treat each component as a unit thermodynamic process. Each component can be represented as a single continuous flow process and thereby its primary function is described.

In the case of control system modelling, there is frequently a less direct link between physical process and control function. For example, the physical processes in a full authority digital electronic control (FADEC) are immensely complex solid state electron movements within the control. These processes are of no direct interest. What is of interest is the fact that they can represent mathematical algorithms used to control the engine. Similarly, the mechanics of a more traditional hydro-mechanical control are thought of only as mathematical control functions.

The above observations suggest that the only practical means of modelling a control system for a gas turbine is along functional lines. The primary requirements for purposes of EHM system design for a control model may be simply stated as follows:

a)   It must provide complete and accurate representation of the control inputs to the engine.

b)   It must be suitable for use as a means of specifying engine test procedures and for subsequent interpretation of test results.

c)   It must be capable of simulating degradation and/or faults at the major component level of the control itself. It should be possible to embed these faults as data changes rather than modification of the control model.

As an example of the level of control system model used in the design of EHM systems, Figure 10 shows the overall block diagram for the F404-GE-400 engine control and Figure 11 shows the detailed block diagram for the Main Fuel control portion of the model. As can be seen, the model is comprised of those primary functions judged to be necessary for examination of control action of both static and dynamic type.

FAULT MODEL DEVELOPMENT

Modelling of engine faults is predicated on the singular notion that it must provide an adequate representation of the cause of the apparent engine problem. It has been argued that without an adequate scientific basis upon which to build an understanding of these cause/effect relationships, it will never be possible to generalize the design techniques to other engine programs. While there is no specific form of fault model, all have been generalized such that they can be used to represent the same type of fault in another engine.

Turbomachinery Faults

As discussed previously, most turbomachinery losses are presented as stage data or empirical data that can be used to modify stage data. This fact is fundamental to all turbomachinery fault modelling at GasTOPS Ltd.

Considering the axial flow compressor, losses in a given blade row occur in four main ways:

1)   blade surface profile losses
2)   annulus wall losses
3)   secondary flow losses
4)   shock losses

Characterization of faults as one or a combination of these effects is thus desirable since data are more readily available. It is emphasized that the modelling of faults must be presented as a modification of stage characteristics as discussed in the following sections of this lecture note.

The general approach taken by GasTOPS Ltd. in the development and implementation or turbomachinery faults is summarized in Figure 12.

For a given fault type (i.e. tip clearance increase, blade surface roughness variation, fouling, foreign object damage, erosion, etc.) and overall severity level, a fault severity factor is assigned to each individual stage with the aid of a Fault Severity Assignment Table, of which Table 1 is typical.

Individual stage fault severities are evaluated by:

$$FS_i = k_{FSi} \cdot FS_{ov}$$

The reference (maximum stage efficiency) performance points of each stage (ϕ'_{ref}, ζ'_{ref}, η'_{ref}) are then evaluated using a Reference Point Modification Table (see Table 2) and the reference points of the "healthy" compressor stages (ϕ_{ref}, ζ_{ref}, η_{ref}). That is, for each stage, i:

$$k_\phi, k_\zeta, k_\eta = f(FS_i)$$

$$and \; \phi'_{ref} = k_\phi \cdot \phi_{ref}$$

$$\zeta'_{ref} = k_\zeta \cdot \zeta_{ref}$$

$$\eta'_{ref} = k_\eta \cdot \eta_{ref}$$

Stage Number	Relative Fault Severity (k_{FS})
1	0.1
2	0.3
3	0.5
4	0.7
5	1.0
6	1.0
7	1.2
8	1.3

Table 1   Typical Fault Severity Assignment

Fault Severity	k_ϕ	k_ζ	k_η
0	1.00	1.00	1.00
1	0.96	0.99	0.95
2	0.92	0.98	0.90
3	0.88	0.97	0.85
4	0.84	0.96	0.80
5	0.80	0.95	0.75
6	0.76	0.94	0.70
7	0.72	0.93	0.65
8	0.68	0.92	0.60
9	0.64	0.91	0.55
10	0.60	0.90	0.50

Table 2   Reference Point Modification

Having determined the reference operating conditions of each stage, generalized stage performance correlations for efficiency and temperature rise, as shown in Figure 13 and 14, are used to evaluate the stage characteristics of the "faulted" compressor. Recall that the stage pressure rise coefficient may be obtained from the stage efficiency and temperature rise coefficient by:

$$\psi = \eta_s \cdot \zeta$$

The faulted stage characteristics are then "stacked" to obtain an estimate of overall compressor performance.

In summary, the fault model for a specific mode of axial compressor degradation contains the following elements:

1. A Fault Severity Assignment Table which, given an overall fault severity level, specifies the fault severity to be assigned to each stage.

2. A Reference Point Modification Table which may be used, along with fault severity and the healthy compressor reference points, to determine the reference operating conditions of each stage.

3. A generalized stage efficiency correlation

$$\eta_s/\eta'_{ref} = f \; (\zeta/\zeta'_{ref}) \; / \; (\phi/\phi'_{ref})$$

4. A generalized stage temperature rise coefficient correlation:

$$\zeta/\zeta'_{ref} = f(\phi/\phi'_{ref}, Fault \; Severity)$$

Tip Clearance Model

A tip clearance fault model for an axial flow compressor has been developed by GasTOPS Ltd. based on the results of Smith [13]. Generalized plots of Smith's data are given in Figure 15 and the equivalent Reference Point Modification Factor Table for Smith's results can be summarized as follows:

ϵ	k_ϕ	k_ζ	K_η
.0080	1.000	1.000	1.000
.0142	1.009	0.971	0.989
.0253	1.023	0.928	0.967
.0364	1.035	0.878	0.962

The 0.8% tip clearance results have been used as a datum since the generalized efficiency plot for this clearance value closely matches the generalized efficiency curve used by GasTOPS Ltd. to model "healthy" compressor stages.

Figure 16 presents the estimated change in overall compressor performance for a fault severity equal to 5. Note that the percentage flow reduction is approximately 3% while the percentage

efficiency reduction is about 2 points. This 2:3, efficiency/flow, reduction is similar to published results as indicated in Figure 17.

Control System Faults

Basic turbomachinery tends to be fairly reliable; however, when faults do occur they tend to be very expensive. On the other hand, a much larger number of faults occur due to problems with the control system components. While less expensive to repair than the basic engine, there are more of them and they tend to tie up the entire aircraft. Such problems range from sensor problems through to actual changes within the control logic hardware.

As discussed previously, these faults are modelled by modifying the function that is affected by the fault. As an example, a commonly encountered problem is in service stalls, some of which can be traced to faulty acceleration fuel schedules embedded within the main fuel control. Figure 11 shows this function of the MFC on the F404-GE-400 engine. Faults such as a worn cam, can readily be represented by modifications to the fuel schedule as shown in the figure.

MODEL VALIDATION

The development of confidence in the results produced by a computer model is inevitably a mixture of judgement and comparison with actual test results. GasTOPS Ltd. has, over the past 12 years, developed models of the following engines.

AIRBORNE	INDUSTRIAL & MARINE
GE J85	GE LM2500
GE F404	GE MS3000
P&W J57	P&W FT4
P&W JT15D	P&W FT12
P&W FT6	DDA 570K
DDA T56	SOLAR SATURN
DDA 250	WCL 352
AVCO LTS101	RR SPEY
	RR AVON

Most of these models are component based models used primarily for control systems investigations; however several of them have been developed from stage characteristics and are in constant use in the development of EHM techniques.

All of the models have been validated to a greater or less extent by comparison with engine tests thus developing confidence in the method. In the case of the F404-GE-400 engine, this model is in an advanced state of development and has been validated by comparison with test data provided by the National Research Council of Canada as well as extensive field data obtained from flight recorders fitted to the CF-18 aircraft. Figure 18 provides comparison with NRC test data indicating a very close fidelity to the actual engine.

Comparison of the dynamic performance of the F404-GE-400 engine yields similarly close results. Figure 19 shows a slam acceleration on takeoff as recorded by the on-board flight data recorder. The model performance is superimposed. The reader should note that the model is that of a nominal engine whereas, the flight data is from a specific unit.

Perhaps the most difficult area of the current model to validate is the fault models; however, even this area has shown quite good comparisons with available test data. Table 3 shows comparative data for an engine which had an HP turbine fitted with out-of-specification blades. In this particular case, data was available from the manufacturer as noted in the table. The comparison is self evident.

Table 3

F404 Performance Deviations at IRP Due to HP Turbine Blade Tip Clearance Increase

	Manufacturers Data	Model Prediction
T_{56}/θ	+ 2.1%	+ 0.5%
$N_1/\sqrt{\theta}$	+ 0.4%	0.0%
$N_2/\sqrt{\theta}$	− 1.8%	− 3.0%
$W_{fm}/\sqrt{\theta}\delta$	− 5.2%	− 7.8%
P_{s3}/δ	− 8.7%	−10.8%
P_{56}/δ	−14.3%	−14.8%
A_8	+14.5%	+16.6%
F_g/δ	− 9.0%	− 8.9%

In addition to a static comparison, it was possible to obtain additional verification by examining the engine dynamics. Figure 20 shows the flight recorded takeoff traces for the right and left engines. Figure 21 shows a simulation of the same situation. Again the comparison is self evident.

APPLICATION TO PERFORMANCE MONITORING

The foregoing described a model that is regarded by GasTOPS Ltd. as an essential tool in the development of performance monitoring systems. The following sections will describe the use of the model for this purpose.

The earliest version of this type of performance model was trialed by the Canadian Navy in 1983/84 [15]. This particular model described the FT4/FT12 engines fitted to the DDH-280 destroyer. It was a manual system insofar as data

collection was concerned. No fault libraries were used; instead, the model was run repeatedly by the operator looking for a best match with the measurement. He could select both the type of fault and its severity in seeking a match with the measurements. In addition, multiple faults could be embedded simultaneously.

A number of observations from this trial are noteworthy.

(1) The instrumentation was found to be problematic. This was unknown to the ships company up to that time.

(2) Operator running of the model was very time consuming and unless the match with measurements was quite clear the result was often ambiguous.

(3) It quickly became apparent that a _definitive_ pronouncement of the existence of a specific fault could never be made from the computer analysis. The ambiguities suggested a probabilistic statement would be more appropriate.

(4) Trending of the data, even when scatter was reduced, left the operator with no sound basis for deciding what to do. In other words a _logical_ method of declaring the fault was (a) real and (b) severe enough to make a decision had to be found.

(5) The existing measurement suite did not necessarily provide appropriate diagnostic parameters. In fact, _direct_ inspection/comparison of engine measurement signatures was not very effective in exposing problems.

This last observation is perhaps the most important. It suggested that future work should concentrate on a systematic examination of parameters which could be computed from the measurements. These parameters would then be used as indicators of faults or emerging problems with the engine. Such parameters became known at GasTOPS Ltd. as engine health indices.

The concept of an engine health index suggests that some combination of measured and/or computed parameters would be:

(1) sensitive to the fault in question
(2) insensitive to measurement scatter.

To expect unambiguous fault isolation from a single health index is perhaps asking too much: however, the parameter must be usable in conjunction with other health indices in order to build an engine fault signature which results in unambiguous diagnosis.

To establish the sensitivity of a proposed health index to a specific fault, the computer models discussed previously have proven to be invaluable tools. The steps involved are:

(1) proposal of a parameter as a means of isolating a fault
(2) running of the model in any or all operating regimes with faults modelled at various levels of severity
(3) examination of the sensitivity and potential ambiguity of the proposed parameter.

This work lead to a number of interesting parameters. For example, the relationship between the fan and compressor spool speeds was found to be extremely sensitive to problems with misrigged or improperly controlled variable compressor geometry on the F404 engine. The F404 intake airflow rate was also found to be a useful indicator of HP turbine damage; however, as shown in Figure 22 the behaviour of this health index varied considerably over the running range of the engine. Figure 23 summarizes the various health indices which have been successfully used to assess F404 engine performance under both steady state and transient operating conditions.

The second major effort was to establish that each parameter was insensitive to measurement scatter. Some model assessments were conducted but since data were readily available from the monitoring equipment, it was decided to obtain real engine data. Figure 24 shows a histogram of fan rotor acceleration times obtained from more than 10,000 F404 takeoff recordings and 250 different engines. Figure 25 presents the N_1 acceleration time trend plots from three specific engines. It is evident from Figures 24 and 25 that individual engine performance variations are small and that the N_1 acceleration time health index can be used to discriminate between engines of varying performance levels. Indeed, this health index has been used as a reliable indicator of F404 fuel metering, exhaust nozzle scheduling and HP spool blade damage faults.

A major factor in the amount of performance scatter for engines which incorporate variable gas path geometry systems is the tolerances allowed on the setup of these systems [16]. As indicated in Figure 26, the engine model can be used to simulate the effects of these tolerances and to develop correction factors or procedures to account for them. In the case of the F404 engine, the application of these correction factors resulted in a reduction in data scatter by a factor of 2 to 3.

FAULT LIBRARIES

The foregoing examples suggest the need to establish a list of common operational problems. For every fault, it is

necessary to undertake the work of establishing a method of fault isolation and diagnosis. This leads again and again to the model and the evaluation of potentially useful health indices. The complete complement of health indices comprise what has become known (at least at GasTOPS Ltd.) as the engine fault signature.

While the fault modelling effort was proven to be a most effective means of establishing cause/effect relationships and the discovery of useful health indices, it rapidly became apparent that any direct use of the model in an on-line capacity was prohibitively expensive in time and in computer capacity. It was therefore decided to approach the issue of diagnosis from the perspective of presenting the fault signature to a predetermined library of faults. The concept is shown graphically in Figure 27.

For a given measurement suite, the data is reduced to ambient conditions and the health indices computed. The difference between the current measured health indices and a known baseline provides a set of differences with which to undertake a search of the library of predetermined fault patterns.

This process is readily implemented on a computer in a fashion that permits a list of possible faults on the basis of "best fit", "2nd best fit", etc. It is emphasized that this step represents a best fit to the current measurements. It does not necessarily represent the most probable fault.

The reordering of the "best fits found" to most probable causes is established from a second library of most common problems which was the starting point in the process of establishing the health indices. The library of most common problems is a statistical database which provides frequency of event information for each fault. By weighting the quality of the data fit and the frequency of occurrence to a specific fault a list of most probable faults can be produced.

Access to the library of fault signatures is a computer search problem. Early efforts by GasTOPS Ltd. utilized in-house software developed for this purpose; however, the emergence of practical rule based expert systems makes it possible to purchase software tailored to this type of problem. The combination of fault libraries and an expert system shell makes for an efficient diagnostic module that can be used on-line.

MONITORING SYSTEM APPLICATIONS

The development of a method of diagnosis has allowed GasTOPS Ltd. to develop application systems which are useful as an element in an overall engine monitoring program [17]. In general, these application systems fall into three categories as described below:

Assessment of Periodic Engine Tests

The most fundamental element of a performance monitoring system is the ability to assess data obtained from periodic tests. In the aircraft application, this test is conducted either on the wing or more commonly in an engine test cell after a repair.

The procedure followed is very much similar to that of the previous section; however, from a system interface viewpoint, the presentation of results is important. Figure 28 shows a typical output as presented to a test cell operator. In addition to the test conditions, the as-measured and corrected (for ambient condition, power level and variable geometry effects) health index values are displayed along with their respective baseline values. Parameters which exceed pre-determined limits are assigned a "status" value which is dependent on the magnitude of the performance deviation(s). The status indicators are then related to potential component problems and a written recommendation is presented to the operator for decision/action purposes. It is noteworthy that the test cell operator still exercises final judgement, but is guided in his decision by the recommendations provided by the diagnostic system.

Trending of Health Indices

A working trend package consists of the ability to collect data, compute the health indices discussed previously and to present deviations in these health indices as a function of time. A typical trend plot is shown in Figure 29. This plot shows the variation in the parameter within the framework of upper and lower acceptable limits and in the specific case shown indicates a progressively deteriorating situation. Once the data falls outside the limits a flag is set by the software indicating to the operator that a fault is developing. The fault type is identified and where possible the rate of progression is tied to numbers of hours before action is taken.

The ability to provide some early warning of pending faults is critical to the success of a monitoring program. In the case of the F404, a lead time of 10 days allows for rescheduling of aircraft and the planning of work in the engine repair shop. Clearly this is a function of the rate of engine deterioration which in turn is a function of the operation. Despite the obvious statistical/operational variation, a health index only becomes truly worthwhile when it provides the operator with some advance warning of the event.

Dynamic Event Analysis

Intuitively, operators of gas turbines are aware that the first signs of engine distress are most likely to occur during

a transient. Under these conditions, the operating point of the compressor is traversing a path relatively close to surge; the temperatures are typically 100-200° hotter than steady state conditions. Similarly, the rate of growth of the casing is different from the rotors which changes blade tip clearances, seal clearance, etc. These physical effects are difficult to quantify; however, there is little doubt in the industry that a deteriorated engine has smaller margins available for handling transient situations than does a healthy engine. Under these conditions, dynamic events occur such as compressor stall, over temperature, etc. These events afford an opportunity for performance analysis to be used, provided reasonable data records are available.

Most modern flight recorders contain the capability to capture data at the rate of from 5 to 10 hz. These data are momentarily held in a rotating log of approximately 40-60 seconds on a first in - first out basis. This feature allows the system to capture a transient record surrounding an event.

The availability of transient information extends the range of possible health indices. These can include such parameters as the rates of change, maximum values, or specific fuel control parameters; however, the process of qualifying any of these as a valid health index is identical to those for steady state analysis.

For example, one particularly useful indicator of F404 engine transient misbehaviour has been the fuel acceleration schedule parameter, W_f/P_c. A number of stalls on takeoff lead to an investigation of problems in this area. It was found that the fuel was scheduled using this parameter and that the parameter could be computed from the data in the rotating log. Figure 30 presents the fuel acceleration schedule parameter recordings obtained before and after the removal of a Main Fuel Control (MFC) from an F404 engine which experienced a flameout on takeoff.

In general, the development of methods to assess problems related to dynamic events has proven to be remarkably productive. One must realize that the event must be dealt with by the maintenance crew. This places the burden of establishing cause on them. Without diagnostic tools, they normally resort to changing field replaceable units such as fuel controls until the problem appears to go away. This is unsatisfactory at best and usually leads to unnecessary expense driven partly by changeout of the wrong component and partly by the high costs of testing various attempted fixes.

FUTURE WORK

Considerable progress has been made in the field of performance analysis

methods for application to engine health monitoring.

To a large extent, this progress has been paced by the availability of component fault modelling techniques capable of systematically investigating the effects of common engine problems on overall performance.

The models described herein have successfully demonstrated the basic methodology of fault investigation leading to the definition of fault libraries based on proven health indices. Nevertheless, there is considerable scope for additional work.

a) Cause/Effect Relationships

As previously stated for those engine problems which we related to design such as tip clearances, variable geometry rigging, etc. there is adequate stage data available in the literature to develop a good fault model. These, in turn, allow the investigation/development of health indices for a given engine. However, for many faults, empirical data simply do not exist. In general, these cases fall into the category of operational damage caused by poor quality fuel, severe thermal damage and foreign object damage. These forms of damage are not parameters of the design and are thus not commonly investigated from the perspective of the impact on performance.

There is very considerable scope for research into the cause/effect relationship of these forms of damage. Furthermore, it is emphasized that the researcher need not have access to complete engines. It has been demonstrated that stage data obtainable from rigs is completely adequate for the purpose and indeed is preferable since it affords the opportunity to develop more generalized descriptions of the phenomena.

b) Fault Library Extension

While the author's company has had considerable success with both marine and airborne engines, the number of proven health indices and the extent of the fault library is quite small. There is much scope for additional studies to qualify new health indices which deal with less significant faults and to improve the quality of diagnosis for those already considered.

The work of fault library extension can readily be extended to consider different or more comprehensive measurement suites. Work to date has been restricted to only the measurement suite provided by the existing instrumentation.

c) Damage Avoidance Strategies

As more becomes known about the cause/effect relationships of damage mode/measurement combinations, it becomes interesting to speculate on the extent of damage caused by various operational strategies.

Currently, the best that we can do is to recognize the damage; however, further work might suggest that specific operations are much more costly than others and can be avoided or minimized. Such investigations may eventually lead to onboard expert system advisors to the pilot which would provide him with options to achieve the same goal.

All of the above work can be accomplished with the aid of gas turbine models as described in this lecture note. It is anticipated that full development of these capabilities will enable designers to fully specify EHM systems during the course of engine development to the level where they are largely proven at the time the engine is fielded.

References

1. MacMillan, W.L. "Propulsion Systems Technology Drives & Issues for the 1990's" AGARD Highlights, Sept. 1989

2. Kandl, M.G., and Groghan, D.A. "U.S. Navy LM2500 Gas Turbine Condition Monitoring Development Program" ASME 80-GT-158, 1980

3. Urban, L.A. "Parameter Selection for Multiple Fault Diagnostics of Gas Turbine Engines" AGARD-CP-165, 1974

4. Saravanamuttoo, H.I.H. "Gas Path Analysis for Pipeline Gas Turbines" Proceedings of 1st Symposium on Gas Turbine Operations and Maintenance National Research Council of Canada, 1974

5. Muir, D.E., Saravanamuttoo, H.I.H., and Marshall, D.J. "Health Monitoring of Variable Geometry Gas Turbines for the Canadian Navy" ASME J. of Engr. for Gas Turbines & Power Vol. III, April 1989

6. Muir, D.E. "Axial Flow Compressor Modelling for Engine Health Monitoring Studies" M.Eng. Thesis, Carleton Univ., Ottawa, Canada, 1988

7. Robbins, W.H., and Dugan, J.F. "Predictions of Off-Design Performance of Multi-Stage Compressors NASA SP-36, 1965

8. Stone, A. "Effects of Stage Characteristics and Matching an Axial Flow Compressor Performance" Trans ASME, Vol. 80, p. 1273 1958

9. Doyle, M.D. and Dixon, S.L. "The Stacking of Compressor Stage Characteristics to Give an Overall Compressor Performance Map" Aeronautical Quarterly, Nov. 1962

10. Saravanamuttoo, H.I.H. and Fawke, A.J. "Simulation of Gas Turbine Dynamic Performance" ASME Paper No. 70-GT-23, 1970

11. Seldner, K., Mikaloew, J.R. and Blaha, R.J. "Generalized Simulation Technique for Turbojet Engine System Analysis" NASA TN D-6610, 1972

12. MacIsaac, B.D. and Saravanamuttoo, H.I.H. "A Comparison of Analog, Digital and Hybrid Computer Techniques for Simulation of Gas Turbine Performance" ASME Paper No. 75-GT-127, March 1974

13. Smith, L.H. Jr. "Casing Boundary Layers in Axial Flow Compressors" From Flow Research on Blading L.S. Dzung, Elsevier Pub. 1970

14. Richardson, J.H. et al "Causes of High Pressure Compressor Deterioration in Service" AIAA 79-1234

15. MacGillivray, P.J., MacIsaac, B.D., and Saravanamuttoo, H.I.H. "Development of Diagnostic Models for Marine Gas Turbines" ASME Paper No. 84-GT-221, 1984

16. Muir, D.E.; Rudnitski, D.M. and Cue, R.W. "CF-18 Engine Performance Monitoring" Paper #7, AGARD CP-448

17. Cue, R.W. and Muir, D.E. "Engine Performance Monitoring and troubleshooting Techniques for the CF-19 Aircraft" ASME Paper 90-GT-357, June 1990
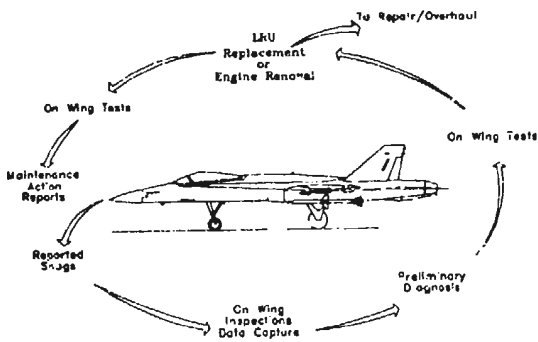
Figure 1-a   Flight Line Repair Environment
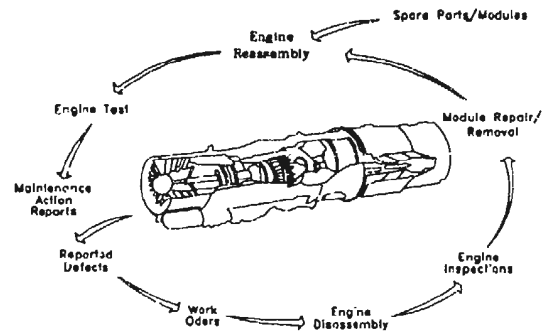
Figure 1-b   Engine Repair Shop Environment
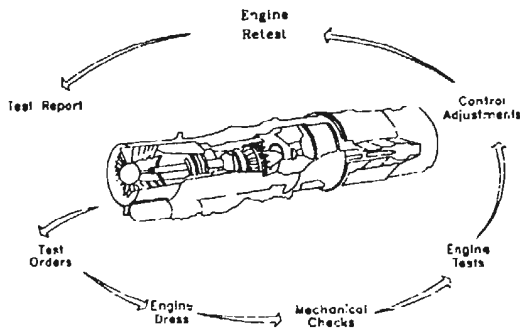
Figure 1-c   Engine Test Environment
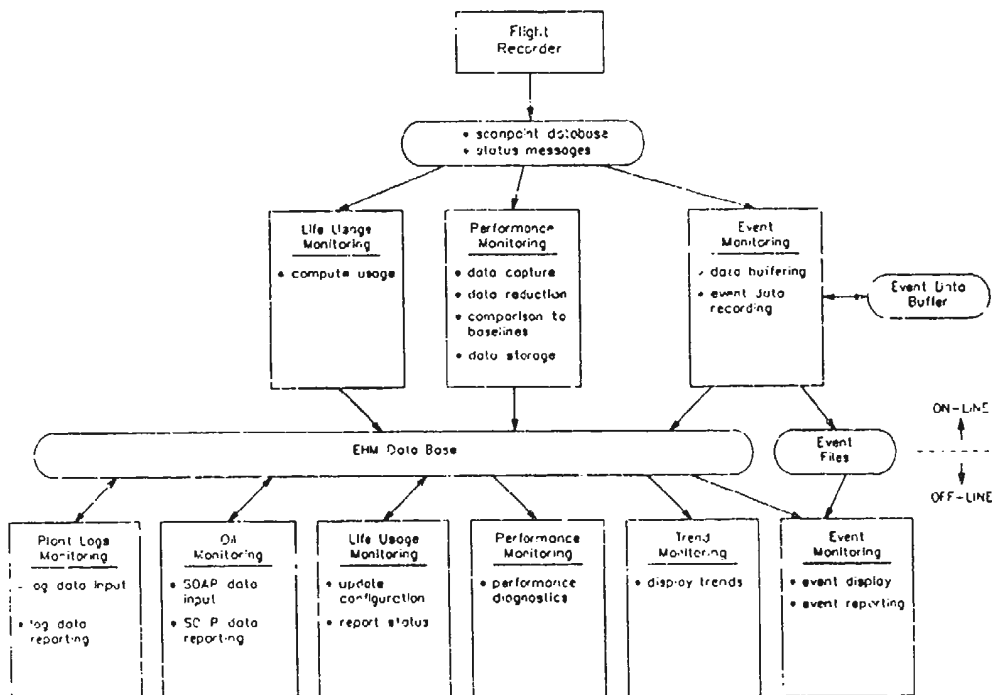
Figure 2   Overview of EHM System
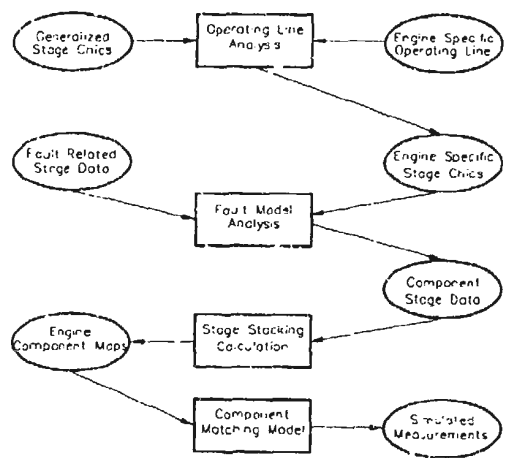
Figure 3   Overall Modelling Concept
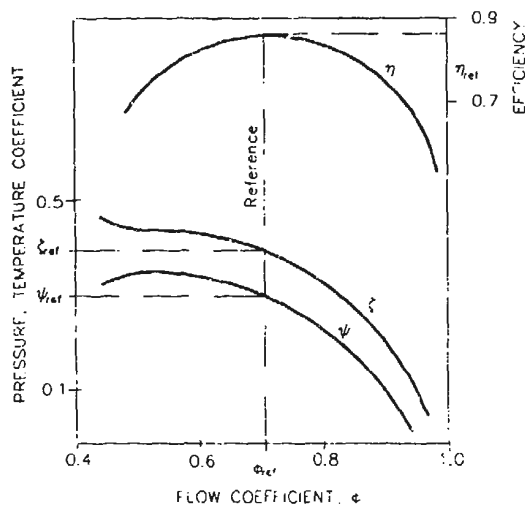
Figure 4   Compressor Stage Characteristics
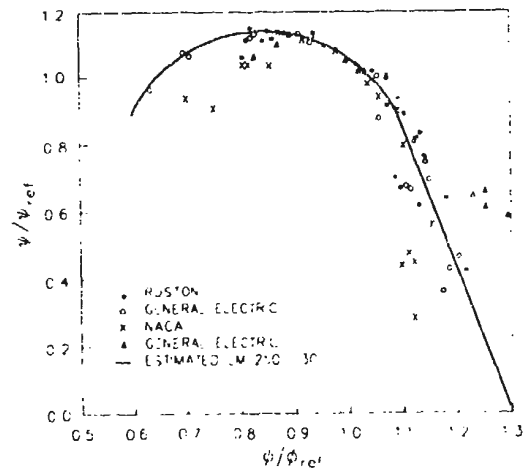
Figure 5   Generalized Stage Pressure Rise Coefficient
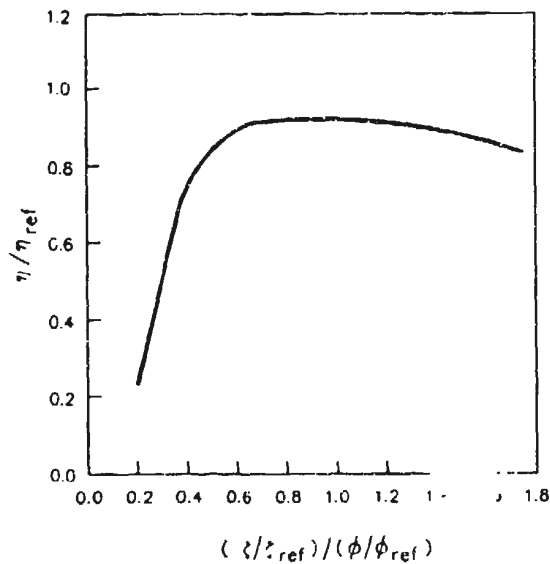
Figure 6   Generalized Stage Efficiency Characteristic
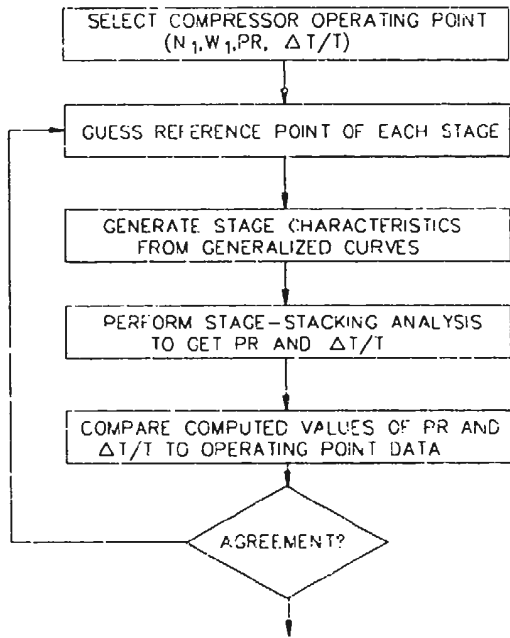
Figure 7   Flowchart for Compressor Characteristic Development
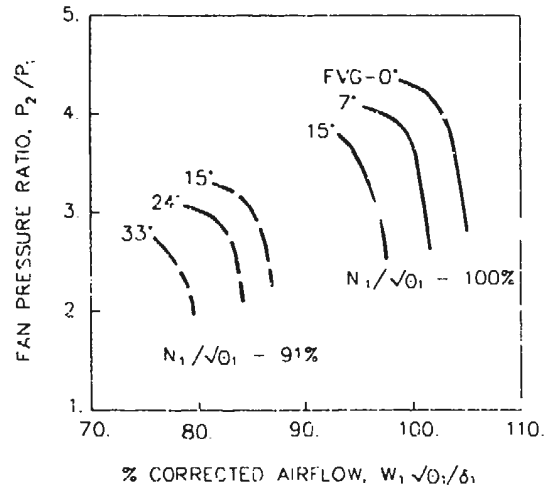
Figure 8   Estimated F404-GE-400 Fan Characteristic
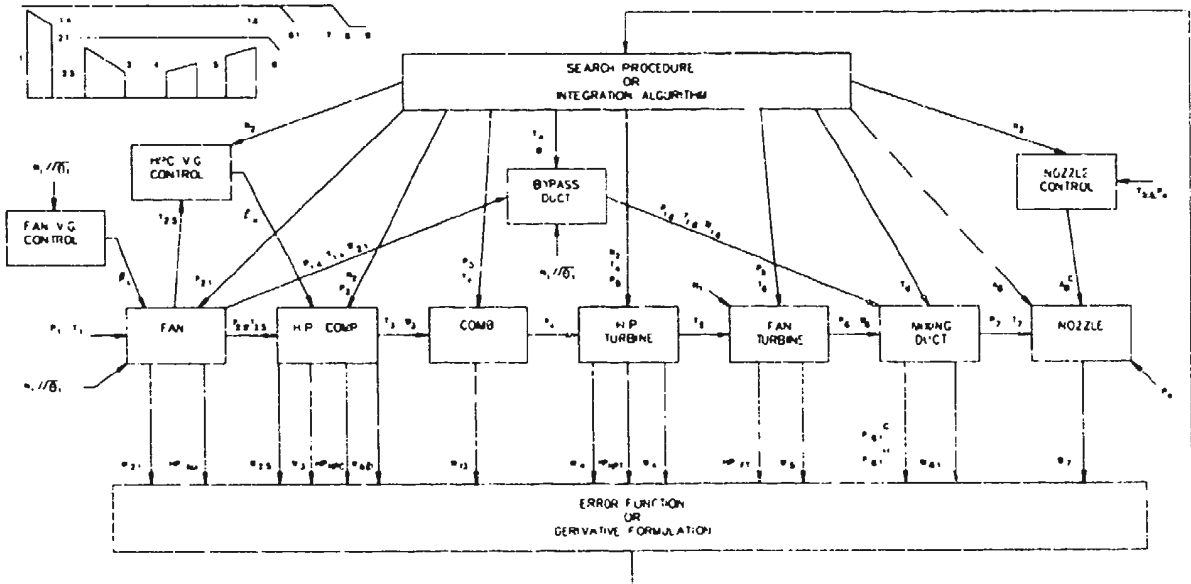
Figure 9   Overall Block Diagram for F404-GE-400 Engine Model
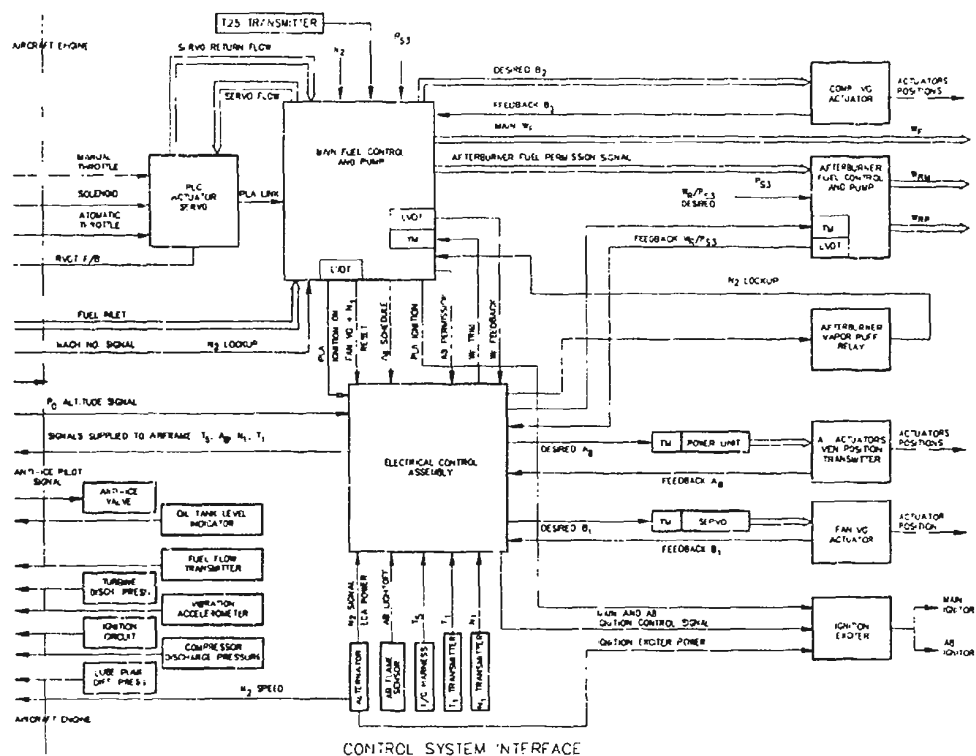
Figure 10 Overall Control System Structure
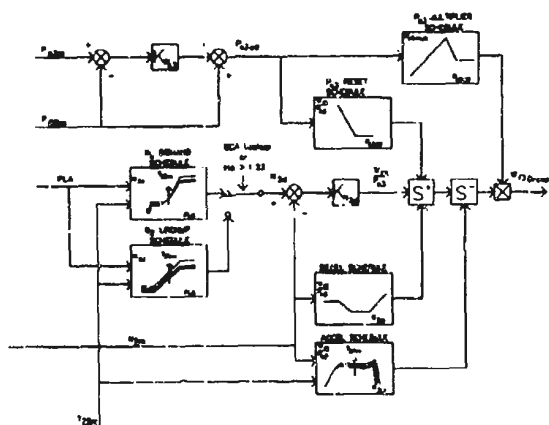
Figure 11 Main Fuel Control Model
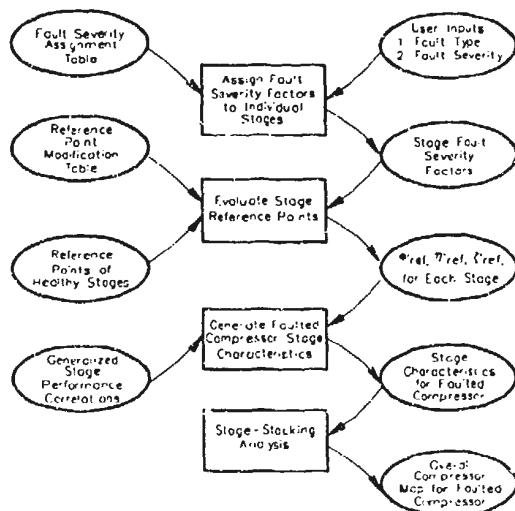
Figure 12 Axial Compressor Fault Modelling
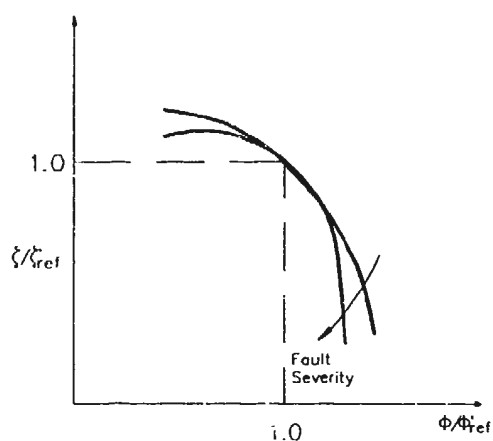
Figure 13 Typical Variation in Stage Pressure Rise due to Degradation
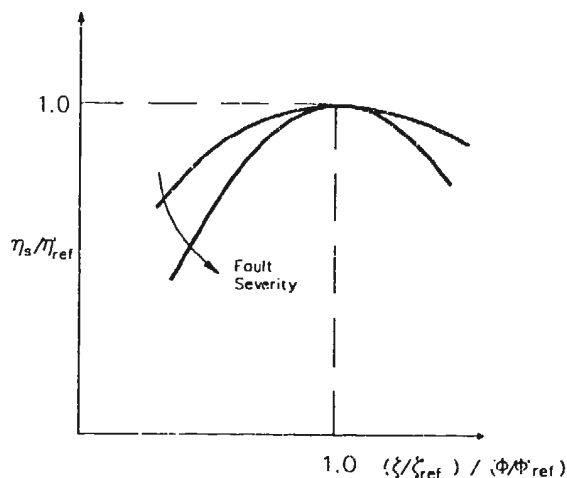
Figure 14 Typical Variation in Stage Efficiency due to Degradation
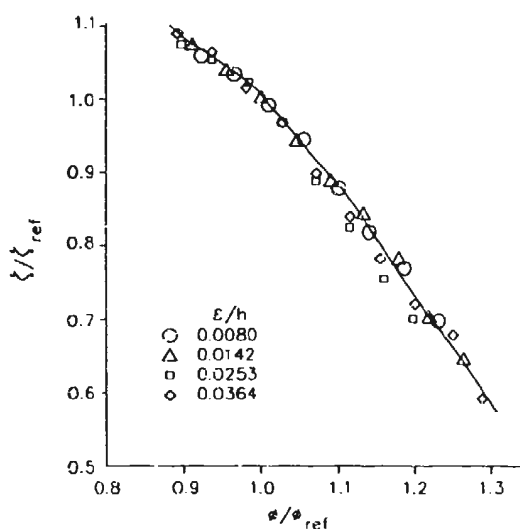
Figure 15 Generalized Stage Tip Clearance Correlation (Smith Data Ref.)
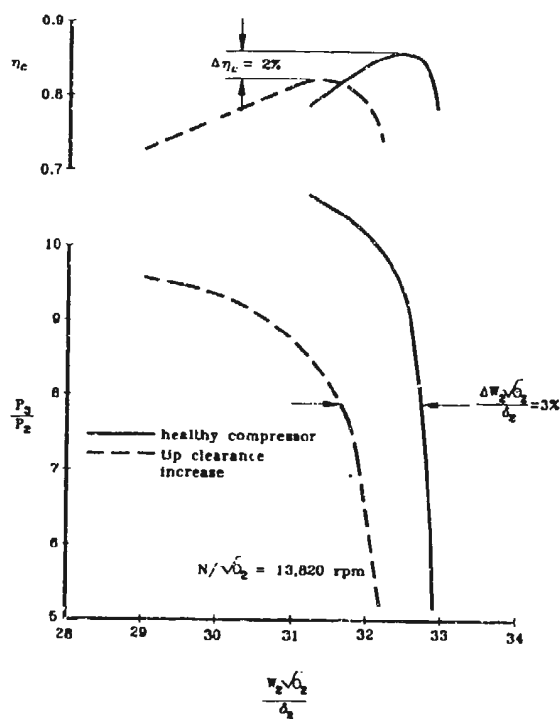
Figure 16 Predicted Influence of Tip Clearance on Axial Compressor Performance
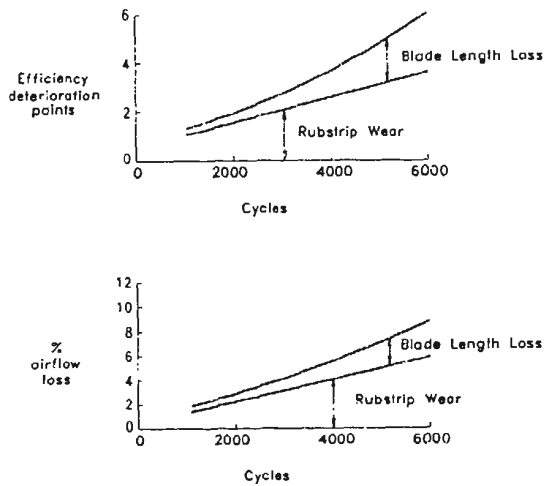
Figure 17　Influence of Tip Clearance on High Pressure Compressor Performance (Ref. 14)
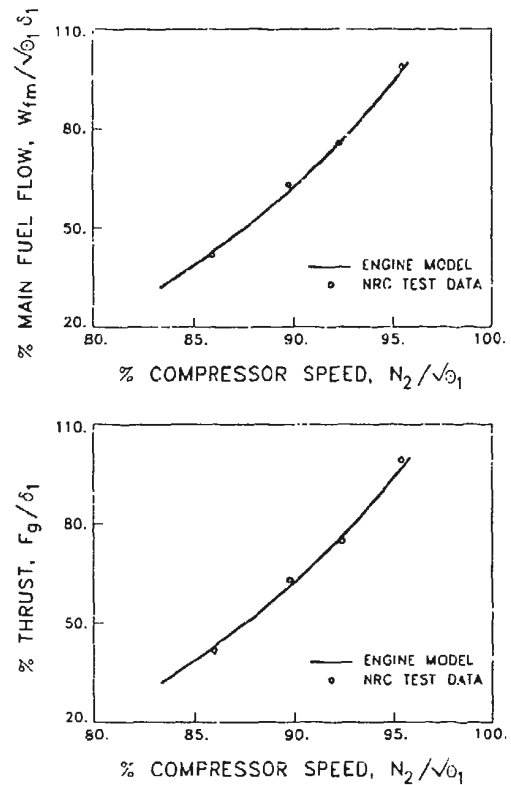
Figure 18　Steady State Performance of F404-GE-4(.) Engine
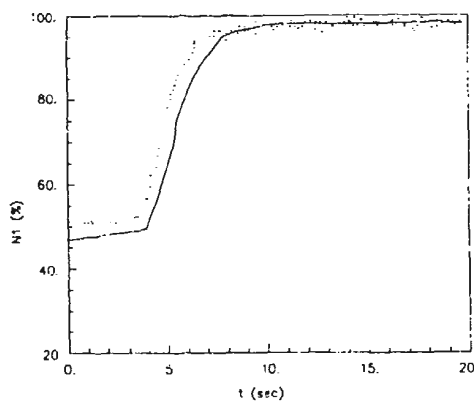
Figure 19-a　Comparison of Model Fan Speed Performance with Flight Data
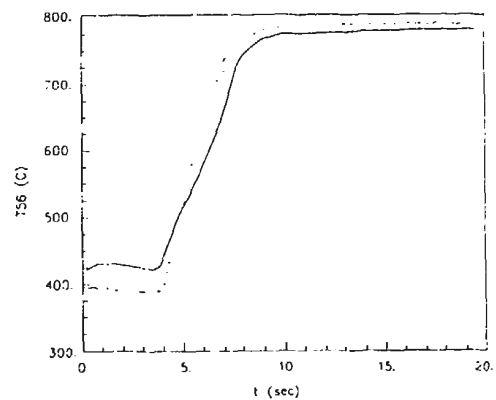
Figure 19-b　Comparison of Model EGT Performance with Flight Data
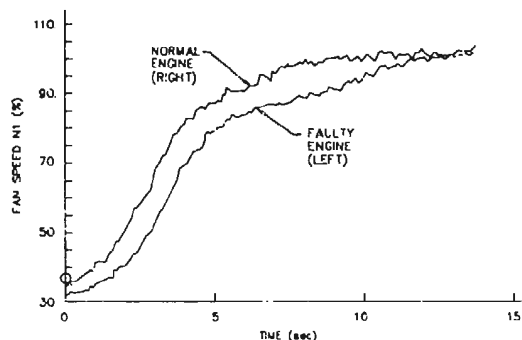
Figure 20   Flight Record of Engine
Dynamic Performance with
Damaged HP Turbine
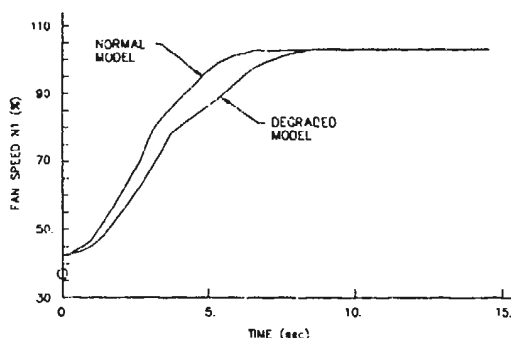
Figure 21   Model Prediction of Engine
Dynamic Performance with
Damaged HP Turbine
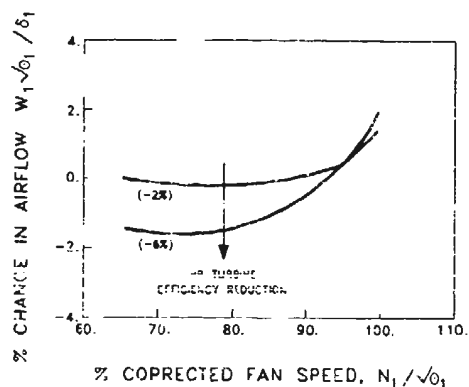
Figure 22   Air Flow Variation with
Engine Operating Level with
HP Turbine Damage

STEADY–STATE	TRANSIENT
Airflow	N Accel Time
N_2/N_1	N_2/N_1
Thrust	Maximum Thrust
Fuel Flow	Fuel Ratio Units
CJP	Minimum VEN Position
EGT	
EPR	

Figure 23   F404 Engine Health Indices
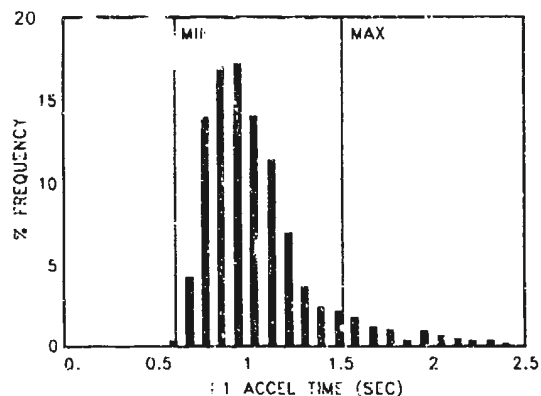
Figure 24   Histogram of N_1 Acceleration
Times Over Many Flights
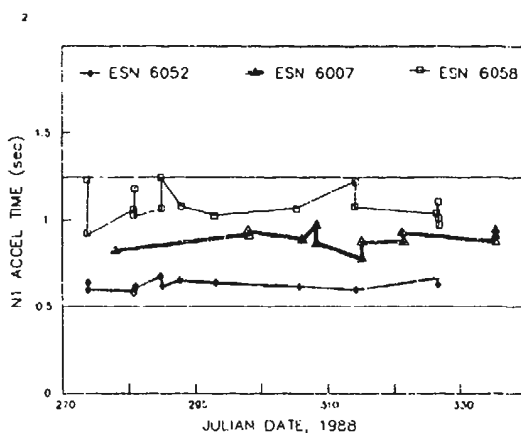
Figure 25   Trend Plots of Different
F404-GE-400 Engines

Figure 27 Fault Diagnostic Procedure
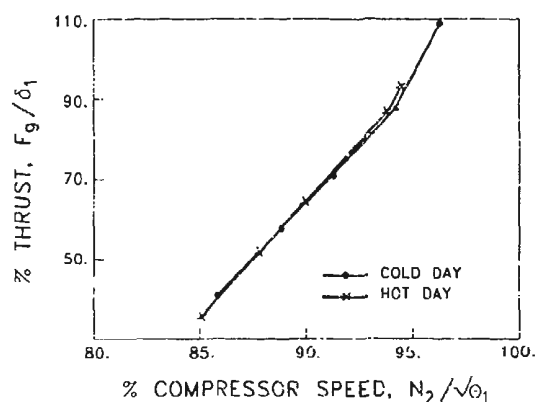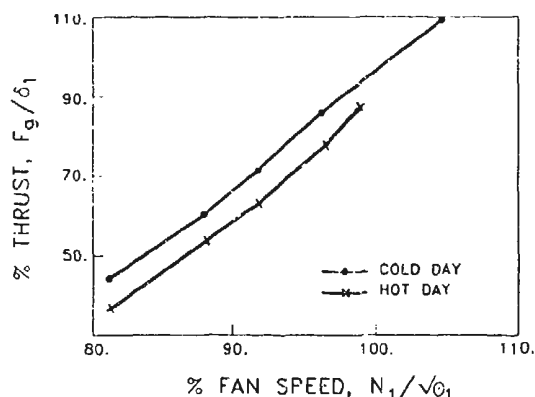
Figure 26 The Effect of Choice of
Engine Baseline Parameter on
Data Scatter
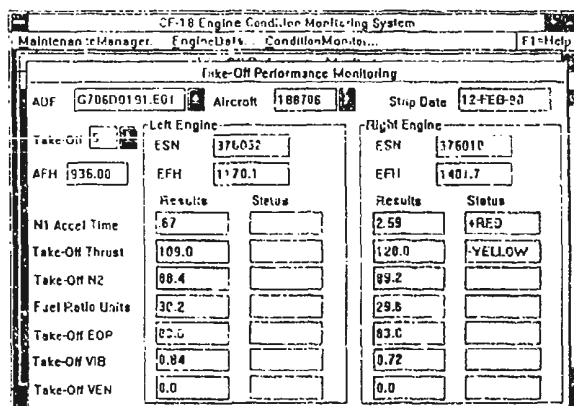
Figure 28-a Typical Diagnostic Output
to Operator
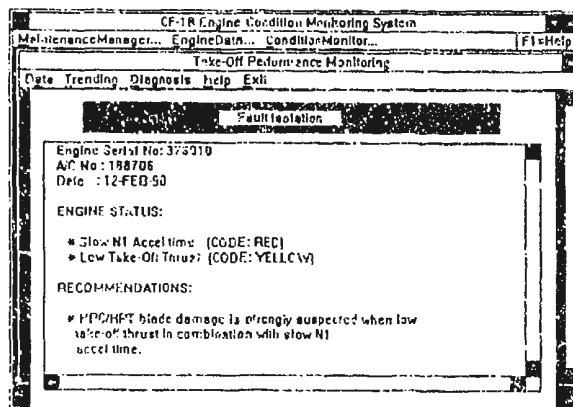
Figure 28-b Typical Diagnosis Provided
to Operator

CF-18 EHM — PERFORMANCE TREND RECORD FOR ENGINE 6148
PARAMETER: N1 75-85% ACCEL TIME   DATE: 29-09-88

MAINTENANCE SUMMARY

A- ADP No. : KKK001   TIME :   795.0
   SN 6148 (R) — LPT MODULE CHANGED

B- ADP No : VM1234   TIME :   821.0
   SN 6148 (R) — FOD CHECK — NO FAULT FOUND (SERV)
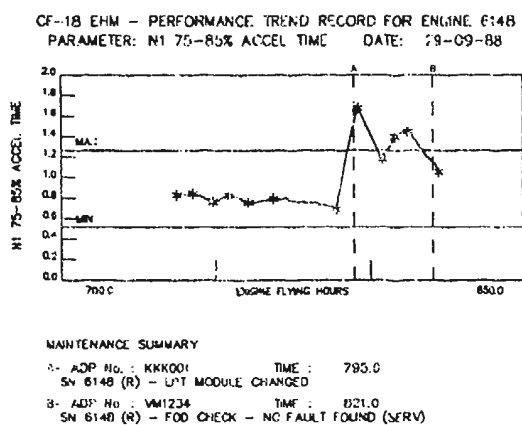
Figure 29   Typical Trend Plot of Health Index
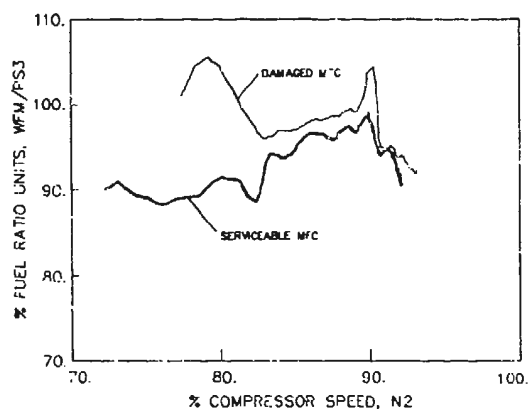
Figure 30   Transient Record of Damaged Main Fuel Control

REPORT DOCUMENTATION PAGE

1. Recipient's Reference	2. Originator's Reference	3. Further Reference	4. Security Classification of Document
	AGARD-LS-183	ISBN 92-835-0674-X	UNCLASSIFIED

5. Originator	Advisory Group for Aerospace Research and Development North Atlantic Treaty Organization 7 Rue Ancelle, 92200 Neuilly sur Seine, France

6. Title	STEADY AND TRANSIENT PERFORMANCE PREDICTION OF GAS TURBINE ENGINES

7. Presented on	27th—28th May 1992 in Cambridge, MA, United States, 9th—10th June 1992 in Neubiberg, Germany and 11th—12th June in Châtillon/Bagneux (near Paris), France.

8. Author(s)/Editor(s)	9. Date
Various	May 1992

10. Author's/Editor's Address	11. Pages
Various	190

12. Distribution Statement	This document is distributed in accordance with AGARD policies and regulations, which are outlined on the back covers of all AGARD publications.

13. Keywords/Descriptors

Aerothermodynamics	Predictions
Gas turbine engines	Computerized simulation
Engine condition monitoring	Aircraft engines
Performance	

14. Abstract

This Lecture Series covers topics of aero-thermodynamic performance prediction methods for gas turbine engines with respect to steady and transient operation. This includes advanced cycle calculation methods, also taking into account variable cycle engine types. A very important objective is the consideration of installation effects, i.e. Reynolds number and inlet distortions, as well as advanced control concepts for increasing engine surge margins. In addition to these topics, individual papers include practical considerations in designing the engine cycle, dynamic simulation, inlet distortion effects in aircraft propulsion system integration, "smart" engines, performance and health monitoring models.

This Lecture Series, sponsored by the Propulsion and Energetics Panel of AGARD, has been implemented by the Consultant and Exchange Programme.

AGARD-LS-183

Aerothermodynamics
Gas turbine engines
Engine condition monitoring
Performance
Predictions
Computerized simulation
Aircraft engines

AGARD Lecture Series 183
Advisory Group for Aerospace Research and
Development, NATO
STEADY AND TRANSIENT PERFORMANCE
OF GAS TURBINE ENGINES
Published May 1992
190 pages

This Lecture Series covers topics of aero-thermodynamic performance prediction methods for gas turbine engines with respect to steady and transient operation. This includes advanced cycle calculation methods, also taking into account variable cycle engine types. A very important objective is the consideration of installation effects, i.e. Reynolds number and inlet distortions, as well as advanced control concepts for increasing engine surge

P.T.O.

AGARD-LS-183

Aerothermodynamics
Gas turbine engines
Engine condition monitoring
Performance
Predictions
Computerized simulation
Aircraft engines

AGARD-LS-183

Aerothermodynamics
Gas turbine engines
Engine condition monitoring
Performance
Predictions
Computerized simulation
Aircraft engines

AGARD Lecture Series 183
Advisory Group for Aerospace Research and
Development, NATO
STEADY AND TRANSIENT PERFORMANCE
OF GAS TURBINE ENGINES
Published May 1992
190 pages

This Lecture Series covers topics of aero-thermodynamic performance prediction methods for gas turbine engines with respect to steady and transient operation. This includes advanced cycle calculation methods, also taking into account variable cycle engine types. A very important objective is the consideration of installation effects, i.e. Reynolds number and inlet distortions, as well as advanced control concepts for increasing engine surge

P.T.O.

AGARD-LS-183

Aerothermodynamics
Gas turbine engines
Engine condition monitoring
Performance
Predictions
Computerized simulation
Aircraft engines

AGARD Lecture Series 183
Advisory Group for Aerospace Research and
Development, NATO
STEADY AND TRANSIENT PERFORMANCE
OF GAS TURBINE ENGINES
Published May 1992
190 pages

This Lecture Series covers topics of aero-thermodynamic performance prediction methods for gas turbine engines with respect to steady and transient operation. This includes advanced cycle calculation methods, also taking into account variable cycle engine types. A very important objective is the consideration of installation effects, i.e. Reynolds number and inlet distortions, as well as advanced control concepts for increasing engine surge

P.T.O.

margins. In addition to these topics, individual papers include practical considerations in designing the engine cycle, dynamic simulation, inlet distortion effects in aircraft propulsion system integration, "smart" engines, performance and health monitoring models.

This Lecture Series, sponsored by the Propulsion and Energetics Panel of AGARD and the Consultant and Exchange Programme of AGARD presented on 27th—28th May 1992 in Cambridge, MA, United States, 9th—10th June 1992 in Neubiberg, Germany and 11th—12th June 1992 in Châtillon/Bagneux (near Paris), France.

ISBN 92-835-0674-X

AGARD

NATO ✈ OTAN

7 RUE ANCELLE · 92200 NEUILLY-SUR-SEINE

FRANCE

Téléphone (1)47.38.57.00 · Télex 610 176
Télécopie (1)47.38.57.99

L'AGARD ne détient pas de stocks de ses publications, dans un but de distribution générale à l'adresse ci-dessus. La diffusion initiale des publications de l'AGARD est effectuée auprès des pays membres de cette organisation par l'intermédiaire des Centres Nationaux de Distribution suivants. A l'exception des Etats-Unis, ces centres disposent parfois d'exemplaires additionnels; dans les cas contraire, on peut se procurer ces exemplaires sous forme de microfiches ou de microcopies auprès des Agences de Vente dont la liste suite.

CENTRES DE DIFFUSION NATIONAUX

ALLEMAGNE
Fachinformationszentrum,
Karlsruhe
D-7514 Eggenstein-Leopoldshafen 2

BELGIQUE
Coordonnateur AGARD-VSL
Etat-Major de la Force Aérienne
Quartier Reine Elisabeth
Rue d'Evere, 1140 Bruxelles

CANADA
Directeur du Service des Renseignements Scientifiques
Ministère de la Défense Nationale
Ottawa, Ontario K1A 0K2

DANEMARK
Danish Defence Research Board
Ved Idractsparken 4
2100 Copenhagen Ø

ESPAGNE
INTA (AGARD Publications)
Pintor Rosales 34
28008 Madrid

ETATS-UNIS
National Aeronautics and Space Administration
Langley Research Center
M/S 180
Hampton, Virginia 23665

FRANCE
O.N.E.R.A. (Direction)
29, Avenue de la Division Leclerc
92322 Châtillon Cedex

GRECE
Hellenic Air Force
Air War College
Scientific and Technical Library
Dekelia Air Force Base
Dekelia, Athens TGA 1010

ISLANDE
Director of Aviation
c/o Flugrad
Reykjavik

ITALIE
Aeronautica Militare
Ufficio del Delegato Nazionale all'AGARD
Aeroporto Pratica di Mare
00040 Pomezia (Roma)

LUXEMBOURG
Voir Belgique

NORVEGE
Norwegian Defence Research Establishment
Attn: Biblioteket
P.O. Box 25
N-2007 Kjeller

PAYS-BAS
Netherlands Delegation to AGARD
National Aerospace Laboratory NLR
Kluyverweg 1
2629 HS Delft

PORTUGAL
Portuguese National Coordinator to AGARD
Gabinete de Estudos e Programas
CLAFA
Base de Alfragide
Alfragide
2700 Amadora

ROYAUME UNI
Defence Research Information Centre
Kentigern House
65 Brown Street
Glasgow G2 8EX

TURQUIE
Milli Savunma Başkanlığı (MSB)
ARGE Daire Başkanlığı (ARGE)
Ankara

LE CENTRE NATIONAL DE DISTRIBUTION DES ETATS-UNIS (NASA) NE DETIENT PAS DE STOCKS
DES PUBLICATIONS AGARD ET LES DEMANDES D'EXEMPLAIRES DOIVENT ETRE ADRESSEES DIRECTEMENT
AU SERVICE NATIONAL TECHNIQUE DE L'INFORMATION (NTIS) DONT L'ADRESSE SUIT.

AGENCES DE VENTE

National Technical Information Service (NTIS)	ESA/Information Retrieval Service European Space Agency	The British Library Document Supply Division
5285 Port Royal Road	10, rue Mario Nikis	Boston Spa, Wetherby
Springfield, Virginia 22161	75015 Paris	West Yorkshire LS23 7BQ
Etats-Unis	France	Royaume Uni

Les demandes de microfiches ou de photocopies de documents AGARD (y compris les demandes faites auprès du NTIS) doivent comporter la dénomination AGARD, ainsi que le numéro de série de l'AGARD (par exemple AGARD-AG-315). Des informations analogues, telles que le titre et la date de publication sont souhaitables. Veuiller noter qu'il y a lieu de spécifier AGARD-R-nnn et AGARD-AR-nnn lors de la commande de rapports AGARD et des rapports consultatifs AGARD respectivement. Des références bibliographiques complètes ainsi que des résumés des publications AGARD figurent dans les journaux suivants:

Scientifique and Technical Aerospace Reports (STAR)
publié par la NASA Scientific and Technical
Information Division
NASA Headquarters (NTT)
Washington D.C. 20546
Etats-Unis

Government Reports Announcements and Index (GRA&I)
publié par le National Technical Information Service
Springfield
Virginia 22161
Etats-Unis

(accessible également en mode interactif dans la base de
données bibliographiques en ligne du NTIS, et sur CD-ROM)

AGARD

NATO ⊕ OTAN

7 RUE ANCELLE · 92200 NEUILLY-SUR-SEINE

FRANCE

Telephone (1)47.38.57.00 · Telex 610 176
Telefax (1)47.38.57.99

DISTRIBUTION OF UNCLASSIFIED
AGARD PUBLICATIONS

AGARD does NOT hold stocks of AGARD publications at the above address for general distribution. Initial distribution of AGARD publications is made to AGARD Member Nations through the following National Distribution Centres. Further copies are sometimes available from these Centres (except in the United States), but if not may be purchased in Microfiche or Photocopy form from the Sales Agencies listed below.

NATIONAL DISTRIBUTION CENTRES

BELGIUM
Coordo
Etat-Ma
Quartier
Rue d'E

CANADA
Director
Dept of
Ottawa,

DENMARK
Danish
Ved Idra
2100 Co

FRANCE
O.N.E.R
29 Aven
92322 C

GERMANY
Fachinfo
Karlsruh
D-7514 L

GREECE
Hellenic Air Force
Air War College
Scientific and Technical Library
Dekelia Air Force Base
Dekelia, Athens TGA 1010

ICELAND
Director of Aviation
c/o Flugrad
Reykjavik

ITALY
Aeronautica Militare
Ufficio del Delegato Nazionale all'AGARD
Aeroporto Pratica di Mare
00040 Pomezia (Roma)

nent

ARD

Pintor Rosales 14
28008 Madrid

TURKEY
Milli Savunma Başkanlığı (MSB)
ARGE Daire Başkanlığı (ARGE)
Ankara

UNITED KINGDOM
Defence Research Information Centre
Kentigern House
65 Brown Street
Glasgow G2 8EX

UNITED STATES
National Aeronautics and Space Administration (NASA)
Langley Research Center
M/S 180
Hampton, Virginia 23665

THE UNITED STATES NATIONAL DISTRIBUTION CENTRE (NASA) DOES NOT HOLD
STOCKS OF AGARD PUBLICATIONS, AND APPLICATIONS FOR COPIES SHOULD BE MADE
DIRECT TO THE NATIONAL TECHNICAL INFORMATION SERVICE (NTIS) AT THE ADDRESS BELOW.

SALES AGENCIES

National Technical
Information Service (NTIS)
5285 Port Royal Road
Springfield, Virginia 22161
United States

ESA/Information Retrieval Service
European Space Agency
10, rue Mario Nikis
75015 Paris
France

The British Library
Document Supply Centre
Boston Spa, Wetherby
West Yorkshire LS23 7BQ
United Kingdom

Requests for microfiches or photocopies of AGARD documents (including requests to NTIS) should include the word 'AGARD' and the AGARD serial number (for example AGARD-AG-315). Collateral information such as title and publication date is desirable. Note that AGARD Reports and Advisory Reports should be specified as AGARD-R-nnn and AGARD-AR-nnn, respectively. Full bibliographical references and abstracts of AGARD publications are given in the following journals:

Scientific and Technical Aerospace Reports (STAR)
published by NASA Scientific and Technical
Information Division
NASA Headquarters (NTT)
Washington D.C. 20546
United States

Government Reports Announcements and Index (GRA&I)
published by the National Technical Information Service
Springfield
Virginia 22161
United States

(also available online in the NTIS Bibliographic
Database or on CD-ROM)

END
FILMED